Cranfield University

Christian Omgba-Essama

Numerical Modelling of Transient Gas-Liquid Flows (Application to Stratified & Slug Flow Regimes)

School of Engineering

PhD Thesis

Cranfield University

School of Engineering
Applied Mathematics and Computing Group

PhD Thesis

Academic Year 2003-4

Christian Omgba-Essama

Numerical Modelling of Transient Gas-Liquid Flows (Application to Stratified & Slug Flow Regimes)

Supervisor: Prof C. P. Thompson

April 2004

This thesis is submitted in partial fulfilment of the requirements
for the degree of Doctor of Philosophy

© Cranfield University, 2004. All rights reserved. No part of this publication may be reproduced without the written permission of the copyright holder.

Abstract

A new methodology was developed for the numerical simulation of transient two-phase flow in pipes. The method combines high-resolution numerical solvers and adaptive mesh refinement (AMR) techniques, and can achieve an order of magnitude improvement in computational time compared to solvers using conventional uniform grids.

After a thorough analysis of the mathematical models used to describe the complex behaviour of two-phase flows, the methodology was used with three specific models in order to evaluate the robustness and accuracy of the numerical schemes developed, and to assess the ability of these models to predict two physical flow regimes, namely stratified and slug flows.

The first stage of the validation work was to examine the physical correlations required for an accurate modelling of the stratified smooth and wavy flow patterns, and a new combination of existing correlations for the wall and interfacial friction factors was suggested in order to properly predict the flow features of the experimental transient case investigated.

The second and final phase of the work dealt with the complex and multi-dimensional nature of slug flow. This flow regime remains a major and expensive headache for oil producers, due to its unsteady nature and high-pressure drop. The irregular flow results in poor oil/water separation, limits production and can cause flaring. The modelling approached that was adopted here is based on the two-fluid model, which can theoretically follows each formed slug and predicts its evolution, growth and decay, as it moves along the pipe.

However, the slug flow study, performed here through a test case above the Inviscid Kelvin-Helmholtz transition from stratified to slug flow, showed that the incompressible two-fluid model used is unable to accurately predict most of the features of this complex flow. Mechanisms such as the interfacial wave formation, the slug growth and propagation, although observed from the simulations, cannot be accurately determined by the model.

Acknowledgments

This work has been undertaken within the second stage of the Transient Multiphase Flows (TMF) Co-ordinated Research Project. The Author wish to acknowledge the contributions made to this project by the Engineering and Physical Sciences Research Council (EPSRC) and to the following industrial organisations: - ABB; AEA Technology; BG International; BP Exploration; Chevron; Conoco; Enterprise Oil; Granherne; Institutt for Energiteknikk; Institut Francais du Petrole; Marathon Oil; Mobil North Sea; Norsk Hydro; Scandpower; TotalFinaElf. The Author wishes to express his sincere gratitude for this support.

In addition, I would like to express my gratitude to my supervisor Prof Chris Thompson for giving me the opportunity to carry out the research into the fascinating subject of multiphase flow modelling. I like to thank him for the fruitful discussions we had, his advices and his support throughout these years.

I would also like to thank all my former and present colleagues and friends from the Applied Mathematics And Computing (AMAC) group, whose advice, patience, support, companionship, and laughter have added so much enjoyment to this experience. Special thanks are due to Jean Charpin, Shane Dickson, Alexandre Dugarry, George Goudinakis, Cesare Guardino, Shan Fu, Pierre-Yves Lesage, Patrick Lezeau, Pauline Loilier, Tim Myers, Peter Sherar, Homa Sutherland, Julian Turnbull, Kath Tipping, Rachael Wiseman, and Judith Weissinger. Of course, it would have not been quite so much fun without Eric Tchambak, Will Rawes, Jonathan Montgomery, Sarah Laskey and Sam Allababidi from the Process and System Engineering Department.

In particular, I would like to convey my appreciation to Dr James Nelson for proof-reading my thesis, and express my sincere gratitude to my former colleague and technical advisor Dr Lahcen Hanich, without whose friendship and help with everything concerning fluid flow modelling, I am not certain that this work could ever have been completed.

A special thank is given to all my friends around the world for their support and encouragement, and to everyone from the Cranfield Football Team that I have known over the years for allowing me to win a couple of trophies, and making my student life a memorable one.

Finally, I dedicate this thesis to my parents for their love, support and understanding throughout this experience, and offer my unqualified thanks to the rest of my family, in particular my elder brother Thierry, and my dear friend Astride, for offering me their shoulders when I most needed it.

To my parents Celestine and Francois Omgba.

Contents

List of Figures

List of Tables

1 Chapter 1 – Introduction

1.1 Background

The research described in this thesis deals with issues related to both mathematical and numerical methods for solving multiphase flows. The author performed some of this work as part of a project on **t**ransient **m**ultiphase **f**low (TMF) [Hewitt, 2002], initiated and funded by the UK Engineering and Physical Sciences Research Council (EPSRC) and by the oil and gas industry and their contractors.

Many systems do not involve the flow of a single homogenous material (phase) such as gas, liquid or solid. Instead complex combinations of two or more of these phases predominate; with gas-liquid, gas-solid, liquid-solid, liquid-liquid, gas-liquid-liquid and even gas-liquid-solid flows frequently occurring in both nature and technology. For example, clouds are droplets of liquid moving in a gas. Oil, gas and water can coexist in rock. Near the surface of the Earth, particles are moved by interacting with air or water, resulting in the shaping of geological features. In the realm of human endeavours, boiling heat transfer is the workhorse of the energy industry, involving gas bubbles nucleating, growing, and coalescing. Chemical processing involves mixing, emulsifying, and catalysis in a myriad of flow scales, and finally, we drink carbonated beverages from soda water to champagne, and eat emulsions and suspensions such as mayonnaise.

The widespread presence of these multi-fluid systems suggests the utility of a general technique of description to understand their behaviour. However, each of these systems has distinguishing characteristics that keep any particular multiphase model from being generally applicable. The result is that many disjoint modelling communities use their own specific formulation and approximations, slowing our progress in better understanding these complex flows. In the present study we focus on gas-liquid two-phase flows. They are commonly encountered in many types of process equipment from boilers and condensers to refrigerators, heat exchangers and even air conditioners. They are also prevalent in hydrocarbon recovery onshore and offshore where oil and gas are currently transported through pipelines. In the early 1970s, Beggs & Brill (1973) stated that more than half of the natural gas gathered in the United States at the time flowed in two-phase pipelines.

In addition to being the most common of the two-phase cases, gas-liquid flow is also the most complex since it combines the characteristics of a deformable interface with those of a compressible phase. This means that for a specified channel design and inclination, and for a given fluids flowrate fed into the system, the gas-liquid interface can arrange itself into a

large variety of forms. As a result many investigators have concluded that, although theoretically possible, it is simply too difficult to solve this two-phase flow problem using the classic Navier-Stokes equations of fluid dynamics. This has led to the adoption of a phenomenological approach in which the flow distributions are classified into several distinct "patterns" enabling the main characteristics of each group to be studied separately.

This chapter begins with a description of the potential flow regimes in gas-liquid horizontal flows, followed by a more detailed description of the objectives of the present study and concludes by a brief summary of each of the subsequent chapters included in this thesis. The research described here led to the development of a computational framework called **EMAPS** (**E**ulerian **M**ultiphase **A**daptive **P**ipeline **S**olver), which is presented in Appendix A, and will be constantly mentioned throughout the thesis.

1.2 Two-Phase Flow Regimes

As already mentioned, when oil and gas flow together in a pipeline, they can arrange themselves in a number of different configurations called **flow patterns** or **flow regimes**. Each flow pattern is characterised by a relatively similar distribution of the two fluids and their interfaces. Transition from one flow pattern to another takes place whenever a major change occurs in the geometry of the gas-liquid interface. However, classification and description of the flow distributions into recognised patterns is still often a very subjective process. The simple reason is that two-phase flow patterns and their behaviour are highly complex and far from being well understood. The recent book by Levy (1999) describes our present state of knowledge about flow regimes in all pipe inclinations and highlights the complications, shortcomings and differences in our understanding. In this thesis, we focus on horizontal or nearly horizontal pipes, and show in Figure 1.1 the typical flow patterns presented in the literature [Mandhane et al., 1974; Taitel & Dukler, 1976; Barnea, 1987; Petalas & Aziz, 1998]. These include:

1. **Dispersed-Bubble flow:** At high liquid flowrates and for a wide range of flowrates, small gas bubbles are dispersed throughout a continuous liquid phase. Due to the effect of buoyancy these bubbles tend to accumulate in the upper part of the tube.

2. **Stratified flow:** At low liquid and gas flowrates, gravitational effects cause total separation of the two phases. This results in the liquid flowing along the bottom of the tube and the gas flowing along the top with a **smooth** interface. If the gas velocity is increased, the interfacial shear forces increase, rippling the liquid surface and producing a **wavy** interface.

3. **Slug flow:** As the gas and liquid flowrates are increased further, the stratified liquid level grows and becomes progressively wavier until eventually the whole cross-section of the pipe is blocked by a wave. The resultant "lump" of liquid called a

"slug" is then accelerated by the gas flow, surging along the pipe, and scooping up the liquid film in front as it progresses. A region containing an elongated gas bubble moving over a thin liquid film then follows this slug. Hence an intermittent regime develops in which elongated bubbles and liquid slugs alternately surge along the pipe.

4. **Annular flow:** At even higher gas flowrates, the gas pushes through the centre of the pipe leaving a ring or annulus of liquid around the inside of the tube which, due to gravity, is thicker at the bottom. Some liquid may also be entrained in the gas core as small-dispersed droplets.

A variety of other flow regimes have been reported in the literature, some of which are illustrated in Figure 1.1. In many cases, new names have been introduced to better define the distribution of the two-phase. For instance, the terms *annular-wavy* or *stratified-wavy* have been used to identify the presence of waves at the gas-liquid interface. Similarly, plug or semi-annular wording has been offered to describe transitional flow patterns, such as between bubble and slug or again between slug and annular flow. We consider here all such variations as sub-regimes of a specific flow pattern, and in the case of gas-liquid horizontal flows, we therefore need to recognize only the four major groups of flow regimes already identified: bubble, slug, stratified, and annular.

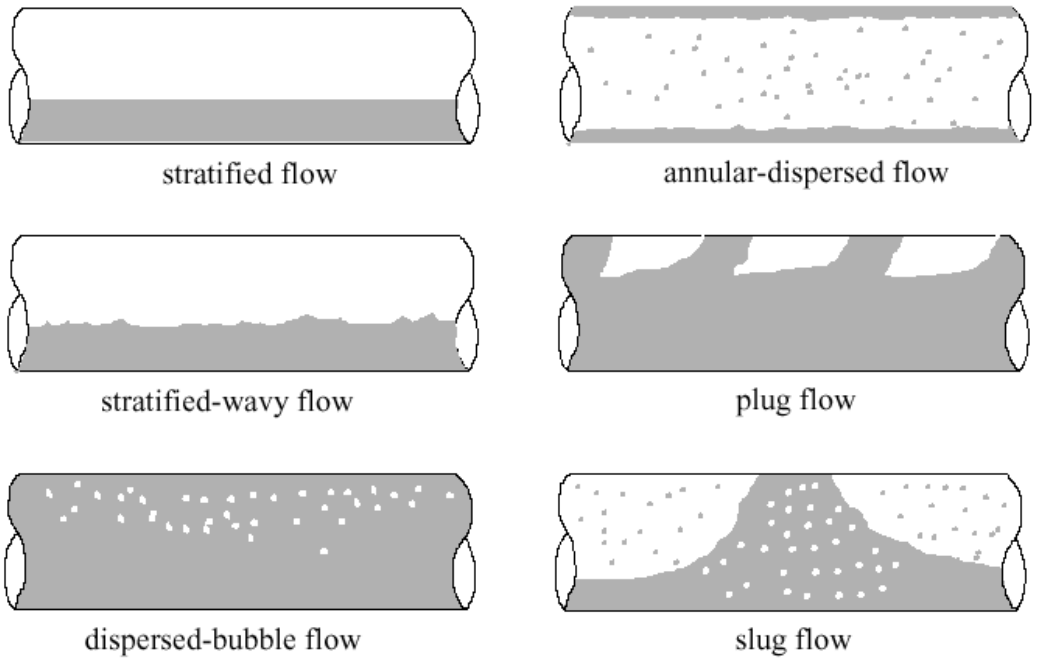

Figure 1-1: Horizontal Gas-Liquid Flow Patterns (Shaha, 1999)

In discussing each of the major types of flow patterns, it is necessary not only to specify such global properties as the pressure drop and the volumetric gas fraction, but also the conditions that determine the transition from one flow pattern to another. Furthermore, the

interface areas and the transfer processes at the interfaces need to be covered. Also, because the geometry at the interface is quite complex, it is often necessary to simplify it considerably to obtain an analytical representation. Finally, it would be naïve to expect that a single mathematical expression or empirical correlation could adequately describe the many existing variations of each flow regime. As matter of fact, several expressions have been developed to describe the conditions encountered within a single flow pattern and it can be quite difficult to choose among them. Some of these expressions will be reviewed in detail in subsequent chapters, exclusively for the stratified and slug flow patterns, which constitute the main targets of the current study.

1.3 Thesis Objectives

We are particularly interested in time-dependent phenomena in long pipelines in the petroleum industry. Although they are normally designed to operate under steady-state conditions, transient phenomena are frequently encountered in pipelines. These phenomena occur from changes in operational conditions such as a change in inlet flow rates or exit pressures (imposed transients) or from induced terrain slugging (these are natural transients due to the pipe geometry).

A good knowledge of the flow characteristics, such as the operating flow regime, the pressure drop, the liquid holdup or the maximum slug length, is therefore very important to properly design two-phase flow lines, fluid treating and separation facilities. However, the prediction of these flow characteristics for oil and gas flows is, at present, based either on incomplete mathematical models or on experimental data obtained from small diameter pipelines with water and air typically being the operating fluids. Hence, there is still a need to develop reliable mathematical models for two-phase hydrocarbon flows in large diameter pipelines.

However, the derivation of the "right" model is far from being achieved for unsteady multiphase flow problems encountered in nature or industrial applications and the numerical modelling of such flows remains a difficult and challenging task for researchers, mainly due the chaotic distribution of turbulent interfaces between the different phases. Hence, the main objectives of this thesis are:

- The evaluation of the limitations of the current modelling tools and if necessary the development of mathematical and physical models for transient two-phase flow in pipelines, which accurately describe the complexity of the flow features involved.
- The development of efficient and robust numerical solvers, which are applicable to a wide variety of industrially relevant problems.
- The development of accurate discretisations: second-order accuracy in space and time (in combination with good gridding strategies) can significantly reduce numerical errors and hence, allow better prediction of the physics of the problem.

- The design of intelligent algorithms that will automatically and efficiently adapt locally the computing strategy to the nature of the solution and to the accuracy required. Here the main tool will be **a**daptive **m**esh **r**efinement (AMR), and we will expect our approach to support local adaptation in space and time, giving maximum efficiency.

Because of the diverse nature of two-phase flow regimes, particular effort has been devoted to the stratified flow and hydrodynamic slug flow regime in horizontal pipes. These flows are particularly challenging for computational schemes, and resolving them accurately will not only improve our understanding of gas-liquid flows but also provide a reliable tool for future predictions.

However, investigating slug flow is made difficult by its transient nature and the multi-dimensional fluid dynamic process that characterizes it. Because the flow is highly complex and unstable, it is difficult to predict parameters such as the pressure drop, and the heat and mass transfer, which are required for design purposes.

Past studies have considered steady-state slug flow, in which the slug moves at constant velocity, and the slug characteristics are averaged. Knowledge of these averaged values alone, and without information about the longitudinal distribution, may be inadequate for design purposes, for example, slug catchers, which should prevent slugs from propagating downstream the system, are designed on the basis of the maximum slug length and not on the average.

Therefore, as a final objective of this research, we will simulate the transient development of the gas and liquid distribution during slug flow as well as understand the dependence of flow parameters on the slug characteristics such as the slug and bubble lengths. This aspect of the study will be covered in the penultimate chapter of this thesis.

1.4 Chapters Outline

The thesis is structured into five main chapters (Chapters 2 to 6) that are followed by a short conclusion (Chapter 7) where the main findings and achievements of the research are summarized and suggestions for possible further work are given.

To develop a successful two-phase model requires elements from many scientific areas, and we believe that it will be counter-productive in this thesis to encapsulate in one chapter the literature review of all the necessary parameters. Instead, we will present in every chapter, a small review of the key elements used for our modelling endeavour.

Chapter 2, "**Two-Phase Flow Models**", covers an extensive review and description of the mathematical models used to represent gas-liquid two-phase flows. It is split into three

main parts. The first one deals with the various modelling formulations existing in the literature, as well as a brief review of the three main commercial packages used in the petroleum industry for simulating transient two-phase flows. The second part discusses the general process of deriving or averaging multiphase flow equations, and the forms of the constitutive relations required to close the derived set of equations. The third section presents three specific mathematical formulations that we have implemented during the course of this thesis. A thorough study of their hyperbolicity as well as their stability limit is also provided in this final section.

Chapter 3, "**Numerical Methods**", focuses on the algorithmic techniques developed and implemented to solve the physical models presented in the second chapter. This chapter also contains three main parts. The first one describes the explicit finite volume approach adopted in this study, and reports the various conservative flux schemes implemented, as well as the developed numerical schemes for the non-conservative terms appearing in some two-phase flow models. The second part discusses issues related to the selection of the time step or appropriate boundary conditions, which are constraints required by most numerical schemes in order to converge properly to a reliable solution. The final section presents the results from the simulation of simple test cases used to validate both single-phase basic models and two-phase flow models implemented in the present study.

Chapter 4, "**Adaptive Mesh Refinement (AMR)**", describes a specific spatial and temporal technique for speeding the convergence of numerical models developed and resolving more accurately complex features of the flows simulated. Compared to non-adaptive schemes, AMR schemes are undeniably complicated and contain many elements, which require careful co-ordination. Hence, the main objective of this chapter is to explain the methodology and intricacies of the AMR algorithm that we have implemented. Therefore, the chapter starts by a short review of adaptive mesh schemes, and the reasons, which motivate the AMR strategy that was chosen. Then, follows a lengthy description of the two most important features of any mesh refinement scheme, which are its hierarchical grid data structure and the refinement process itself. Next we present two interesting consequences of the inter-grid communication, namely the boundary conditions and the mass conservation process.

The effort required to correctly program the AMR algorithm is considerable, with a complete implementation requiring tens of thousands of code lines to express the core algorithm. Therefore the last part of this chapter presents simulations demonstrating that the resultant computational benefits make this effort worthwhile. Finally, the chapter is closed by a summary of the work, a list of conclusions that were drawn, and a few suggestions as to how this work could be usefully extended.

Chapter 5, "**Stratified Flow Modelling**", describes the first practical applications of the mathematical and numerical models developed. It aims at better understanding the phase interactions in both steady and transient two-phase stratified flows. The closure laws for wall and interfacial shear stress are the main uncertainties for the stratified flow models used here, therefore, a review and validation study of these key terms constitute the two

major parts of this chapter. Based on the quantitative analysis of the interfacial structure, new steady state expressions for shear stresses are derived and advocated for further stratified flow modeling purposes.

Chapter 6, "**Slug Flow Modeling**", examines the validity of one of the developed two-fluid models to predict the complex features of hydrodynamics slug flow. The chapter starts by explaining the mechanisms of slug flow formation following experimental observations. Then, we present a literature review of the key parameters (length, frequency, velocity) for an accurate prediction of slug flow, followed by a brief description of the various approaches used in the literature to numerically model this complex flow regime.

The chapter continues with the analysis of the numerical simulations of a slug flow test case, investigating mechanisms such as slug initiation, growth and propagation using the validated stratified flow model described in Chapter 5. Finally, we conclude with some suggestions in order to improve the predictions of our incompressible code as well as the current commercial codes.

1.5 References - 1

- **Barnea D., (1987)** "A unified model for prediction flow pattern transitions in the whole range of pipe inclination". *Int. J. Multiphase Flow,* **13**, 1-12.

- **Beggs H. D., & Brill J. P., (1973),** "A study of two-phase flow in inclined pipes". *Journal of Petroleum Technology, Transactions*, **25**, 607-617, May 1973.

- **Hewitt G. F., (2002)** "Joint Project on Transient Multiphase Flows (TMF3)". *http://www.cranfield.ac.uk/sme/amac/tmf/tmf3_prospectus_final_version_may_2nd_2002.pdf* (visited on the 02/12/2003)

- **Levy S., (1999)** "Two-Phase Flow in Complex Systems". *John Wiley & Sons, Inc*.

- **Mandhane J. M., Gregory G. A., and Aziz K., (1974)** "A flow pattern map for gas-liquid flow in horizontal pipes". *Int. J. Multiphase Flow*, **1**, 537-553.

- **Petalas N., & Aziz K., (1998)** "A Mechanistic Model for Multiphase Flow in Pipes". *49th Annual Technical Meeting of the Petroleum Society of the Canadian Institute of Mining, Metallurgy and Petroleum*, **Paper 98-39**, Calgary, Canada, June 8-10.

- **Taitel Y., & Duckler A. E., (1976)** "A Model For Predicting Flow Regime Transitions in Horizontal and Near-Horizontal Gas-Liquid Flow". *AIChE Journal*, **22 (1)**, 47-55.

- **Shaha J., (1999)** "Phase Interactions in Transient Stratified Flow". *PhD thesis*, Department of Chemical Engineering, Imperial College, London, UK.

2 Chapter 2 - Two-Phase Flow Models

2.1 Introduction

Two-phase gas-liquid flows consist of interacting phases that are distributed in a complex way in space and time. The boundaries between the phases are delineated by interfaces, and the major difficulties in the mathematical description and subsequent prediction of the behaviour of a two-phase flow arise because of the presence of these interfaces. The properties that characterize the flow can vary considerably across the interface and in some cases are discontinuous. Despite the apparent self-organisation of the flow into flow regimes or flow patterns, each of which has a reasonably distinct average interfacial topology, the interfaces themselves can fluctuate widely in space and time and appear to have limitless degrees of freedom.

The governing equations describing two-phase flow systems, coupled with accurate numerical resolution techniques, should provide a tool for investigating and predicting the mean flow features with an understanding of the limitations and uncertainties in their specifications. However, building the physical model is probably the most important part of the modelling process because numerical models developed from inappropriate conceptual models can have large uncertainties that are difficult to quantify, and may lead to results that differ significantly from the physical systems they seek to describe. In pipeline engineering applications, errors in flow and transport predictions could be contentious, dangerous, or very costly, but the complexity of the flow behaviour means that confidence in a conceptual model is developed through an iterative process of characterization, model building, prediction, field-testing, calibration, and refinement.

We are particularly interested in time-dependent phenomena in long pipelines operating under two-phase stratified and slug flow conditions. Therefore, our objective is to develop a generic mathematical model capable of predicting the complex behaviour of these two flow regimes. Before we present some of the models that were investigated during the course of this thesis, we start the chapter by a review of various mathematical models found in the literature, followed by an overview of transient one-dimensional models used by commercially available simulators.

A two-phase flow is considered as a field that is subdivided in many single-phase regions with moving boundaries between the phases. Differential balance equations for each sub-region can be derived with the appropriate interfacial boundary conditions, or so called "jump conditions" to match the conditions either side of the interface. Thus in theory, it is possible to describe a two-phase flow using local instantaneous variables. However, the resulting equations are computationally intractable and averaging techniques are generally used to derive practical two-phase flow equations. Hence, the next section presents a short note on the averaging techniques used in the literature, followed by a description of a full set of a one-dimensional compressible two-fluid equations obtained using an ensemble averaging technique [Drew & Passman, 1999].

One of the areas of controversy in multiphase modelling is the expression of constitutive relations or closure laws used for practical applications. Hence, the next section contains a description of two constitutive laws used for regularizing two-phase flow equations, namely the interfacial pressure correction and the virtual mass force. It also contains a short introduction of frictional drag laws, which constitute the main algebraic source terms in all mathematical models presented in this study.

We conclude the chapter by two sections describing three specific models that were implemented in the EMAPS code. The penultimate section deals with the formulation of their governing equations, while the last one evaluates their stability via a characteristics analysis, and derives the limit of hyperbolicity, or range of applicability, of these models.

2.2 Review of Two-Phase Mathematical Models

Two-phase flows commonly occur in nature and in a multitude of other settings. They are not only of academic interest but are found in a wide range of engineering applications such as chemical plants, nuclear reactors or gas and oil pipelines. Because of obvious differences among these flows, and the complexity of various flow patterns encountered, many forms of descriptive equations representing their behaviour have been developed and are discussed by various authors [Stewart & Wendroff, 1984; Soo, 1990].

Despite the numerous variations and forms of mathematical models found in the literature, they can be classified, in the Eulerian framework, in three separate groups, namely:

- **H**omogeneous **E**quilibrium **M**odel (HEM)
- **D**rift-**F**lux **M**odel (DFM)
- **T**wo-**F**luid **M**odel (TFM)

A more detailed description of these three generic models is given in the following sub-sections.

2.2.1 Homogeneous Equilibrium Model (HEM)

The simplest formulation for the hydrodynamics of a two-phase mixture is referred to as the homogeneous equilibrium model (HEM). In this model, one assumes that the velocity, temperature and pressure of the phases or components are equal. This assumption is based on the belief that differences in these three variables (and chemical potential if chemical reactions are considered) will promote momentum, energy, and mass transfer between the phases rapidly enough so that thermodynamic equilibrium is reached. This will be the case for drag-dominated flows where the two phases are strongly coupled and their relative velocities equalise over short spatial length scales. For example, when one phase is finely dispersed in another phase, a large interfacial area is generated and, under certain circumstances, this assumption can be made; e.g., bubbly flow of air in water or steam in water at high pressures.

The governing equations of the HEM model resemble those of a pseudo-fluid with mixutre properties. They are, therefore, similar to the single-phase Euler equations with appropriate source terms [Corradini, 1997; Garcia et al., 2000]. To close the model and obtain the mixture properties, a thermodynamic equation of state that links the two phases is used. However, the multiphase transport properties, the viscosity and thermal conductivity, are a matter of concern for the model, because it is not clear whether one should average their effect in an area-average, mass average or volume-average sense. In many situations, such as for pressure drop calculations, the mixture transport properties are arbitrarily averaged on a volume or mass basis. However, these averaging schemes are not exact and are usually corrected by fitting coefficients to a set of experimental data. In other situations the effect of multiple phases is neglected and the liquid or gas property values for the viscosity and thermal conductivity are used. For example, when the amount of liquid in the pipe is large (low quality or void fraction), the viscosity can be taken to be that of the liquid.

A modified version of the model for one-dimensional isothermal gas-liquid flows is presented in Section 2.6.1. It is characterized by a separate continuity equation for each phase and a single momentum equation. Several investigators [Mori et al., 1976; Sharma et al., 1985; Ramos, 1995] have used this model for various engineering applications ranging from pressure wave propagation in pipelines to magma propagation in volcanic conduits. But critical comments on the applicability of the HEM model can be found in the review papers by Stewart & Wendroff (1984) and Manninen & Taivassalo (1996), and it is advisable to always check the validity of the equilibrium assumptions, whenever it is used, by comparing with more accurate theoretical models. For example, rapid acceleration or pressure changes cannot always be accurately modelled with the HEM model; i.e., shock wave propagation through a multiphase medium. This is especially true when the pressure change is large compared to the ambient pressure, or any of the driving potentials are large, relative to their reference values. Such a 'rule-of-thumb' is very crude and one must carefully consider the timescales for equilibration of these driving potentials with allowable characteristic times for the problem of interest.

2.2.2 Drift-Flux Model (DFM)

In multiphase flows, gravity and centrifugal forces tend to cause velocity differences between the phases. To account for these, a group of models has been developed that uses a single momentum equation with an additional term to represent the effect of velocity differences between the phases. Depending on the exact formulation of the equations used to determine the velocity differences (and the personal preference of the author), this model is referred by various names, such as the drift-flux model [Zuber & Findlay, 1965], the mixture model [Ishii, 1975], the algebraic-slip model [Pericleous & Drake, 1986] or the local-equilibrium model [Johansen et al., 1990]. Here, the drift-flux designation will be used, because it is the name given by the first authors who dealt with the model.

As previously mentioned, the salient feature of the drift-flux model is that the restriction on equal phase velocities is relaxed and the momentum exchange between the phases and the pipe is modelled separately with different velocities, e.g., gas and liquid velocities. The relaxation of equal velocities is most important when the densities between the phases are quite different in the presence of a gravitational potential field or large pressure gradients. Given a density difference, buoyancy effects tend to induce a drift velocity of the dispersed phase in the continuous phase. A measure of this density difference is the Atwood ratio that is defined in Table 11.1. It can be seen that, as this density ratio approaches zero, the HEM model would become more valid because the drift velocity would be reduced as the buoyancy of the lighter phase diminishes. The remaining assumptions of equal temperatures and pressures of the phases are usually retained in most applications. This is because it is usually assumed that the rates of mass and energy exchange are large enough to promote equilibrium. Once again a check with a more detailed model is recommended.

The governing equations for the drift-flux model are not presented here, but can be found in the thesis by Theron (1989) and Bonzoni-Gavage (1991) as well as numerous articles [Pauchon et al., 1994; Boure, 1997; Masella, 1997; Faille & Heintze, 1999; Fjede & Karlsen, 1999; and Romate, 2000]. For isothermal flows, the model will be similar to the HEM model; it is therefore given in the form of a continuity equation for each phase and one momentum equation for the motion of the mixture. However, there are two important differences in the equations that one should notice. Firstly, the two continuity equations do not use the same velocity and secondly the momentum equation requires an algebraic correlation or a sub-model, based on a force balance for dispersed phases, for the computation of the relative velocities. The form of the constitutive equations for the relative velocities varies in the different mixture models. The basic assumption in this formulation is that a local equilibrium is established over short a spatial length scale. Due to the requirement of a strong coupling between the phases, the drift-flux model is more suited to liquid-particle mixtures than gas-particle mixtures.

2.2.3 Two-Fluid Model (TFM)

The final type of multiphase model is the multiple fluid model (better known as the two-fluid model designating two phases or components). This model treats the general case of modelling each phase or component as a separate fluid with its own set of governing balance equations. In general, each phase has its own velocity, temperature and pressure. The velocity difference, as in the drift-flux model, is induced by density differences. The temperature difference between the phases is fundamentally induced by the time lag of energy transfer between the phases at the interface as thermal equilibrium is reached. If the multiphase system involves rapidly changing flow conditions due to area changes in steady flow or transient conditions then the time lag for reaching thermal equilibrium between the phases may become significant in comparison to the characteristic time it takes for flow conditions to change. According to Corradini (1997), one may estimate this condition by computing a characteristic Fourier number (Table 11.1) for the system under expected flow conditions. Hence, when thermal nonequilibrium becomes important, one must include the possibility of a temperature difference by separate energy balances in a multiphase model.

The modelling of pressure nonequilibrium is much more complex [Ishii, 1975]. The pressure difference between two phases is caused by three main effects: surface energy of a curved interface, mass transfer, and dynamic effects.

In the first case the simple existence of an interface (probably curved) requires that some pressure difference exist between the phases. This pressure difference is proportional to the interfacial surface tension and inversely proportional to the radius of curvature and is usually neglected in most applications. The second effect is noticeable when the mass flux due to phase change is large at the interface between the phases; e.g., large evaporation or condensation rates. The final effect occurs when one phase has a larger pressure relative to the other phase due to very rapid energy deposition or pressurization effects.

A common example of an induced dynamic pressure difference is the flow of a mixture of air bubbles and water through a converging-diverging nozzle. If the rate of flow is high and the area change is dramatic enough, the liquid will depressurize quickly as it passes through the nozzle thereby leaving the vapor bubbles at a higher pressure. This dynamic pressure difference will cause the vapor bubbles to grow, overexpand and then oscillate around a new mean pressure [Corradini, 1997]. This example takes on the second effect for steam bubbles in water because mass transfer would also be present. The magnitude of pressure nonequilibrium between the phases is inversely proportional to the time scale of the rate of phase change or external pressure oscillations. For most applications of two-fluid modelling this pressure nonequilibrium is usually neglected; i.e., only when the rate of phase change and pressure oscillations become of equal time scales does this nonequilibrium effect become important. One way to estimate this is to compare the flow velocity to the speed of sound in the multiphase system (note that computing a mixture sound speed is not a straightforward task): i.e., only when the flow velocity approaches or exceeds the multiphase sound speed would the pressure nonequilibrium become important.

The two-fluid model equations are given in Section 2.6.3 for isothermal flows. They are formulated by considering the transfer processes of each phase separately, in terms of two sets of conservation equations that govern the balance of mass and momentum for each phase. One should note that when a two-fluid model is used, a number of interfacial transport coefficients are defined, which require constitutive relation models to complete the overall model. This approach has the advantage that the actual transport processes can be rigorously defined. However, one is required to model these kinetic processes in detail, which implies a much greater depth of experimental data and insight.

By using a separate momentum equation for each phase and two independent velocity fields in the formulation, it is anticipated that the model will properly take into account the dynamic interactions between phases. Thus, it is expected that two-fluid models can be more useful to the analyses of wave propagation and flow regimes identification than the simpler mixture models (HEM, DFM). In particular, if the two-phases are weakly coupled so that the waves can propagate in each phase with different velocity, the two-fluid model should be used to study these phenomena. The second application to the analysis of the flow regimes can be explained by the fact that the changes of flow regimes occur mainly due to the instabilities of the interfaces, and the interfacial transfer of momentum governs the dynamics and stability of interfaces.

2.3 Commercial Software

Early studies on transient two-phase flow were conducted in the nuclear industry, as it became mandatory to predict the transient flow behaviour during potential Loss-of-Coolant Accidents (LOCAs) for licensing Pressurized Water Reactors (PWRs). Due to the nature of the two phases (steam/water), very fast transients and heat transfer phenomena were involved. Numerous large codes using a six-equation, two-fluid model such as TRAC [LASL, 1984], RELAPS5 [Shieh et al., 1994] or CATHARE [Bestion, 1990] were developed for this purpose. On the other hand, most of the transient phenomena encountered in the oil and gas industry are comparatively slow. Ruptures and pigging operations represent the extreme case of transients that can occur in a pipeline. Thus, the development of a tool that could predict the flow behaviour of hydrocarbon systems under different types of flow condition was needed. From numerous studies of different aspects of transient two-phase flows, some investigators have implemented and developed one-dimensional software since the early 1980's. Below is a brief summary of the three major two-phase flow simulators commercially available for the petroleum industries.

2.3.1 OLGA, PeTra

In 1983, IFE and SINTEF [Bendiksen et al., (1986, 1991)] jointly started the development of **OLGA**, the first commercial software for pipelines transportation. Originally, it used a

classic two-fluid model, but subsequent developments have led to the implementation of an extended dynamic two-fluid model that assumes the possible existence of three different phases, namely gas, liquid film and liquid droplets. A separate mass equation is applied to each of these three phases. Two momentum equations, one for the gas and possible liquid droplets and the other for the liquid film, are utilised. An energy conservation equation for the mixture is also used. In this six-equation model, two basic flow pattern classes are considered: distributed (bubble and slug flow) and separated (stratified and annular-mist flow). The transition between the two flow patterns is based on the assumption of a continuous average void fraction and is determined according to a minimum slip concept, where the flow pattern yielding the minimum gas velocity is chosen. Comparisons of experimental or field data against OLGA predictions [Bendiksen et al., 1986; Klemp, 1987; Ellul et al., 1991; Rygg & Ellul, 1991] have shown good agreement.

OLGA is one of the market-leading simulators for transient multiphase flow of oil, water and gas in wells and pipelines. However, based on recent R&D especially within three-phase slug flow, Statoil has developed a prototype of a next generation multiphase flow simulation tool named **PeTra** [Larsen et al., 1997]. This prototype still lacks much of the functionality and robustness found in the latest OLGA 2000 version, therefore a new simulator, which combines the best from OLGA & PeTra is currently being developed by Scandpower Petroleum Technology and will commercially replace OLGA in the future.

2.3.2 PLAC, ProFES

The **P**ipe**L**ine **A**nalysis **C**ode (**PLAC**) has been developed by AEA Petroleum Services since 1987. This transient multiphase hydrocarbon simulator for pipeline systems is based on the structure of the nuclear code TRAC (Transient Reactor Analysis Code), and therefore employs a two-fluid model formulation considering mass, momentum and energy equations for each phase. The partial differential equations are solved using the Stability Enhancing Two-Step (SETS) method described by [Mahaffy, 1982] and in the software technical manual [AEA Technology, 1996]. The necessary closure laws for interfacial friction, heat and mass transfer are provided via the use of mechanistic models or accepted correlations. Only two flow pattern maps are used for the entire range of inclination angles. Some studies [Black et al., 1990; Philbin & Butcher, 1992] using PLAC confirmed its accuracy when compared to experimental data and demonstrated its practical applications and capabilities to support field development.

A restructuration of the PLAC code in the late 1990's led to the development of an integrated software environment called **ProFES** (**Pro**duced **F**luids **E**ngineering **S**oftware), which is now commercialised by AEA Technologies Services.

2.3.3 TACITE

Developed since 1990, **TACITE** [Pauchon et al., (1993, 1994)] is a drift-flux model for the hydrocarbon mixtures in pipeline networks. It was conceived under a joint research

program between the French Petroleum Institute (IFP) and the oil company TotalFinaElf. The model solves a set of four conservation equations: one for the mass of each phase, one for the mixture momentum, and one for the mixture energy. Information about the slip between phases is obtained from a steady-state flow regime dependent relationship. To determine flow patterns, a new concept is introduced; it assumes that there are only two basic flow patterns: separated flow (stratified or annular) and dispersed flow with bubbles or droplets [Fabre et al., 1989]. Intermittent flow is then considered as a combination of these two patterns. A set of closure laws validated with extensive experimental results is used and physical properties are determined via a thermodynamic package. The set of four conservation equations is then solved using an explicit time advancing method. Comparisons for steady-state conditions with experimental and field data showed good agreements.

2.4 Derivation of Two-Phase Conservation Equations

In general, two formulation methods are possible when deriving equations that describe two-phase flows. These formulations actually represent fundamentally different ways of thinking about such flows and, hence, provide complementary insight into the method chosen here. The first is the particle-source-in-cell method where the dispersed phase is treated from a Lagrangian point of view in which the individual particles are tracked. The continuous phase is seen from an Eulerian point of view with the effect of the dispersed phase entering through source terms in the conservation equations. This method, also known as the Eulerian-Lagrangian formulation, is physically intuitive but is not computationally practical for other than very dilute dispersed phases.

The second method is the two-fluid model in which each phase is seen from an Eulerian point of view. This method regards the phases as two superimposed continua, much like two mixed gases, and defines local averaged quantities for each of them at each point of the physical space. The degree to which this description is accurate depends on how dispersed and dense each phase is, similar to the applicability of the continuum flow assumption in single-phase flows. Although not as accurate as the first method, the two-fluid model is the only alternative for practical computations when the dispersed phase is very dense. It is therefore the method chosen here.

Several authors [Ishii, 1975; Drew, 1983; Daniels et al., 2003] have made rigorous derivations of the two-fluid model. The usual procedure is to write, based on the principles of continuum mechanics as elucidated in standard fluid mechanics books [Truesdell & Rajagopal, 2000], the local instantaneous conservation equations for mass, momentum and energy separately for each phase, together with the appropriate molecular transport properties. Conservation laws are also written for the infinitesimally thin boundary layer between the two phases. Several authors refer to these equations for the interfaces as "jump conditions". However, the instantaneous equations, while physically valid, are intractable

computationally even using supercomputers, because the phases and their interfaces are constantly changing with position and time. This condition is analogous in single-phase flow to using the local instantaneous Navier-Stokes equations to solve a turbulent flow problem. As with turbulent flow, the solution is to average the equations and the corresponding interfacial conditions.

If done rigorously, averaging techniques lead to a computationally tractable and accurate set of equations that approximate the mean values of the desired flow variables and interfacial transfer effects. However, derivation of the conservation laws for two-phase flow by these methods is highly mathematical and to some extent can be viewed as a separate subject within two-phase flow. Therefore, the technical details of the derivation process will not be presented here, but instead a short description of various averaging procedures found in the literature, followed by a presentation of a one-dimensional set of equations obtained using a particular type of averaging technique.

2.4.1 Averaging Procedures

A number of different averaging methodologies have been proposed in the literature. They vary significantly, but usually are found to lead to equivalent forms of averaged balance equations. However, the physical variables that appear in each of the averaged balance equations involve different physical interpretations. A number of workers have made significant contributions to the development of averaged equations including Ishii (1975), Yadigaroglu & Lahey (1976), Mathers et al. (1978), Nigmatulin (1979), Drew (1983), Lahey & Drew (1988), and Daniels et al. (2003). The publications cited above are by no means an exhaustive list but have been selected because they are representative of all the different approaches that have been adopted in the literature. These various approaches can be summarized as:

1. Spatial (volume or area averaging), with no averaging in time;
2. Time averaging, with no spatial averaging;
3. Ensemble averaging, with no averaging in space;
4. Ensemble/space averaging or time/space averaging.

Hence, the averaging process involves taking averages in time, space, over an ensemble or in some cases in combination. Daniels et al. (2003) pointed that, if carried out correctly, the averaging process acts as a filter removing information that occurs below certain length and time scales. This has two important consequences: firstly, the averaged equations will only be able to resolve flow features down to the limits defined by the averaging process, and secondly, in order to solve the averaged equations the information lost or filtered out by the averaging process will have to be supplied by extra constitutive relations, this is the so called “closure problem”, which will be tackled later in this chapter.

Drew & Passman (1999) reviewed the different averaging techniques, their advantages and drawbacks, and suggested that any averaging procedure should lead to averaged flow

parameters that are continuous and have continuous first derivatives. However, there are some difficulties with the continuity of the first derivatives if they are spatially averaged. For example if we area-average on a cross-section, then the first derivatives becomes discontinuous each time an interface becomes tangential to the averaging plane.

One possible way out of the conceptual difficulties with the use of spatial averages is to use ensemble-averaging techniques as proposed by Drew (1983), Joseph & Lundgren (1990), and Drew & Passman (1999). An ensemble-average is viewed as more general than the other averaging techniques and the set of equations, presented below, were obtained using this technique.

2.4.2 One-Dimensional Conservation Equations

Formulations derived from rigorous averaging techniques generally lead to a full set of three-dimensional equations. However, in many engineering systems, such as long pipelines, the geometry of the system will constrain the fluid motion to be largely in one dimension. Therefore, a pragmatic approach to developing a practical mathematical model is to integrate these derived 3D equations of motion over a cross-section and obtain a suitable one-dimensional two-fluid model or area averaged set of equations.

For isothermal flows in a pipe with constant diameter, using time-average [Chan & Banerjee, 1981] or ensemble-average [Park et al., 1998] techniques, lead to the same set of one-dimensional conservation equations, which are:

Mass conservation:

$$\frac{\partial \rho_k R_k}{\partial t} + \frac{\partial}{\partial x}\left(\rho_k R_k V_k\right) = \Gamma_k \tag{2.1}$$

Momentum conservation:

$$\begin{aligned}\frac{\partial \rho_k R_k V_k}{\partial t} + \frac{\partial}{\partial x}\left(\rho_k R_k V_k^2\right) = &-R_k \frac{\partial P_k}{\partial x} - \Delta P_{ki} \frac{\partial R_k}{\partial x} + \frac{\partial}{\partial x}\left[R_k\left(\tau_k + \tau_k^{Re}\right)\right] \\ &+ M_{kw} + M_{ki} + \Gamma_k V_{ki} - \rho_k R_k g \sin\beta\end{aligned} \tag{2.2}$$

where β is the pipe inclination from horizontal (Figure 2-1) and variables ρ_k, P_k, R_k, and V_k are respectively the fluid density, pressure, volume fraction and velocity of phase-k. The parameter ΔP_{ki} is known as the pressure correction term, while τ_k and τ_k^{Re} represent respectively the viscous stress and the Reynolds or turbulent viscous stress. The terms M_{ki} and M_{kw} describe respectively the interfacial and wall shear stresses. The mass transfer is expressed using Γ_k while V_{ki} gives the interfacial velocity for each phase.

Three extra relations supplement the mass and momentum conservation equations presented above. The first one is an algebraic constraint that expresses the fact the volume fractions of the two phases must sum to one, and the next two are the mass and momentum interfacial jump conditions, all given by:

$$\sum_k R_k = 1 \tag{2.3}$$

$$\sum_k \Gamma_k = 0 \tag{2.4}$$

$$\sum_k M_{ki} + \Gamma_k V_{ki} = 0 \tag{2.5}$$

The subscript **i** indicates an interfacial term while the subscript **k** can take value 1 or 2 to describe one phase or the other, but in subsequent models presented in this chapter, it will have the index value G or L clearly labeling either the gas or the liquid phase.

Equations (2.1) – (2.5) will be refered as the **generic two-fluid model** and they can be used to model any two-phase flow system where a one-dimensional fluid motion is appropriate. However, the model is incomplete, as it contains 22 unknowns for only 7 equations. Therefore, additional constitutive relations are required to close and solve this generic model.

Though some correlations for the Reynolds viscous stress τ_k^{Re} have been postulated [Park et al., 1998], many other researchers [Lahey & Drew, 1988] believe that it is not possible to model this term accurately in two-phase flow. As a consequence, it is not often taken into consideration and will be neglected in the present study. As for the viscous stress τ_k, it has a minor effect on the flows considered here, so it is also neglected as well as the mass transfer Γ_k between the phases. Hence, the generic two-fluid model is reduced to 6 equations for 14 unknowns (8 variables: ρ_k, P_k, R_k, V_k + 6 closure terms: ΔP_{ki}, M_{kw}, M_{ki}).

The required constitutive relations are complicated functions of the fluid velocities and their local properties, as well as the two-phase flow patterns. They sometimes contain derivative terms, and can therefore change the structure of the generic two-fluid model, its convective terms, and subsequently its wave propagation behaviour. Most of these closure relations are presented in the following section.

2.5 Forms of Constitutive Relations

The purpose here is not to enumerate all the constitutive equations presented in the literature for pressure, interfacial force or wall shear terms, but to briefly show the various

approaches adopted by researchers in modelling these terms, and clarify some of the assumptions made in deriving two specific two-fluid models presented in Section 2.6.

2.5.1 Closure Laws for Pressure Terms

The pressure terms in the momentum equation (2.2) appear in the literature in three equivalent formulations. For completeness, these forms are:

$$R_k \frac{\partial P_k}{\partial x} + \Delta P_{ki} \frac{\partial R_k}{\partial x} \quad = \quad \frac{\partial (R_k P_k)}{\partial x} - P_{ki} \frac{\partial R_k}{\partial x} \quad = \quad \frac{\partial R_k \Delta P_{ki}}{\partial x} + R_k \frac{\partial P_{ki}}{\partial x} \qquad (2.6)$$

(a) (b) (c)

where the ΔP_{ki} is defined by $\Delta P_{ki} = P_k - P_{ki}$. This term is often referred in the literature as a pressure correction term, and will be later renamed Pc is Section 2.6.3.

Hence, to close the generic two-fluid model, additional relations need to be supplied to link the four distinct pressure terms (P_k, P_{ki}, k = G, L) that appear in the system of equations. Depending on the pressure formulation and the extra closure relations, various two-fluid models have been proposed in the literature. This complicates the process of selecting a specific model for practical applications, especially that the underlying assumptions used to obtain these closure relations are not always clarified.

2.5.1.1 Phase Pressure: P_k

The pressure in a compressible fluid is related to the temperature and density of the fluid through a thermodynamic equation of state. However, for isothermal flows considered here, the phase pressure equation only depends upon the fluid density, and can be given as:

$$P_k = P_k(\rho_k) \qquad (2.7)$$

The usual method of modelling pressure differences between the fluids is to assume that the pressure is equal in both phases. In this case, the two-fluid model is referred to as a single-pressure model (SPM). If, as previously discussed, one finds that pressure nonequilibrium between the phases is important, one must introduce a local constitutive relation that accounts for this pressure difference due to dynamic and interfacial effects. In this case, the two-fluid model is refered as a two-pressure model (TPM).

Many examples using a TPM formulation can be found in the literature [Ransom & Hicks, 1984; Glimm et al., 1999; Saurel & Abgrall, 1999; Chung et al., 2002], and more and more researchers try to adopt this formulation, even for flow where there is an instantaneous pressure equilibrium, as the resulting model appears to be more stable for numerical

purposes. However, as some of the closure relations for the TPM are still not clarified, the simple SPM approach will be adopted here for further studies.

2.5.1.2 Interfacial Phase Pressure: P_{ki}

The difference between the two interfacial pressures is generally related to the surface tension force, and appears to depend on the flow pattern considered. When this force becomes important, Barnea & Taitel (1993) suggested an expression for the stratified flow regime while Drew & Passman (1999) gave an alternative expression for bubbly flow. Both relations are given as:

$$\begin{cases} P_{Gi} - P_{Li} = \sigma \dfrac{\partial h_L^2}{\partial x^2} & \textit{Stratified flow} \\ P_{Gi} - P_{Li} = \dfrac{2\sigma}{r_B} & \textit{Bubbly flow} \end{cases} \tag{2.8}$$

where σ is a constant surface tension, h_L is the height of the liquid in the pipe if stratified flow, and r_B is the radius of bubbles.

However, the simplest way to obtain the interfacial pressure difference is to assume equal interface pressure, thereby neglecting the effect of surface tension. Mathematical models considered later in this chapter always use the equal interfacial pressure assumption and therefore adopt the following relation:

$$P_{Gi} = P_{Li} = P_I \tag{2.9}$$

2.5.1.3 Pressure Correction Term: $\Delta P_k = P_k - P_{ki}$

Early two-fluid models (TRAC, OLGA) did not consider this term in their formulation. However, its inclusion in the momentum equations allows, for example, an accurate propagation of gravity waves in stratified flow, and can have a significant effect on the hyperbolicity of the model. Therefore, recent models tend to include it in their formulation and, as a consequence, numerous expressions depending on the flow regime abound in the literature. In what follows, an account of pressure correction closure models for stratified and dispersed bubbly flow is given.

Stratified Flow

In stratified flow, the pressure correction is generally associated to the hydrostatic head, and Barnea & Taitel (1996) obtained their expression by averaging the liquid pressure P_L over any cross-section as:

$$P_L = \frac{1}{A_L}\int_0^{h_L}[P_{Li} + \rho_L g\cos\beta(h_L - y)]b\,dy \tag{2.10}$$

where b is the chord length [b(y)] and β is the angle of the pipe with the horizontal (Figure 2-1). Using the Leibnitz rule for differentiation, they obtained:

$$\frac{\partial(P_L A_L)}{\partial x} = \frac{\partial(P_{Li} A_L)}{\partial x} + A_L \rho_L g\cos\beta\frac{\partial h_L}{\partial x} \tag{2.11}$$

A similar expression is obtained for the gas phase; hence for a constant cross-section, combining Equations (2.11) and (2.6c) gives the following relations:

$$\begin{cases} \dfrac{\partial R_L \Delta p_L}{\partial x} = R_L \rho_L g\cos\beta\dfrac{\partial h_L}{\partial x} \\ \dfrac{\partial R_G \Delta p_G}{\partial x} = R_G \rho_G g\cos\beta\dfrac{\partial h_L}{\partial x} \end{cases} \tag{2.12}$$

Many authors [Taitel & Dukler, 1976; Watson, 1990; Barnea & Taitel, (1993, 1996)] use the above pressure correction expression in their momentum equations. Therefore, it is the same expression that will be used later in the incompressible two-fluid model presented in Section 2.6.

However, other expressions exist in the literature. Bestion (1990) proposed the following algebraic relation for the thermal hydraulic code CATHARE:

$$\Delta P_G = \Delta P_L = R_L R_G(\rho_L - \rho_G)gD \tag{2.13}$$

while different algebraic expressions, based on the distribution of hydrostatic pressures in the tube, are often used by researchers [Lahey & Drew, 1988; De Henau & Raithby, 1995; Masella et al., 1998]. The relations are given by:

$$\begin{cases} \Delta P_L = \rho_L gD\cos\beta\left(-\dfrac{1}{2}\cos\dfrac{\gamma}{2} + \dfrac{1}{3\pi R_L}\sin^3\dfrac{\gamma}{2}\right) \\ \Delta P_G = -\rho_G gD\cos\beta\left(\dfrac{1}{2}\cos\dfrac{\gamma}{2} + \dfrac{1}{3\pi R_G}\sin^3\dfrac{\gamma}{2}\right) \end{cases} \tag{2.14}$$

where D is the pipe diameter, γ is the angle subtended by the liquid wetted perimeter, and it is related to the liquid volume fraction by the relation $R_L=(\gamma-\sin\gamma)/2\pi$.

Dispersed Bubbly Flow

The pressure correction term is sometimes considered as a stabilizing term for two-fluid models, and as such it is often neglected in favour of the virtual mass term in numerous codes [Pokharna et al., 1997] dealing with dispersed flows. However, Drew & Passman (1999) presented a detailed study of closure models for bubbly flows and proposed the following relation:

$$\begin{cases} P_G - P_{Gi} = 0 \\ P_L - P_{Li} = \xi\left(Re_L, R_L\right)\rho_L\left(V_G - V_L\right)^2 \end{cases} \tag{2.15}$$

They suggested that for dilute flow, ξ=1/4 when the boundary layer remains attached to the spherical particle, and for low Reynolds number flows, the calculation of the averaged fields indicates that ξ = -9/32.

Some authors take into account pressure corrections for all configurations in such a way that they always have a conditionally hyperbolic system for the test cases studied. Toumi (1996), Coquel et al. (1997), and Bestion (1990) suggested the following expression:

$$\Delta P_G = \Delta P_L = \delta\left(R_k, \rho_k\right)\left(V_G - V_L\right)^2 \tag{2.16}$$

$$\text{with} \qquad \delta = \begin{cases} \xi\rho_L R_G & \text{Toumi } (\text{Toumi, 1996}) \\ \dfrac{\rho_G\rho_L R_G R_L}{\rho_G R_G + \rho_L R_L} & \text{CATHARE } (\text{Bestion, 1990}) \end{cases}$$

where ξ is an adjustable coefficient used to ensure that the resulting two-fluid model remains hyperbolic during numerical simulations. Toumi (1996) justified the choice of the pressure correction term (2.16) by assuming that gas and liquid expressions might be equal in order to satisfy the mixture momentum equation and that they must vanish when the gas velocity is equal to the liquid velocity:

$$\Delta P_{ki} \to 0 \quad \text{as} \quad \left(V_G - V_L\right) \to 0 \tag{2.17}$$

The pressure correction (2.15) does not satisfy the equal value requirement for the gas and liquid expressions, but Drew & Passman (1999) explained its derivation using the "Bernoulli theorem" for the variation of pressure in a flowing inviscid fluid. And it is a similar expression, modified following Toumi (1996) approach, which will be used in the single pressure model (SPM) proposed in Section 2.6.3.

2.5.2 Interfacial Stress Term: M_{ki}

The interfacial stress term M_{ki} arises from stresses acting on the interface. It is the most crucial transfer law in modelling multiphase isothermal flows, and can be expressed [Ishii, 1975] as a linear combination of several important physical forces, namely:

$$M_{ki} = M_{ki}^{D} + M_{ki}^{V} + M_{ki}^{B} + M_{ki}^{L} + M_{ki}^{C} \tag{2.18}$$

where the superscripts D, V, B, L, and C stand for the steady-state **d**rag, **v**irtual mass, **B**asset, **l**ift, and **c**ollision forces respectively. Closure models for the interfacial drag and virtual mass forces are presented in the next sub-sections. As for the Basset force, Cheng et al. (1985) claimed that its effect was quite small in two-phase flow systems, so it will not be considered here, nor will the lift and collision forces, for which Ishii & Mishima (1984) suggested that their functional forms are not well known.

2.5.2.1 Interfacial Shear Force

In all specific two-phase flow models described later, the virtual mass force mentioned in the next sub-section will be neglected, making the interfacial drag law the only crucial closure term for modelling two-phase flows that were investigated in this thesis.

The total interfacial shear force greatly depends upon the flow regime considered, and despite its great importance, it remains the greatest shortcoming of conventional two-fluid models and its real expression is not always known accurately. However, Ishii & Mishima (1984) suggested modelling it as the combination of two terms as:

$$M_{ki}^{D} = \left\langle -\tau_{ki} \cdot \nabla R_{k} \right\rangle_{x} + \overline{M}_{ki} \tag{2.19}$$

The first term on the right-hand side represents the effect of the interfacial shear and the void gradient, and is particularly important for a separated flow. The second term is the generalized area-averaged particle drag and is important for a dispersed flow.

Separated Flow

In a stratified or annular flow, the contribution of the interfacial shear and void gradient is the dominant drag force. Ishii & Mishima (1984) have shown that, for separated flows in a tube, it can be given as:

$$M_{ki}^{D} \cong \left\langle -\tau_{ki} \cdot \nabla R_{k} \right\rangle_{x} = -\tau_{Gi} \frac{S_{i}}{A} \tag{2.20}$$

where A is the pipe cross-section and S_i is the wetted perimeter of the interface or the gas core, which will be defined in Chapter 5. The constitutive relation for the gas interfacial shear stress τ_{Gi}, which will be renamed τ_I in the remaining of the thesis, is given in terms of the standard interfacial friction factor as:

$$\tau_I = \frac{1}{2} f_I \rho_G (V_G - V_L) \left| V_G - V_L \right| \tag{2.21}$$

There are a number of correlations for the interfacial friction factor f_I. They depend upon the fluid's local properties and the flow regime. They are not presented here, but will be reviewed in Chapter 5 in the case of stratified flow.

Dispersed Bubble Flow

The average drag force on a single particle or drop or bubble is the force felt by that object as it moves steadily through the surrounding fluid. It is usually given in terms of a dimensionless coefficient C_D, where the drag force for a dispersed bubble flow is defined as:

$$\overline{M}_{Gi} = -\frac{3}{4} \frac{\rho_L R_G C_D}{D_B} \overline{V}_r \left| \overline{V}_r \right| \tag{2.22}$$

Here, the drag coefficient C_D is assumed to be a function of the gas volume fraction R_G, the bubble diameter D_B, the relative velocity $\overline{V}_r$ and the liquid viscosity. The dependence of C_D on these parameters has been studied and many correlations for the drag coefficient C_D have been suggested in the literature. They are summarized in the book by Clift et al. (1978), and the reference papers by Ishii & Zuber (1979) and Tomiyama et al. (1998).

The important point, however, is that the averaged local relative velocity $\overline{V}_r$ must be approximated based on the drift flux formulation [Ishii & Mishima, 1984] and not as the difference between the area averaged mean velocities of phases $\left(\overline{V}_r \neq V_r = V_G - V_L\right)$. The difference between these two relative velocities can be very large. The reason is that in the one-dimensional formulation, two completely different effects cause slip, Vr, between two phases; i.e., the local relative motion between two phases at a local point and the integral effect of the phase and velocity distributions arising due to the area averaging [Zuber & Findlay, 1965; Ishii, 1977].

2.5.2.2 Virtual Mass Force

The virtual mass term in Equation (2.18) represents the interphase force, which results from the displacement of adjacent fluid mass in the case of relative acceleration between the

phases. The form of the virtual mass term in realistic two-phase flows is not known exactly and thus different computer codes for nuclear thermal hydraulics simulations [Bestion, (1990); Tiselj & Petelin, (1997)] use different forms of the virtual mass term. Drew et al. (1979) asserted that the most general form of the virtual mass contains first order space and time derivatives, and can be expressed as:

$$M_I^V = c_{vm}\rho_L R_G \left\{ \frac{\partial V_r}{\partial t} + V_L \frac{\partial V_G}{\partial x} - V_G \frac{\partial V_L}{\partial x} + (\kappa - 1) V_r \frac{\partial V_r}{\partial x} \right\} \qquad (2.23)$$

where V_r is the relative velocity, and the parameter κ should be a function of the gas volume fraction with the value 2 for $R_G \to 0$ and 0 for $R_G \to 1$. In the hydraulics codes RELAP5 and PDE2 [Tiselj & Petelin, 1997], the parameter κ is set equal to 1. Toumi & Kumbaro (1996) also used the same value of κ in their numerical model, and in all three cases, the liquid density ρ_L in (2.23) is replaced by the product of the liquid volume fraction R_L by the mixture density ρ_M. The corresponding expression used is therefore:

$$M_I^V = c_{vm}\rho_M R_L R_G \left[\left(\frac{\partial V_G}{\partial t} + V_L \frac{\partial V_G}{\partial x} \right) - \left(\frac{\partial V_L}{\partial t} + V_G \frac{\partial V_L}{\partial x} \right) \right] \qquad (2.24)$$

The open parameter c_{vm} in the virtual mass term can be used to adjust the interfacial momentum coupling with respect to different flow regimes. For idealised dispersed droplet or bubbly flow, a value of $c_{vm} = 0.5$ has been derived from classical potential flow [Drew & Passmann, 1999]. For completely separated flows (e.g. stratified flow) it is expected that c_{vm} tends to zero, but in the case of churn-turbulent two-phase flow with strong interfacial momentum coupling, a value of $c_{vm} > 0.5$ might be more appropriate. For slug-flow, Ishii & Mishima (1984) calculated a factor of $c_{vm} = 3.3$ to 5 depending on the form of slugs.

To account for the interaction effects between phases, Zuber (1964) suggested using the following expression of the virtual mass coefficient

$$c_{vm} = \frac{1}{2}\left(\frac{1 + 2R_d}{1 - R_d} \right) \qquad (2.25)$$

where R_d is the discontinuous phase fraction. However, Toumi & Kumbaro (1996) suggested defining c_{vm} by a condition necessary to obtain a hyperbolic system. Thus for their set of equations they found that the system is hyperbolic if:

$$c_{vm} \geq c_{vm}^0 = \sqrt{4c(1-c)} \qquad (2.26)$$

where c is a concentration term defined as follows:

$$c = \frac{\rho_G R_G}{\rho_G R_G + \rho_L R_L} \tag{2.27}$$

In the same way, the hyperbolicity of PDE2 code was achieved by a minor modification of the RELAP5 virtual mass coefficient c_{vm} [Tiselj & Petelin, 1997], given as:

$$c_{vm-RELAP5} = \begin{cases} \dfrac{1-2R_G}{2-2R_G} & R_G < 0.5 \\ \dfrac{3-2R_G}{2} & R_G > 0.5 \end{cases} \tag{2.28}$$

$$c_{vm-PDE2} = \begin{cases} \dfrac{1+2R_G}{2-2R_G} & R_G < 0.5 \\ \sqrt{\left[\dfrac{3-2R_G}{2R_G}\right]^2 - \dfrac{(R_G-1)(2R_G-1)}{(1+R_G\rho_G/\rho_L - R_G)^2}} & R_G > 0.5 \end{cases} \tag{2.29}$$

In conclusion, it is worth noting that for many interesting cases, the inclusion or neglect of the virtual mass force in the phasic momentum does not appreciably change the momentum results. However, the inclusion of this term with its temporal and spatial derivative terms has an effect on the hyperbolicity of the system and the numerical scheme. Although it adds an extra complexity on the numerical scheme, Watanabe et al. (1990) claimed that the virtual mass force improves the computation efficiency of the solution scheme.

2.5.3 Wall Shear Stress: M_{kw}

The wall shear stress represents the stresses acting on the phase at the wall. Different methodologies have been proposed to calculate it and are reviewed in the book by [Levy, 1999]. The wall shear stress is generally based on closure laws derived from fully developed steady state two-phase flows, and usually given as:

$$\mathrm{M_{kw}} = \mathrm{T_{kw}} = -\frac{\tau_k \mathrm{S_k}}{\mathrm{A}} \tag{2.30}$$

where S_k is the part of the wall wetted by phase k and τ_k is the wall shear stress of the same phase. The constitutive relation for the wall shear stress is given in term of the standard wall friction factor f_k as:

$$\tau_k = \frac{1}{2} f_k \rho_k V_k |V_k| \tag{2.31}$$

Correlations for gas and liquid wall frictions abound in the literature, as it is common practice to model two-phase wall friction factors using single-phase pipe formulas. These single-phase relations are not presented here, but they will be reviewed in Chapter 5.

2.6 Formulation of Specific Models

Three particular models were implemented and investigated during the course of the thesis; they all assume that the liquid phase is incompressible and that the flow of the two-phase mixture is isothermal.

2.6.1 HEM-3 (Homogeneous Equilibrium Model)

This model is recommended whenever the two phases are strongly coupled (bubble flow for example), such that the responses of the two phases are simultaneous and the wave propagation is firmly interlocked. However, in the present study, it has been mainly used for the algorithmic development and assessment of the numerical solvers that will be described in the next chapter because, while being physically realistic, it avoids two important numerical issues related to most two-fluid models: the presence of non-conservative flux terms, and the ill-posedness of the governing equations.

As already mentioned, this model assumes that all phases move at the same mixture velocity V_M. It is characterised by a combined momentum equation for all phases, but a separate mass conservation equation for each phase. The three one-dimensional equations that constitute the model are therefore:

- **Conservation of gas mass**

$$\frac{\partial \rho_G R_G}{\partial t} + \frac{\partial \rho_G R_G V_M}{\partial x} = 0 \tag{2.32}$$

- **Conservation of liquid mass**

$$\frac{\partial \rho_L R_L}{\partial t} + \frac{\partial \rho_L R_L V_M}{\partial x} = 0 \tag{2.33}$$

- **Conservation of total momentum**

$$\frac{\partial}{\partial t}\left(\rho_M V_M\right) + \frac{\partial}{\partial x}\left(\rho_M V_M^2 + P\right) = T_w - \rho_M g \sin\beta \tag{2.34}$$

where the mixture density ρ_M and the mixture wall shear stress T_w are defined by:

$$\rho_M = \rho_G R_G + \rho_L R_L \tag{2.35}$$

$$T_w = -\frac{1}{2D} f_w \rho_M V_M |V_M| \tag{2.36}$$

The conservation of energy is not enforced explicitly: the flow is assumed to be isothermal. The liquid is assumed to be incompressible and the gas density is linked to the pressure P via a thermodynamic law such as Equation (2.7) or equivalent $(\rho_G = \rho_G(P))$.

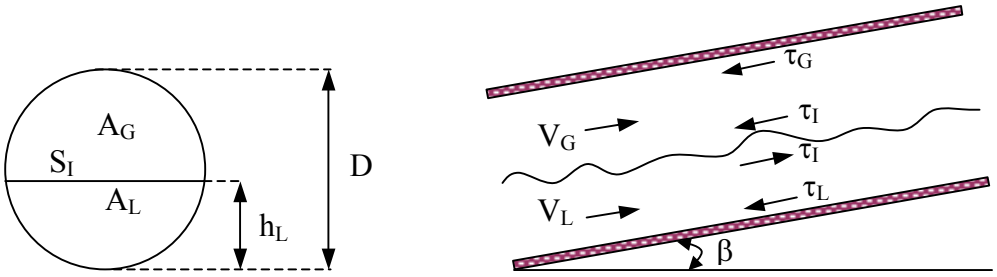

Figure 2-1: Cross-section and side views of a stratified flow in a circular pipe

2.6.2 PFM-2 (Pressure Free Model)

One of the peculiar features of most two-fluid models is the non-conservative aspect of the governing equations. Hence, efficient numerical methods developed for single-phase conservative systems cannot be used for solving these two-fluid models and new methods should be designed for their numerical computation. This lengthy and difficult modelling process can be avoided if a specific two-fluid model presented by Watson (1990) is used. A brief description of the model derivation steps now follows (see Appendix B for a more detailed presentation).

Consider the generic system of equations (2.1)-(2.5) and assume that the gas and liquid phases are incompressible, and that the two-phase mixture flows in a gravitationally separated configuration in a circular pipe of diameter **D** inclined at an angle β to the horizontal, as shown in Figure 2-1. Then using the pressure correction formulation (2.6b) and the stratified flow correlations (2.12), the following conservation equations can be derived:

- A total mass conservation is obtained by summing the gas and liquid mass balance equation (2.1), giving:

$$\frac{\partial}{\partial t}\left(\rho_L R_L + \rho_G R_G\right) + \frac{\partial}{\partial x}\left(\rho_L R_L V_L + \rho_G R_G V_G\right) = 0 \qquad (2.37)$$

- A global momentum equation is obtained by combining the gas and liquid equation (2.2) so as to eliminate the interfacial pressure P_I:

$$\frac{\partial}{\partial t}\left(\rho_L V_L - \rho_G V_G\right) + \frac{\partial}{\partial x}\left(\frac{1}{2}\rho_L V_L^2 - \frac{1}{2}\rho_G V_G^2 + \left(\rho_L - \rho_G\right) g \cos\beta \, h_L\right) = H \qquad (2.38a)$$

with

$$H = -\left(\rho_L - \rho_G\right) g \sin\beta + \left(\frac{1}{A_L} + \frac{1}{A_G}\right)\tau_I S_I + \frac{\tau_G S_G}{A_G} - \frac{\tau_L S_L}{A_L} \qquad (2.38b)$$

where S_I represents the interfacial wetted perimeter while S_G and S_L are the gas and liquid wetted perimeters, all defined in Chapter 5. The parameter τ_I is the interfacial shear stress defined by Equation (2.21), while τ_G and τ_L are respectively the gas and liquid wall shear stresses, both defined by Equation (2.31).

The mass and momentum equations (2.37) and (2.38) must be supplemented by two more relationships. The first one is obtained from the geometric constraint that the areas occupied by the liquid and gas phases must fill the pipe, so that:

$$A_L + A_G = A, \qquad \text{or} \qquad R_L + R_G = 1 \qquad (2.39)$$

The other condition is obtained from the original gas and liquid mass conservation equations. Since the phases are assumed to be incompressible, dividing the mass conservation equations by the appropriate density and adding them leads to the following relation:

$$\frac{\partial}{\partial x}\left(R_L V_L + R_G V_G\right) = 0 .$$

Hence, a second algebraic constraint (2.40) is obtained from the above equation, where $Q(t)$ is a known function of time dependent on the inlet flow rates.

$$R_L V_L + R_G V_G = Q(t), \qquad (2.40)$$

Therefore, the four original gas and liquid mass and momentum equations (2.1)-(2.2) have been reduced to just two differential conservative equations (2.37) and (2.38), and two

algebraic equations (2.39) and (2.40). The resulting system of equations is very practical for stratified flows and suitable for numerical computations.

Though the common interfacial pressure may be obtained directly from one of the gas or liquid momentum equation, or perhaps more elegantly from their sum, it was never evaluated when using this model. Therefore, the name given to the implemented model is **PFM-2**, which stands for **P**ressure **F**ree **M**odel, and the value 2 indicates the total number differential equations that constitute the model.

2.6.3 SPM-4 (Single Pressure Model)

The PFM-2 model presented above is restricted to fluid flow cases with constant properties, as the liquid and gas compressibility were ignored. This approach may be adequate for some two-phase flow patterns calculations but it fails to predict for example the true nature of slug movement in pipelines when the change in the volume of the gas due to compressibility effects becomes important. Therefore, a more general system of four equations based on the generic two-fluid model was analysed and implemented.

The model still treats the liquid phase as incompressible, but considers the gas phase as compressible obeying a thermodynamic equation of state. It is named **SPM-4** because it assumes a single pressure is common to both gas and liquid phases. The system of mass and momentum conservation equations that constitute the model is given as:

- **Gas & Liquid Mass Conservation**

$$\begin{cases} \dfrac{\partial \rho_G R_G}{\partial t} + \dfrac{\partial \rho_G R_G V_G}{\partial x} = 0 \\ \dfrac{\partial \rho_L R_L}{\partial t} + \dfrac{\partial \rho_L R_L V_L}{\partial x} = 0 \end{cases} \tag{2.41}$$

- **Gas & Liquid Momentum Conservation**

$$\begin{cases} \dfrac{\partial \rho_G R_G V_G}{\partial t} + \dfrac{\partial \rho_G R_G V_G^2}{\partial x} = -R_G \dfrac{\partial P}{\partial x} + B_{fG} + T_I + T_{Gw} \\ \dfrac{\partial \rho_L R_L V_L}{\partial t} + \dfrac{\partial \rho_L R_L V_L^2}{\partial x} = -R_L \dfrac{\partial P}{\partial x} - P_c \dfrac{\partial R_L}{\partial x} + B_{fL} - T_I + T_{Lw} \end{cases} \tag{2.42}$$

where B_{fk} is the body or gravity force for phase-k defined by $\left(B_{fk} = -\rho_k R_k g \sin\beta\right)$. The term T_{kw} is the wall shear stress for phase-k defined by Equations (2.30)-(2.31) while T_I is the interfacial shear stress defined by Equations (2.20)-(2.21) for separated flows and by Equation (2.22) for dispersed flows.

From the generic two-fluid model (2.1)-(2.2), it can be seen that the gas pressure correction has been neglected $(\Delta P_{Gi} = 0)$ as suggested by Drew & Pasmann (1999) and that the liquid pressure correction term has been renamed P_c. Two expressions of this term were investigated here; one is given by Equation (2.15) while the other one is used by the TRIUMPH code [Bonizzi et al., 2001] and it is defined as:

$$P_c = \rho_L R_L g \cos\beta \frac{dh_L}{dR_L}, \qquad \Rightarrow \qquad P_c \frac{\partial R_L}{\partial x} = \rho_L R_L g \cos\beta \frac{\partial h_L}{\partial x} \tag{2.43}$$

2.7 Hyperbolicity Analysis of Specific Models

In this section, a study of the characteristics or the hyperbolicity of the specific models presented above is performed. Discussions about whether non-real characteristics should be allowed abound in the literature [Stewart, 1979; Arai, 1980; Prosperetti & Satrape, 1989]. Those in favour note that, in general mathematical terms, the most serious pathology associated with complex characteristics is the destruction of the continuous dependence on the initial data at short scales, and that any numerical discretisation procedure would introduce a minimum resolvable scale and enough dissipation, so that any problems associated with smaller scales are irrelevant in practice.

However, while analysing the stability of a broad range of incompressible two-fluid models, Prosperetti & Satrape (1989) showed that the stability is independent of the wavelength, implying that if the existence of complex characteristics leads to instability at short scales, the same instability will also be present at all scales. Hence, a non-hyperbolic model is bound to be unstable and any numerical result to the contrary must be a consequence of an excessively dissipative numerical scheme or, possibly, a slow growth rate of the instability.

It is, therefore, necessary to always check the hyperbolicity of any specific model used. Not only does the characteristic analysis give the range of validity of the model, but it may also be useful in developing numerical methods used to solve the physical model.

Before proceeding with the three specific models presented in the previous section, it is convenient to note that their governing equations can be algebraically manipulated into the following matrix or primitive form:

$$M_A \frac{\partial \Psi}{\partial t} + M_B \frac{\partial \Psi}{\partial x} = S \tag{2.44}$$

where M_A and M_B are two non-singular square matrices of coefficients which are functions of the dependent flow variables. The vector Ψ contains the dependent flow variables or

primitive variables, while the vector S expresses the algebraic source terms for the interfacial and wall transfers of mass and momentum.

Hence, the dependence of their solution on prescribed initial data or the study of their characteristics can be reduced to an investigation of the equation:

$$\det\left(M_B - \lambda M_A\right) = 0 \tag{2.45}$$

where λ is a characteristic value.

2.7.1 HEM-3

Consider the primitive vector Ψ with $\Psi^T = \left(R_L, V_M, \rho_G\right)$, then the HEM-3 system of equations (2.32)-(2.34) can be written in primitive formulation (2.44) using the following matrices:

$$M_A = \begin{bmatrix} -\rho_G & 0 & R_G \\ \rho_L & 0 & 0 \\ \Delta\rho V_M & \rho_M & R_G V_M \end{bmatrix}, \qquad M_B = \begin{bmatrix} -\rho_G V_M & \rho_G R_G & R_G V_M \\ \rho_L V_M & \rho_L R_L & 0 \\ \Delta\rho V_M^2 & 2\rho_M V_M & C_G^2 + R_G V_M^2 \end{bmatrix} \tag{2.46}$$

where $\Delta\rho = \rho_L - \rho_G$ is the density difference and $C_G^2 = \dfrac{\partial P}{\partial \rho_G}$ is the square of the gas speed of sound.

The eigenvalues λ_k of the homogeneous equilibrium model based on the equations are then obtained by solving Equation (2.45). Combining matrices M_A and M_B from Equation (2.46) gives the following matrix:

$$M_B - \lambda M_A = \begin{bmatrix} -\rho_G\left(V_M - \lambda\right) & \rho_G R_G & R_G\left(V_M - \lambda\right) \\ \rho_L\left(V_M - \lambda\right) & \rho_L R_L & 0 \\ \Delta\rho V_M\left(V_M - \lambda\right) & \rho_M\left(2V_M - \lambda\right) & C_G^2 + R_G V_M\left(V_M - \lambda\right) \end{bmatrix} \tag{2.47}$$

Thus, setting the determinant of the matrix (M_B-λM_A) to zero leads to the following relation:

$$\begin{aligned} \rho_L R_G\left(V_M - \lambda\right)^2\left(\rho_M\left(2V_M - \lambda\right) - \Delta\rho R_L V_M\right) - \\ \rho_G\rho_L\left(V_M - \lambda\right)\left(C_G^2 + R_G V_M\left(V_M - \lambda\right)\right) = 0 \end{aligned} \tag{2.48}$$

Expanding Equation (2.48) gives the following characteristic polynomial:

$$\rho_L \rho_M R_G \left(V_M - \lambda\right)\left[\lambda^2 - 2V_M\lambda + V_M^2 - C_G^2 \frac{\rho_G}{\rho_M R_G}\right] = 0 \tag{2.49}$$

Hence, the three eigenvalues of the HEM-3 model are:

$$\begin{cases} \lambda_1 = V_M - C_M \\ \lambda_2 = V_M \\ \lambda_3 = V_M + C_M \end{cases} \tag{2.50}$$

where ρ_M is the mixture density defined by Equation (2.35) and the parameter C_M is the homogeneous speed of sound given by the following expression:

$$C_M = \left[\frac{\rho_G}{\rho_M R_G}\right]^{1/2} C_G \tag{2.9}$$

It should be noted that the three eigenvalues are always real; therefore, the HEM-3 is always hyperbolic, confirming a result that is already known in the literature.

2.7.2 PFM-2

Consider the primitive vector $\Psi = \left(R_L, V_G\right)^T$, then it is possible to rewrite the PFM-2 set of conservative equations (2.37)-(2.38) using the matrix formulation (2.44). However, this process is cumbersome and left to Appendix B. Only the matrices M_A and M_B used in the primitive formulation are given here:

$$M_A = \begin{bmatrix} \Delta\rho & 0 \\ \rho_L \dfrac{V_r}{R_L} & -\left(\rho_G + \rho_L \dfrac{R_G}{R_L}\right) \end{bmatrix}, \tag{2.51a}$$

$$M_B = \begin{bmatrix} \Delta\rho V_G & -\Delta\rho R_G \\ \rho_L V_L \dfrac{V_r}{R_L} + \Delta\rho g \cos\beta \dfrac{A}{A'_L} & -\left(\rho_G V_G + \rho_L V_L \dfrac{R_G}{R_L}\right) \end{bmatrix} \tag{2.51b}$$

where $\Delta\rho = \rho_L - \rho_G$ is the density difference and $V_r = V_G - V_L$ is the relative velocity.

The characteristic polynomial of the PFM-2 model is obtained by solving Equation (2.45). Combining matrices (2.51a) and (2.51b) gives:

$$M_B - \lambda M_A = \begin{bmatrix} \Delta\rho(V_G - \lambda) & -\Delta\rho R_G \\ \rho_L \frac{V_r}{R_L}(V_L - \lambda) + \Delta\rho g \cos\beta \frac{A}{A'_L} & -\left(\rho_G(V_G - \lambda) + \rho_L(V_L - \lambda)\frac{R_G}{R_L}\right) \end{bmatrix} \quad (2.52)$$

Thus, setting the determinant of the matrix (M_B - λM_A) to zero, gives the following characteristic polynomial:

$$\begin{aligned} &-\frac{\Delta\rho(V_G - \lambda)}{R_L}\left[\rho_G R_L (V_G - \lambda) + \rho_L R_G (V_L - \lambda)\right] \\ &+\frac{\Delta\rho R_G}{R_L}\left[\rho_L V_r (V_L - \lambda) + \Delta\rho g \cos\beta \frac{A_L}{A'_L}\right] = 0 \end{aligned} \quad (2.53)$$

By dividing the previous equation by $\Delta\rho/R_L$, the following characteristic polynomial is obtained:

$$\begin{aligned} &-\lambda^2(\rho_G R_L + \rho_L R_G) + 2\lambda(\rho_G R_L V_G + \rho_L R_G V_L) - C_0 = 0 \\ &\text{with} \quad C_0 = \left(\rho_G R_L V_G^2 + \rho_L R_G V_L^2 - \Delta\rho g \cos\beta \frac{R_G A_L}{A'_L}\right) \end{aligned} \quad (2.54)$$

Let $\chi = \frac{\rho_G R_L}{\rho_L R_G}$, then if Equation (2.54) is divided by $\frac{1}{\rho_L R_G}$, the characteristic polynomial becomes:

$$-\lambda^2(1 + \chi) + 2\lambda(V_L + \chi V_G) - \left(V_L^2 + \chi V_G^2 - \frac{\Delta\rho g \cos\beta A_L}{\rho_L A'_L}\right) = 0 \quad (2.55)$$

Hyperbolicity Condition

For the quadratic (2.55) to have real characteristics, its discriminant Δ^S, which is given below, must always be greater than or equal to zero.

$$\Delta^S = \left(V_L + \chi V_G\right)^2 - \left(1+\chi\right)\left(V_L^2 + \chi V_G^2 - \frac{\Delta\rho g \cos\beta A_L}{\rho_L A'_L}\right)$$

$$\Delta^S = -\chi\left(V_G - V_L\right)^2 + \left(1+\chi\right)\frac{\Delta\rho g \cos\beta A_L}{\rho_L A'_L} \tag{2.56}$$

Thus, satisfying the hyperbolicity condition $\Delta^S \geq 0$ gives a simple relation also known as the **I**nviscid **K**elvin **H**elmholtz (IKH) condition (Section 5.4.3), and defined as:

$$\boxed{\left(V_G - V_L\right)^2 \leq \frac{\Delta\rho\left(\rho_L R_G + \rho_G R_L\right)}{\rho_G \rho_L} g\cos\beta \frac{A}{A'_L}} \tag{2.57}$$

Eigenvalues

Providing that $\Delta^S \geq 0$ or that the hyperbolicity condition (2.57) is satisfied, the two real characteristics of the PFM-2 model are given by:

$$\begin{cases} \lambda_1 = \dfrac{\left(V_L + \chi V_G\right) - \sqrt{\Delta^S}}{1+\chi} \\ \lambda_2 = \dfrac{\left(V_L + \chi V_G\right) + \sqrt{\Delta^S}}{1+\chi} \end{cases} \tag{2.58}$$

where the discriminant Δ^S is given by Equation (2.56) and the density ratio χ is defined by the following equation:

$$\chi = \frac{\rho_G R_L}{\rho_L R_G} \tag{2.59}$$

2.7.3 SPM-4

Consider the primitive vector Ψ with $\Psi^T = \left(R_L, V_G, V_L, \rho_G\right)$, then the SPM-4 system of equations (2.41)-(2.42) can be written as Equation (2.44) using the following matrices:

$$M_A = \begin{bmatrix} -\rho_G & 0 & 0 & R_G \\ 1 & 0 & 0 & 0 \\ 0 & \rho_G R_G & 0 & 0 \\ 0 & 0 & \rho_L R_L & 0 \end{bmatrix}, \tag{2.60a}$$

$$M_B = \begin{bmatrix} -\rho_G V_G & \rho_G R_G & 0 & R_G V_G \\ V_L & 0 & R_L & 0 \\ 0 & \rho_G R_G V_G & 0 & R_G C_G^2 \\ P_c & 0 & \rho_L R_L V_L & R_L C_G^2 \end{bmatrix} \tag{2.60b}$$

where $C_G^2 = \dfrac{\partial P}{\partial \rho_G}$ is the square of the gas speed of sound.

2.7.3.1 Characteristic Polynomial

The eigenvalues λ_k of the single pressure model (SPM-4) are obtained by solving $\det(M_B - \lambda M_A) = 0$, where:

$$M_B - \lambda M_A = \begin{bmatrix} -\rho_G (V_G - \lambda) & \rho_G R_G & 0 & R_G (V_G - \lambda) \\ (V_L - \lambda) & 0 & R_L & 0 \\ 0 & \rho_G R_G (V_G - \lambda) & 0 & R_G C_G^2 \\ P_c & 0 & \rho_L R_L (V_L - \lambda) & R_L C_G^2 \end{bmatrix} \tag{2.61}$$

Hence,

$$\det[M_B - \lambda M_A] = -(V_L - \lambda)\det[M_1] - R_L \det[M_2] \tag{2.62}$$

with

$$M_1 = \begin{bmatrix} \rho_G R_G & 0 & R_G (V_G - \lambda) \\ \rho_G R_G (V_G - \lambda) & 0 & R_G C_G^2 \\ 0 & \rho_L R_L (V_L - \lambda) & R_L C_G^2 \end{bmatrix} \tag{2.63a}$$

and

$$M_2 = \begin{bmatrix} -\rho_G (V_G - \lambda) & \rho_G R_G & R_G (V_G - \lambda) \\ 0 & \rho_G R_G (V_G - \lambda) & R_G C_G^2 \\ P_c & 0 & R_L C_G^2 \end{bmatrix} \tag{2.63b}$$

The determinant of the matrix M_1 can be easily calculated and it is given by:

$$\det[M_1] = -\rho_L \rho_G R_L R_G^2 (V_L - \lambda)\left(C_G^2 - [V_G - \lambda]^2\right) \tag{2.64}$$

The determinant of the matrix M_2 is calculated as follows:

$$\det[M_2] = -\rho_G (V_G - \lambda)\begin{vmatrix} \rho_G R_G (V_G - \lambda) & R_G C_G^2 \\ 0 & R_L C_G^2 \end{vmatrix} + P_c \begin{vmatrix} \rho_G R_G & R_G (V_G - \lambda) \\ \rho_G R_G (V_G - \lambda) & R_G C_G^2 \end{vmatrix}$$

$$\det[M_2] = -\rho_G^2 C_G^2 R_G R_L (V_G - \lambda)^2 + \rho_G R_G^2 P_c \left(C_G^2 - [V_G - \lambda]^2\right) \tag{2.65}$$

Combining Equations (2.62), (2.64) and (2.65), and dividing the obtained expression by $\left(\rho_G \rho_L R_L R_G^2\right)$, gives the following characteristics polynomial:

$$\boxed{(V_L - \lambda)^2 \left(C_G^2 - [V_G - \lambda]^2\right) + (V_G - \lambda)^2 \left(\chi C_G^2 + \frac{P_c}{\rho_L}\right) - C_G^2 \frac{P_c}{\rho_L} = 0} \tag{2.66}$$

where the parameter χ is the density ratio given by Equation (2.59).

In the next section, the hyperbolicity of the SPM-4 model for two different expressions of the pressure correction term P_c will be determined using the small perturbation method. In the first case, P_c is equal to the hydrostatic term defined by Equation (2.43), and in the second case, the pressure correction term is given similarly to Equation (2.16) as a function of the relative or slip velocity between the gas and liquid phases. This latter case will be called the bubbly correction term while the former will be named the stratified correction term.

Before proceeding, define the dimensionless parameters:

$$\tilde{\lambda} = \frac{\lambda - V_G}{C_G}, \qquad \hat{p} = \frac{P_c}{\rho_L C_G^2}, \qquad \theta = \frac{V_r}{C_G} = \frac{V_G - V_L}{C_G} \tag{2.67}$$

Then by dividing equation (2.66) by C_G^4, the characteristic polynomial becomes:

$$\boxed{\left(\tilde{\lambda} + \theta\right)^2 \left(1 - \tilde{\lambda}^2\right) - \tilde{\lambda}^2 [\chi + \hat{p}] + \hat{p} = 0} \tag{2.68}$$

Expanding equation (2.68), gives the following expression:

$$\left(\tilde{\lambda}^2 + 2\theta\tilde{\lambda} + \theta^2\right) - \left(\tilde{\lambda}^4 + 2\theta\tilde{\lambda}^3 + \theta^2\tilde{\lambda}^2\right) - \tilde{\lambda}^2\left(\chi + \hat{p}\right) + \hat{p} = 0$$

$$\boxed{-\tilde{\lambda}^4 - 2\theta\tilde{\lambda}^3 + \tilde{\lambda}^2\left(1 + \chi - \theta^2 + \hat{p}\right) + 2\theta\tilde{\lambda} + \left(\theta^2 - \hat{p}\right) = 0} \qquad (2.69)$$

2.7.3.2 Perturbation Analysis

The eigenvalues of SPM-4 system of equations are the roots of the characteristic polynomial (2.66). These roots can be computed analytically using a very lengthy and tedious process (Ferrari method for example), but here, their first order approximation will be derived using a perturbation method around the small parameter $\theta = V_r / C_G$, similar to the work of Toumi (1996) and Masella (1997).

For the vast majority of flows encountered in pipelines, the relative velocity V_r, which characterises the slip velocity between the two phases, is in general of order of a metre per second, while the speed of sound in the gas is of order of 200 to 300 meters per second depending on the composition of the gas. Consequently the parameter θ remains small and it appears reasonable to develop the eigenvalues according to this parameter.

The perturbation method around a small parameter is explained in detail in many numerical textbooks. Here, we shall recall the 1964 lemma due to Goursat [Masella, 1997], which is required for first order root approximation.

Lemma (Goursat)

Consider a polynomial function $P(x,\theta)$ of a small parameter θ, with real coefficients in x, given by:

$$P(x,\theta) = P_0(x) + \theta P_1(x) + \frac{\theta^2}{2} P_2(x) \qquad (2.70)$$

where $P_0(x)$, $P_1(x)$ and $P_2(x)$ are three polynomials with real coefficients.

We look for the roots of the polynomial $P(x,\theta)$ in the neighbourhood of a root x_0 of the polynomial $P_0(x)$. We distinguish two cases depending on whether x_0 is a single or a double root of $P_0(x)$.

Case a): if x_0 is a single root of the polynomial $P_0(x)$, then there exist a first order approximation function $x(\theta)$, differentiable in θ, such that $P(x(\theta),\theta) = 0$. The function $x(\theta)$ is given by:

$$x(\theta) = x_0 + \theta z_1 + o(\theta) \tag{2.71}$$

where z_1 is defined as:

$$z_1 = -\frac{P_1(x_0)}{P_0'(x_0)} \tag{2.72}$$

and P_0' is the first derivative of the polynomial $P_0(x)$.

Case b): if x_0 is a double root of the polynomial $P_0(x)$, then there exist two first order approximation functions $x(\theta)$ and $y(\theta)$, such that $P(x(\theta),\theta) = P(y(\theta),\theta) = 0$. The functions $x(\theta)$ and $y(\theta)$ are given by:

$$x(\theta) = x_0 + \theta z_1 + o(\theta) \quad \text{and} \quad y(\theta) = x_0 + \theta z_2 + o(\theta) \tag{2.74}$$

where z_1 and z_2 are the roots of the quadratic function:

$$P_0''(x_0)z^2 + 2P_1'(x_0)z + P_2(x_0) = 0 \tag{2.75}$$

and P_0'' is the second derivative of the polynomial $P_0(x)$, while P_1' is the first derivative of the polynomial $P_1(x)$.

Stratified Pressure Correction

For stratified flow, the expression $P_c \frac{\partial R_L}{\partial x}$ in Equation (2.43) is generally replaced by the following hydrostatic expression:

$$P_c \frac{\partial R_L}{\partial x} = \rho_L R_L g\cos(\beta)\frac{\partial h_L}{\partial x} = \rho_L \frac{A_L}{A_L'} g\cos(\beta)\frac{\partial R_L}{\partial x}$$

where h_L is the liquid height, A_L is the liquid cross section area and $A_L' = \frac{dA_L}{dh_L}$.

Hence, we have the hydrostatic term $P_c = \frac{A_L}{A_L'}\rho_L g\cos(\beta)$, and the dimensionless term $\left(\hat{p} = \frac{P_c}{\rho_L C_G^2} = \frac{A_L g\cos\beta}{A_L' C_G^2}\right)$. Then, the characteristic equation (2.69) can be rewritten as:

$$-\tilde{\lambda}^4 + \tilde{\lambda}^2(1 + \chi + \hat{p}) - \hat{p} + 2\theta\tilde{\lambda}(1 - \tilde{\lambda}^2) + \theta^2(1 - \tilde{\lambda}^2) = 0 \tag{2.76}$$

Combining relations (2.70) and (2.76) leads to the following polynomial expressions:

$$\begin{cases} P_0(\tilde{\lambda}) = -\tilde{\lambda}^4 + \tilde{\lambda}^2(1+\chi+\hat{p}) - \hat{p} \\ P_1(\tilde{\lambda}) = 2\tilde{\lambda}(1-\tilde{\lambda}^2) \\ P_2(\tilde{\lambda}) = 2(1-\tilde{\lambda}^2) \end{cases} \tag{2.77}$$

Hence, the zeros of the polynomial $P_0(\tilde{\lambda})$ are given by solving the following relation:

$$-\tilde{\lambda}^4 + \tilde{\lambda}^2(1+\chi+\hat{p}) - \hat{p} = 0 \tag{2.78}$$

Set $y = \tilde{\lambda}^2$, Equation (2.78) becomes a quadratic:

$$y^2 - y(1+\chi+\hat{p}) + \hat{p} = 0 \tag{2.79}$$

The discriminant of equation (2.79) is given by:

$$\begin{aligned} \Delta^S &= (1+\chi+\hat{p})^2 - 4\hat{p} = \left(1+\chi+\hat{p}-2\sqrt{\hat{p}}\right)\left(1+\chi+\hat{p}+2\sqrt{\hat{p}}\right) \\ \Delta^S &= \left(\chi+\left[1-\sqrt{\hat{p}}\right]^2\right)\left(\chi+\left[1+\sqrt{\hat{p}}\right]^2\right) \end{aligned} \tag{2.80}$$

Δ^S is always positive if $\hat{p} \geq 0 \Rightarrow \cos\beta \geq 0$

Hence, the two roots of Equation (2.79) are given by the following expression:

$$\begin{cases} y^+ = \dfrac{(1+\chi+\hat{p}) + \sqrt{\Delta^S}}{2} \\ y^- = \dfrac{(1+\chi+\hat{p}) - \sqrt{\Delta^S}}{2} \end{cases} \tag{2.81}$$

It can be shown that the two roots are positive; for the first one y^+ it is obvious (all terms are positive), and for the second root y^-, we can find a positive minimum limit, viz.

$$y^- \geq y^-_{min} = \frac{(1+\chi+\hat{p}) - \sqrt{\Delta^S_{max}}}{2}$$

and $$\Delta = (1+\chi+\hat{p})^2 - 4\hat{p} < (1+\chi+\hat{p})^2 = \Delta^S_{max}$$

so $$y^- \geq y^-_{min} = 0$$

Hence, the four eigenvalues of Equation (2.78) can be expressed as:

$$\begin{cases} \tilde{\lambda}_1 = -\sqrt{y^+} \\ \tilde{\lambda}_2 = -\sqrt{y^-} \\ \tilde{\lambda}_3 = \sqrt{y^-} \\ \tilde{\lambda}_4 = \sqrt{y^+} \end{cases} \tag{2.82}$$

Because the four eigenvalues in (2.82) are single root, we can only apply the **case a)** of the lemma of Goursat to obtain the first order approximation term z of the eigenvalues.

From Equation (2.77), the derivative of the zero order polynomial $P_0(\tilde{\lambda})$ is given by:

$$P_0'(\tilde{\lambda}) = -2\tilde{\lambda}\left(2\tilde{\lambda}^2 - [1 + \chi + \hat{p}]\right) \tag{2.83}$$

so, the generic expression of z is then given by:

$$z = -\frac{P_1(\tilde{\lambda})}{P_0'(\tilde{\lambda})} = \frac{(1 - \tilde{\lambda}^2)}{2\tilde{\lambda}^2 - (1 + \chi + \hat{p})} \tag{2.84}$$

and for the four reduced eigenvalues $\tilde{\lambda}_{1,2,3,4}$, we have the following expressions:

$$\begin{cases} z_{1,4} = \dfrac{1 - y^+}{2y^+ - (1 + \chi + \hat{p})} \\ z_{2,3} = \dfrac{1 - y^-}{2y^- - (1 + \chi + \hat{p})} \end{cases} \tag{2.85}$$

The reduced eigenvalues expression is then given by:

$$\begin{cases} \tilde{\lambda}_1 = -\sqrt{y^+} + \theta z_{1,4} \\ \tilde{\lambda}_2 = -\sqrt{y^-} + \theta z_{2,3} \\ \tilde{\lambda}_3 = \sqrt{y^-} + \theta z_{2,3} \\ \tilde{\lambda}_4 = \sqrt{y^+} + \theta z_{1,4} \end{cases} \tag{2.86}$$

Hence for the stratified correction term, the four eigenvalues are real, provided that $\cos\beta >= 0$, and their expression is given as:

$$\begin{cases} \lambda_1 = V_G - C_G\sqrt{y^+} + V_r\dfrac{1-y^+}{2y^+ - (1+\chi+\hat{p})} \\ \lambda_2 = V_G - C_G\sqrt{y^-} + V_r\dfrac{1-y^-}{2y^- - (1+\chi+\hat{p})} \\ \lambda_3 = V_G + C_G\sqrt{y^-} + V_r\dfrac{1-y^-}{2y^- - (1+\chi+\hat{p})} \\ \lambda_4 = V_G + C_G\sqrt{y^+} + V_r\dfrac{1-y^+}{2y^+ - (1+\chi+\hat{p})} \end{cases} \tag{2.87}$$

Bubbly Pressure Correction

In this case, the pressure correction term is given by:

$$P_c = \xi\rho_L v_r^2 \qquad \Rightarrow \qquad \hat{p} = \xi\theta^2 \tag{2.88}$$

Equations (2.78) or (2.79) can then be rewritten as:

$$-\tilde{\lambda}^4 + \tilde{\lambda}^2(1+\chi) + 2\theta\tilde{\lambda}(1-\tilde{\lambda}^2) + \theta^2(-\tilde{\lambda}^2 + \xi\tilde{\lambda} + 1 - \xi) = 0 \tag{2.89}$$

Combining relations (2.70) and (2.89) leads to the following polynomial expressions:

$$\begin{cases} P_0(\tilde{\lambda}) = -\tilde{\lambda}^2(\tilde{\lambda}^2 - (1+\chi)) \\ P_1(\tilde{\lambda}) = 2\tilde{\lambda}(1-\tilde{\lambda}^2) \\ P_2(\tilde{\lambda}) = 2(-\tilde{\lambda}^2 + \xi\tilde{\lambda} + 1 - \xi) \end{cases} \tag{2.90}$$

The zero order approximation of the reduced eigenvalues is given by $P_0(\tilde{\lambda}) = 0$, which leads to:

$$\begin{cases} \tilde{\lambda}_1 = -\sqrt{1+\chi} \\ \tilde{\lambda}_{2,3} = 0 \\ \tilde{\lambda}_4 = \sqrt{1+\chi} \end{cases} \tag{2.91}$$

- The eigenvalues $\tilde{\lambda}_1$ and $\tilde{\lambda}_4$ are single roots, so we can apply **case a)** of the lemma of Goursat to find the first order approximation of those roots.

$$P_0'(\tilde{\lambda}) = -2\tilde{\lambda}\left(2\tilde{\lambda}^2 - [1+\chi]\right) \tag{2.92}$$

Hence,
$$z_{1,4} = -\frac{P_1(\tilde{\lambda}_{1,4})}{P_0'(\tilde{\lambda}_{1,4})} = \frac{1-\tilde{\lambda}_{1,4}^2}{2\tilde{\lambda}_{1,4}^2 - (1+\chi)} = \frac{-\chi}{1+\chi} \tag{2.93}$$

and, the single root eigenvalues are given by:

$$\tilde{\lambda}_{1,4} = \mp\sqrt{1+\chi} + \theta z_{1,4} \tag{2.94}$$

- The eigenvalue $\tilde{\lambda}_{2,3}$ is a double root, so we apply **case b)** of the lemma of Goursat to find the first order approximations z_2 and z_3 of the double root. According to the lemma, $z_{2,3}$ are the solutions of the following quadratic expression:

$$P_0''(\tilde{\lambda}_{2,3})z^2 + 2P_1'(\tilde{\lambda}_{2,3})z + P_2(\tilde{\lambda}_{2,3}) = 0 \tag{2.95}$$

From the system of equations (2.90), the following expressions are derived:

$$\begin{cases} P_0''(\tilde{\lambda}) = -12\tilde{\lambda}^2 + 2(1+\chi) \\ P_1'(\tilde{\lambda}) = -6\tilde{\lambda}^2 + 2 \end{cases} \tag{2.96}$$

Then Equation (2.95), combined with Equations (2.90) and (2.96), gives the following quadratic:

$$z^2(1+\chi) + 2z + (1-\xi) = 0 \tag{2.97}$$

The discriminant of Equation (2.97) is given by:

$$\Delta^D = 1 - (1-\xi)(1+\chi) \tag{2.98}$$

which leads to:

$$z_{2,3} = \frac{-1 \mp \sqrt{\Delta^D}}{1+\chi} \qquad \text{if } \Delta^D > 0 \tag{2.99}$$

The expression of the reduced eigenvalues is then given by:

$$\begin{cases} \tilde{\lambda}_1 = -\sqrt{1+\chi} + \theta z_{1,4} \\ \tilde{\lambda}_2 = \theta z_2 \\ \tilde{\lambda}_3 = \theta z_3 \\ \tilde{\lambda}_4 = \sqrt{1+\chi} + \theta z_{1,4} \end{cases} \tag{2.100}$$

Hence, for the bubbly correction term, the four eigenvalues are real, provided that $\Delta^D >= 0$, and their expression is given as:

$$\begin{cases} \lambda_1 = V_G - C_G\sqrt{1+\chi} - V_r\dfrac{\chi}{1+\chi} \\ \lambda_2 = V_G - V_r\dfrac{\left(1+\sqrt{\Delta^D}\right)}{1+\chi} \\ \lambda_3 = V_G - V_r\dfrac{\left(1-\sqrt{\Delta^D}\right)}{1+\chi} \\ \lambda_4 = V_G + C_G\sqrt{1+\chi} - V_r\dfrac{\chi}{1+\chi} \end{cases} \tag{2.101}$$

Hyperbolicity Condition

The condition of hyperbolicity for the bubbly correction term is given by $\Delta^D \geq 0$ and implies that:

$$\begin{aligned} &\Rightarrow \quad 1-(1-\xi)(1+\chi) \geq 0 \\ &\Rightarrow \quad (1-\xi) \leq \frac{1}{1+\chi} \\ &\boxed{\Rightarrow \quad \xi > \xi_0 = \frac{\chi}{1+\chi} = \frac{\rho_G R_L}{\rho_G R_L + \rho_L R_G}} \end{aligned} \tag{2.102}$$

For the special case where there is no pressure correction term $(\xi = 0)$, but the slip or relative velocity between the two phases is not null, Equation (2.98) gives $\Delta^D = -\chi$, which means the roots $\lambda_{2,3}$ are always complex, and the single pressure model SPM-4 is never hyperbolic. This result obtained by the perturbation method, confirms a finding that can be easily demonstrated when the two phases are assumed incompressible, like in the PFM-2 model.

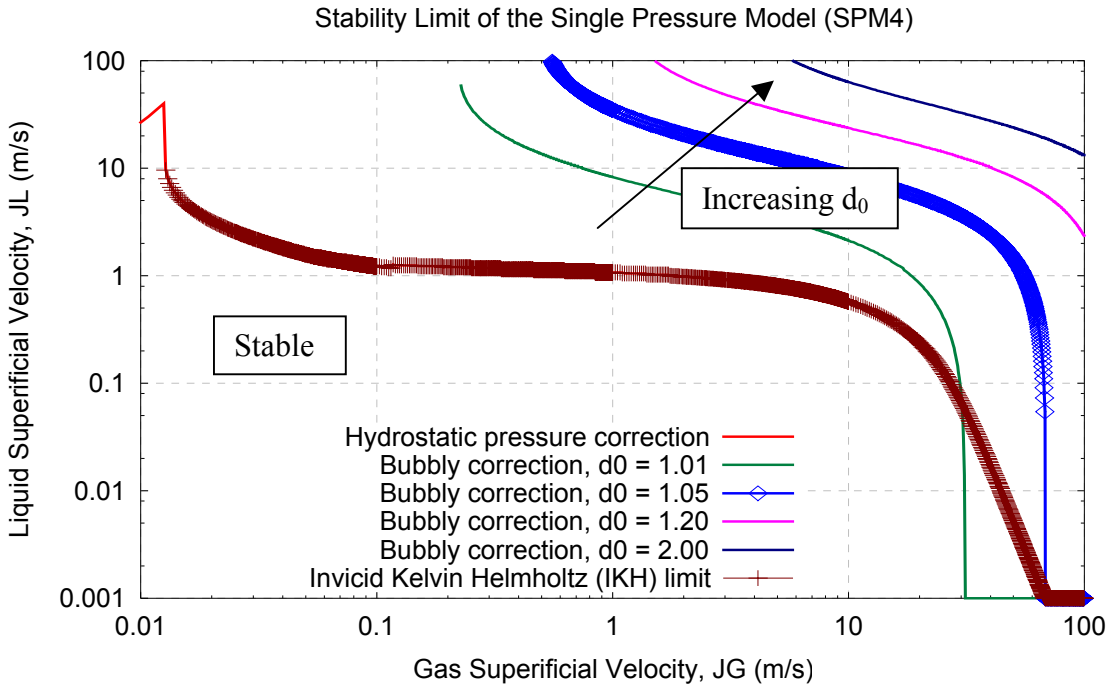

Figure 2-2: Hyperbolicity Limit of the Single Pressure Model (SPM-4)

However, selecting for example $\xi = d_0\xi_0$ in Equation (2.88), with the bubble correction factor $d_0 > 1.0$, results in the four approximate eigenvalues always being real, and consequently the SPM-4 system of equations being hyperbolic.

Figure 2-2 presents, in gas-liquid superficial velocity axes, the stability limit of the single pressure model for the hydrostatic pressure correction and various coefficients of the bubble correction factor d_0. The stability limit using the hydrostatic pressure correction term is the same as the IKH limit (2.57) obtained from an incompressible model. And although, we can improve the stability limit by increasing the bubble correction factor, there is no guarantee that the resulting model accurately describes the physical flow features and main characteristics that we seek to simulate.

2.8 Conclusion

After reviewing the modelling approaches existing in the literature, we have presented in this chapter three specific models that we have implemented for the applications described later in this thesis. These three models are the HEM-3 (Homogeneous Equilibrium Model), and two two-fluid models, one incompressible: the PFM-2 (Pressure-Free Model), and the other one compressible: the SPM-4 (Single Pressure Model).

For numerical purposes and a better understanding of the main characteristics of these models, we have performed their stability analysis, more specifically, we have analysed their hyperbolicity condition. Hence, we have shown that the homogeneous equilibrium model is always hyperbolic, and that the two-fluid incompressible model is hyperbolic for flow conditions below the inviscid Kelvin Helmholtz (IKH) condition (2.57). We have also shown that the four approximate eigenvalues of SPM-4 model are always real. However, it should be noted that these approximate eigenvalues are only valid for the small parameter $\theta \leq 5\%$, or more specifically, the relative flow velocity V_r should be less than 15 m/s if gas speed of sound is 300 m/s.

Furthermore, the reader should be warned against a confusion sometimes found in the literature, which suggests that the single pressure model SPM-4 is always hyperbolic. Though the approximate eigenvalues are always real, the true eigenvalues can be complex, and a numerical evaluation of these reveals that the condition of hyperbolicity or limit of validity of the SPM-4 model is similar to the two-fluid incompressible model PFM-2 i.e. critical flow above the same IKH condition (2.57).

2.9 References - 2

- **AEA Technology (1996).** "PLAC User Guide and Technical Manual", PC version 5.3, (January 1996)

- **Arai M., (1980)** "Characteristics and stability analyses for two-phase flow equation systems with viscous terms". *Nuclear Science and Engineering,* **74**, 77-83.

- **Barnea D., & Taitel Y., (1993)** "Kelvin-Helmhotz stability criteria for stratified flow: viscous versus non-viscous (inviscid) approaches". *Int. J. Multiphase Flow,* **19 (4)**, 639-649.

- **Barnea D., & Taitel Y., (1996)** "Stratified three-phase flow in pipes – Stability and transition". *Chemical Engineering Communication,* **Vols. 141-142**, 443-460.

- **Bestion D., (1990)** "The Physical Closure Laws in the CATHARE Code". *Nuclear Engineering Design*, **124**, 229-245.

- **Bendiksen K., Malnes D., Moe R., and Nuland S. (1991)** "The Dynamic Two-Fluid Model OLGA: Theory and Application". *SPE Production Engineering*, **6**, 171-180.

- **Bendiksen K., Brandt I., Fuchs P., Linga H., Malnes D., and Moe R., (1986)** "Two-Phase Flow Research at SINTEF and IFE: Some Experimental Results and a Demonstration of the Dynamic Two-Phase Flow Simulator", presented at the 1986 Offshore Northern Seas Conference, Stavanger, (1986).

- **Benzoni-Gavage S, (1991)** "Analyse numerique des modèles hydrodynamiques d'écoulements diphasiques instationaires dans les reseaux de production petrolières. Thèse de doctorat de l'Université Claude Bernard, Lyon I, 10 Decembre 1991.

- **Black P. S., Daniels L. C., Hoyle N. C., and Jepson W. P., (1990)** "Studying Transient Multiphase Flow using The Pipeline Analysis Code (PLAC)". *Journal of Energy Resources Technology*, **112**, 25-29, (March 1990).

- **Bonizzi M., Issa R. I., and Kempf M. H. W., (2001)** "Modelling of gas entrainment in horizontal slug flow". *Proceedings of the ICMF 2001 Conference*, **Paper 402**, May 27 – June 1, New Orleans, USA.

- **Boure J. A., (1997)** "Wave Phenomena and One-dimensional Two-Phase Models, Part III: General Case; Generalized Drift Flux Models; Other Two-Fluid Models". *Multiphase Science and Technology*, **9**, 63-107.

- **Chan A. M. C., & Banerjee S., (1981)** "Refilling and Rewetting of a Hot Horizontal Tube. Part II: Structure of a Two-Fluid Model". *Journal of Heat Transfer*, **103**, 287-292.

- **Cheng M-S., Chang K-S., and Lee S-J., (2002)** "Numerical solution of hyperbolic two-fluid two-phase flow model with non-reflecting boundary conditions". *International Journal of Engineering Science*, **40**, 789-803.

- **Chung L. Y., Drew D. A., and Lahey Jr. R. T., (1985)** "An Analysis of Wave Propagation in Bubbly Two Component Two-Phase Flow". *Journal of Heat Transfer*, **107**, 402-408.

- **Clift R., Grace J. R., and Weber M. E., (1978)** "Bubbles, Drops, and Particles". *Academic Press*.

- **Coquel F., Amine K. E., Godlewski E., Perthame B., and Rascle P., (1997)** "A numerical method using upwind schemes for the resolution of two-phase flows", *Journal of Computational Physics*, **136**, 272-288.

- **Corradini M. L., (1997)** "Fundamentals of Multiphase Flow". Department of Engineering Physics, University of Wiscosin. **N.B.** The Internet link for this book is no longer valid, but do check http://silver.neep.wisc.edu/~WINS/publications.html.

- **Daniels L. C., Guardino C., and Thompson C. P., (2003)** "An Implicit Two-Phase Compressible Flow Solver For Pipelines". *Multiphase Science and Technology*, **21 (3)**, 335-349.

- **De Henau V., & Raithby G. D., (1995)** "A Transient Two-Fluid Model for the Simulation of Slug Flow in Pipelines – I. Theory". *Int. J. Multiphase Flow*, **21 (3)**, 335-349.

- **Drew D. A., (1983)** "Mathematical modeling of two-phase flows". *Annual Review of Fluid Mechanics*, 1**5**, 261-291.

- **Drew D., Cheng L., and Lahey Jr. R. T., (1979)** "The analysis of virtual mass effects in two-phase flow". *Int. J. Multiphase Flow*, **5**, 233-242.

- **Drew D. A., & Passman S. L., (1999)** "Theory of Multicomponent Fluids". *Applied Mathematical Sciences*, **135**, Springer.

- **Ellul I. R., Delacroix M. P., King P. E., and W. A. Finlay W. A., (1991)** "The Use of Dynamic Simulation in Offshore Multiphase Pipeline Design". *5th L.F.P. and T.U. Multiphase Production International Conference,* Cannes, France (June, 1991).

- **Faille I., & Heintze E., (1999)** "A rough finite volume scheme for modelling two-phase flows in a pipeline". *Computers & Fluids,* **28**, 213-241.

- **Fabre J., Line A., and Peresson L., (1989)** "Two-Fluid/Two-Flow-Pattern Model for Transient Gas-Liquid Flow in Pipes". *4th BHRA Multiphase Flow International Conference*, Nice, France, (June 1989).

- **Fjelde K. K., & Karlsen K. H., (1999)** "High resolution hybrid primitive-conservative upwind schemes for the drift-flux model". *RF Rogaland Research report*, Preprint 1999-023, Bergen, Norway.

- **Garcia J. R., Corberan J. M., and Gascon L. L., (2000)** "A Conservative Scheme for 1D Homogeneous Two-Phase Flow". *AMIF-ESF Workshop – Computing Methods for Two-Phase Flow*, **Paper 25**, Aussois, France, January 12-14.

- **Glimm J., Saltz D., and Sharp D. H., (1999)** "Two-phase modelling of a fluid mixing layer". *Journal of Fluid Mechanics,* **378**, 119-143.

- **Ishii M., (1975)** "Thermo-Fluid Dynamic Theory of Two-Phase Flow". *Eyrolles*, Paris.

- **Ishii M., (1977)** "One-Dimensional Drift-Flux Model and Constitutive Equations for Relative Motion Between Phases in Various Two-Phase Flow Regimes". *Argonne National Lab Report, ANL 77-47* , October 1977.

- **Ishii M., & Zuber N., (1979)** "Relative Motion and Interfacial Drag Coefficient in Dispersed Two-Phase Flow of Bubbles, Drops and Particles". *AIChE Journal*, **25**, 843-855.

- **Ishii M., & Mishima K., (1984)** "Two-Fluid Model and Hydrodynamic Constitutive Relations". *Nuclear Engineering and Design*, **82**, 107-126.

- **Johansen S. T., Anderson N. M., and De Silva S. R., (1990)** "A two-phase model for particle local equilibrium applied to air classification of powers". *Power Technology*, **63**, 121-132.

- **Joseph D. D., & Lundgren T. S., (1990)** "Ensemble Averaged and Mixture Theory Equations". *Int. J. Multiphase Flow,* **16**, 35-42.

- **Klemp S., (1987)** "Practical Design Experiences with the OLGA Code". *Multiphase Technology and Consequences for Field Development Forum*, Stavanger, Norway (October 1987).

- **Lahey Jr. R. T., & Drew D. A., (1988)** "Three Dimensional Time and Volume Averaged Conservation Equations of Two-Phase Flow". *Advances in Nuclear Science Technology,* **20**, 1-69.

- **Larsen M., Hustvedt E., Hedne P., and Straume T., (1997)** "Petra: A Novel Computer Code for Simulation of Slug Flow". *SPE 38841*, 1-12.

- **LASL [Los Alamos Scientific Laboratory], (1984)** "TRAC-PF1: An Advanced Best-Estimated Computer Program for Pressurized Water Reactor Analysis", *Report LA-9944-MS, NUREG/CR-3567*, (February 1984).

- **Lyczkowski R. W., Gidaspow D., Solbrig C. W., and Hughes E. D., (1978)** "Characteristics and Stability Analyses of Transient One-Dimensional Two-Phase Flow Equations and Their Finite Difference Approximations". *Nuclear Science and Engineering,* **66**, 378-396.

- **Mahaffy J. H., (1982)** "A stability-Enhancing Two-Step Method for Fluid flow Calculations". *Journal of Computational Physics*, **46**, 329-341.

- **Manninen M., & Taivassalo V., (1996)** "On the mixture model for multiphase flow". *VTT Publications 288*, 1-67.

- **Masella J. M., (1997)** "Quelques Méthodes Numeriques Pour Les Ecoulements Diphasiques Bi-Fluide En Conduites Pétrolières". *PhD Thesis*, Université de Pierre et Marie Curie, Paris 6.

- **Masella J. M., Tran Q. H, Ferre D., and Pauchon C., (1998)** "Transient simulation of two-phase flows in pipes". *Int. J. Multiphase Flow,* **24**, 739-755.

- **Mathers W. G., Ferch R. L., Hancox W. T., and McDonald B. H., (1978)** "Equations For Transient Flow-Boiling In A Duct". *2nd CSNI Specialist Meeting on Transient Two-Phase Flow,* June 11-13, Paris, France, 59-82.

- **Mori Y., Hijikata K., and Ohmori T., (1976)** "Propagation of a pressure wave in two-phase flow with very high void fraction". *Int. J. Multiphase Flow*, **2**, 453-464.

- **Nigmatulin R. I., (1979)** "Spatial Averaging in the Mechanics of Heterogeneous and Dispersed Systems". *Int. J. Multiphase Flow*, **5**, 353-385.

- **Park J. W., Drew D. A., and Lahey Jr. R. T., (1998)** "The analysis of void propagation in adiabatic monodispersed bubbly two-phase flows using an ensemble-averaged two-fluid model ". *Int. J. Multiphase Flow*, **24**, 1205-1244.

- **Pauchon C., Dhulesia H., Lopez D., and Fabre J. (1993)** "TACITE: A Comprehensive Mechanistic Model for Two-Phase Flow", presented at the 6th International Conference on Multiphase Production, Cannes, France, (June 1993).

- **Pauchon C., Dhulesia H., Binh Cirlot G., and Fabre J., (1994)** "TACITE: A Transient Tool for Multiphase Pipeline and Well Simulation", *SPE 28545* presented at the SPE Annual Technical Conference, New Orleans, LA, USA (September 1994).

- **Pericleous K. A., & Drake S. N., (1986),** "An Algebraic Slip Model of PHOENICS for Multiphase Applications". Numerical Simulation of Fluid Flow and Heat/Mass Transfer Processes. (Eds. Markatos N. C., Tatchell D. G., Cross M., & Rhodes N.) *Lecture Notes in Engineering 18,* Berlin, Springer-Verlag.

- **Philbin M., & Butcher G., (1992),** "Multi-phase flow in oil and gas pipelines: simulation of transient phenomena", *Pipes & Pipelines International,* p 20, (November-December 1992).

- **Pokharna H., Mori M., and Ransom V. H., (1997)** "Regularization of two-phase flow models: A comparison of numerical and differential approaches". *Journal of Computational Physics*, **134**, 282-295.

- **Prosperetti A., & Satrape J., (1990)** "Stability of two-phase flow models". Two-Phase Flows and Waves, *Springer-Verlag*, **IMA 26**, 98-117.

- **Ramos J. I., (1995)** "One-dimensional, time dependent, homogeneous two-phase flow in volcanic conduits". *International Journal for Numerical Methods in Fluids,* **21**, 253-278.

- **Ramshaw J. D., & Trapp J. A., (1978)** "Characteristics, Stability and Short-Wavelength Phenomena in Two-Phase Flow Equation Systems". *Nuclear Science and Engineering,* **66**, 93-102.

- **Ransom V. H., & Hicks D. L., (1984)** "Hyperbolic Two-Pressure Models for Two-Phase Flow". *Journal of Computational Physics*, **53**, 124-151.

- **Romate J. E., (1998)** "An approximate Riemann solver for a two-phase flow model with numerically given slip relation". *Computers & Fluids,* **27**, 455-477.

- **Romate J. E., (2000)** "Developing a second-order TVD scheme for one-dimensional two-phase flow model", *AMIF-ESF Workshop – Computing Methods for Two-Phase Flow*, **Paper 22**, Aussois, France, January 12-14.

- **Rygg O. B., & Ellul I. R., (1991)** "The Dynamic Two-Phase Flow Modeling Live Crude Lines Under Rupture Conditions". *23rd Annual Offshore Technology Conference*, Houston, Texas, (May, 1991).

- **Saurel R., & Abgrall R., (1999)** "A Multiphase Godunov Method for Compressible Multifluid and Multiphase Flows". *Journal of Computational Physics,* **150**, 425-467.

- **Sharma Y., Scoggins Jr. M. W., Shoham O., and Brill J. P., (1985)** "Simulation of transient two-phase flow in pipelines", *2nd International Conference on Multi-Phase Flow*, London, 19-21 June, England, **Paper C4**, 141-152.

- **Shieh A. S., Ransom V. H., and Krishnamurthy R., (1994)** "RELAPS5/MOD3 Code Manual. Volume 6: Validation of Numerical Techniques in RELAPS5/MOD3". Idaho National Engineering Laboratory, *Report NUREG/CR-5535, EGG-2596*.

- **Soo S. L., (1990)** "Multiphase Fluid Dynamics". *Science Press and Gower Technical*.

- **Stewart H. B., (1979)** "Stability of two-phase flow calculations using two-fluid model". *Journal of Computational Physics*, **3**, 259-270.

- **Stewart H. B., & Wendroff B., (1984)** "Two-Phase Flow: Models and Methods". *Journal of Computational Physics*, **56**, 363-409.

- **Taitel Y., & Duckler A. E., (1976)** "A Model For Predicting Flow Regime Transitions in Horizontal and Near-Horizontal Gas-Liquid Flow". *AIChE Journal*, **22/1**, 47-55.

- **Theron B., (1989)** "Ecoulements instationnaires intermittents de gas et de liquide en conduite horizontale". These Institut National Polytechnique, Toulouse.

- **Tiselj I., & Petelin S., (1997)** "Modelling of Two-Phase Flow with Second-Order Accurate Scheme". *Journal of Computational Physics*, **136**, 503-521.

- **Tomiyama A., Kataoka I., Zun I., and Sakaguchi T., (1998)** "Drag coefficients of single bubbles under normal and microgravity conditions". *JSME Int. J., Series B: Fluids Thermal Eng.*, **41 (2)**, 472-479.

- **Toumi I., (1996)** "An Upwind Numerical Method for Two-Fluid Two-Phase Flow Models". *Nuclear Science Engineering*, **123**, 147-168.

- **Toumi I., & Kumbaro A., (1996)** "An Approximate Linearised Riemann Solver for a Two-Fluid Model". *Journal of Computational Physics*, **124**, 286-300.

- **Truesdell C., & Rajagopal K. R., (2000)** "An Introduction to the Mechanics of Fluids". *Birkhauser Verlag AG*.

- **Watanabe T., Hirano M., Tanabe F., and Kamo H., (1990)** "The effect of virtual mass force term on the numerical stability and efficiency of systems calculations". *Nuclear Engineering and Design*, **120**, 181-192.

- **Watson M., (1990)** "Non Linear Waves in Pipeline Two-Phase Flows". Proceedings of the 3rd International Conference on Hyperbolic Problems, Uppsala, Sweden, (June 1990), Studentliterratur, Lund.

- **Yadigaroglou G., & Lahey R. T. Jr, (1976)** "On the various forms of the conservation equations in two-phase flow". *Int. J. Multiphase Flow*, **2**, 477-494.

- **Zuber N., (1964)** "On the Dispersed Two-Phase Flow in Laminar Flow Regime". *Chemical Engineering Science*, **19**, 897-917.

- **Zuber N., & Findlay J. A., (1965)** "Average Volumetric Concentration in Two-Phase Flow Systems". *Trans. ASME J. Heat Transfer*, **87**, 453-68, (November 1965).

3 Chapter 3 - Numerical Methods

3.1 Introduction

The governing equations described in the previous chapter cannot be solved analytically except for very simple cases, and for physical problems of interest, there is no alternative to computational methods for resolving these equations. Therefore, this chapter deals with the approach and resolution techniques that were used to handle these systems of equations.

The chapter starts with a brief description of various numerical approaches for solving two-phase flow models, as well as an explanation of the one that was adopted in this thesis. Following is the general formulation of the governing equations describing these models and their numerical discretisations. Then a presentation of the numerical schemes for conservative terms is given, followed by the methods adopted for non-conservative terms existing in the equations. The next section describes constraints imposed on the numerical schemes, notably the time step restriction and the boundary conditions.

The last two sections deal with validation test cases for the numerical schemes implemented. Firstly, we present the results of these schemes for two well-known model equations (Burgers and Shallow Water). The cases from these two single-phase models are used as a test-bed for the convergence and accuracy of our numerical methods; they provide confidence in the numerical schemes, as analytical solutions for the selected cases are known. Secondly and finally, we describe various test cases that were used to validate the three specific two-phase flow models presented in the previous chapter.

A small summary, reporting the findings from the numerical schemes and cases tested, will conclude the chapter, as well as the recommendation choice for the methods adopted.

3.2 Numerical Approach

Over the past two decades, important advances have taken place in computational fluid dynamics (CFD) with the aim of increasing numerical accuracy through the development of high-resolution schemes [Harten, 1983; Yee, 1989], improving efficiency through devising better solvers and solution algorithms [Patankar, 1981], and increasing the use of multigrid and mesh refinement techniques.

While all these advances have led to accurate, robust and efficient numerical solvers for the simulation of single phase flows, the developments in multi-fluid solution algorithms have lagged behind compared to single-fluid algorithms, partly because of the higher computational cost involved, and partly due to the numerical difficulties (non-hyperbolic and non-conservative model issues) associated with the simulation of multiphase flows.

Despite these difficulties, successful numerical methods have been designed for the computation of two-fluid models. These algorithms can be divided into two groups based on the treatment of the pressure term. The first group includes segregated pressure-based solution algorithms and among them one finds the inter-phase slip algorithm (IPSA) and its variants devised by Spalding (1980, 1983), the implicit multi-field algorithms (IMF) proposed by Harlow & Amsdem (1975), Stewart (1979), and Mahaffy (1982), or the implicit method embodied in the TRIOMPH code at Imperial College [Issa & Kempf, 2003].

[Darwish & Moukalled, 2001] have recently reviewed this group of methods, which generally use a finite volume approach on staggered grids. Unfortunately, in contrast with the widespread information available on the solution algorithms of their single-fluid counterparts, much less information is available on multifluid solution procedures, a fact that has confined their implementation to a small community, slowed their development, and isolated them from the newer developments in single-fluid flow algorithms (all speed flows, etc.).

Furthermore, their lack of generality has led many researchers to develop a second group of algorithms, which includes approximate Riemann solvers, upwind methods, flux splitting methods and other high resolution shock-capturing methods [Stadke et al., 1994; Toumi, 1996; Tiselj & Petelin, 1997; Faille & Heinze, 1999; Romate 2000] for two-phase models. All these methods are generally adaptation of single-phase versions, and reviewing these single-fluid schemes is beyond the scope of this thesis.

There is no clear indication in the literature for the selection of an appropriate numerical scheme for two-phase flow applications. Therefore, the approach adopted here is based on this second group of methods because they are much simpler to implement, and their widespread description makes them easy to generalize, which is an important development aspect when designing a solution algorithm for many mathematical models.

However, our purpose is not to create or devise new numerical schemes. Hence, following the approach of Saurel & Abgrall (1999) for their two-fluid algorithm, we will use or combine of existing single-fluid schemes so that they can handle the three specific models (HEM-3, PFM-2 and SPM-4) described in the previous chapter.

It should be noted that various mathematical concepts, such as convergence, consistency and stability, which are useful in determining the success of numerical algorithms, are not investigated in this chapter but can be found in many numerical textbooks [Hirsch, 1990;

Laney, 1998]. Hence, the following sections only describe the numerical schemes that were implemented in the EMAPS framework.

3.3 Formulation & Discretisation of Equations

3.3.1 General Formulation

The governing equations of the three specific models presented in the previous chapter fall in two different categories of numerical formulation and therefore, require different numerical schemes or resolution techniques. The homogeneous model HEM-3 and the incompressible model PFM-2 model are known as **conservative** systems defined by:

$$\frac{\partial Q}{\partial t} + \frac{\partial F}{\partial x} = S \tag{3.1}$$

where **Q** is a vector field of conservative variables, typically mass and momentum. The vectors **F** and **S** are algebraic functions of Q only, and respectively express the fluxes and source terms appearing in the appropriate model.

On the other hand the single pressure model SPM-4 is a **non-conservative** system and can be expressed as:

$$\frac{\partial Q}{\partial t} + \frac{\partial F}{\partial x} = H\frac{\partial Q}{\partial x} + S \tag{3.2}$$

where the first term $H\partial Q/\partial x$ in the right hand side of Equation (3.2) is a matrix-vector product that contains all the non-conservative terms present in the model. The remaining vectors Q, F and S have similar meanings to those of the conservative formulation (3.1). For completeness, the vector and matrix forms, of the three specific models mentioned in this section, are explicitly given in Appendix C.

3.3.2 Discretisation of Equations

The approach adopted here is the finite difference method, widely used in computational fluid dynamics (CFD) and described in many numerical textbooks [Fletcher, 1988; Hirsch, 1990; LeVeque, 1990; Toro, 1997; and Laney 1998]. The essence of this method is to replace partial derivatives in the governing flow equations with algebraic difference quotients, resulting in a system of discrete difference equations for the dependent variables at each grid or mesh cell. For the conservative system (3.1), the finite difference discretisation leads to the following expression:

$$Q_j^{n+1} = Q_j^n - \tau\left(\hat{F}_{j+1/2} - \hat{F}_{j-1/2}\right) + \Delta t S_j \tag{3.3}$$

where Δt is the time step, $\tau = \dfrac{\Delta t}{\Delta x}$ (with Δx the mesh size), and $\hat{F}$ is the numerical flux, which expression defines the numerical conservative scheme. The subscript **j** represents the mesh cell index, while the superscripts **n** and **n+1** are time indexes, representing respectively the old and new or updated time values.

For the non-conservative formulation (3.2), the finite difference discretisation can be expressed as:

$$Q_j^{n+1} = Q_j^n - \tau\underbrace{\left(\hat{F}_{j+1/2} - \hat{F}_{j-1/2}\right)}_{\text{NFT}} + \Delta t\underbrace{\left(H\frac{\partial Q}{\partial x}\right)_j}_{\text{NCT}} + \Delta t S_j \qquad (3.4)$$

The numerical flux term (NFT), the non-conservative term (NCT) and the source term S_j in expressions (3.3) or (3.4) can be evaluated at the old or new time increment (n or n+1) leading to either an explicit or an implicit numerical method. As for choosing between these two types of approaches, we opt for explicit schemes because they are relatively easy to set up and program. Advantages and disadvantages of these two approaches can be found in the book by Wendt (1996) or in the paper by Yee (1989).

It should be noted that the conservative formulation (3.1) and its discretisation (3.3) are fully embodied in their respective non-conservative expressions (3.2) and (3.4), in which cases the matrix coefficient H is set to zero. Therefore, the non-conservative formulation and discretisation, which are more generic than their conservative counterparts, were used to construct the single solution algorithm that has been implemented in the EMAPS framework.

Hence, to advance explicitly the vector solution Q in time for any of the mathematical models studied, we use the following expression:

$$Q_j^{n+1} = Q_j^n + \Delta Q_j \qquad (3.5)$$

where the increment vector ΔQ at a mesh point labelled **j** is derived from the non-conservative expression (3.4) and is given by:

$$\Delta Q_j = -\tau\left(\hat{F}_{j+1/2} - \hat{F}_{j-1/2}\right)^n + \Delta t\left(H\frac{\partial Q}{\partial x}\right)_j^n + \Delta t S_j^n \qquad (3.6)$$

The superscript **n** in Equation (3.6) means that the increment vector is obtained using old time step solution vectors Q^n, for example the numerical source term value at mesh cell j is defined by $S_j^n = S\left(Q_j^n\right)$.

The numerical expressions for the flux term $\hat{F}$, referred to here as conservative flux methods, are given in the next section, while the numerical expressions for $\left(H\partial Q/\partial x\right)_j^n$, known as non-conservative terms methods will be defined in Section 3.5.

3.4 Methods for the Conservative Flux

The numerical flux schemes that we have implemented can be classified, in terms of accuracy, as first order, second order and high-resolution methods (second order in the smooth regions of the solution and first order where there are discontinuities or shocks in the solution).

They are grouped into two categories, namely central and upwind methods. Originally, we focused on central schemes, because we needed a general-purpose solver for hyperbolic conservative systems describing multiphase flow phenomena. These schemes were selected so that they do not require any algebraic manipulation of the Jacobian of the flux vector, or any knowledge of the characteristics of the model simulated.

Although the central flux schemes can be easily used to solve any conservative one-dimensional model, they were sometimes found not to be accurate and robust for some flow situations. Therefore, a second group of numerical flux methods based on the knowledge of the model characteristics were implemented to deal with these problems.

Hence, the first part of this section describes the four central schemes investigated, while the second part presents the two characteristics based schemes that were implemented.

3.4.1 Central Schemes

3.4.1.1 Lax-Friedrichs

This scheme is the simplest and most common explicit method found in numerical textbooks [Hirsch, 1990; Toro, 1997]. It belongs to the Lax family of central schemes, and it is first order in space and time. Its intercell flux expression is given as:

$$\hat{F}_{j+1/2}^{LF} = \frac{1}{2}\left(F_{j+1}^n + F_j^n\right) - \frac{1}{2\tau}\left(Q_{j+1}^n - Q_j^n\right) \qquad (3.7)$$

where the numerical flux value at mesh point j is defined by $F_j^n = F\left(Q_j^n\right)$ with the function F representing the physical expression of the flux terms described by the mathematical model under investigation.

3.4.1.2 Ritchmyer (Lax-Wendroff Two-Step)

Most numerical schemes are based directly on finite difference approximations to the Partial Differential Equations (PDEs). An exception is the Lax-Wendroff central scheme, which is based on the Taylor series approximations. The book by Hirsch (1990) describes the one-step version of the scheme and it is not repeated here. It is second-order accurate in time and space, but requires an evaluation of the flux vector Jacobian when using it. On the other hand, the two-step scheme that follows removes the need to compute the Jacobian of the flux vector resulting in a gain in computational time and simpler programming.

Two different versions of the two-step scheme exist in the literature, the McCormack version, which is popular in the Aeronautics community, and the Richtmyer version, which is described here. These two versions lead to almost identical solutions, but in our view the Richtmyer version is the most effective and simpler one to implement. It is characterised by an intermediate first step applying the Lax-Friedrichs scheme to midpoints, and a second step that is the application of a leapfrog scheme (for a description of the leapfrog scheme, see for instance the book by Hirsch (1990). In the conservative formulation, this second order flux scheme is defined by:

$$\hat{F}^{RI}_{j+1/2} = F\left(\overline{Q}_{j+1/2}\right) \tag{3.8a}$$

where the intermediate vector solution $\overline{Q}_{j+1/2}$ is given as:

$$\overline{Q}_{j+1/2} = Q^{n}_{j+1/2} - \frac{\tau}{2}\left[F\left(Q^{n}_{j+1}\right) - F\left(Q^{n}_{j}\right)\right] + \frac{\Delta t}{2} S\left(Q^{n}_{j+1/2}\right) \tag{3.8b}$$

The average vector $Q^{n}_{j+1/2}$ is expressed as follows:

$$Q^{n}_{j+1/2} = \frac{1}{2}\left(Q^{n}_{j+1} + Q^{n}_{j}\right) \tag{3.8c}$$

Note that the implementation of the Richtmyer scheme is actually done in the reverse order (from relation (3.8c) to (3.8a)) to the one presented above.

3.4.1.3 Force

The Lax-Friedrichs and Richtmyer schemes presented above are almost never used for practical fluid flow applications. The first one is extremely diffusive and will damp most flow features, and the second scheme is dispersive (like most second order schemes), and may induce numerical spurious waves, or oscillatory solutions, which are termed “wiggles”. To avoid the well known ill-effects of these two schemes, Toro (1997)

proposed a simple deterministic **f**irst-**or**der **ce**ntred scheme (**force**), in which the intercell flux is in fact an arithmetic mean of the Lax-Friedrichs flux (3.7) and the Richtmyer flux (3.8). It is therefore given by:

$$\hat{F}^{force}_{j+1/2} = \frac{1}{2}\left[\hat{F}^{LF}_{j+1/2} + \hat{F}^{RI}_{i+1/2}\right] \tag{3.9}$$

3.4.1.4 Flux Corrected Transport (FCT)

This method developed by Boris & Book (1973) and Book et al. (1975) was the first high-resolution scheme to introduce the concept of limiters in the literature. It can be seen as a "predictor/corrector" method in which a large amount of diffusion is introduced in the predictor stage, and an (almost) equal amount of anti-diffusion is introduced in the corrector stage. However, the anti-diffusion is limited so that no new maximum or minimum can appear in the solution, nor can existing extrema be accentuated.

Let Q^n be the previous time step solution, and $\widetilde{Q}$ be the new updated solution generated by the second-order Ritchmyer scheme (3.8), then the FCT algorithm described below consists of five steps, and can be found in the second volume of the book by [Fletcher, 1988].

1. Generation of diffusive fluxes

$$F^{d}_{j+\frac{1}{2}} = \nu_{j+\frac{1}{2}}\left(Q^{n}_{j+1} - Q^{n}_{j}\right) \tag{3.10a}$$

2. Diffusion of the solution

$$Q^{d}_{j} = \widetilde{Q}_{j} + \left(F^{d}_{j+\frac{1}{2}} - F^{d}_{j-\frac{1}{2}}\right) \tag{3.10b}$$

3. Generation of anti-diffusive fluxes

$$F^{ad}_{j+\frac{1}{2}} = \mu_{j+\frac{1}{2}}\left(\widetilde{Q}_{j+1} - \widetilde{Q}_{j}\right) \tag{3.10c}$$

4. Limitation of the anti-diffusive fluxes

$$S = \text{sign}\left(F^{ad}_{j+\frac{1}{2}}\right)$$

$$F^{cad}_{j+\frac{1}{2}} = S.\max\left[0, \min\left(S.\left(\widetilde{Q}_{j+1} - Q^{d}_{j}\right), \left|F^{ad}_{j+\frac{1}{2}}\right|, S.\left(\widetilde{Q}_{j+2} - Q^{d}_{j+1}\right)\right)\right] \tag{3.10d}$$

5. Generation of intercell flux

$$\hat{F}^{FCT}_{j+\frac{1}{2}} = F^{cad}_{j+\frac{1}{2}} - F^{d}_{j+\frac{1}{2}} \tag{3.10e}$$

For our algorithm, the diffusion and anti-diffusion coefficients ν and μ have been taken constants, and both equal to 0.125 as suggested by Lezeau & Thompson (1999).

3.4.2 Characteristics Based Schemes

We have implemented two schemes that use the maximum eigenvalue or characteristic of the model studied. The first one is a first-order scheme while the second one is a high-resolution scheme using the Total Variation Diminishing (TVD) approach [Harten, 1983]. Theses two schemes were selected because they do not use a local Riemann solution [Toro, 1997], and can therefore be applied to any system of conservation laws without a full knowledge of the characteristic waves. They are respectively known as Rusanov and TVD Lax- Friedrichs, and are described below.

3.4.2.1 Rusanov

For general non-linear systems in one dimension, the simplest characteristic based flux scheme is the first order Rusanov scheme, for which the intercell flux takes the form:

$$\hat{F}^{RUS}_{j+1/2} = \frac{1}{2}\left[F\left(Q^{n}_{j}\right) + F\left(Q^{n}_{j+1}\right) - \lambda_{j+1/2}\left(Q^{n}_{j+1} - Q^{n}_{j}\right)\right] \tag{3.11a}$$

where $\lambda_{j+1/2}$ is an average wave speed value. Various choices are possible for its estimate, but here we use the upper bound of the absolute values of the characteristic speeds in either cell as suggested by Trangenstein (2000). Hence, it is given by:

$$\lambda_{j+1/2} = \max\left(\max_{k}\left|\lambda^{k}_{j}\right|, \max_{k}\left|\lambda^{k}_{j+1}\right|\right), \quad k = 1, N_{eq} \tag{3.11b}$$

where N_{eq} is the total number of partial differential equations in the model, for example two for the incompressible two-fluid model PFM-2 and three for the HEM-3 model.

3.4.2.2 TVD Lax-Friedrichs

In order to limit the excessive diffusion generated by the Lax-Friedrichs scheme, Yee (1989) proposed a TVD version of the scheme using the van Leer (1979) MUSCL approach. The resulting scheme is still slightly more dissipative than the use of the first-order upwind scheme. Therefore variations of this scheme have been recently presented in the literature, a simplified version was suggested by Barmin et al. (1996) while the version implemented here was proposed by Tóth & Odstrčil (1996) as:

$$\hat{F}^{TVDLF}_{j+1/2} = \frac{1}{2}\left[F\left(Q^{L}_{j+1/2}\right) + F\left(Q^{R}_{j+1/2}\right)\right] - \frac{1}{2\tau}\Phi^{LR}_{j+1/2} \qquad (3.12a)$$

The left and right state vectors denoted by Q^L and Q^R are formed from an intermediate state $Q^{n+1/2}$ (3.12c) and the limited differences $\delta\overline{Q}^{n}$ (3.12f) as:

$$Q^{L}_{j+1/2} = Q^{n+1/2}_{j} + \frac{1}{2}\delta\overline{Q}^{n}_{j}, \qquad Q^{R}_{j+1/2} = Q^{n+1/2}_{j+1} - \frac{1}{2}\delta\overline{Q}^{n}_{j+1} \qquad (3.12b)$$

The intermediate vector or predictor step value is given by:

$$Q^{n+1/2}_{j} = Q^{n}_{j} - \frac{\tau}{2}\left[F\left(Q^{n}_{j} + \tfrac{1}{2}\delta\overline{Q}^{n}_{j}\right) - F\left(Q^{n}_{j} - \tfrac{1}{2}\delta\overline{Q}^{n}_{j}\right)\right] + \frac{\Delta t}{2}S\left(Q^{n}_{j}\right) \qquad (3.12c)$$

The dissipative limiter Φ^{LR} in Equation (3.12a) is a function of Q^{LR} (some symmetric average vector of Q^L and Q^R), and of the spatial difference vector $\delta Q^{LR} = Q^R - Q^L$. Yee (1989) originally defined $\Phi^{LR} = \delta Q^{LR}$ not making use of any characteristic wave speed, but as already mentioned this leads to a very diffusive scheme. Hence, to reduce the numerical diffusion, Barmin et al. (1996) and Tóth & Odstrčil (1996) multiplied Φ^{LR}_{Yee} by the local courant number and proposed the following relation:

$$\Phi^{LR} = \frac{\Delta t}{\Delta x}\lambda^{max}_{j+1/2}\left(Q^{R} - Q^{L}\right) \qquad (3.12d)$$

Cockburn et al. (1989) used the expression (3.11b) for their value of $\lambda^{max}_{j+1/2}$ in the above equation. In this case, the scheme has the same diffusion coefficient as the Rusanov scheme described in the previous section, and should be called MUSCL-Rusanov instead of TVD Lax-Friedrichs. Here, we use the relation proposed by Barmin et al. (1996), which is computationally less expensive than the expression (3.11b). This relation was also adopted by Tóth & Odstrčil (1996) and it is given as:

$$\lambda^{max}_{j+1/2} = \max\left|\lambda_{k}\left(\frac{Q^{L} + Q^{R}}{2}\right)\right|, \quad k = 1, Neq \qquad (3.12e)$$

There are many flux limiter functions defined in the literature [Yee, 1989; Tóth & Odstrčil, 1996], but for the limited differences $\delta\overline{Q}^{n}$ in Equations (3.12b) and (3.12c), we opt for the simple Minmod function described by Equation (3.14), and therefore use the following relation:

$$\delta\overline{Q}^{n}_{j} = \text{Min mod}\left(Q^{n}_{j} - Q^{n}_{j-1}, Q^{n}_{j+1} - Q^{n}_{j}\right) \qquad (3.12f)$$

The programming of the TVD Lax-Friedrichs scheme does not exactly follow the description given above. Therefore, the proper sequence for implementing this scheme is (3.12f), (3.12c), (3.12b), (3.12e), (3.12d) and (3.12a).

3.5 Methods for the Non-Conservative Terms

The generic discretisation (3.4) involves flux conservative terms, which can be expressed using any of the numerical flux schemes described above, and non-conservative terms $H\partial Q/\partial x$ that need to be dealt with more carefully. Several types of simple spatial discretisation for these terms have been implemented and are listed below:

3.5.1 MinMod Scheme

Coquel et al. (1997) suggested this type upwind discretisation for their two-fluid model, and proposed the following relation:

$$\left(H\frac{\partial Q}{\partial x}\right)_j^n = \frac{H_j^n}{\Delta x}\,\text{Min mod}\left(Q_{j+1}^n - Q_j^n,\, Q_j^n - Q_{j-1}^n\right) \tag{3.13}$$

where the Minmod function is defined by:

$$\text{Min mod}(x,y) = \frac{1}{2}\left(\text{sign}(x)+\text{sign}(y)\right)\min\left(|x|,|y|\right) \tag{3.14}$$

The discretisation (3.13) is first order in space and was named Minmod-1 in the EMAPS framework. It was found to be very diffusive; therefore a second order version proposed by Harten (1989) was implemented. It is given by:

$$\left(H\frac{\partial Q}{\partial x}\right)_j^n = \frac{H_j^n}{\Delta x}\,\text{Min mod}\left[2\left(Q_{j+1}^n - Q_j^n\right), \frac{1}{2}\left(Q_{j+1}^n - Q_{j-1}^n\right), 2\left(Q_j^n - Q_{j-1}^n\right)\right] \tag{3.15}$$

where the function

$$\text{Min mod}(x,y,z) = \begin{cases} \text{s.min}\left(|x|,|y|,|z|\right) & \text{if } \text{sign}(x)=\text{sign}(y)=\text{sign}(z) \\ 0 & \text{otherwise} \end{cases} \tag{3.16}$$

The non-conservative terms discretisation (3.15) was named Minmod-2 in the code.

3.5.2 Centred Scheme

A simple central discretisation has also been implemented for the non-conservative terms. It is second order in space, and is given by:

$$\left(H \frac{\partial Q}{\partial x} \right)_j^n = H_j^n \frac{Q_{j+1}^n - Q_{j-1}^n}{2\Delta x} \tag{3.17}$$

This centred spatial discretisation usually generates spurious oscillations; therefore the non-conservative terms are generally expressed using the second-order Minmod-2 scheme described above.

3.6 Constraints on Numerical Methods

For the numerical schemes described above to successfully simulate physical problems, appropriate boundary conditions need to be implemented. The approach adopted for these conditions is described later in this section, but first we present the procedure of selecting time step Δt used by the computational schemes, because while the user may freely specify the mesh size Δx, the time step size is usually restricted to the stability condition of the particular numerical scheme used.

3.6.1 Time Step Size

The mathematical models and numerical schemes described above were implemented in an adaptive mesh refinement (AMR) framework. The full details of this automatic spatial refinement technique will be presented in the next chapter, and a short description can be found in the paper by Omgba-Essama et al. (2000).

Hence, the spatial discretisation length Δx is generally dictated by the AMR scheme depending upon the desired accuracy. As for the time step Δt appearing in the discrete equations, the explicit formulation of the numerical schemes constrains its size with the usual Courant-Friedrichs-Levy (CFL) number. It is therefore given by:

$$\Delta t = CFL \frac{\Delta x}{\lambda_{max}^n} \tag{3.18}$$

where CFL is a positive coefficient restricted to a limiting value, usually one. The closer this coefficient is to its upper limit, the more efficient is the numerical time marching scheme. For all the numerical schemes described above, except for FCT, their stability

analysis requires the value *CFL <= 1*, but for the FCT scheme, Sod (1985) showed that the CFL value should be less than 0.5.

The term λ_{max}^{n} in Equation (3.18) is the largest wave speed present throughout the domain at time level n. It is estimated for the mathematical models HEM-3, PFM-2 and SPM-4 as the largest absolute value of their analytical characteristics defined in the first chapter. Hence, for a system of k differential equations in a computational domain with M cells (Figure 3-1), this term is given as:

$$\lambda_{max}^{n} = \max_{j}\left\{\max_{k}\left|\lambda_{j}^{k}\right|\right\} \quad \text{for} \quad j = 1,\cdots,M; \quad k = 1, Neq \tag{3.19}$$

It should be noted that for the single pressure model SPM-4, the approximate eigenvalues described in the previous chapter are only valid for the small relative velocities compared to gas speed of sound ($V_r/C_G < 5\%$). Therefore to obtain the eigenvalues for this model, we use a combination of analytical approximate values and numerical exact values calculated by the numerical recipes [Press et al., 1992] function "HQR" for solving arbitrary matrix eigenvalues.

3.6.2 Boundary Conditions

For a computing domain [0, L] discretised into M computing cells of length Δx, we need special conditions at the boundary positions x = 0 and x = L as illustrated in Figure 3-1. These boundary conditions are expected to provide for example the numerical fluxes $\hat{F}_{1/2}$ and $\hat{F}_{M+1/2}$, which are required by finite difference discretisation such as (3.3) or (3.4) in order to advance the extreme cells 1 and M to the next time level.

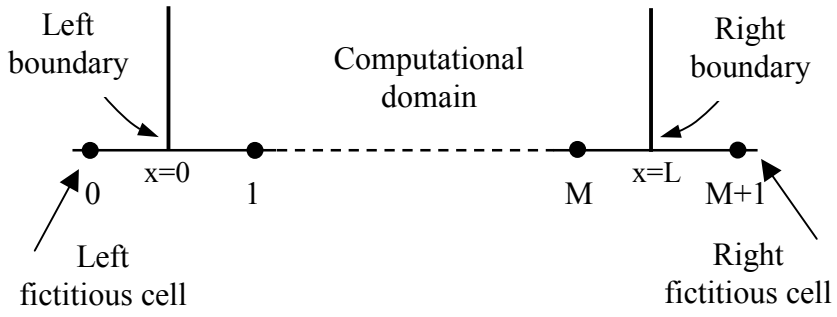

Figure 3-1: Boundary Conditions. Fictitious cells outside the computational domain are created (Toro, 1997)

For each mesh cell of the computational domain, two numerical fluxes are required to update the vector solution Q_j^n. However, for cells 1 and M, which are adjacent to the left

and right boundaries respectively, we only have one intercell flux. Hence, some special procedure needs to be implemented. Let us consider the left boundary x = 0. As mentioned by Toro (1997), one possibility is to assume a boundary function $Q_1(t)$ prescribed there. Then we could define an intercell flux at the boundary by setting $\hat{F}_{1/2} = F(Q_1(t))$.

A more attractive alternative, which is adopted in EMAPS, is to specify a *fictitious* (also referred to as *ghost* or *dummy*) *cell* 0 to the left of the boundary x = 0 together with a cell average Q_0^n, at each time level n, so that the missing intercell flux $\hat{F}_{1/2}$ can be solved using (Q_0^n, Q_1^n). For the right boundary, we prescribe a fictitious cell M+1 and a cell average Q_{M+1}^n to find the intercell flux $\hat{F}_{M+1/2}$. The prescription of these fictitious states or boundary conditions depends entirely on the physics of the particular problem at hand.

3.7 Numerical Validation of Single-Phase Models

Since there are no non-trivial analytical solutions to two-phase flow problems against which to compare the numerical results, confidence in the numerical simulations is enhanced by utilizing other unrelated numerical schemes or by solving mathematically similar problems with known solution from other disciplines. This motivated the validation work on single-phase models. Two simple and well-known one-dimensional systems, namely the Burgers and Shallow water equations, were used to analyse and assess the accuracy and robustness of the numerical schemes implemented. Their description is presented in this section.

3.7.1 Inviscid Burgers Model

3.7.1.1 Equation

The inviscid Burgers equation is a single non-linear equation given in conservative form by equation (3.20). The simplicity of its convective term makes this scalar equation a very suitable model for testing computational algorithms for flows where severe gradients or shocks are anticipated.

$$\frac{\partial u}{\partial t} + \frac{\partial (u^2/2)}{\partial x} = 0 \qquad (3.20)$$

The variable u in relation (3.20) is the fluid flow axial velocity, and although this inviscid equation is mainly used nowadays for algorithmic and not physical purposes, it should be mentioned that the original Burgers equation, which is reviewed and studied by Benton & Platzman (1972), contains a viscous term and it is special case of some mathematical models of turbulence.

3.7.1.2 Analytical Solution (Riemann Problem)

For any scalar conservation equation, or any system of conservation laws such as the one-dimensional Euler equations, the Riemann problem [Toro, 1997; Laney, 1998] has uniform initial conditions on a finite spatial domain, except for a single jump discontinuity. For the Burgers equation, the initial data are given by:

$$u(x,0) = \begin{cases} u_L & x < x_d \\ u_R & x > x_d \end{cases} \tag{3.21}$$

where $\mathbf{u_L}$ and $\mathbf{u_R}$ are constant left and right velocity values, and $\mathbf{x_d}$ is the location of the discontinuity.

The Riemann problem has an exact analytical solution, and the form of this solution depends on the relation between u_L and u_R. If ($\mathbf{u_L > u_R}$), the solution is called a shock wave, while it is referred to as a rarefaction wave in the opposite case. For $x_d = 0$ in expression (3.21), the exact solution as described in the book by Toro (1997) is:

$$\left.\begin{array}{l} u(x,t) = \left.\begin{cases} u_L & \text{if} \quad x < St \\ u_R & \text{if} \quad x > St \end{cases}\right\} \quad \text{if} \quad u_L > u_R \\ \qquad S = \dfrac{1}{2}(u_L + u_R) \\ u(x,t) = \left\{\begin{array}{lll} u_L & \text{if} & x/t \le u_L \\ \dfrac{x}{t} & \text{if} & u_L < \dfrac{x}{t} < u_R \\ u_R & \text{if} & x/t \ge u_R \end{array}\right\} \quad \text{if} \quad u_L \le u_R \end{array}\right. \tag{3.22}$$

The parameter **S** is the shock wave velocity, the speed at which the discontinuity travels. If the discontinuity position x_d is different from zero, then the above solution remains valid providing that x is replaced by $(x-x_d)$.

A more detailed discussion on the solutions of the Riemann problem for the inviscid Burgers equation can be found in numerical textbooks [LeVeque, 1992; Toro, 1997]. For general analysis of other solutions of the Burgers equation, we refer the reader to the paper by Benton & Platzman (1972) and the book by Whitham (1974).

3.7.1.3 Numerical Results

The results presented in Figure 3-2 are for a shock wave case at 1.5 sec, where the initial velocities are $u_L = 1$ m/s, and $u_R = 0.5$ m/s, and the initial shock position is $x_d = 0.2$.

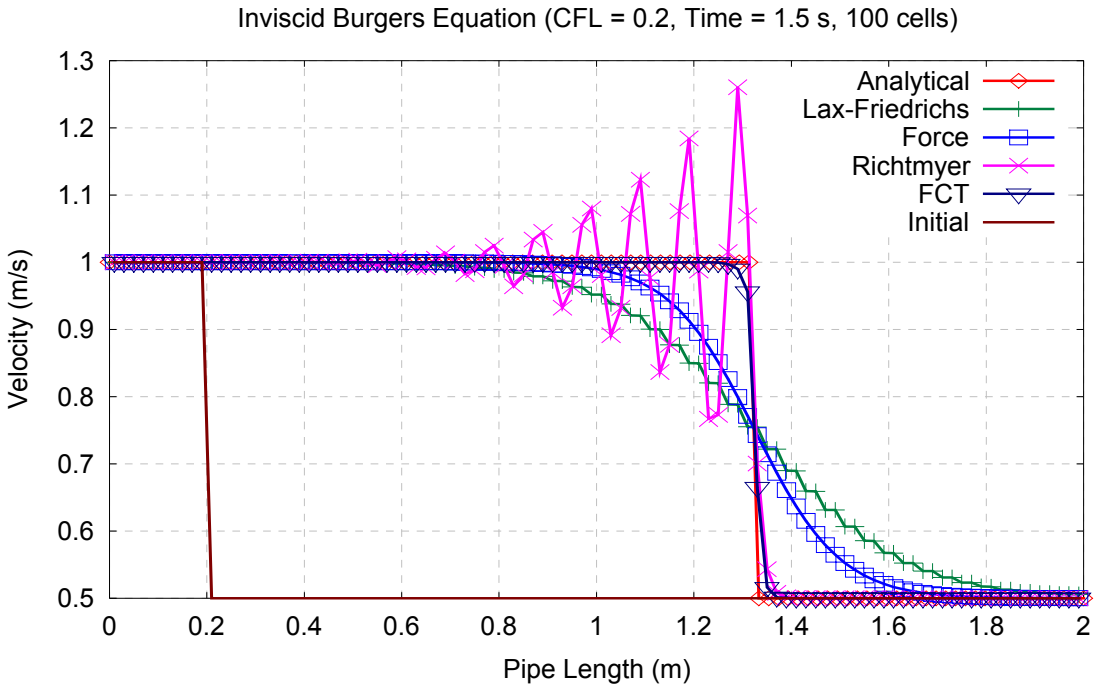

Figure 3-2: Burgers results for central schemes at time = 1.5 s, using 100 cells.

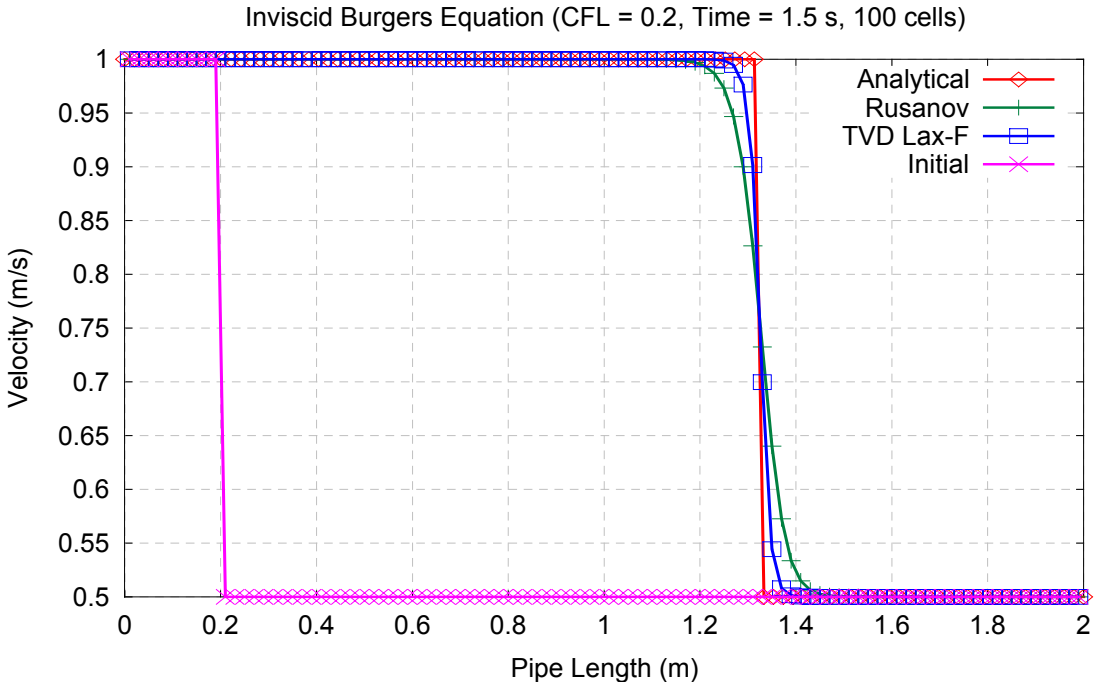

Figure 3-3: Burgers results for upwind schemes at time = 1.5 s, using 100 cells.

The pipe length is 2 m, and the number of cells is set to 100 giving a mesh size Δx of 0.02 m. Figure 3-2 shows the comparative results for all the central schemes described in Section 3.4.1, while Figure 3-3 compares the results of the two characteristics based schemes described in Section 3.4.2 with the analytical solution (3.22).

All the simulations presented in Figures 3-2 and 3-3 use a CFL value of 0.2 to calculate the time step. Though not providing the most accurate results for the test in hand, this value was selected for all single-phase flow validations for two reasons. Firstly, because it highlights a bit better the differences between the numerical schemes evaluated, and secondly and more importantly because it is the CFL value generally used for two-phase flow simulations presented later in this thesis.

In general, the characteristic-based schemes are less diffusive and more accurate than the central ones. But for the Burgers equation, we found that the FCT scheme is the most accurate, followed closely by the TVD Lax-Friedrichs scheme, then the Rusanov and Force schemes. The Lax-Friedrichs results appear the least accurate of all the numerical results, as the scheme easily spreads the initial cell discontinuity over many cells while advancing in time.

As for the Ritchmyer scheme, it is very dispersive and generates spurious oscillations near the discontinuity, which may be unstable for long or more complex simulations, and probably crash the code as a result. Therefore, we will no longer consider this scheme alone for further numerical simulations; however it will still be used by the FCT and the Force schemes, as it remains one of the building blocks of these schemes.

3.7.2 Shallow Water Model

3.7.2.1 Equations

This system describes the height **h** of a free water surface in a stream with velocity **u** [Whitham, 1974]. It was selected for numerical validation, not only because of known analytical solutions, but also because its system of equations is analogous to the two-phase incompressible model PFM-2 presented in the first chapter, see the paper by Watson (1990) for similarities. Referring to the conservative formulation (3.1), the shallow water equations can be written as follows:

$$Q = \begin{pmatrix} h \\ hu \end{pmatrix}, \qquad F = \begin{pmatrix} hu \\ hu^2 + \dfrac{gh^2}{2} \end{pmatrix}, \qquad S = \begin{pmatrix} 0 \\ 0 \end{pmatrix} \tag{3.23}$$

where **g** is the gravitational acceleration constant. The physical properties of the flow are directly related to the mathematical properties of the model simulated, and in the case of the

shallow water system, we can obtain the two characteristic velocities $\lambda_{1,2}$ by calculating the eigenvalues of J, the Jacobian of the flux vector F.

$$J = \frac{\partial F}{\partial Q} = \begin{pmatrix} 0 & 1 \\ -u^2 + gh & 2u \end{pmatrix} \tag{3.24}$$

These velocities represent the speed of propagation of the two wave fronts (see Figure 3-4) and are given as:

$$\lambda_{1,2} = u \pm \sqrt{gh} \tag{3.25}$$

3.7.2.2 Analytical Solution (Dam Break Problem)

The dam break test simulates the rupture of a barrier placed across a channel. The initial conditions for this physical problem are:

$$h(x,0) = \begin{cases} h_L & x < 0 \\ h_R & x > 0 \end{cases} \qquad \text{and} \qquad u(x,0) = 0. \tag{3.26}$$

Louaked & Hanich (1998) presented the analytical solution for this problem as:

$$h(x,t) = \begin{cases} h_L & \frac{x}{t} \le -\sqrt{gh_L} \\ \left(\frac{1}{9g}\right)\left[2\sqrt{gh_L} - \frac{x}{t}\right]^2 & -\sqrt{gh_L} \le \frac{x}{t} \le \left(u_m - \sqrt{gh_m}\right) \\ h_m & \left(u_m - \sqrt{gh_m}\right) \le \frac{x}{t} \le s \\ h_R & s \le \frac{x}{t} \le \infty \end{cases} \tag{3.27}$$

$$u(x,t) = \begin{cases} 0 & \frac{x}{t} \le -\sqrt{gh_L} \\ \left(\frac{2}{3}\right)\left[\sqrt{gh_L} + \frac{x}{t}\right] & -\sqrt{gh_L} \le \frac{x}{t} \le \left(u_m - \sqrt{gh_m}\right) \\ u_m & \left(u_m - \sqrt{gh_m}\right) \le \frac{x}{t} \le s \\ 0 & s \le \frac{x}{t} \le \infty \end{cases} \tag{3.28}$$

The terms $\mathbf{h_m}$ and $\mathbf{u_m}$ are defined in function of the wave propagation velocity **s** as:

$$h_m = \frac{1}{2}\left[\sqrt{1+\frac{8s^2}{gh_R}} - 1\right]h_R \tag{3.29}$$

$$u_m = s - \frac{gh_R}{4s}\left[1+\sqrt{1+\frac{8s^2}{gh_R}}\right] \tag{3.30}$$

where **s** is the positive real solution of the following equation:

$$u_m + 2\sqrt{gh_m} - 2\sqrt{gh_L} = 0 \tag{3.31}$$

The root finding program for solving Equation (3.31), and consequently deriving the dam break analytical solution, uses an iterative scheme such as the dichotomy method, which can be found in the numerical recipes book [Press et al., 1992]. However, this exact solution was kindly provided to us by Dr Hanich, one of the authors of the paper mentioned above.

3.7.2.3 Numerical Results

The initial heights for the test simulated were $h_L = 0.1$ and $h_R = 0.5$ with a discontinuity located at 0.5 m, which is half of the axial distance used for the simulation.

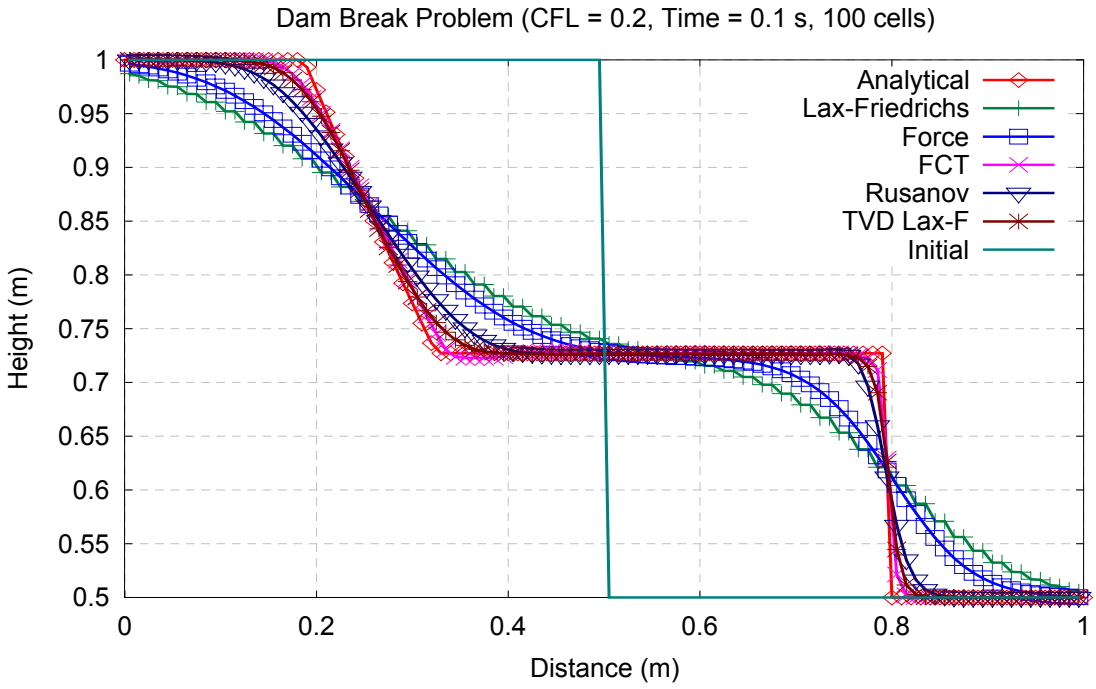

Figure 3-4: Shallow Water [Dam Break]. Height Profile at T = 0.1s for Central and Upwind Schemes.

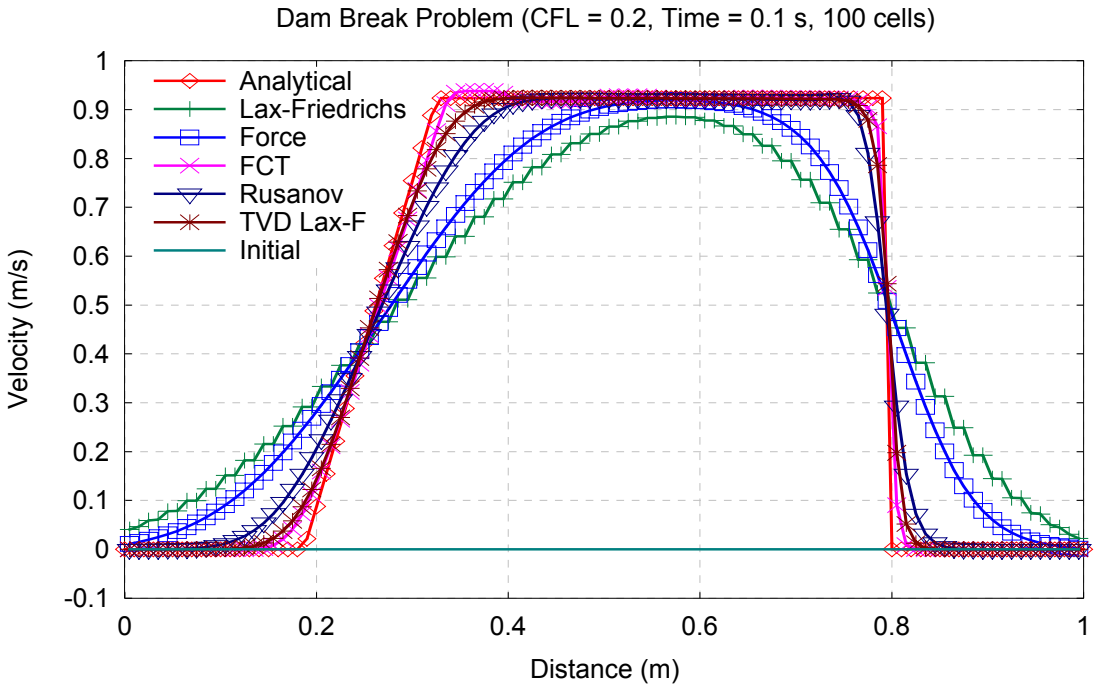

Figure 3-5: Shallow Water [Dam Break]. Velocity Profile at T = 0.1s for Central and Upwind Schemes.

Figures 3-4 and 3-5 show the height and velocity profiles obtained with the Shallow Water model at 0.1 second when using the central and upwind schemes previously described. In terms of accuracy, we found identical trends to those of the Burgers equation. The high-resolution FCT and TVD Lax-Friedrichs schemes remain the most accurate while the Force and Lax-Friedrichs are the least accurate ones.

The Lax-Friedrichs scheme is so dissipative that it easily damps discontinuities and can lead to the disappearance of shock fronts for long simulations, even with fine meshes. This fact is undesired for some two-phase flow simulations, in particular slug flow where the front of the slug can be viewed as a hydraulic jump. Therefore, this scheme will not be considered for two-phase flow simulations, leaving only four flux schemes, two central (Force and FCT) and two upwind ones (Rusanov and TVD Lax-Friedrichs) for evaluation.

It should be noted that other numerical tests were performed with this model [Omgba-Essama, 1999], and with the single-phase Euler equations [Omgba-Essama, 2000]. They are not reported here because our primary focus is on multiphase flows, and because they lead to similar conclusions to those mentioned above, concerning the accuracy and robustness of the numerical schemes implemented.

3.8 Numerical Validation of Two-Phase Models

In this section, we present various test cases for validating the three specific models described in the first chapter. The purpose of these tests is not necessarily to assess the ability of the physical models to accurately predict salient two-phase flow features for problems of interest, but to evaluate the accuracy and robustness of the numerical methods in predicting simple cases found in the literature, with known or unknown analytical solutions.

3.8.1 IFP Test-Case

3.8.1.1 Problem Summary

The French Petroleum Institute (IFP) proposed this simple but meaningful test case in order to evaluate the numerical performance of our implementation. An isothermal gas-liquid simulation of a long horizontal pipeline of constant diameter is performed. For a given combination of inlet flow rates and outlet pressure, there exists a steady-state solution. The gas mass flow rate is then quickly doubled. As a result, a volume fraction wave propagates down the line. When it reaches the outlet, the line has settled in a different steady state. The specifications of the problem are as follows:

- Length of the pipeline: 10 km
- Diameter of the pipeline: 0.146 m
- Operating fluids: air and water (ρ_G variable, $\rho_L = 1000 kg/m^3$)
- Flow temperature: $T = 5\ ^{\circ}C$

The objective of this test is not only to correctly predict the holdup wave propagation, but also to evaluate the ability of the numerical schemes to handle frictional source terms, which have a major effect in the pipeline problems we are interested in. For this test case only the HEM model was used, as comparisons with TACITE drift-flux model are possible, and therefore only the wall friction factor f_w in relation (2.36) is required for the two-phase mixture and it was taken constant and equal to 0.02.

3.8.1.2 Initial & Boundary Conditions

Figure 3-6 describes the operating conditions for this test case. The inlet liquid mass flowrate is constant and equal to 20 kg/s, while the gas mass flowrate is initially equal to 0.2 kg/s, then it is doubled to 0.4 kg/s in a linear ramp between t = 1000s and t = 1010s.

The outlet pressure is kept fixed at 10 bar, and referring to equation (2.7) relating the gas density to the pressure, the perfect gas law is utilized and expressed as:

$$\frac{P}{\rho_G T} = \frac{P_{norm}}{\rho_{norm} T_{norm}} \tag{3.32}$$

where the normal conditions are given by: P_{norm}= 1 bar, T_{norm}= 300 K, ρ_{norm} = 1 kg/m^3.

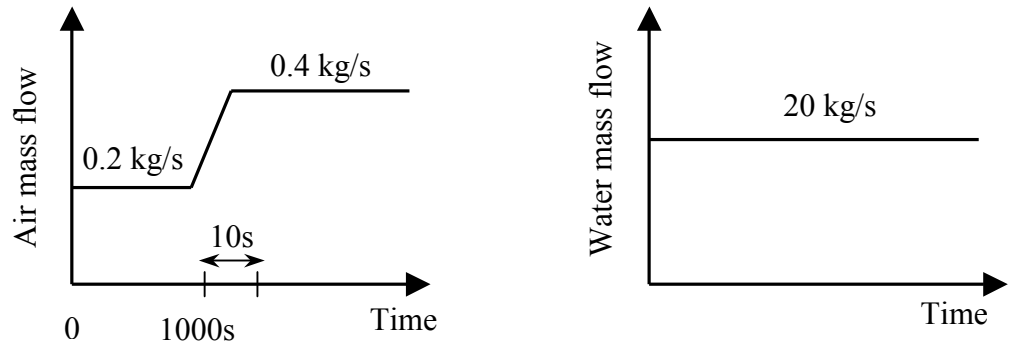

Figure 3-6: Schematic of operating conditions for the IFP test case

3.8.1.3 Numerical Results (HEM-3)

Various effects have been studied using the homogeneous equilibrium model (HEM-3) in combination with the numerical schemes described earlier in this chapter, and they are reported in this section.

FCT Diffusion Effect

The diffusion (d) and anti-diffusion (ad) coefficients implemented in the FCT scheme described in Section 3.4.1.4 were suggested by Lezeau & Thompson (1999), and are both set equal to a constant value of 0.125. As already mentioned, these coefficients work perfectly well for most problems with discontinuities and suppress unwanted oscillations, giving highly accurate resolutions for all single-phase flow cases presented in the previous sections. However, for two-phase flow problems, they sometimes lead to artificial wiggles near the discontinuity (Figure 3-7), so we performed an analysis of the effect of these diffusive coefficients for the IFP test case.

The results of slightly varying the diffusion coefficient while keeping the anti-diffusion coefficient constant are presented in Figure 3-7. They show that increasing the diffusion coefficient by a small amount such as 1%, can remove the unwanted numerical wiggles, while maintaining a sharp resolution of the discontinuities. Therefore, the implementation of the FCT scheme was modified accordingly and all two-phase flow numerical results presented in this thesis were obtained with the FCT scheme that uses constant coefficient values 0.126 and 0.125 for diffusion and the anti-diffusion parameters respectively.

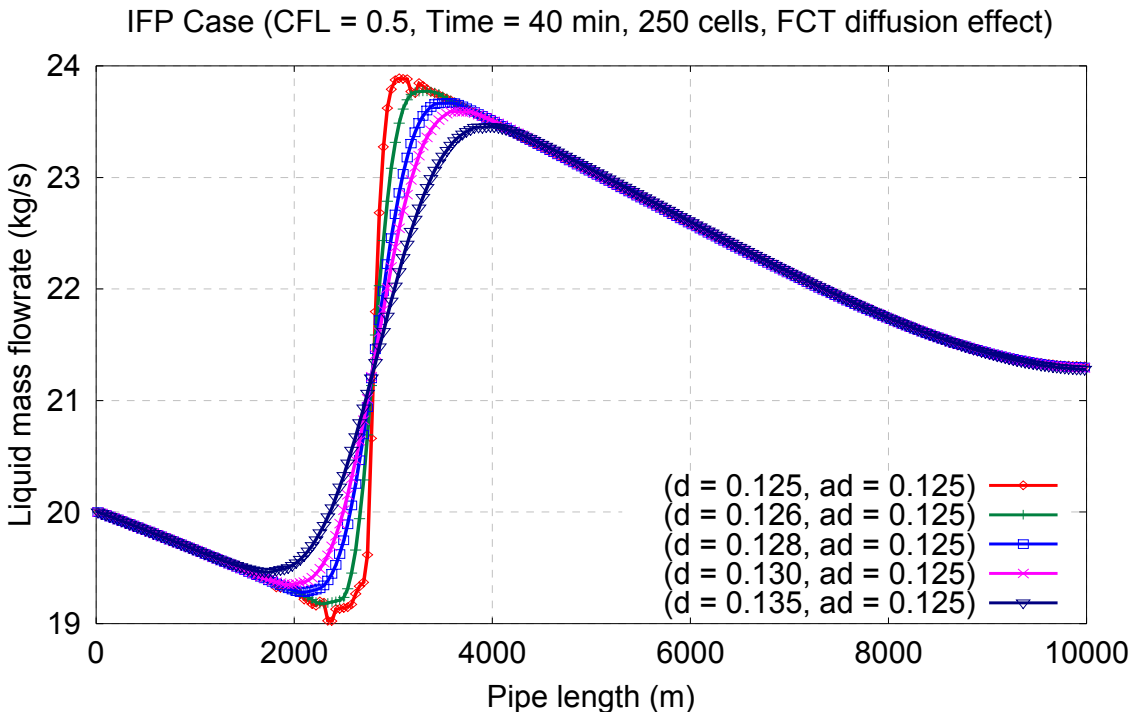

Figure 3-7: HEM-3 [IFP Case]. Effect of the FCT diffusion and anti-diffusion coefficients

Schemes Comparison

Figure 3-8 summarises the solutions obtained on a uniform grid ($\Delta x = 40$ m) for a one-hour simulation with different numerical schemes. These results show that while a global variable such as the pressure drop can be accurately predicted by any of the numerical methods implemented, even first order ones, other quantities such as holdup or mass flowrates require high-resolution schemes for an accurate description of their behaviour.

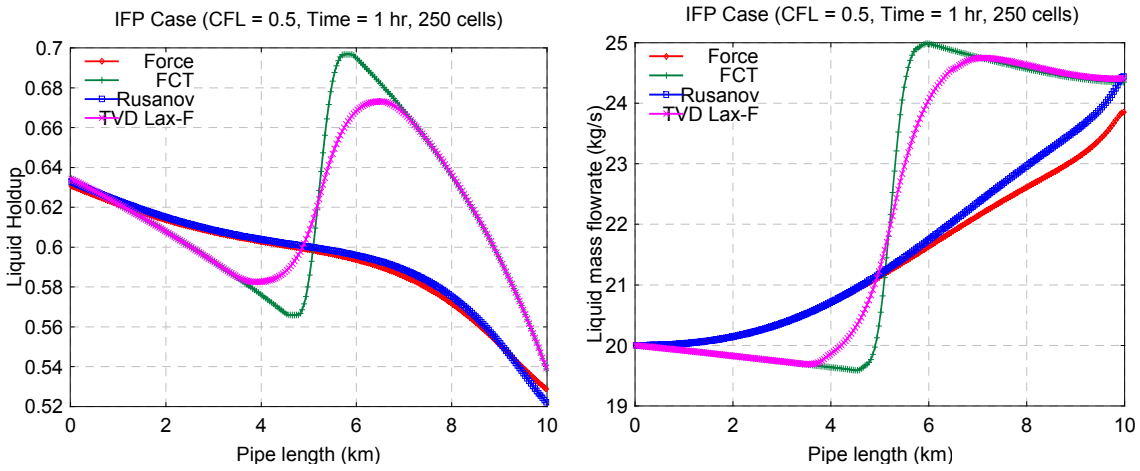

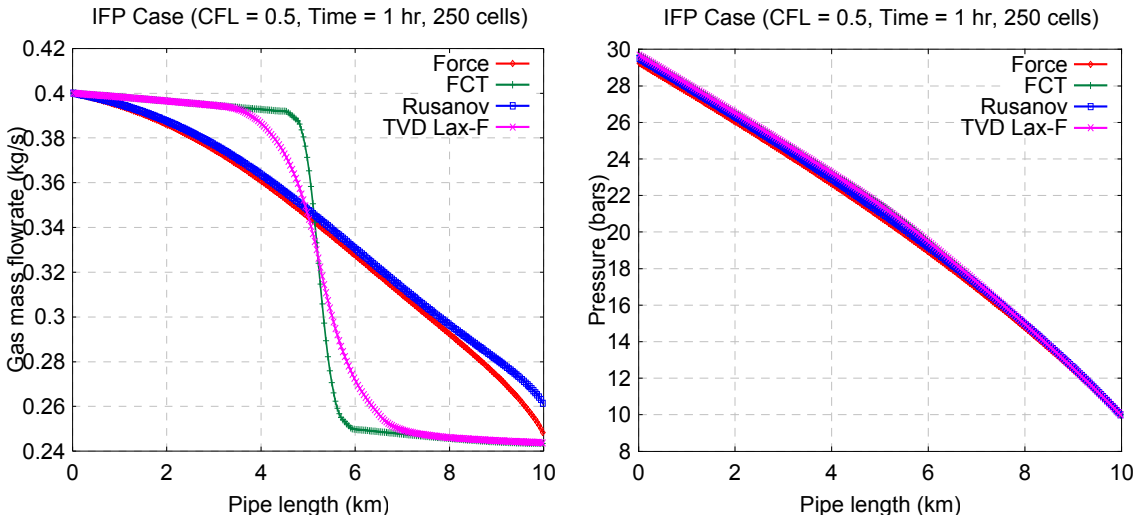

Figure 3-8: HEM-3 [IFP Case]. Numerical schemes comparison for the liquid hold-up and mass flowrate (top), the gas mass flowrate and common pressure (bottom) at t = 1 h.

Mesh Refinement Effect

Figure 3-9 summarises the behaviour of the numerical solutions obtained using the TVD Lax-Friedrichs scheme with different grid sizes. The results show that the finer the mesh size is, the more convergent the solution is, evidence of a well-behaved numerical model.

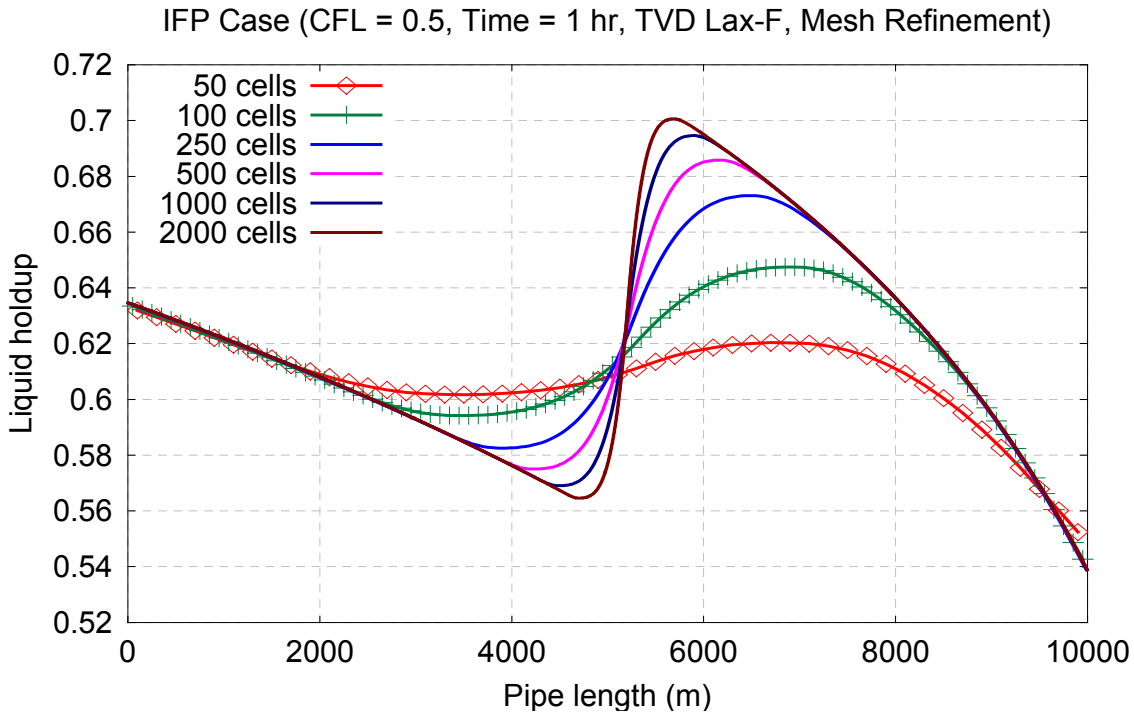

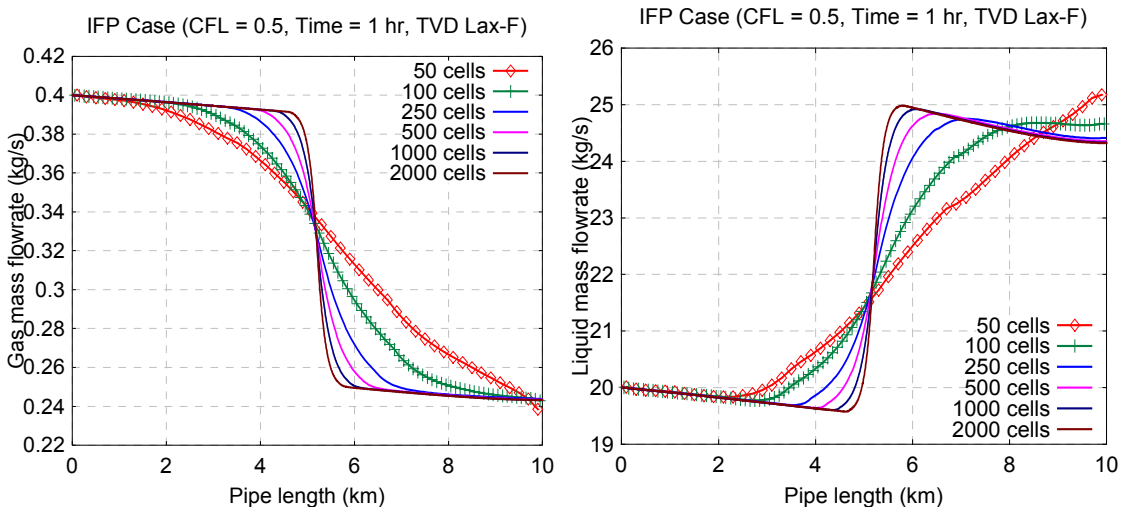

Figure 3-9: HEM-3 [IFP Case]. Mesh Refinement for the liquid holdup (top), the gas and liquid mass flowrates (bottom) at time = 1 hour, using the TVD Lax-Friedrichs scheme.

Flow Evolution

Figure 3-10 presents the time evolution of the liquid holdup and gas mass flowrate at different time steps using the FCT scheme. These results are in good agreement with those obtained by TACITE commercial software, and reported by Lezeau & Thompson (1999).

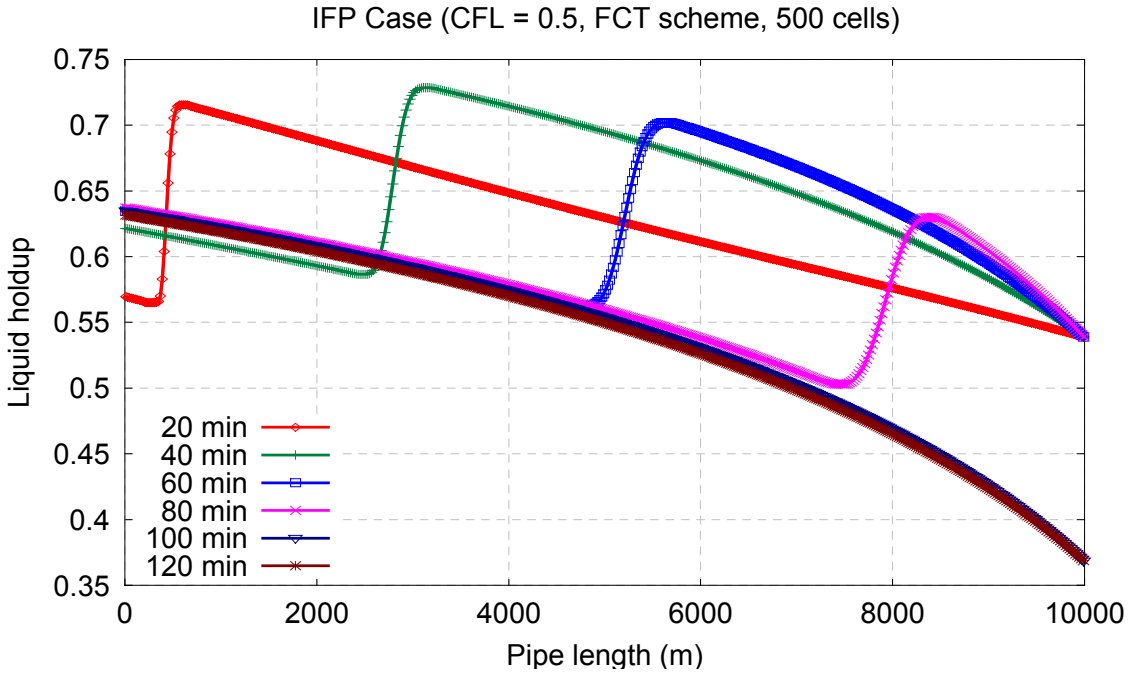

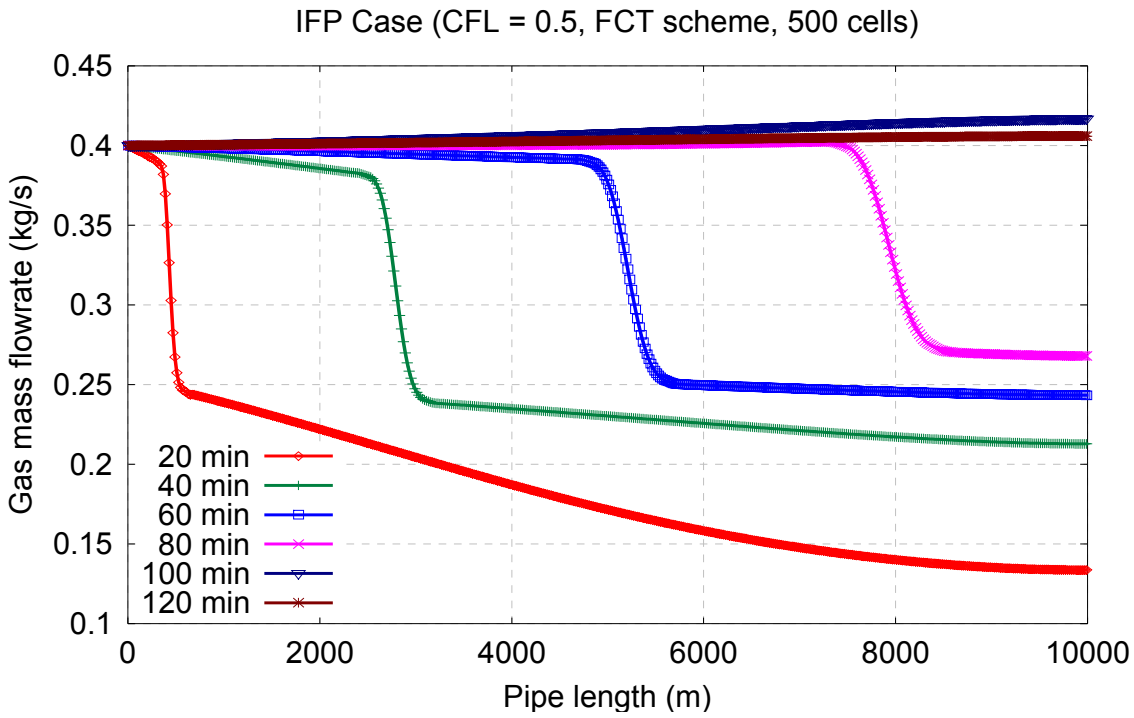

Figure 3-10: HEM-3 [IFP Case]. Time evolution of the liquid hold-up (top) and the gas mass flowrate (bottom) using the FCT scheme with 500 grid cells.

All the numerical results presented for the IFP case clearly demonstrate the importance of high-resolution numerical schemes. As with single-phase cases, the FCT and the TVD Lax-Friedrichs are the only viable schemes for simulations over a long period of time. For the IFP case, low-order schemes such as Force or Rusanov dissipate the strength of the holdup front discontinuity (Figure 3-8) in a way that it can disappear in time, even with the use of fine grid cells.

3.8.2 Water Faucet Case

3.8.2.1 Problem Summary

This popular problem, devised by Ransom (1987), consists of a liquid stream entering a vertical solution space at the top and falling under the action of gravity to form a stream of uniformly decreasing cross-section. It is illustrated schematically in Figure 3-11, and the specifications of the problem are given as:

- Length of the vertical pipe: 12 m
- Diameter of the vertical pipe: 1 m
- Operating fluids: air and water ($\rho_G = 1.16$ kg/m^3, $\rho_L = 1000$ kg/m^3)

- Flow temperature: T = 50 °C

The objective of the problem is to test the interaction of the body force terms with temporal and convective acceleration terms in the momentum formulation. A temporal acceleration exists in the initial part of the transient and the initial uniform volume fraction profile is convected out of the system as the fluid accelerates through the solution domain. These features test the void propagation characteristic and stability of the numerical solution method. The diffusive character of the numerical method is also tested since a discontinuity in void fraction is propagated through the solution space and the extent that the discontinuity is smeared can be quantitatively established.

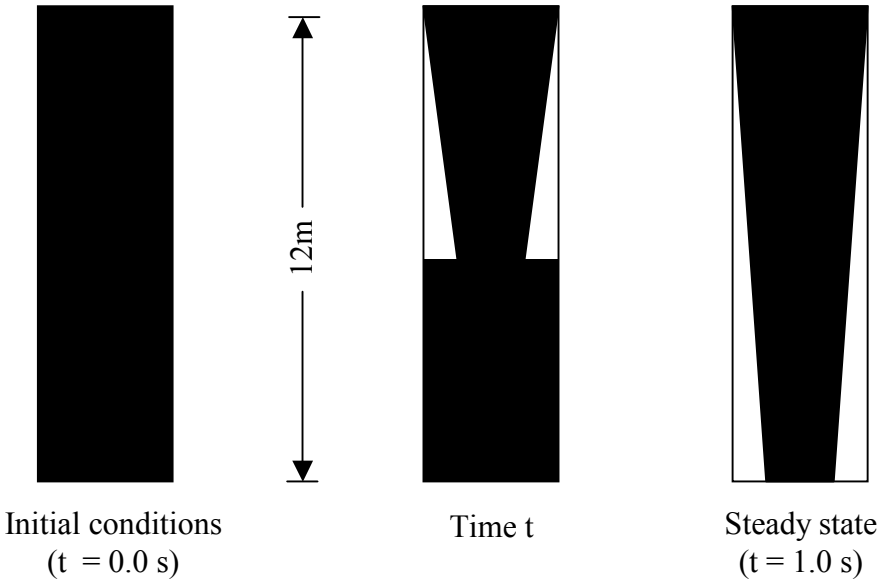

Figure 3-11: Schematic of the water faucet test case

The incompressible two-fluid model (PFM-2), in which both wall friction and interfacial friction are omitted, was used to simulate this test case, and the numerical results obtained from this model will be compared to the simple analytical solution that will be presented in Section 3.8.2.3.

3.8.2.2 Initial & Boundary Conditions

Initially (t = 0 s), the tube is filled with a uniform column of water at velocity of 10 m/s surrounded by a stagnant gas (V_{G0} = 0 m/s), such that the gas volume fraction is 0.2. The thermodynamic properties of system at the initial state are assumed constant at values appropriate for air-water mixture and are 50°C for the temperature and 1 bar for the pressure.

The boundary conditions at the inlet or top of the tube are similar to the initial input data, and are given as:

- Inlet gas void fraction = 0.2
- Inlet liquid velocity = 10 m/s
- Inlet gas velocity = 0 m/s

The only outflow boundary condition at the bottom of the tube is constant atmospheric pressure (1 bar). However, because we use the incompressible two-fluid model to simulate this problem, we do not enforce explicitly this condition, but consider the bottom of the tube as an open boundary for the conservative variables used by the model.

3.8.2.3 Analytical Solution

Transient

The fact that the transient solution of the water-faucet has a particularly simple analytical expression has made this test case one of the most popular test-beds for validating numerical methods for two-phase flow models. This transient analytical solution is derived in this section, by assuming that the liquid phase is incompressible and that pressure variation terms in the liquid phase are ignored.

Moreover, with the additional assumptions of no wall and interfacial friction, the liquid-phase momentum equation, resulting from equation (2.2), only contains nonzero terms for the temporal and spatial acceleration and the body force, and it is given by:

$$\frac{\partial V_L}{\partial t} + V_L \frac{\partial V_L}{\partial x} = g \tag{3.33}$$

Assuming no mass transfer, the associated differential equation for the liquid phase volume fraction is established from continuity considerations (2.1) and is expressed as:

$$\frac{\partial R_L}{\partial t} + V_L \frac{\partial R_L}{\partial x} + R_L \frac{\partial V_L}{\partial x} = 0 \tag{3.34}$$

The solution for the liquid velocity and volume fraction response can be obtained in closed form since Equation (3.34) is a single hyperbolic partial differential equation having real characteristics. The characteristic curves are defined by:

$$dx = V_L dt \tag{3.35}$$

which is the path of a liquid particle, and along this path, Equation (3.33) can be integrated directly to obtain the following expression for the liquid velocity:

$$V_L = V_{L0} + g(t - t_0) \tag{3.36}$$

Where V_{L0} is the initial or boundary velocity corresponding to the point x_0, t_0. The corresponding length coordinate along the particle path is obtained by integration of Equation (3.35) and using the liquid velocity relation (3.36) giving the following relation.

$$x = x_0 + V_{L0}(t - t_0) + \frac{g}{2}(t - t_0)^2 \tag{3.37}$$

Using the solution for the velocity, Equation (3.34) can be integrated to obtain the solution for the liquid fraction along the characteristic curve. In this case two possible solutions are obtained, the first applies if the initial point of the characteristic curve lies on the $t_0 = 0$ (initial value) curve and is:

$$R_L = R_{L0} \tag{3.38}$$

The second corresponds to cases where the initial point on the characteristic curve lies on the $x_0 = 0$ boundary. In this case the liquid volume fraction is given by:

$$R_L = R_{L0}\left[\frac{V_{L0}}{V_{L0} + g(t - t_0)}\right] \tag{3.39}$$

Solving the preceding equations (3.37) and (3.39) to eliminate $(t\text{-}t_0)$, we get the following expression:

$$x = x_0 + \frac{V_{L0}^2}{g}\left[(R_{L0}/R_L - 1) + 0.5(R_{L0}/R_L - 1)^2\right] \tag{3.40}$$

which gives the following liquid holdup and velocity relations:

$$R_L = \frac{R_{L0}V_{L0}}{\sqrt{V_{L0}^2 + 2g(x - x_0)}} \tag{3.41}$$

$$V_L = \sqrt{V_{L0}^2 + 2g(x - x_0)} \tag{3.42}$$

The above liquid holdup and velocity expressions (3.41) and (3.42) are also steady state solutions and can be easily obtained by neglecting the temporal variations in the continuity and momentum equations (3.34) and (3.33). In this case, the initial values (with subscript 0 in this section) are replaced by the inlet boundary values.

To summarize, combining relations (3.36) – (3.38), and equations (3.41) - (3.42) give the following transient solution:

$$R_L(x,t) = \begin{cases} \dfrac{R_L^{inlet} V_L^{inlet}}{\sqrt{\left(V_L^{inlet}\right)^2 + 2g\left(x - x^{inlet}\right)}} & x \le x^{inlet} + V_L^{inlet} t + \dfrac{g}{2} t^2 \\ R_L^{inlet} & \text{otherwise} \end{cases} \tag{3.43}$$

$$V_L(x,t) = \begin{cases} \sqrt{\left(V_L^{inlet}\right)^2 + 2g\left(x - x^{inlet}\right)} & x \le x^{inlet} + V_L^{inlet} t + \dfrac{g}{2} t^2 \\ V_L^{inlet} + gt & \text{otherwise} \end{cases} \tag{3.44}$$

The term x^{inlet} represents the location of the pipe inlet and is generally set to zero; therefore, only specifying the inlet liquid velocity completes the above transient solution.

3.8.2.4 Numerical Results (PFM-2)

The numerical schemes described earlier in this chapter have been applied to the two-fluid incompressible model (PFM-2) in order to evaluate various numerical effects. All the computational results reported in this section were obtained with a CFL value of 0.5.

Scheme Comparison

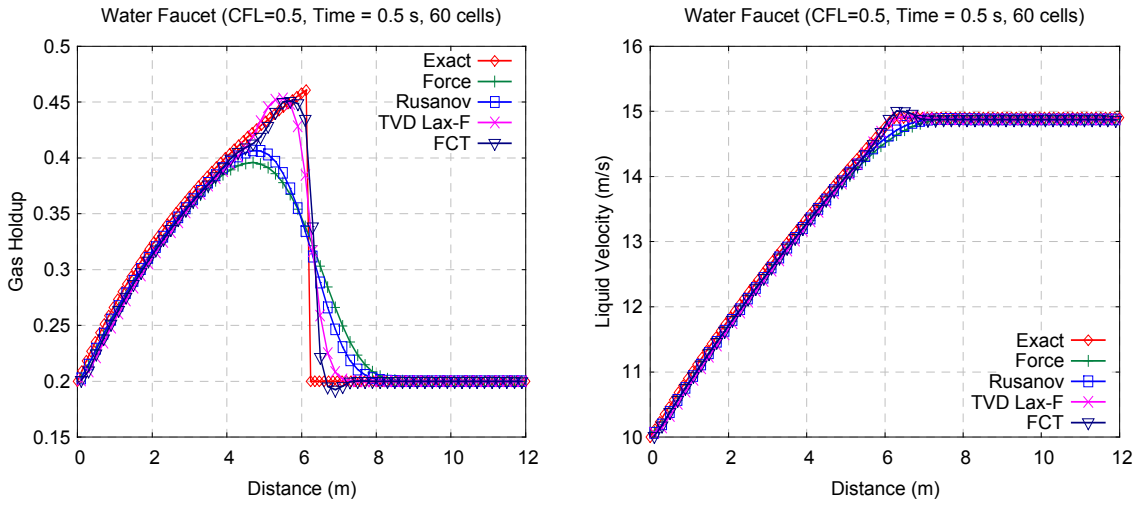

Figure 3-12: PFM-2 [Water Faucet]: Analytical comparison with various numerical schemes for the gas holdup (left) and liquid velocity (right) at time = 0.5 second.

Figure 3-12 presents the numerical results of the gas holdup and liquid velocity profiles, together with their analytical solutions, for four explicit solvers. The results obtained using 60 cells (Δx = 0.2 m) show that all the four numerical solvers accurately predict the liquid velocity profile, but for the gas volume fraction, the best looking results appear to be obtained with the first order schemes, namely Rusanov and Force, contrary to the findings of the previous case (IFP).

The results obtained with high-resolution schemes such as FCT or TVD Lax-Friedrichs (Figure 3-13) produced clearly visible overshoots before and after the front of the gas holdup discontinuity, resulting in a code crash for fine mesh simulations. We emphasize that these oscillatory spikes are not of numerical nature, but rather of mathematical nature, related to the ill-posedness or the non-hyperbolicity of the model used for this particular test case.

Therefore, the massive artificial viscosity embedded in the first order schemes only hide the mathematical instability visible in Figure 3-13, and it is expected that for very fine meshes, the first order schemes will exhibit a similar behaviour to the more accurate high-resolution schemes.

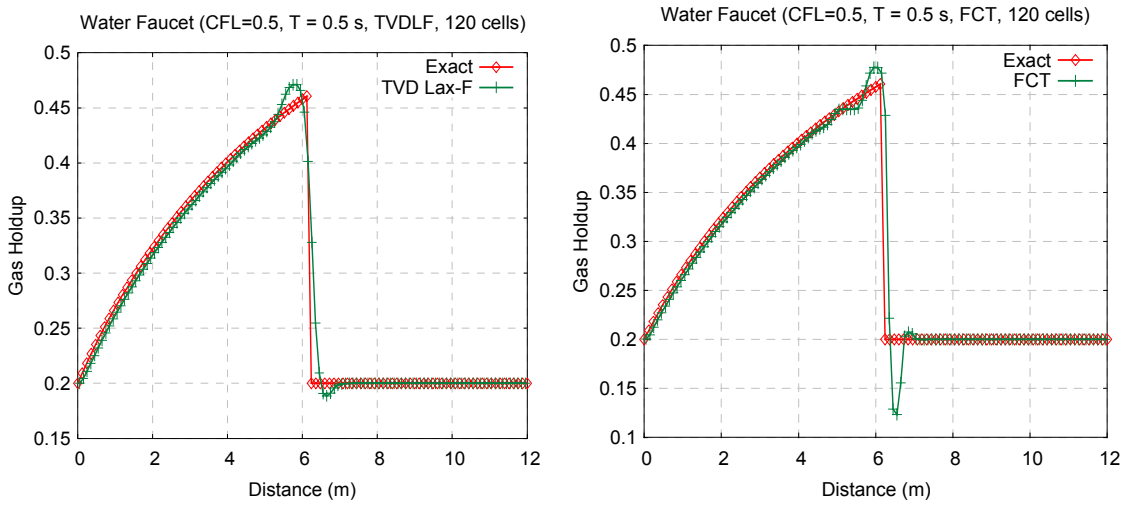

Figure 3-13: PFM-2 [Water Faucet]: Analytical comparison with high-resolution schemes (TVD Lax-F and FCT) for the liquid holdup at time = 0.5 second.

Mesh Refinement

Figure 3-14 shows a grid convergence study of the gas void fraction profile, at time = 0.5 second, computed with the Rusanov scheme. The plot shows typical first order behaviour in terms of spatial accuracy, and bears very close resemblance to Toumi (1995) and Paillere et al. (2003) results that were obtained using two-fluid pressure based models and respectively an approximate Riemann solver and a flux vector splitting solver named AUSM+ (Advection Upwind Splitting Method) as numerical schemes.

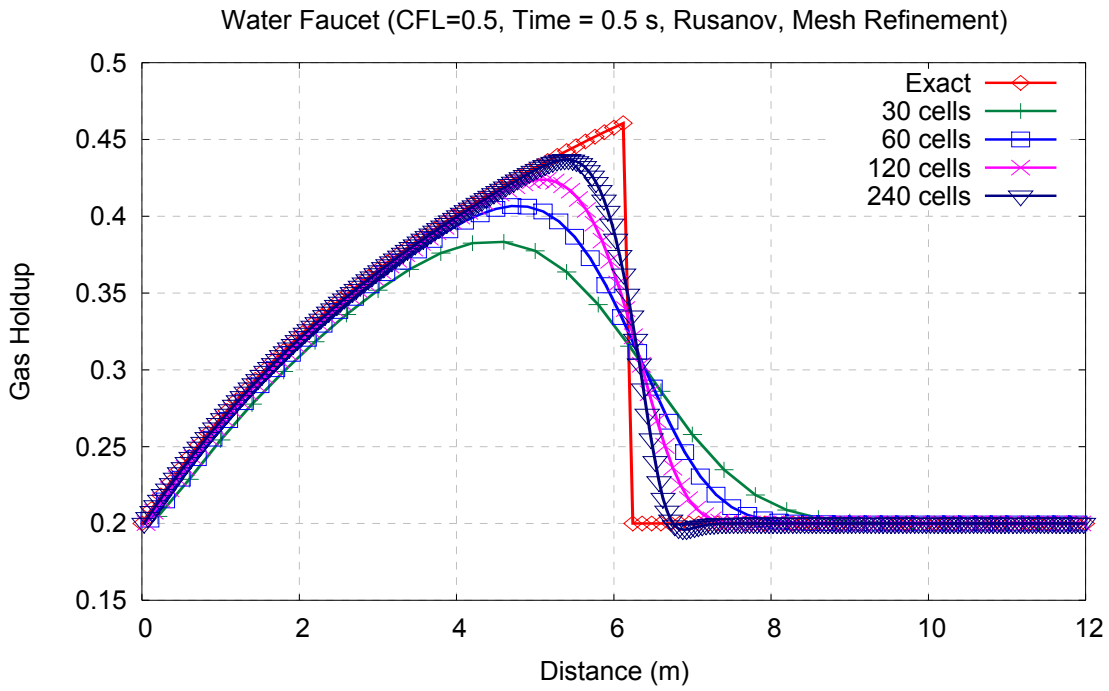

Figure 3-14: PFM-2 [Water Faucet]: Mesh Refinement for the gas holdup at time = 0.5 second, using the first order Rusanov scheme.

As already mentioned, a very small and almost invisible overshoot appears in Figure 3-14 for 240 cells. If we were to plot the results for finer meshes (i.e. 1200 cells) like some researchers in the literature, then bigger overshoots similar to the ones in Figure 3-13 will be visible in the numerical solutions.

Flow Evolution

The calculations were carried out for a range of time-step size in order to demonstrate the temporal convergence of the numerical schemes. For the specific initial and boundary conditions simulated, a steady state solution is theoretically attained in 0.85 second, when the void fraction discontinuity reaches the pipe outlet, thus the calculations were carried out to at least 1.0 second to also test the numerical convergence to steady state.

Figure 3-15 presents the time evolution of the gas void fraction (top) and the liquid velocity (bottom) profiles obtained using the first order scheme Force with 200 cells. An agreement with the analytical solutions is observed, proving the ability of the numerical scheme to correctly predict the flow features for the water faucet problem. The acceleration of the liquid velocity is also clearly visible in Figure 3-15, starting from 10 m/s at the inlet to more than 18 m/s at the outlet at “steady state”.

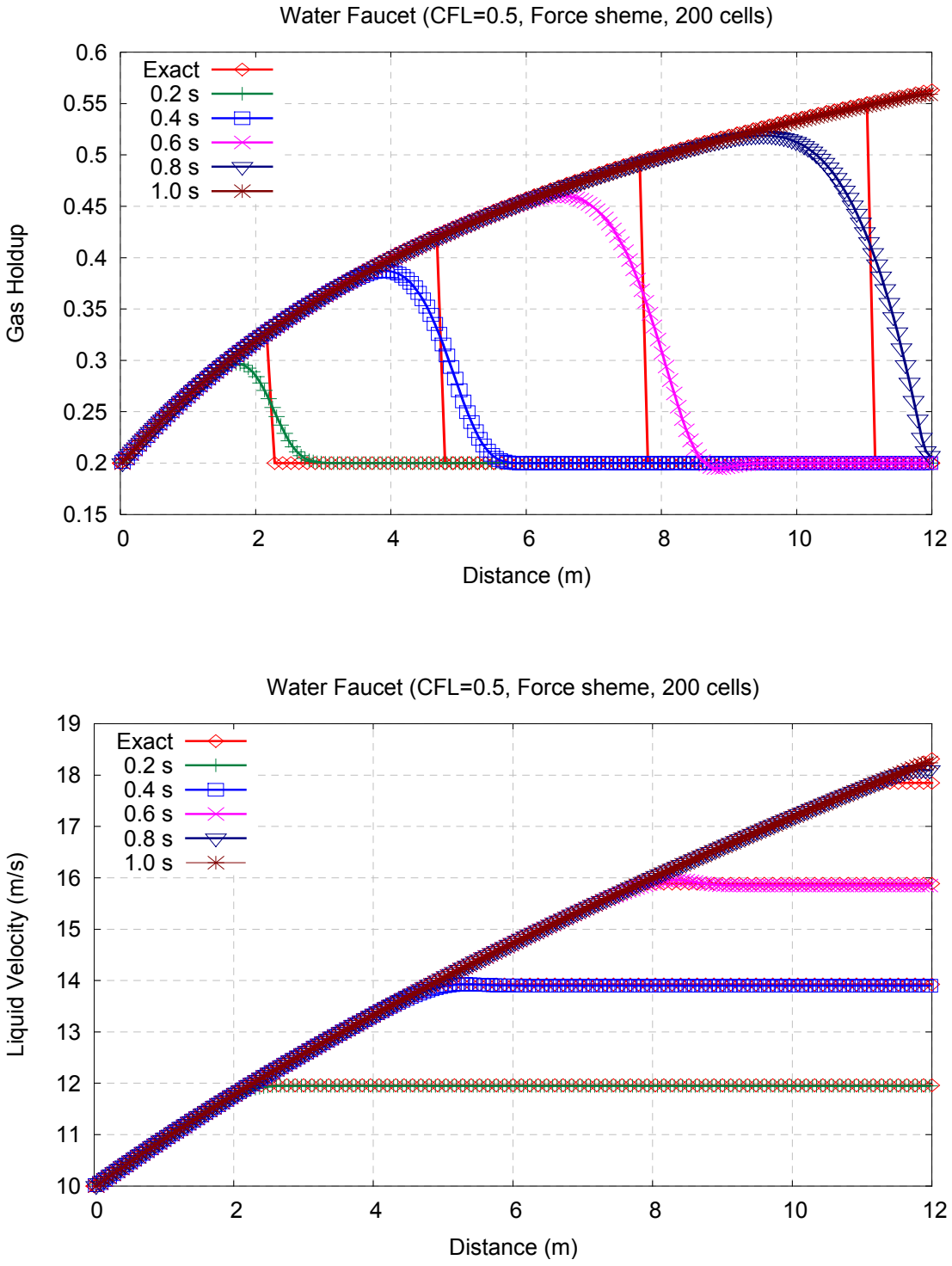

Figure 3-15: PFM-2 [Water Faucet]: Time evolution of the gas holdup (top) and liquid velocity (bottom) using the first order centred scheme (Force) with 200 cells.

3.8.3 Stratified Flow Case

3.8.3.1 Problem Summary

A horizontal duct is divided into two equal length parts by a diaphragm; each part contains water and air, the former lying below the latter. The depth of the water is somewhat greater on the left of the diaphragm than on the right. The problem is illustrated schematically in Figure 3-16, and its specifications are given as:

- Length of the horizontal pipe: 10 m
- Diameter of the horizontal pipe: 1 m
- Operating fluids: air and water (ρ_G = 1.16 kg/m^3, ρ_L = 1000 kg/m^3)
- Atmospheric flow conditions: (T = 20 $^\circ$C, P = 1 bar)

The objective of the simple case proposed by Youngs (1987) is to assess the ability of the model and numerics to predict stratified wave structures, which is one of the primary goals of this study. At the beginning of the simulation, the diaphragm is supposed suddenly to break; the task is then to calculate what happens during the next few seconds, during which the water and air are set in motion, in opposite directions, as gravity waves travel from the diaphragm-rupture point towards the two ends.

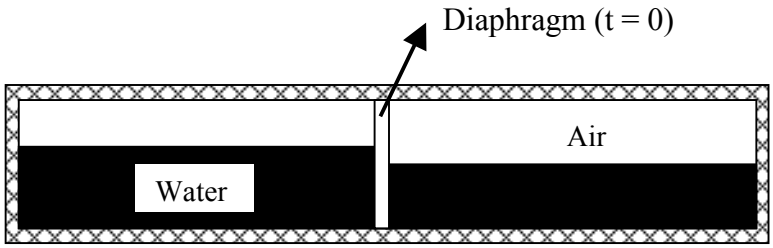

Figure 3-16: Schematic diagram of the stratified flow problem

The two–fluid incompressible model (PFM-2) is used, but without allowance for the interfacial friction between the phases. The wall friction between the fluids and the pipe wall is also neglected, suppressing the momentum transfer between the phases. However, the effects of gravity are accounted for by way of the appropriate sources in the momentum equations for the two fluids. These sources are obtained from the presumption that the pressure variation in the vertical direction is hydrostatic, and account for the influence of the cross-sectional shape is taken into consideration.

In the original paper Youngs (1987) considered two cases, differing in respect of the postulated cross-section of the duct. In the first case, the cross-section is square, whereas in

the second case it is circular. And though an analytical solution [Kurasaki & Spalding, 1979] based on the shallow water theory exists for the square cross-section, in this study, we only consider the circular cross-section case, because all the mathematical models developed in this study assumed a circular duct shape by default. Therefore, for comparative purposes, our numerical results will be assessed in relation to the other numerical results presented by others researchers in the literature.

3.8.3.2 Initial & Boundary Conditions

The volume fraction of water on the left-hand side of the diaphragm is 0.51, and that on the right hand side is 0.49. Initially, both fluids are at rest ($V_L = V_G = 0$ m/s); and the pressure in the air is at atmospheric conditions on both sides of the diaphragm.

For the boundary conditions, the duct is closed at both ends; this forces the velocities of the two fluids to be zero at the two ends of the duct ($V_L = V_G = 0$ m/s at x = 0 and x =10 m).

3.8.3.3 Numerical Results (PFM-2)

Various numerical effects are presented in this section for the stratified test case. The computational results for the fluid volume fractions and velocities presented here are at different time steps with various grid cells, and all were performed using a CFL value of 0.5.

Scheme Comparison

Using 100 grid cells, we compare in Figure 3-17 the FCT and TVD Lax-Friedrichs results for the liquid holdup, the gas and liquid velocities versus the duct length. The graphs are shown for two time values, 5.0 s (left) and 10.0 s (right), and we can see from the figure that there is very little difference between these two high-resolution schemes for the liquid holdup.

However, for the fluid velocities the differences are clearly visible with the FCT scheme providing the most accurate predictions in both simulations. For both the gas and liquid, the absolute peak velocity is more than twice in the case of the FCT compared to the TVD Lax-Friedrichs scheme. This is undoubtedly due to huge amount of numerical viscosity or diffusion embedded in the latter scheme, justifying the selection of the FCT scheme as our preferred numerical method for the incompressible two-fluid model.

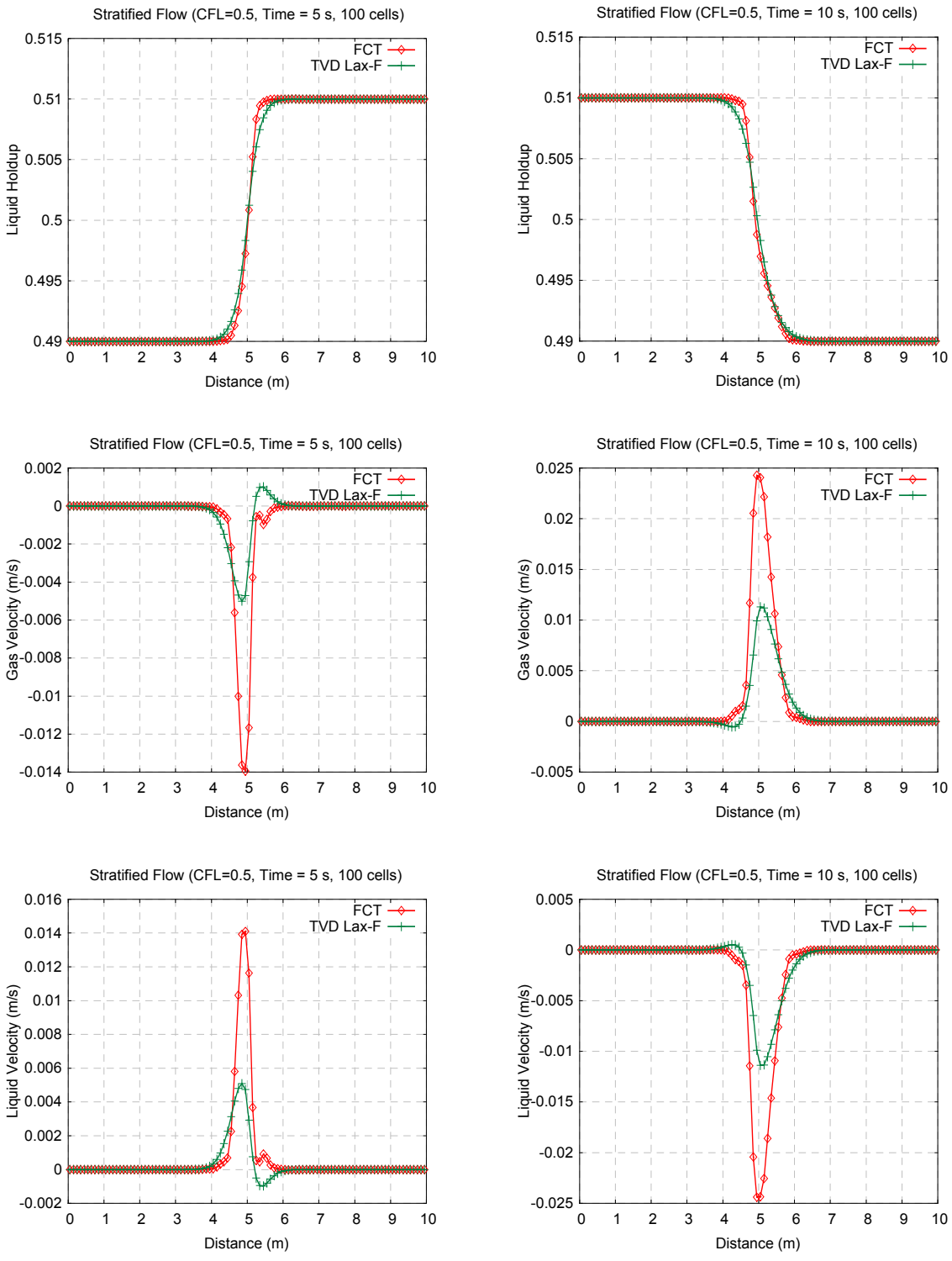

Figure 3-17: PFM-2 [Stratified Flow]: Comparison of FCT and TVD Lax-Friedrichs schemes for the liquid holdup (top), the gas velocity (middle) and the liquid velocity (bottom) at time = 5.0 s (left) and time = 10.0 s (right).

Mesh Refinement

In Figures 3-18 and 3-19, we present the effect of spatial refinement for the most diffusive of the high-resolution schemes that we implemented (TVD Lax-Friedrichs), and as expected, we found that the results are more accurate for finer meshes.

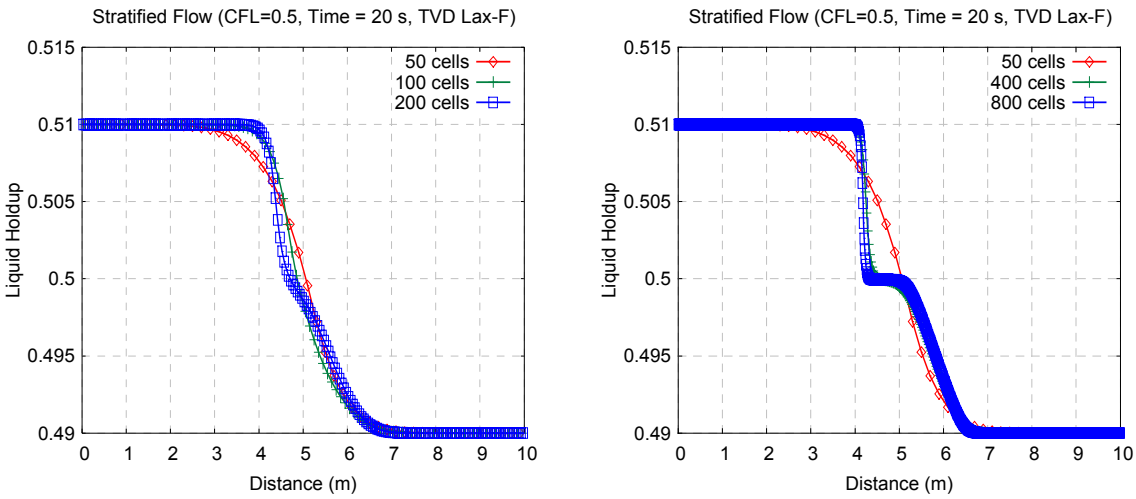

Figure 3-18: PFM-2 [Stratified Flow]: Mesh refinement for the liquid holdup at time = 20 seconds using the high-resolution scheme TVD Lax-Friedrichs.

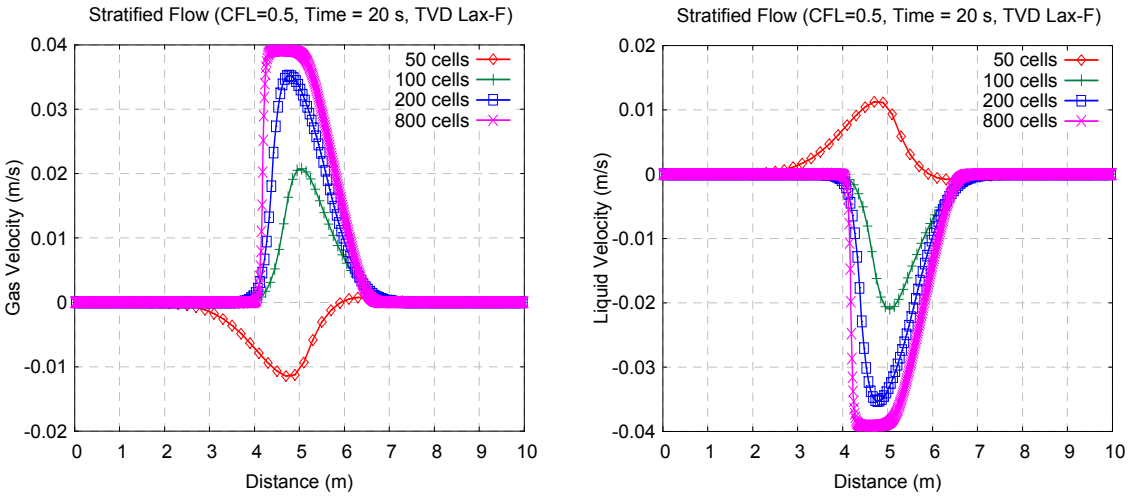

Figure 3-19: PFM-2 [Stratified Flow]: Mesh refinement for the gas (left) and liquid (right) velocities at 20 seconds using the TVD Lax-Friedrichs scheme.

Figure 3-18 shows the liquid holdup at 20 seconds for various mesh sizes, and we can see that there is no difference in the profile between 400 and 800 cells, proving that the numerical scheme has converged to a reliable solution. This figure also shows that for these two finer meshes, there is a step change or sort of contact discontinuity in the holdup profile, which is not visible with coarser meshes for which the high artificial viscosity smoothes the holdup profile near the discontinuity, thereby suppressing the step change feature.

Figure 3.19 presents the gas and liquid velocities, also at 20 seconds, for various mesh sizes, and we can see that from 100 cells onward, the prediction pattern is similar to the one observed with the holdup profile, where we had an improved accuracy for finer meshes. However, with the coarsest mesh (50 cells), we observed a very peculiar behaviour, where the discontinuity wave appears in the opposite direction to what it is expected, emphasizing once again the importance of carefully selecting the mesh size for a particular simulation.

Flow Evolution

To demonstrate the temporal convergence of the FCT scheme for the stratified case, we carried out simulations using various times, and the results obtained are summarized in Figure 3-20 for the liquid holdup and in Figure 3-21 for the gas and liquid velocities. These results are in agreement with the ones presented in the literature [Youngs, 1987], which revealed alternating profiles every five seconds for all the flow parameters (holdup and velocities) shown here.

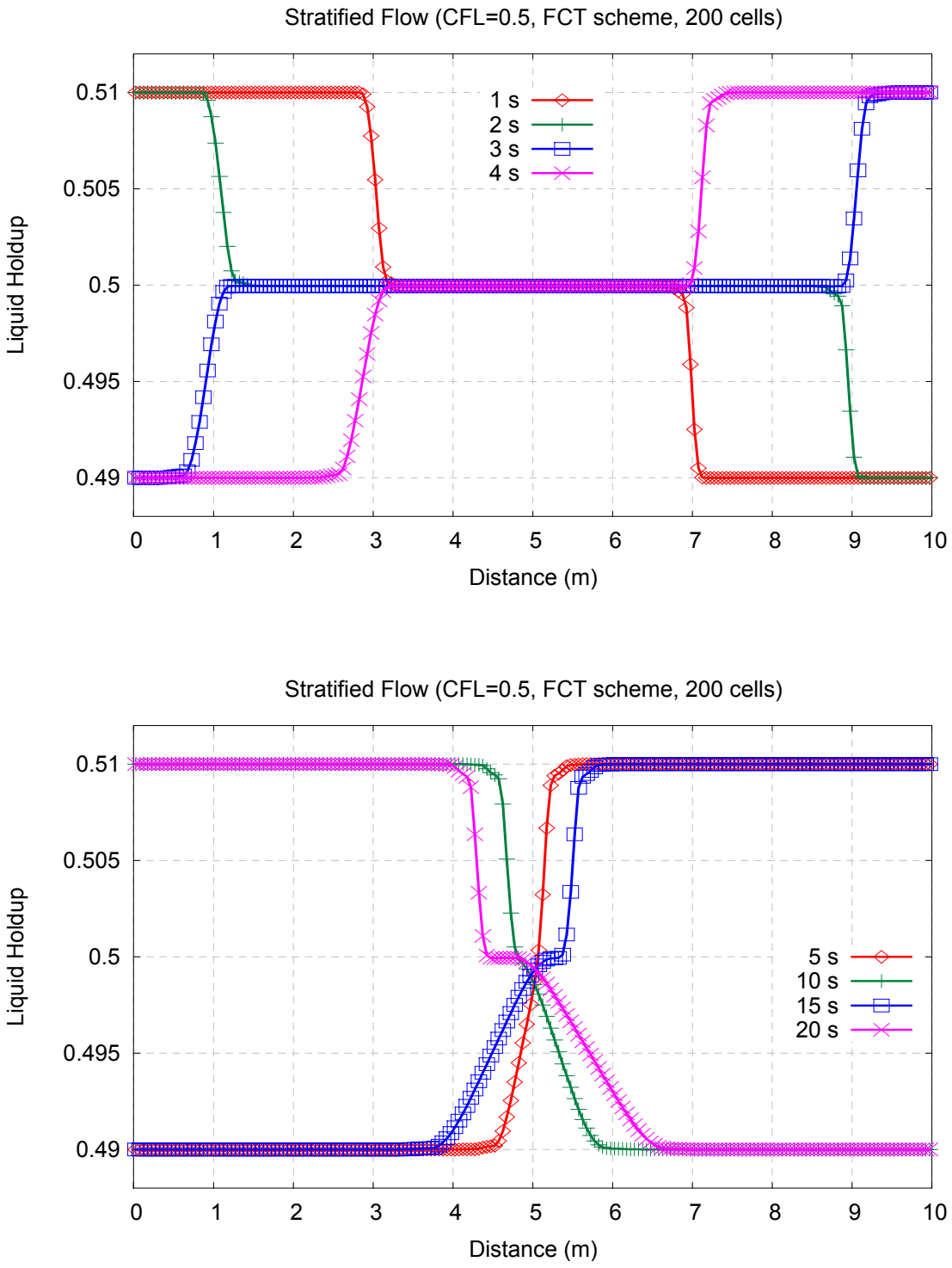

Figure 3-20: PFM-2 [Stratified Flow]: Time evolution of the liquid holdup using the TVD Lax-Friedrichs scheme with 200 grid cells.

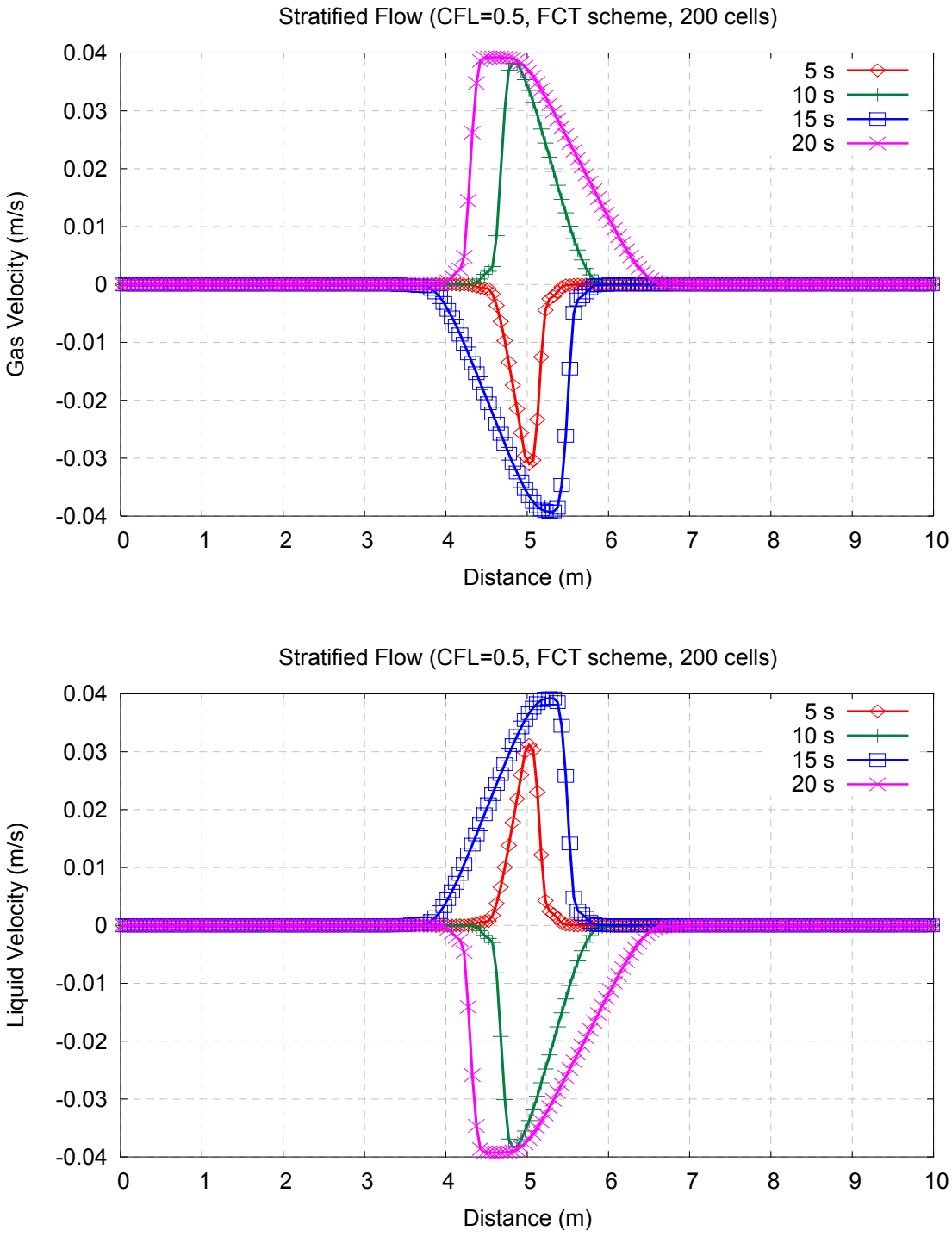

Figure 3-21: PFM-2 [Stratified Flow]: Time evolution of the gas (top) and liquid (bottom) velocities using the TVD Lax-Friedrichs scheme with 200 grid cells.

3.8.4 Sedimentation Case

3.8.4.1 Problem Summary

The problem consists of a long vertical pipe initially filled with stationary gas and liquid in a fully homogeneous mixture. As time proceeds, gravity acts downwards, and particles of light fluid rise and particles of dense fluid fall. Eventually, the dense phase collects at the bottom of the pipe and the light fluid collects at the top of the pipe.

The problem is illustrated schematically in Figure 3-22, and its specifications are given as follows:

- Length of the vertical pipe: 7.5 m
- Diameter of the vertical pipe: 1 m
- Operating fluids: air and water (ρ_G variable, $\rho_L = 1000$ kg/m^3)
- Atmospheric flow conditions: ($T_{inlet} = 20\ ^{\circ}C$, $P_{outlet} = 1$ bar)

The primary objective of this test case is to evaluate the single-pressure model (SPM-4) numerical scheme described earlier in the chapter. The computational results are sensitive to numerical diffusion in the volume fraction equations if incompressible flow is assumed. Hence, this problem provides a good test for the prediction abilities of the SPM-4 numerics that we have implemented.

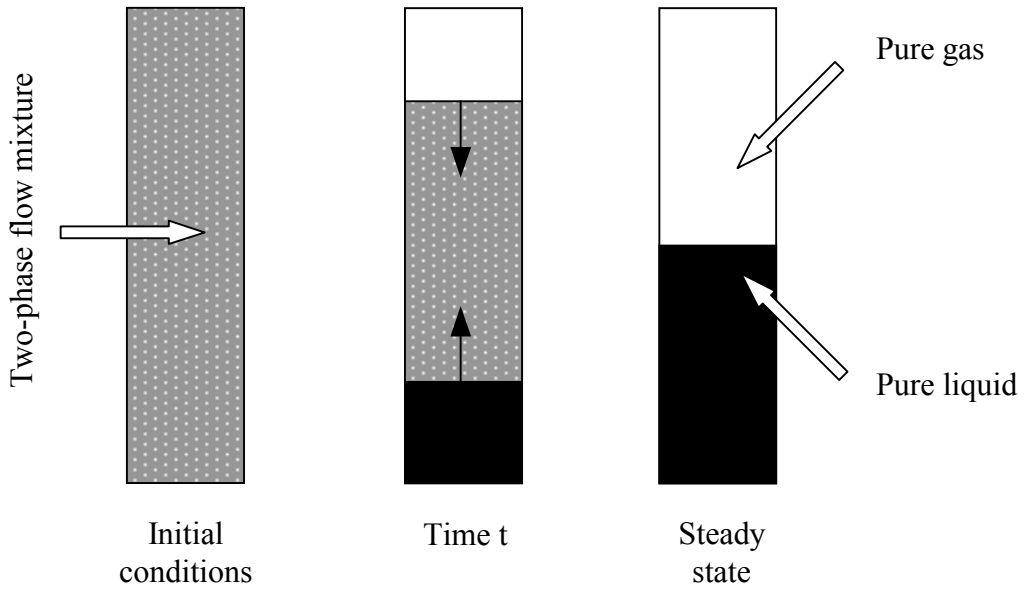

Figure 3-22: Schematic diagram of the sedimentation problem

Analytical Solution

Youngs (1987) who also proposed this test case stated that when the two fluid densities ρ_G and ρ_L are chosen to be almost equal, an analytical solution exits. However, the expression of this exact solution was not provided, therefore, air and water are used here as fluids similarly to Coquel et al. (1997) and Paillère et al. (2003), and our results will be compared to ones of these later researchers.

3.8.4.2 Initial & Boundary Conditions

At the beginning of the simulation (time = 0), the two fluids are at rest everywhere in the vertical pipe [V_G (x) = V_L (x) = 0 m/s], such that the gas volume fraction is 0.5. The thermodynamic properties of system at this initial state are assumed constant at atmospheric conditions (20°C for the inlet temperature and 1 bar for the outlet pressure).

These initial thermodynamics properties are the same throughout the simulation, as for the other boundary conditions, the duct is closed at both ends, forcing gas and liquid velocities to be null at the ends of the duct ($V_L = V_G = 0$ m/s at x = 0 and x =7.5 m).

3.8.4.3 Numerical Results (SPM-4)

In order to evaluate various numerical effects, a combination of the TVD Lax-Friedrichs scheme (3.12) and the MinMod-2 scheme (3.15) has been applied to the single pressure model (SPM-4), respectively for the conservative and non-conservative terms of the system. The computational results of these effects for the sedimentation test case are presented in this section, where all the simulations were performed using a stable CFL value of 0.5, and neglecting the wall and interfacial frictions.

Mesh Refinement

Figure 3-23 summarises the behaviour of the gas holdup profile obtained using our combined TVD Lax-Friedrichs / MinMod-2 scheme with different grid sizes. The results shown are a little bit diffusive in general, but the finer the mesh size is, the more accurate is the solution of the two-fluid model, evidence of a well-behaved numerical method.

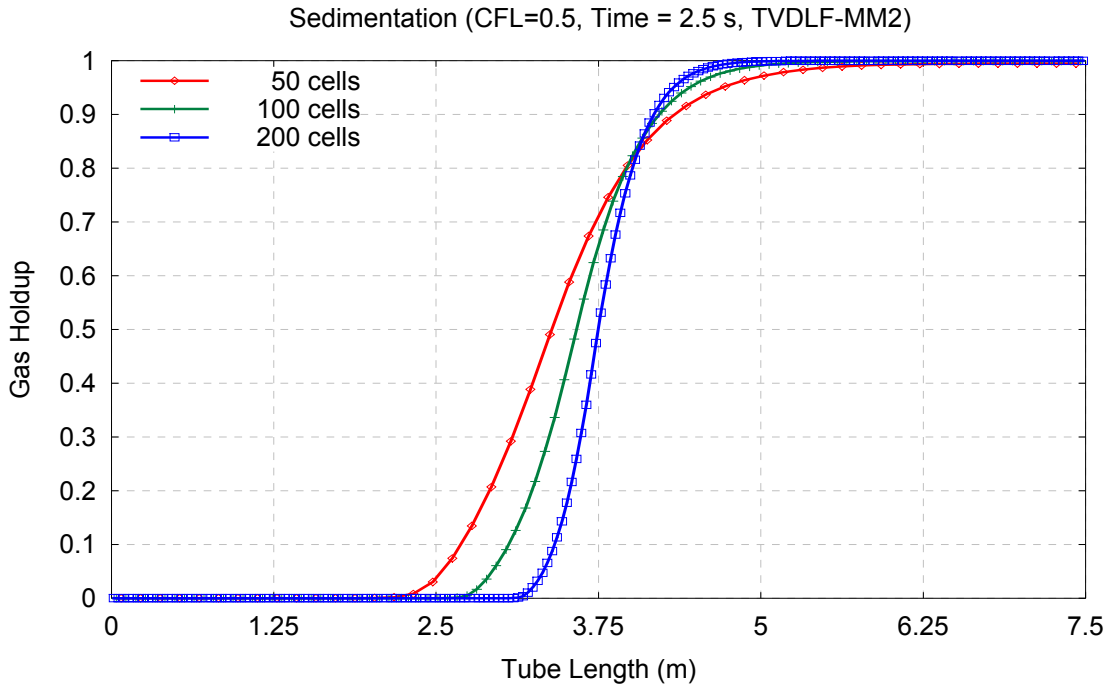

Figure 3-23: SPM-4 [sedimentation]: Mesh Refinement for the gas holdup at 2.5 seconds using the combination TVD Lax-Friedrichs and Minmod-2 schemes.

Flow Evolution

In Figure 3-24, we present the time evolution of the gas holdup at different times using the combined TVD Lax-F/ MinMod-2 scheme with 200 grid cells. These results are in good agreement with those described in the literature [Coquel et al., 1997; Paillère et al., 2003], and show that as the time increases, the initially mixed two phases evolve naturally toward full separation with the denser fluid on the bottom half of the vertical tube and lighter fluid on the top half. And after 2.5 seconds, the gas holdup profile can be considered as the steady state solution where the gas and liquid phases are well separated, with a void fraction below 0.01 in the region of ‘‘pure’’ water, and a void fraction above 0.99 in the region of pure air.

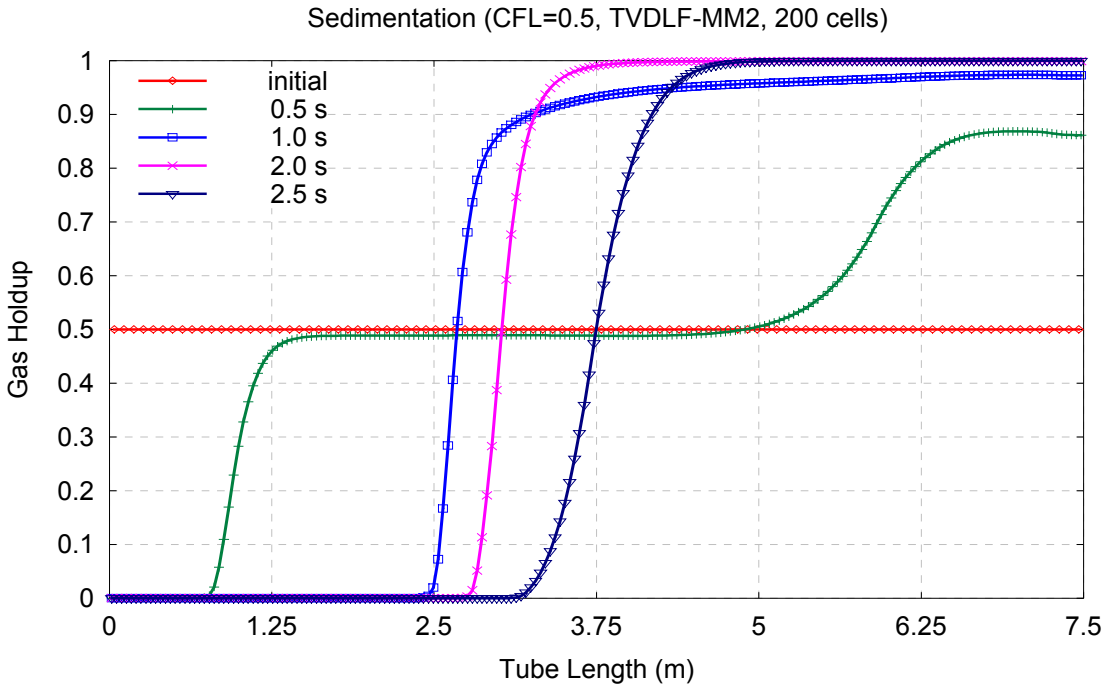

Figure 3-24: SPM-4 [sedimentation]: Time evolution of the gas holdup profile using the combined TVD Lax-Friedrichs / Minmod-2 scheme with 200 grid cells.

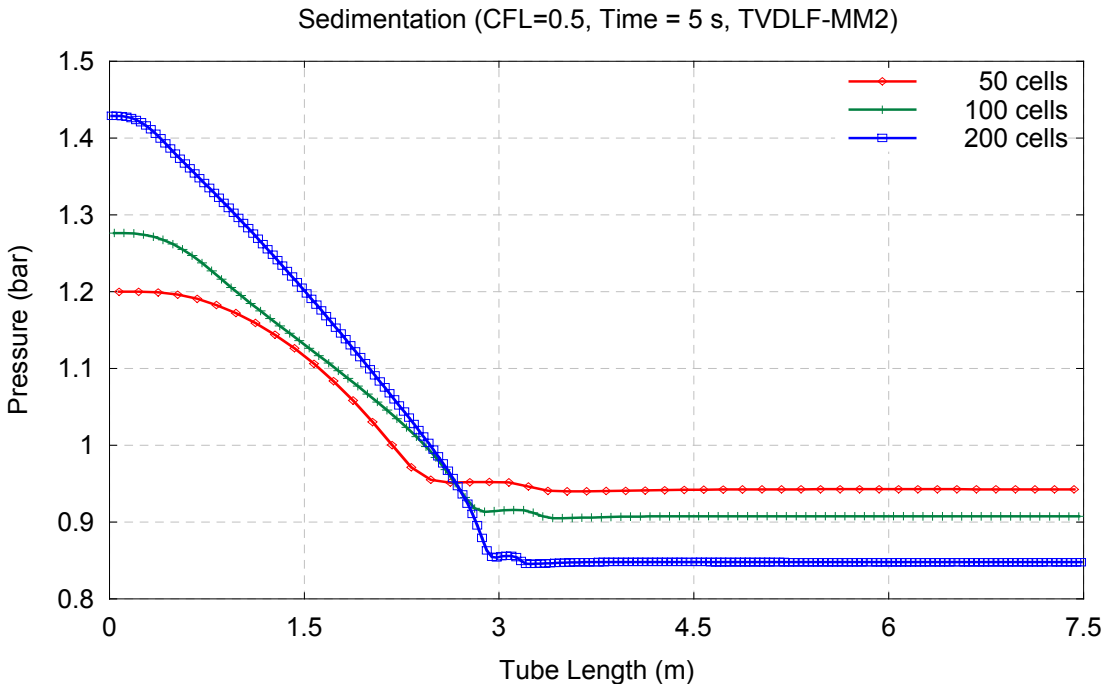

Figure 3-25: SPM-4 [sedimentation]: Steady state profile for pressure using the combined TVD Lax-Friedrichs / Minmod scheme with various mesh sizes.

Steady State Results

When the interfacial friction factor is neglected, Youngs (1987) stated that the steady state solution of the sedimentation case is reached after 4.0 seconds, we therefore present in Figure 3-25 the pressure profile from our model obtained after 5.0 seconds. Although, there is a 15% deviation between the atmospheric pressure at the pressure value in the gas region, we found that the numerical scheme developed for our two-fluid compressible model computes fairly well the theoretical hydrostatic pressure profile in the liquid region (peak theoretical pressure value is roughly equal to $\rho_L\, g\, h_L + P_{initial} = 1.37$ bar).

The single-pressure model (SPM-4) was developed as an improvement of the incompressible model, and though its current implementation appears robust and accurate, more test cases are necessary to fully validate this complex model.

3.9 Conclusion

We presented in this chapter the finite difference numerical approach that we have adopted for solving the two-phase gas-liquid models mentioned in the previous chapter, and described in detail the numerical schemes that we have implemented and investigated, during the course of this work. We also validated these schemes with both simple single-phase and two-phase flow cases, and the results presented in various figures in this chapter, clearly show that first order schemes such as Lax-Friedrichs or Rusanov are too dissipative, while the second-order Ritchmyer is too dispersive in the neighbourhood of the shock. These facts, which have been known for a long time in the single-phase flow community and reported in many numerical textbooks, are more disturbing for two-phase flow models and generally lead to non-converging solutions or total disappearance of key flow features.

On the other hand, the high-resolution schemes FCT and TVD Lax-Friedrichs work well for our two-phase flow models, and are able to capture strong discontinuities in the flow with a high accuracy. A comparative study of high-resolution schemes presented by Yang & Przekwas (1992), shows that the FCT scheme is one of the most competitive for flows with severe gradients, and the small modification made to this scheme in this work, has proven that our implemented version is very robust and accurate for the conservative models such as the homogeneous model (HEM-3) or the incompressible two-fluid model (PFM-2). It is therefore our default scheme that we advocated for these models. However, for the single-pressure model (SPM-4), the presence of non-conservative terms makes it difficult to use the predictor-corrector FCT scheme and we found that the combined TVD Lax-Friedrichs / MinMod-2 scheme will provide fairly good results.

3.10 References - 3

- **Barmin A. A., Kulikovskiy A. G., and Pogorelov N. V., (1996)** "Shock-Capturing Approach and Nonevolutionary Solutions in Magnetohydrodynamics". *Journal of Computational Physics*, **126**, 77-90.

- **Benton E. R., & Platzman G. W., (1972)** "A Table of Solutions of the One-Dimensional Burgers Equation". *Journal of Applied Mathematics*, **30**, 195-212.

- **Book D. L., Boris J. P., and Hain K., (1975)** "Flux-Corrected Transport II. Generalizations of the Method". *Journal of Computational Physics*, **18**, 248-283.

- **Boris J. P., & Book D. L., (1973)** "Flux-Corrected Transport I. SHASTA, A Fluid Transport Algorithm That Works". *Journal of Computational Physics*, **11**, 38-69.

- **Cockburn B., Lin S.-Y., and Shu C.-W., (1989)** "TVB Runge-Kutta local projection discontinuous Galerkin finite element method for conservation laws III: One-dimensional systems". *Journal of Computational Physics*, **84**, 90.

- **Coquel F., Amine K.E., Godlewski E., Perthame B., and Rascle P., (1997)** "A numerical method using upwind schemes for the resolution of two-phase flows", *Journal of Computational Physics*, **136**, 272-288.

- **Darwish M., & Moukalled F., (2001)** "A Unified Formulation of the Segregated Class of Algorithms for Multifluid Flow at All Speeds". *Numerical Heat Transfer*, Part B, **40**, 99-137.

- **Faille I. & Heintze E., (1999)** "A rough finite volume scheme for modelling two-phase flows in a pipeline". *Computers & Fluids,* **28**, 213-241.

- **Fletcher C. A. J., (1988)** "Computational Techniques for Fluid Dynamics: Specific techniques for Flow Categories", Volume 2. *Springer-Verlag*.

- **Harlow F. M., & Amsden A. A., (1975)** "Numerical Calculations of Multiphase Flow". *Journal of Computational Physics*, **17**, 19-52.

- **Harten A., (1983)** "High Resolution Schemes For Hyperbolic Conservation Laws". *Journal of Computational Physics*, **49 (3)**, 357-393.

- **Hirsch C., (1990)** "Numerical Computation of Internal and External Flows: Fundamentals of numerical discretization", Volume 2. *John Wiley & Sons*.

- **Issa R. I., & Kempf M. H. W., (2003)** "Simulation of slug flow in horizontal and nearly horizontal pipes with the two-fluid model". *International Journal of Multiphase Flow*, 29, 69-95.

- **Kurasaki M., & Spalding D. B., (1979)** "One-dimensional unsteady two-phase flows with interphase slip: A numerical study". *Proc. 2nd Multiphase Flow and Heat Transfer Symposium*, Miami Beach, USA.

- **Laney G. B., (1998)** "Computational Gasdynamics". *Cambridge University Press*.

- **LeVeque R. J., (1990)** "Numerical Methods for Conservation Laws", *Birkhäüuser*.

- **Louaked M., & Hanich L., (1998)** "TVD Scheme for the Shallow Water Equations", *Journal of Hydraulic Research*, **36 (3)**, 363-378.

- **Mahaffy J. H., (1982)** "A Stability-Enhancing Two-Step Method for Fluid Flow Calculations". *Journal of Computational Physics*, **46**, 329-341.

- **Omgba-Essama C., (1998)** "Parallel Computation of Multiphase Flow", 1st year annual review report, Applied Mathematics and Computing Group, Cranfield University, UK.

- **Omgba-Essama C., Hanich L., Thompson C. P., and Lezeau P., (2000)** "Adaptive Grid Refinement for Transient Two-Phase Flows". *AMIF-ESF Workshop, Computing Methods for Two-phase Flows*, Centre Paul Langevin, Aussois (Savoie) France, 12-14 January.

- **Paillere H., Corre C., and Garcia Cascales J. R., (2003)** "On the extension of the AUSM+ scheme to compressible two-fluid models". *Computers & Fluids*, **32**, 891-916.

- **Patankar S. V., (1981)** "Numerical Heat Transfer and Fluid Flow". *Hemisphere, New York*.

- **Press W. H., Flannery B. P., Teukolsky S. A., and Vetterling W. T. (1992)** "Numerical Recipes in Fortran: The Art of Scientific Computing". 2nd edition, *Cambridge University Press*.

- **Ransom V. H. (1987)** "Faucet flow, oscillating manometer, and expulsion of steam by sub cooled water". In G.F. Hewitt, J.M. Delhaye, and N. Zuber, editors, *Numerical Benchmark Tests, Multiphase Science and Technology, Volume 3*. Hemisphere Publishing Corporation.

- **Romate J. E., (2000)** "Developing a second-order TVD scheme for one-dimensional two-phase flow model". *AMIF-ESF Workshop – Computing Methods for Two-Phase Flow*, **Paper 22**, Aussois, France, January 12-14.

- **Saurel R., & Abgrall R., (1999)** "A Multiphase Godunov Method for Compressible Multifluid and Multiphase Flows". *Journal of Computational Physics,* **150**, 425-467.

- **Sod G. A., (1985)** "Numerical Methods in Fluid Dynamics: Initial and Boundary Value Problems". *Cambridge University Press*.

- **Spalding D. B., (1980)** "Numerical Computation of Multi-phase Fluid Flow and Heat Transfer", in C. Taylor and K. Morgan (eds.), *Recent Advances in Numerical Methods in Fluid*, **1**, 139-167.

- **Spalding D. B., (1983)** "Development in the IPSA Procedure for Numerical Computation of Multiphase-Flow Phenomena with Interphase Slip, Unequal Temperatures", in T. M. Shih (ed.), *Numerical Methodologies in Heat Transfer, Proc. Second National Symposium*, 421-436, Hemisphere, New York.

- **Stadtke H., Franchello G., and Worth B., (1994)** "Numerical Simulation of Multi-Dimensional Two-Phase Based on Hyperbolic Flow Equations", *European Two Phase Flow Group Meeting*, Piacenza, Italy, 6-8 June.

- **Stewart H. B., (1979)** "Stability of Two-Phase Flow Calculation Using Two-Fluid Models". *Journal of Computational Physics*, **33**, 259-270.

- **Tiselj I. & Petelin S., (1997)** "Modelling of Two-Phase Flow with Second-Order Accurate Scheme". *Journal of Computational Physics*, **136**, 503-521.

- **Toro E. F., (1997)** "Riemann Solvers and Numerical Methods for Fluid Dynamics". *Springer*.

- **Toth G. & Odstrcil D., (1996)** "Comparison of Some Flux Corrected Transport and Total Variation Diminishing Numerical Schemes for Hydrodynamic and Magneto-hydrodynamic Problems". *Journal of Computational Physics*, **128**, 82-100.

- **Toumi I., (1996)** "An Upwind Numerical Method for Two-Fluid Two-Phase Flow Models". *Nuclear Science Engineering*, **123**, 147-168.

- **Van Leer B., (1979)** "Towards the Ultimate Conservation Difference Scheme V, A Second-Order Sequel to Godunov's Method". *Journal of Computational Physics*, **32**, 101-136.

- **Watson M., (1990)** "Non Linear Waves in Pipeline Two-Phase Flows", Proceedings of the 3rd International Conference on Hyperbolic Problems, Uppsala, Sweden, (June 1990), Studentliterratur, Lund.

- **Wendt J. F., (1996)** "Computational Fluid Dynamics: An Introduction", 2nd edition, *Springer*.

- **Whitham G. B., (1974)** "Linear and Non Linear Waves", *John Wiley & Sons*, Inc.

- **Yang H. Q., & Przekwas A. J., (1992)** "A Comparative Study of Advanced Shock-Capturing Schemes Applied to Burger's Equation". *Journal of Computational Physics*, **102**, 139-159.

- **Yee H., (1989)** "A class of high-resolution explicit and implicit shock-capturing methods". *Von Karman Institute for Fluid Dynamics*, Lecture Series **1989-04**.

- **Youngs D. L., (1987)** "Numerical Benchmark Tests". In G.F. Hewitt, J.M. Delhaye, and N. Zuber, editors*, Multiphase Science and Technology, Volume 3*. Hemisphere Publishing Corporation.

4 Chapter 4 - Adaptive Mesh Refinement (AMR)

4.1 Introduction

Multiphase flows encountered in transportation pipelines generally exhibit multiscale physical phenomena that are extremely difficult to simulate. These flows are time varying in nature with the local phase content and velocity varying with time and position due to turbulence and the passage of the interface. An extreme case of such variations is that of slug flow, which will be studied in Chapter 6, and which is characterized by alternating liquid and gas continuous zones passing along the pipe.

Chapter 6 will show that by using shock-capturing schemes presented in the previous chapter, and very high grid resolution, it is possible to overcome the numerical design difficulties associated with such complex flows. However, it will also be clear that there are often large portions of the flow where a fine grid resolution is not needed. Thus, using a uniform and highly refined grid in these regions represents a tremendous waste of computational effort. In addition, limitations on computational resources often force a compromise on grid resolution, resulting in inaccurate description of some flow features.

Furthermore, the fine grid resolution approach is not computationally attractive for flows in long industrial pipelines, as the number of nodes per unit of length required for these flows is typically one or two order of magnitude greater than the number per unit length used in commercial calculations, therefore a better resolution technique is needed to deal with such flows. In this chapter, we present the **a**daptive **m**esh **r**efinement (**AMR**) scheme, which has been developed to simulate fluid flows with disparate localised and moving features at low cost.

AMR techniques attempt to match the local resolution of the computational grid to the requirements of the local flow solution, by locally and automatically modifying the computational grid. Thus, very fine mesh cells are precisely concentrated and restricted to regions where they are needed, and elsewhere the computational grid may be quite coarse. Such a strategy can dramatically reduce the computational effort required to perform simulations of problems that contain disparate physical length scales. Quirk (1991) estimated, for example, the duration of a detonation simulation to more than two years using an appropriate uniform mesh, whereas a good adaptive mesh refinement will just take seven hours.

4.2 Chapter Outline

Compared to non-adaptive schemes, AMR schemes are undeniably complicated; they contain many elements, which require careful co-ordination. However, because the potential savings are so large, a wide variety of strategies have been developed. Therefore, this chapter starts by a short review of adaptive mesh schemes, and the reasons, which motivate the code AMR paradigm, are explained.

The main objective of this chapter being to explain the methodology and intricacies of the AMR algorithm that we have implemented, the majority of our description will be dedicated to this purpose. Hence, the chapter carries on by a presentation of the principles or premises of the Berger's AMR strategy that was chosen. Then, follows a lengthy description of the two most important features of any mesh refinement scheme, which are its hierarchical grid data structure and the refinement process itself. Next we present two interesting consequences of the inter-grid communication, namely the boundary conditions and the mass conservation process.

The numerical solver, which is also an important aspect in any AMR algorithm, will not be repeated in this chapter, as it is mainly one of the two explicit high-resolution schemes described in the previous chapter (Flux Corrected Transport (FCT) or TVD Lax Friedrichs). But, in order to understand how AMR functions mentioned above are linked together, a *pseudo-code* that accurately describes the sequencing of our adaptive strategy will be presented. This can also be valuable to any person who wishes to implement the ideas described in this chapter.

The effort required to correctly implement the AMR algorithm discussed below is considerable, with a complete implementation requiring tens of thousands of code lines to express the core algorithm. Therefore the last part of this chapter presents simulations demonstrating that the resultant computational benefits make this effort worthwhile. Finally, the chapter is closed by a summary of the work, a list of conclusions that were drawn, and a few suggestions as to how this work could be usefully extended.

4.3 Review of AMR Schemes

The literature for computational simulation of physical phenomena contains a wealth of material about adaptive mesh refinement on both structured and unstructured meshes. However, Mavripilis (1990) points out that the use of unstructured mesh techniques in the computational fluid dynamics (CFD) field constitutes a relatively recent phenomenon, and despite their flexibility in dealing with arbitrary complex geometries, there are several drawbacks associated with unstructured mesh refinement, notably large overheads, which become particularly troublesome for transient flow simulations.

Furthermore, the main advantage of unstructured mesh techniques over structured mesh ones, is their natural ability to discretise complex multidimensional geometries, which is not an issue for one-dimensional models considered in the present study. Therefore, these types of adaptive strategies were not considered here and the interested user is referred to the review papers by Mavripilis (1998) and Lohner (1998) for a complete discussion on unstructured mesh generation and adaptivity issues.

Thus, this section mainly focuses on structured mesh techniques. However, many strategies have been developed with the sole aim of dealing with a specific flow; they serve their special purpose well, but lack generality. Other methods appear unsuited to discontinuities, steep gradients or shock flows. Given this variety, it would serve no purpose to encompass in this chapter a full and lengthy review of adaptive mesh schemes. Instead it is more appropriate that we simply allude to some of the reasoning that has shaped the development of the AMR algorithm. To this end, we briefly touch on two structured adaptive mesh strategies that are frequently applied to compressible flow problems, highlighting their respective advantages and disadvantages.

4.3.1 Mesh Enrichment (Local Cell Refinement)

The first strategy is commonly known as the *local cell refinement*, which is implemented by refining or splitting individual cells one at a time. This approach tends to produce regions that more tightly conform to the spatial structure of the features requiring mesh refinement. However the computational tasks are organised necessarily by operations performed on an individual cell. This leads to indirect addressing and irregular difference schemes to maintain communication among data associated with computational cells on the composite mesh. Moreover, the data structures maintaining the cell refinement need to be closely tied to the finite difference stencils used by the numerical methods. Numerous variations of this type of mesh refinement strategy are reported in the literature and they are reviewed in the thesis by Neeman (1996).

4.3.2 Mesh Redistribution (Moving Mesh Methods)

The second class of adaptive strategies are the *moving mesh methods*, which refine by redistributing mesh points, rather than creating new meshes at different resolutions [Li & Petzold, 1997; Stockie et al., 2001; and Tang & Tang, 2003]. They were developed to handle many non-linear hyperbolic and parabolic problems that contain shocks or other sharp moving fronts, and they are fairly easy to implement. Thus, while they may be useful for a limited class of applications, they are inherently non-uniform, therefore inappropriate for existing uniform grid solvers. In addition, the number of grid cells does not grow, but the complexity of the solution can, so a given mesh size may prove insufficient for some evolving simulation, causing some regions which require very high resolution to “steal” nodes from other regions which are then insufficiently resolved.

4.4 AMR Constraints for Transient Flows

The fact, that there is no standard way of implementing AMR schemes in the literature, has led many researchers to develop numerous variations of the two classes of adaptive grid methods, described in the previous section, and for various multidimensional applications. But despite their undoubted popularity, neither the generic moving mesh methods nor the local cell refinement methods were judged to be suitable for our transient multiphase flow purposes. Nevertheless, these AMR schemes both exhibit, many of the qualities we wished to instil into our algorithm, and many of the disadvantages we wish to avoid. Hence, the following is a list of properties that we have required for our scheme.

- The scheme must be conservative and general purpose – *we want to apply it to a variety of single, two- or three-phase flow problems in which the mesh change should not result in the production or loss of mass, momentum or energy.*
- The scheme must be well suited to unsteady simulations – *our main interest lies in simulating time-dependent or transient multiphase flow problems.*
- No unreasonable constraint should be placed on the numerical solver used to integrate the flow solution – *we hope to employ the adaptive method with both a variety of shock capturing schemes and a number of different flow models.*
- The method should not produce elements that are too small, as this would reduce too severely the timestep allowable for the explicit flow solvers employed.
- The refinement process must be cheap and easy in order to minimise the overheads associated with complex data structure used by adaptive methods.

These criteria severely limit the field of applicable strategies found in the literature, and have led us to opt for the block-structured approach to local refinement proposed by Berger and her collaborators [Berger & Oliger, 1984; Berger & Colella, 1989]. In this approach, the refined regions are not individual cells, but rather large collections of fine cells in each block. As a result, it is possible to reduce the overhead of managing the complex data structures, which describe the computational region. In addition, almost all of the numerical work is done on regular arrays of floating point numbers.

However, the structure of our global implementation follows the approach adopted by Quirk (1991), Neeman (1996), and Boden (1997), which removes much of the complexity of Berger's original scheme, without compromising the quality of the resultant simulations. In order to achieve an easy refinement process for our one-dimensional problems, the bisection technique proposed by Arney (1989) was retained in the present study. This refinement strategy, in which each patch is split into identical sub-patches, was also used by Thompson et al. (1992) to solve the incompressible Navier-Stokes equations, and they reported good results. The AMR scheme in general presents as many obstacles to the programmer as it presents benefits to the user. Therefore, all the various elements of our strategy will be deeply detailed in the following paragraphs, starting with the general principles of the scheme that we have selected.

4.5 Principles of Berger Strategy

Berger developed in the early 1980's an adaptive mesh refinement strategy for hyperbolic systems of conservation that has been successfully applied to simulation of time-unsteady gas-dynamic flows in two dimensions [Berger & Colella, 1989] and three dimensions [Bell et al., 1994]. It enables the simulation of complex problems with reduced computational and storage requirements because it allows computational effort to be concentrated precisely where it is required to maintain high accuracy.

To locally refine the computational grid, Berger adopted a structured mesh approach, which is based on the notion of multiple, independently solvable grids, all of identical type but each of arbitrary size and shape. Therefore, the underlying premise of this strategy is that once individual cells are selected for refinement, the algorithm clusters them to form a collection of cells called a patch or sub-grid on a fine resolution level, and the process is repeated until the finest existing level.

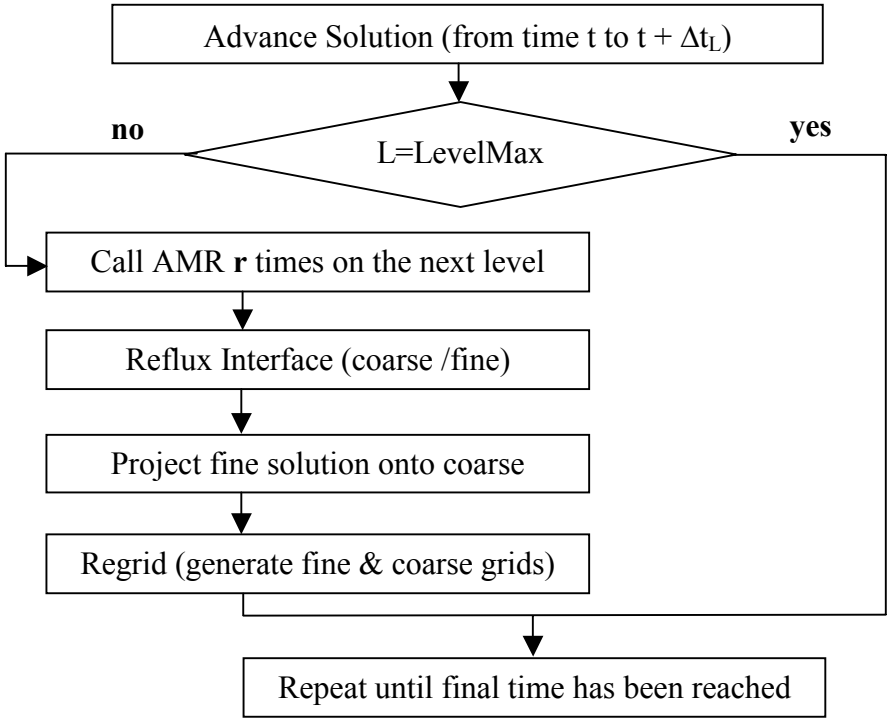

Figure 4-1: AMR Driver: Sequence of Integration.

Thus, all grids of any given resolution that cover a problem domain and given proper boundary information are equivalent in the sense that they can be solved independently by identical means. In essence, the multigrid concept [Brandt, 1977] is adjusted, reducing it from the highly accurate but computationally expensive set of increasingly finely resolved

grids, each covering the entire domain, to a set of resolution *levels*, each employing a disjoint set of sub-grids to cover progressively less of the domain.

Hence, Berger's algorithmic methodology manages a hierarchy of grids. The hierarchy consists of several levels of refinement. On each level L, there is a single grid spacing Δx_L (Figure 4-3), but different levels have different grid spacing related by an integer divisor. The coarsest grid covers the entire physical domain. Within that domain, finer grids cover rectangular sub-regions. Additional refinement may be achieved by recursively placing still finer grids. Finer grids take smaller time-steps, which are proportional to the Δx on the grid. As time evolves, the regions of the physical domain requiring high resolution will in general change, requiring the hierarchy of coarse and finer grids to adapt dynamically to the changing solution.

The time advancement procedure for AMR is recursive (Figure 4-1), and if R is the refinement ratio between levels, $R = \Delta x_L / \Delta x_{L+1}$, then the $L+1^{th}$ level must make R time-steps for every single time-step of the L level, resulting in a multigrid W-cycle for advancing the solution (Figure 4-2). During the recursive evolution, the AMR algorithm must take additional steps to maintain consistency between different levels of refinement. Since error is proportional to a positive power of the grid spacing Δx, the values calculated on finer grids are more accurate than the values of the coarser grids. Wherever fine grid cells overlie coarse grid cells, the coarse grid cells are replaced with the average of the overlying fine cells at the completion of each coarse-grid time-step. An additional step must be taken to maintain conservation at the boundary between coarse and fine grids. Coarse grid cells that adjoin a fine grid but are not overlain by fine grids must be updated using fluxes, which agree with the fluxes that are used on the adjoining fine grid cells. Therefore the AMR algorithm must advance these coarse grid cells using fluxes, which are an appropriate sum of fine grid fluxes on the shared cell faces.

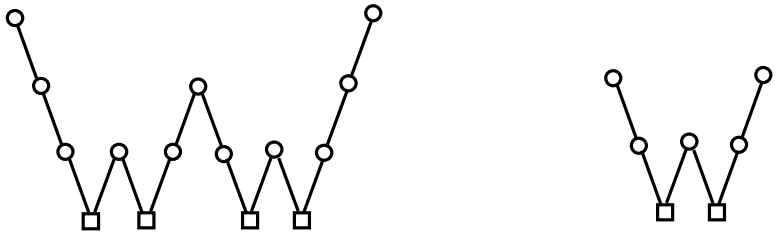

Figure 4-2: Multigrid W cycles (4 and 3 levels of refinement)

Throughout this chapter, we reserve the term patch or sub-grid for a single logical collection of cells, and the term grid for a collection of such patches. Although this AMR patch approach tends to refine additional cells, it has several important advantages over the individual cell refinement or moving mesh strategies. It allows inter-cell communication to be maintained in a more straightforward manner and it is designed so that a small number of computational tasks can be organised in a highly structured fashion. In addition, the

numerical integration routines used to solve the equations on the adaptive grid are easily separated from the structure of the AMR algorithm. This greatly enhances code extendibility, maintenance and generality.

4.6 Data Structure

4.6.1 Overview

Unlike traditional uniform approaches, where only fixed solution vectors and perhaps some additional workspace need to be stored, AMR data structures must satisfy several requirements for an efficient implementation. They must store information on intergrid conditions, solution vectors, and some intermediate results necessary for the finite difference scheme adopted (e.g., solution vector at the previous timesteps). They must contain information on the relationship between different patches at any given time as well as parameters that control time evolution of refinements and regridding criteria. Also, the data structures must allow for easy scheduling of operations on all grids in a way that is transparent for the user. Finally they should contain information on mapping of the data onto a distributed memory system [Berger & Colella, 1989], even though this last requirement is not taken into account in this research.

To this end, we define a hierarchy of data structures, starting from a patch description, through a set of management functions defined on each individual patch to a tree or level structure of patches. Each data structure is defined in term of parameters that define the size and shape of the structure, and define their time evolution. The maximum number of levels and the total number of cells on the coarsest or base level are the only parameters, which need to be provided by the user, for the time being via a text based pre-processor. We are considering integrating in the future, a graphical user interface to make all input parameters easier.

Before describing the patch and level object, which are the major elements of our data structure, and some management functions, we first explain the programming language that we have adopted for implementation purposes.

4.6.2 Implementation Language (Fortran 90)

As mentioned above, AMR systems must manage not only the solution vectors for a large dynamically changing collection of patches, but also the relationships between these patches, between the solution vectors and various other data items. In addition, maximal flexibility is achieved if the manner of describing the data items and relationships allows the data structure to be autonomous: that is, to manage itself, rather than relying on hard-coded management functions.

This complex and subtle nature of the data structure [Berger & Oliger, 1984] has been one of the primary stumbling blocks to the popularity of block-structured AMR among computational scientists. The burdensome coding requirements of grid hierarchy data structures make the development of a general-purpose system in basic programming language like FORTRAN 77 unrealistic. The fact that Fortran 77 does not support, at least explicitly, dynamical memory management, has forced programmers, in the past, to heavily rely on the traditional linear memory model. This leads to unnecessarily lengthy programs that are difficult to read and maintain, even though some of the codes themselves were quite efficient.

Even if a system is designed in a language that supports sophisticated data types, such as C, the enormous variety of structured simulation paradigms leads to a prohibitively high amount of design and implementation. So, to develop an efficient and modular code, we have opted for FORTRAN 90 and exploited its object-oriented features for the data structure management, and the numerical modules. This "new" Fortran not only simplifies the problem of handling dynamic objects with a much more sophisticated structure than simple Fortran arrays, it also allows for better organization of the code by encapsulating data structures and methods to manipulate them in Fortran 90 modules, as well as defining explicit interfaces to user routines.

C++ is the other obvious choice for the data structure implementation, and it is also a popular alternative among AMR researchers [Pember et al., 1995; Neeman, 1996], but this language is not as efficient as Fortran for numerical integration routines, which are used to solve partial differential equations, and which constitute the core of our code.

4.6.3 Patch & Level Description

Almost all Berger types of data structure found in the literature are designed for 2D or 3D problems [Berger & Colella, 1989; Quirk, 1991; Pember et al., 1995]. Although there should be no big change for 1D problems, many features that appear only in higher dimensions can be simplified. Thus a patch object or data type is defined as a Fortran 90 linked list object in the program, and it is characterised by:

- An identifier (integer number associated with each patch)
- The current level of the patch
- The number of cells in the patch
- The refinement flag
- The physical patch location (starting point in 1D grid layout)
- The solution data and buffer vectors for each cell in the patch
- The inlet and outlet interface fluxes.
- A pointer to the parent patch
- Two pointers to children patches (left & right child)
- Two pointers to neighbour patches (next or previous patch on the same level)

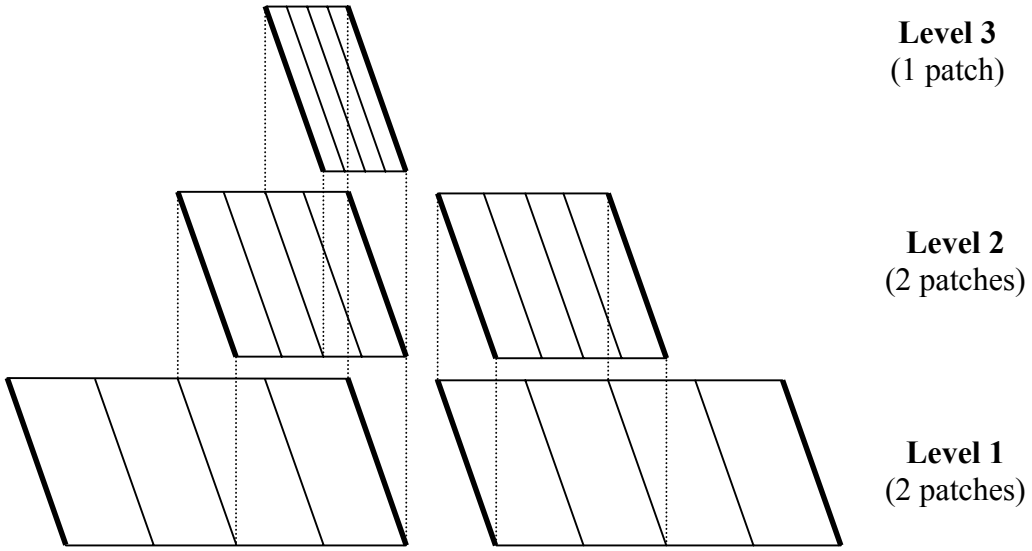

Figure 4-3: Example of grid organisation for adaptive computations.

The AMR algorithm uses a tree or level structure (Figure 4-3) to discretize the flow domain. Similarly to the patch object, a level data type is defined as a double linked list object, and it is characterised by:

- An identifier
- The spatial level resolution or mesh size
- The integration time for all patches on the current level
- A pointer to the first located patch on the level
- Two pointers to neighbour levels (next or previous level on the same hierarchy)

4.6.4 Data Structure Management

Functions associated with the patch or level object consist of three basic operations: creation, deletion and update. These three operations can be split into sub-operations, but among them, they constitute the entire set of tasks required for the data structure management. These same operations are therefore performed either on the entire hierarchy or on a specific data item. For example, a control algorithm has access to each level or to a hierarchy as a whole, while a solver function is applied to each patch of the appropriate level.

4.6.4.1 Management of Data Items

Creation and deletion operate at several levels of complexity depending on the data item. For example, creation of a sub-grid is a four-step process. First, the sub-grid data type is allocated. Next its attributes (identifier, current level, number of cells…) are set. Then, the

solution and buffer vectors are allocated and initialised to null. Finally, the sub-grid is inserted in the grid hierarchy, and appropriate pointers are set to link others sub-grids in the hierarchy structure.

Deletion of a data item operates similarly, but in a reverse order. Deletion does not include the initialisation step, but a transfer step from child to parent patch is executed, just before de-allocating the child patch.

Finally, execution with respect to a data item includes initialisation, injection, projection, input, output and so on. The inter-changeability of these operations promotes flexibility and generality within the data management framework.

4.6.4.2 Transfer operations

Injection and projection are also called prolongation and restriction in the multigrid language. They are used to transfer solution vectors from parent to child patch and vice versa. A simple linear interpolation has been chosen for these operations in the present study, and can be described as follows:

Projection

$$Q_i^c = \frac{1}{2}\left(Q_i^f + Q_{i+1}^f\right) \tag{4.1}$$

Injection

$$\begin{cases} Q_{2i}^f = \frac{3}{4}Q_i^c + \frac{1}{4}Q_{i+1}^c \\ Q_{2i+1}^f = \frac{1}{4}Q_i^c + \frac{3}{4}Q_{i+1}^c \end{cases} \tag{4.2}$$

Where Q is the solution vector, and the subscripts **c** and **f** correspond to **coarse** and **fine** patches or parent and child sub-grids.

4.7 Automatic Grid Refinement Process

The problem of designing an algorithm that automatically adapts a computational grid to an evolving flow solution is not an easy task. But once a correct data structure has been defined and implemented, the refinement process becomes not only less cumbersome but also more intuitive. It can therefore be sub-divided into a sequence of well-defined problems or procedures, which are relatively simple to design and implement. Moreover, the correct co-ordination of these individual procedures ensures robustness and integrity of the AMR algorithm.

4.7.1 Fundamental Principles

Refinement covers coarse sub-domains with patches of higher resolution and it is done according to the following three fundamental principles:

1. The ratio time step over mesh size: $\left(\tau = \frac{\Delta t}{\Delta x} = \frac{\Delta t_c}{\Delta x_c} = \frac{\Delta t_f}{\Delta x_f} \right)$ is kept constant and equal to 2 on all levels. This allows an easy synchronisation of the algorithm and ensures stability of the integration scheme on all patches.

2. At the interface between two patches, either at the same level or at different levels, numerical fluxes are conserved. This is a necessary condition for maintaining accuracy and avoiding reflections [Berger, 1987].

3. A patch at level *w* can only be bordered by patches at levels: *w - 1, w, w + 1*. This is crucial to simplify the treatment of interfaces and is achieved by forcing grid refinement if necessary. This approach also controls accuracy as it smoothes regions of changing mesh size.

In the present study, another principle - fine patches always have the same number of cells as their coarse parents - can be derived from the fact that a bisection technique was chosen as the regridding process. This makes data structures self-similar and facilitates processing.

4.7.2 Elements of the Adaptation Process

The refinement strategy is based on the sub-division of parent or coarse patches, and this process may be split loosely into two operations. First given a grid structure and flow solution we identify regions of large error and flag these regions for refinement. Then, a child patch is created and initialised in a finer level to cover these regions.

The adaptation process given in this section has been rudimentary, but it should help the reader to maintain a sense of direction during the more detailed description of the individual elements that follows.

4.7.2.1 Error Estimation & Flagging for Refinement

In previous AMR work [Berger & Oliger, 1984; Berger & Colella, 1989; Quirk, 1991; Pember et al., 1995], a Richardson-type estimate of the global truncation error was used to identify cells for refinement. The goal was to guarantee a specified level of accuracy throughout a simulation with nearly minimal computational cost. Although there are several important advantages to this process, it is significantly complex to implement and more expensive than more simple gradient detection strategies.

In the present study, we have chosen to start with a Lezeau & Thompson (1998) type of gradient detector, thus the precise flagging procedure can be described as follows: at all

levels, at all time steps, an average gradient is computed for each half of each patch k belonging to level l.

$$\mathrm{Grad}_{l,k,\mathrm{left}} = \sqrt{\frac{\sum_{j=1}^{M}\left(Q_{2,j}-Q_{1,j}\right)^2 + \sum_{i=3}^{N_k/2}\sum_{j=1}^{M}\left(Q_{i,j}-Q_{i-2,j}\right)^2}{M\cdot N_k/2}} \tag{4.3}$$

$$\mathrm{Grad}_{l,k,\mathrm{right}} = \sqrt{\frac{\sum_{i=N_k/2+1}^{N_k}\sum_{j=1}^{M}\left(Q_{i,j}-Q_{i-2,j}\right)^2 + \sum_{j=1}^{M}\left(Q_{N_k,j}-Q_{N_k-1,j}\right)^2}{M\cdot N_k/2}} \tag{4.4}$$

Where N_k is the number of cells in patch k and M is the dimension of the vector of conservative variables or the number of equations of the system solved.

A half patch on level l is then flagged for refinement if its average gradient *Grad* is greater than or equal to the following threshold:

$$t_l = \left(\frac{\sum_{k=1}^{L_p}\mathrm{Grad}_{l,k,\mathrm{left}}^{\gamma} + \mathrm{Grad}_{l,k,\mathrm{right}}^{\gamma}}{2L_p}\right)^{\left(\frac{1}{\gamma}\right)} \tag{4.5}$$

Where L_p is the total number of sub-grids or patches in level l and γ is a parameter, which controls the sensitivity of refinement. The higher γ, the more selective the refinement since t_l will tends towards the L_∞–norm of the average grid gradients. In the current version of the code the value of γ is set to 2 for all existing levels, meaning that an L_2-norm of the gradient is used for selecting automatically regions to be refined.

A further investigation of the effect of this error estimator may be worthwhile for future developments as first results using this average gradient indicate that it often produces larger refined regions than may be desired.

4.7.2.2 Regridding

Regridding creates new patches at a finer level to cover the selected area of refinement at the immediately coarser level. This process is repeatedly performed as the simulation evolves, resulting in an automatic adjustment of the patch configuration on all levels. Note that if the time corresponding to the data on a fine level matches that of the data on a coarser level, we must be at a synchronisation point. Then, regridding may be deferred to some coarse level if it is also appropriate to invoke this process on the coarser level at that time.

As already mentioned, the technique used to generate new patches on a fine level is called bisection. Thus a parent patch, which needs to be refined, is always split in two equal halves and replaced by children grids with half resolution ($\Delta x^f = \Delta x^c/2$).

4.7.2.2.1 Temporal Refinement

The AMR approach adopted here is unique among grid adaptation techniques, in that it employs temporal as well as spatial refinement. Other adaptive grid techniques advance all the grid cells with the same time step, which is often dictated by stability criteria of the finest cells. Temporal refinement allows the coarser grid levels to advance with much larger time steps than the fine levels. In order to impose the temporal refinement, the AMR algorithm uses the CFL criteria (2.18) calculated from the solutions of the coarse grids, even where fine level coverage exists. Updating the coarse grid cells require little computational effort relative to that of updating the finest grid cells.

The AMR algorithm implemented here assumes that the temporal refinement is equal to the spatial refinement, and although there is no limitation on the maximum number of grid levels allowed, we recommend avoiding situations where the solution is needlessly integrated by too many small time steps levels (i.e. finest level > 7). For example, consider a 10 level grid structure in which the cell resolutions of the nine finer levels are increased by a factor of 2. The resulting time step of the finest grid level would be defined as $1/512^{th}$ of the coarsest time step, and such a situation will result in an unnecessary increase in the integration costs and probably the numerical (diffusion) error associated with the solution.

This temporal refinement strategy does not necessarily lead to the optimal timestep for the finer grid levels, and although we have not encountered any problem related to this strategy, it may be worth investigating in the future the alternative approach adopted by Boden (1997) in which the time step is determined for every grid level, from the maximum characteristic speed in its solution, immediately before it is integrated. This results in an unpredictable number of fine grid time steps in every coarse grid time step, however, Boden (1997) estimated that over a whole computation, the ratio of the number of fine to coarse time steps is approximately equal to the spatial refinement factor.

4.7.2.2.2 Refinement Frequency

To the reader of the adaptive grid literature, the philosophy, behind when or how often any adaptive grid structure should be updated, could be construed as an open issue. Several AMR algorithms, notably Berger & Colella (1989) and Bell et al. (1994), do not update the grid structure as often as possible. By far the most expensive part of any computation is the integration of the flow field solution. Any viable adaptive grid algorithm should spend only a tiny proportion of the overall computing time, generating the grid structure and transferring data within it.

By not changing the grid structure whenever possible, adaptive grid algorithms appear to increase efficiency, i.e. they spend less time adapting the grid structure compared with the integration of the grid solution. However, the finer grid levels need to extend sufficiently far beyond the immediate vicinity of the dynamic flow features requiring refinement, in order to ensure adequate coverage during the ensuing time steps. Hence, the longer a grid structure remains unchanged, the greater the proportion of the flow domain that must be covered by fine grid cells [Boden, 1997]. The increased number of cells results in an increased number of computationally expensive cell integrations.

Therefore, maximum efficiency is achieved by adapting the grid structure when and wherever possible, thereby limiting the total amount of processing time spent integrating the solution, because the cost associated with the extra grid adaptation is negligible in comparison. Hence, the philosophy adopted is in agreement with Quirk (1991) and Boden (1997), in that the AMR algorithm presented here does update the grid structure whenever possible, i.e. every time a fine grid solution reaches the same time level as the underlying coarse grid. Figure 4-4 depicts a typical time evolution of a one-dimensional grid structure and the refinement frequency for four levels of integration. Note that, regridding at finer levels only occurs at appropriate step intervals on coarser grids.

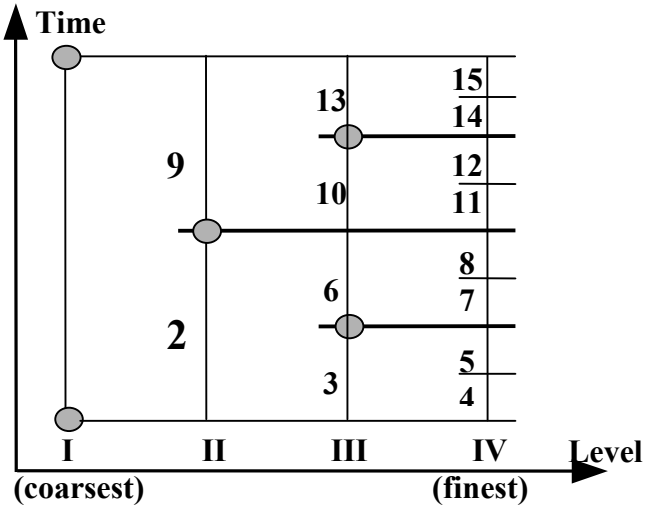

Figure 4-4: Integration Cycle and Refinement Frequency. Regridding at finer levels occurs at appropriate ● step intervals on coarser grids.

4.8 Boundary Conditions

A crucial aspect of any integration algorithm is proper handling of the boundary conditions. Within AMR scheme, we face three different kinds of boundaries. One comes directly with the PDE system, and it describes *external* or physical boundaries of the entire computational domain. The two others are artefacts of the AMR technique, they are

imposed on fine patches whenever they are created in the interior domain, and can be described as *fine-fine* or *fine-coarse* boundary or interface.

To distinguish between these three situations, a flag corresponding to each boundary type is used to tag the left and right boundary cells associated with each patch. The notion of *ghost* or *dummy cells* (Figure 4-5) is also used to facilitate the inter-patch communication.

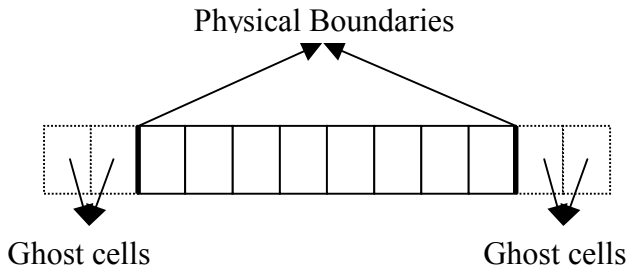

Figure 4-5: Example of ghost or dummy cells.

4.8.1 External boundaries

Physical boundary conditions are problem dependent and require no knowledge of the patch connectivity. Therefore, their implementations are not different from procedures that are often used by schemes employing just a single uniform patch or grid.

4.8.2 Fine-Fine Boundaries

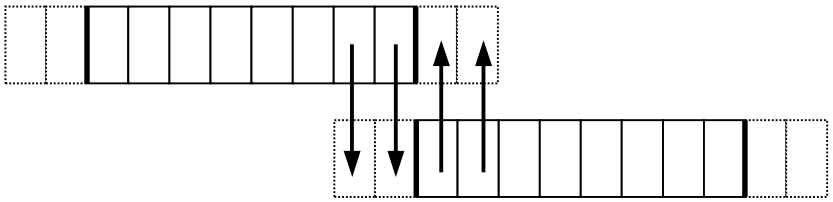

Figure 4-6: Example of fine-fine boundary

This type of boundary occurs when two patches share an edge on the same refinement level (Figure 4-6). It is easy to deal with because there is a one-to-one correspondence between dummy cells bordering each fine patch and cells contained in the adjacent patch. Thus, data in the dummy cells intersecting the neighbouring patch are simply copied from the appropriate cells located in the interior of that neighbouring patch.

4.8.3 Fine-Coarse Boundaries

When setting boundary conditions for fine patches and only coarse patch data are available, the adaptive mesh refinement scheme uses conservative interpolation to define the solution in a fine patch cell. The injection operator (4.2) is used to perform this process.

4.9 Mass Conservation

The final AMR issue discussed in this section is the mass conservation on adaptive meshes, and the algorithm developed here is only valid for conservative systems of equations. We have noted previously that coarse patches are integrated before fine patches. However, fine patches typically produce more accurate results. Therefore, when all levels have been advanced to the same time, the solution obtained on fine patches is used to improve data on coarser patches. This correction step is done in two different sub-steps called here projection down and refluxing.

4.9.1 Projection down

To advance a patch from time t to t + Δt, the numerical explicit solver uses the following conservative expression for every coarse cell not overlain by fine cells.

$$Q_j^{t+\Delta t} = Q_j^t - \tau\left(F_{j+1/2} - F_{j-1/2}\right) \tag{4.6}$$

where Q is the vector solution and F the numerical flux evaluated at time t. But for coarse cells that underlie fine cells, the solution is updated by projecting the overlying fine grid solutions. The interpolation operator (4.1) is used to perform this projection procedure.

An important point here is that projection should occur after refluxing, rather than before, because the projected values reflect the most accurate solution available. If projection occurs before flux correction, then the optimal projected values may be corrected, which is obviously undesirable. If however, correction occurs first, then any corrected values covering a finer patch will be replaced with the projected values, while those on a true fine-to-coarse interface will remain appropriately corrected.

4.9.2 Refluxing

The refluxing process enforces flux conservation at patch interfaces [Berger, 1987] and requires storing the inlet and outlet fluxes for each patch during the numerical time integration. This process is done for coarse cells that share a cell edge with a fine patch boundary, but do not actually underlie any fine level cells. Thus, for one-dimensional problems considered here, the different cases where flux correction is necessary can be arranged in two groups (Figure 4-7). The general procedure for refluxing can be found in the papers by Berger (1987) and Hornung & Trangenstein (1997). Thus, in what follows, we briefly explained the technique using the first case of Figure 4-7a.

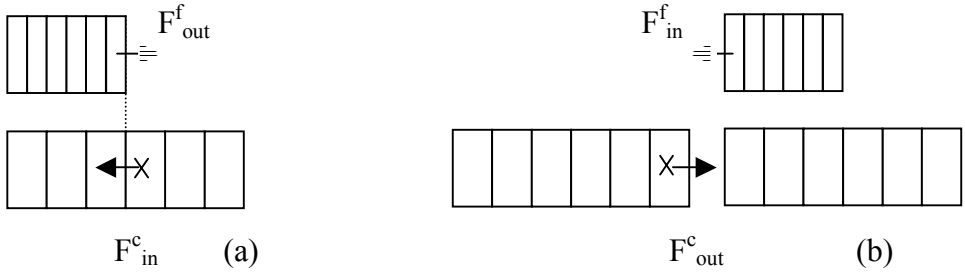

Figure 4-7: Grid interface between fine/coarse patches.

Suppose a coarse cell j shares its left cell face with a fine patch boundary. Let F^c_{in} be the coarse flux at the left cell face of j (i.e. $F^c_{in} = F^c_{j-1/2}$). Thus, the integration step (4.6) can be written:

$$Q_j^{t+\Delta t_c} = Q_j^t - \tau\left(F^c_{j+1/2} - F^c_{in}\right) \tag{4.7}$$

If instead of using a coarse value, the fine flux were used, the update process (4.6) will be written as:

$$Q_j^{t+\Delta t_c} = Q_j^t - \tau\left(F^c_{j+1/2} - \hat{F}^f_{out}\right) \tag{4.8}$$

Where $\hat{F}^f_{out} = \sum_{i=1}^{2} F^f_{out}$ is the summation of fine fluxes accumulated during integration on the fine level from time t to $t + \Delta t_c$.

By using equation (4.7) in (4.8), the following correction expression can be derived:

$$Q_j^{t+\Delta t_c} = \underbrace{Q_j^t - \tau\left(F^c_{j+1/2} - F^c_{in}\right)}_{\text{coarse value}} - \overbrace{\tau\left(F^c_{in} - \hat{F}^f_{out}\right)}^{\text{fine correction}} \tag{4.9}$$

In the same way, the second case (Figure 4-7 b) correction can be expressed as:

$$Q_j^{t+\Delta t_c} = \text{coarse value} + \overbrace{\tau\left(F^c_{out} - \hat{F}^f_{in}\right)}^{\text{flux correction}} \tag{4.10}$$

Thus, the fine or flux correction in (4.9) or (4.10) uses the difference between the two net fluxes to adjust the updated coarse solution, and it is equivalent to repeating the integration of the coarse cell using the sum of the fine patch fluxes instead of the coarse patch flux.

4.10 Coordination of the Complete AMR Algorithm

After defining the initial coarse grid structure and priming it with the solution data, the coordination of the AMR processes can be regarded as a recursive sequence of procedures, which operate on every grid level until the desired point in time is reached. Figure 4-8 depicts a flowchart of this recursive sequence of procedures, which we briefly describe in the following paragraphs.

The algorithm begins with a time step integration of the initial coarse grid (level 1) patch(es) that cover the entire computational domain. Then, an error estimation procedure identifies coarse cells where the solution is not resolved to a given error tolerance, and flagged them as left or right part of the coarse patch. At the next iteration or timestep, these tagged parts of the coarse patch are then spatially refined (with a ratio of 2) to form the level 2 grid structure. As the simulation proceeds, this process is repeated until either the error tolerance is satisfied or a specified maximum level is reached. Hence, as the dynamics evolve in time the important features of the solution move through the computational domain in a way that cannot be predicted a priori.

For the unsteady conservative 1D models developed here, the AMR algorithm uses an explicit high resolution method (FCT or TVD Lax-Friedrichs) to advance the solution on each grid patch. The stability requirement for this method is that a signal not be able to pass entirely through a finite difference cell in any given time-step. This requirement is enforced by restricting the time-step such that $S^*\Delta t/\Delta x < CFL < 1$ where S is the speed of the fastest wave in the problem and CFL is the Courant number specified by the user.

From this we can see that as we move from one level to the next finest with a constant refinement ratio of $R = 2$, the time-steps taken on the finer grids must be reduced by a factor of R. Further, in order for the fine grids to be advanced to the same point in time as the coarse level we must advance them R times for each coarse grid advancement. The time stepping algorithm is recursive: The grids at level L are advanced with a time-step $\Delta t(L)$. The grids at level $L+1$ are advanced R times with time-step $\Delta t(L+1) = \Delta t(L)/R$. Finally, a synchronization step is performed between level L and $L+1$.

The same integration module is used to advance both coarse and fine grids. The stencil for this integrator requires that a certain number of boundary values be supplied for each grid. The boundary values are supplied by either (1) copying from adjacent grids, (2) calling user supplied physical boundary condition functions or (3) interpolating from grids at a coarser level. When interpolating data from coarser grids, we obtain the data on the required sub-patch by a recursive call to this fill algorithm.

The synchronization step is used to ensure that the solutions on the coarse and fine levels remain consistent. It consists of a "**refluxing**" step followed by a "**projection**" also known as an "average-down" step. Since the numerical method discretely respects the conservation laws, it is necessary that the amount of the conserved quantities contained in a fine grid be

the same as that contained in the underlying coarse grid region. The "projection" step is implemented by averaging the fine grid data in a volume weighted fashion down to the coarse grid region covered by the fine grids (Section 4.9).

A conservative scheme updates the solution by computing fluxes across the faces of each finite difference cell. The state of the solution in a cell at the new time is the state at the old time plus the net flux across each of its faces. The fluxes computed on the coarse grid are in general not equal to the cumulative fluxes over the same physical region on the fine grids. The "refluxing" step effectively replaces the coarse grid fluxes with the cumulative fine grid fluxes. The reflux step updates the coarse grid cells adjacent to but not covered by the fine grids with a correction term that represents the difference between the coarse grid and fine grid fluxes.

The core of the AMR algorithm implemented is the region surrounded by a dotted line frame in Figure 4-8. This recursive driver procedure advances the grid solution on level L from time t to t + Δt, and can be described as:

ALGORITHM TO ADVANCE SOLUTION ON LEVEL *L* FROM TIME t TO t + Δt.

1. Advance solution on each patch of level L from time t to t + Δt.
   (a) Set boundary conditions needed to integrate grid in one of the three ways:
      i. Use physical boundary conditions, if applicable
      ii. Otherwise, use data from level L patches, if available (fine/fine)
      iii. Otherwise, interpolate data in time on level $L - 1$ cells underlying the level L boundary cells (fine/coarse)
   (b) Integrate the solution on the grid from time t to t + Δt using an explicit high-resolution scheme (FCT or TVD Lax-Friedrichs).
2. If level L is not finest existing then
   For $J = 1, R$
   Advance the solution on level $L+1$ from $t + (J-1)\ \Delta t/R$ to $t + J\ \Delta t/R$
3. Fix up conservation between level L and level $L+1$ at t + Δt in two ways:
   (a) Reflux:
   In level L cells that share a cell edge with a fine grid interface but do not actually underlie level $L+1$ cells, replace the effect of the coarse grid flux at the shared cell edge with the effect of the fine grid fluxes.
   (b) Project the fine solution onto coarse grid cells:
   In level L cells that underlay level $L+1$ cells, replace the solution in the level L cell by average of the solution in the overlying level $L+1$ cells.
4. If it is time to refine, then apply the error estimator procedure and flag the level L patches for regridding.

As already mentioned, the sequence of operations at each time step Δt forms a W-cycle as in the multigrid method because the time refinement factor R in step 2 is fixed to a constant value 2.

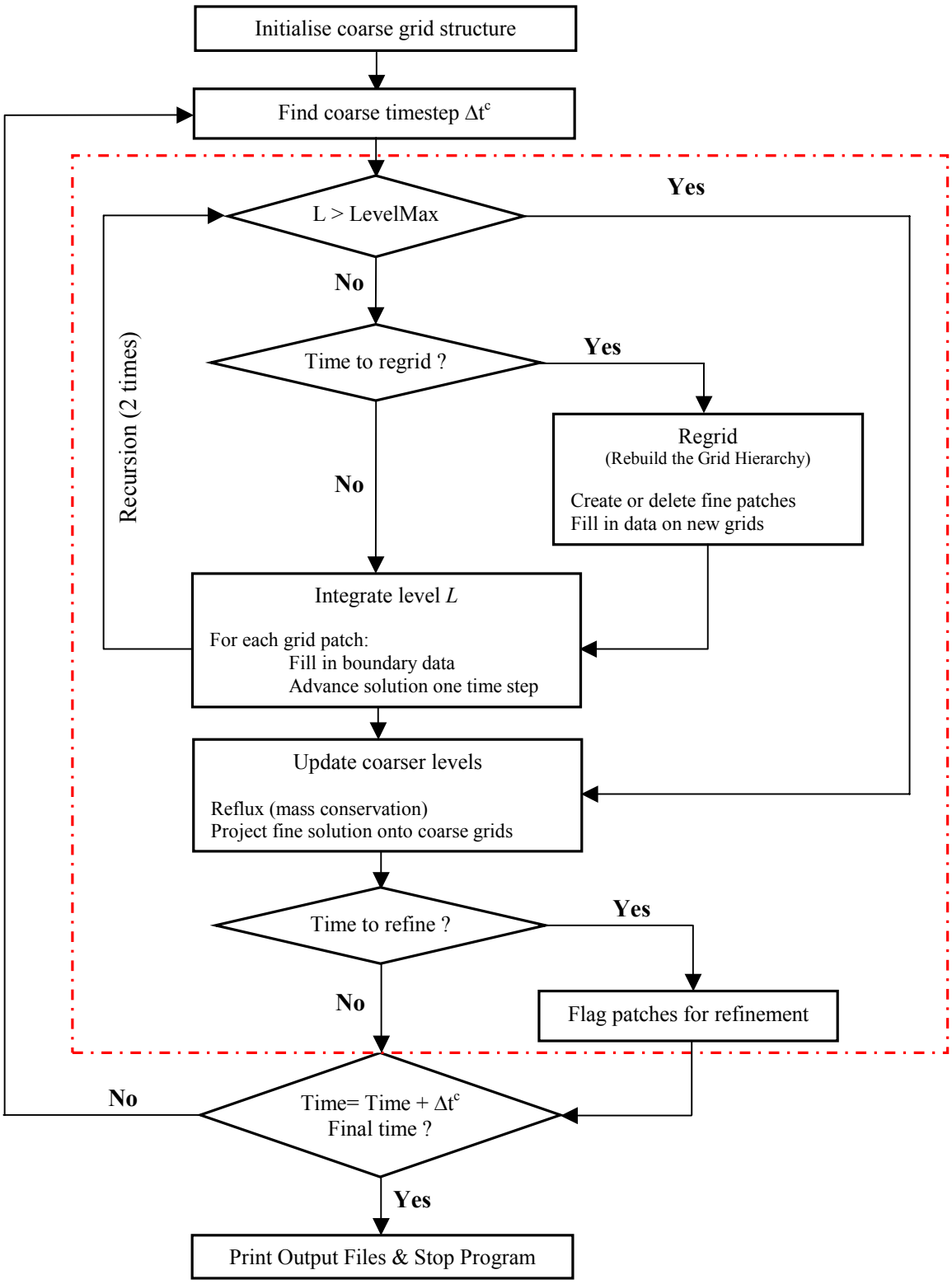

Figure 4-8: Flowchart that describes the adaptive mesh refinement algorithm.

4.11 EMAPS Implementation of AMR

In this section, we present some of the algorithms or Fortran 90 functions that perform the standard operations mentioned in previous sections. The purpose is to provide the reader with some clarifications and insights of the algorithmic details and functions required by the AMR strategy that we have adopted. These algorithms were implemented in the EMAPS framework, and include:

- Control;
- Integration;
- Boundary Collection;
- Regridding;
- Error estimation;
- Flagging;
- Correction;
- Projection.

However, EMAPS does not merely copy the existing AMR algorithms in the literature. Instead, it implements versions of them, which take full advantage of the expressive power of the tree-based data structure, and data management infrastructure that we have adopted, as well as our refinement and regridding strategies. Thus, despite the fact that the AMR strategy in EMAPS is based on the work of Berger and other researchers, these algorithms themselves constitute a significant contribution to the AMR canon.

```
SUBROUTINE TRANSIENT(TIME, TIMEOUT)

    IMPLICIT NONE
    REAL(WP), INTENT(IN)    :: TIMEOUT
    REAL(WP), INTENT(INOUT) :: TIME
    REAL(WP)  :: DT                      !TIME STEP (LOCAL VARIABLE)

    DO WHILE (TIME < TIMEOUT)

       CALL COARSE_TIME_STEP(DT, TIME)  !COMPUTE THE COARSEST TIME STEP
       CALL AMR(TIME, LVL_HANDLE)       !ADAPTIVE MESH REFINEMENT DRIVER
       CALL UPDATE_ALL_BUFFER()

       TIME = TIME + DT                 !UPDATE OR INCREMENT TIME
       NIT2 = NIT2 + 1                  !UPDATE THE NUMBER OF ITERATIONS

       CALL OUTPUT_DUMP_RESULT(TIME, NIT2)
    ENDDO

END SUBROUTINE TRANSIENT
```

Figure 4-9: EMAPS Unsteady or Transient Controller Algorithm.

4.11.1 Control Algorithm

The control algorithm in Figure 4-9 provides for EMAPS the time loop over the chosen number of root level integrations, performing two basic operations: the process of integration itself, and an output operation. Considering that the dotted frame region in Figure 4-8 is the integration process described by the function "**AMR**", and that a separated EMAPS function performs the initialisation of the grid solution, then Figure 4-9 represents the Fortran 90 implementation of the overall code depicted in Figure 4-8.

4.11.2 Integration

Figure 4-10 describes the EMAPS implementation of the AMR recursive algorithm described in Section 4.10. The halting condition for the algorithm is that it has reached an empty level, at which point it returns without computing. Otherwise, the algorithm regrids if appropriate, and advances the input level solution through the function "**INTEGRATE**", which applies the numerical solver for all patches at the current level.

```
RECURSIVE SUBROUTINE AMR(TIME, LEVEL)

    IMPLICIT NONE
    REAL(WP),  INTENT(IN) :: TIME            !TIME OF INTEGRATION
    TYPE(TLEVEL), POINTER :: LEVEL           !LEVEL OF INTEGRATION

    !---LOCAL VARIABLES
    INTEGER   :: I
    REAL(WP)  :: DT                          !LEVEL TIME STEP

    IF (.NOT.ASSOCIATED(LEVEL)) RETURN
    IF (.NOT.ASSOCIATED(LEVEL%FIRST_GRID)) RETURN

    IF (TIME_TO_REGRID(LEVEL)) CALL REGRID() !REBUILD THE GRID HIERARCHY

    CALL INTEGRATE(TIME, LEVEL)              !ADVANCE THE LEVEL SOLUTION
    CALL INIT_CONSERVATIVE_REFLUX(LEVEL)

    IF (LEVEL%ID < LVLMAX) THEN
       DT=TAU*LEVEL%DX

       DO I = 1, RF
         CALL AMR(TIME+(I-1)*DT/RF, LEVEL%NEXT)
       ENDDO

       CALL CORRECT_COARSE_FLUXES(LEVEL%NEXT)
       CALL PROJECT_FINE_SOLUTION(LEVEL%NEXT)
       IF (TIME_TO_REFINE(LEVEL)) CALL SET_LEVEL_FLAGS(LEVEL)
    ENDIF

END SUBROUTINE AMR
```

Figure 4-10: EMAPS AMR Recursive Integration Routine

Then, a call to function "**INIT_CONSERVATIVE_REFLUX**" initialises the current level patches inlet and outlet fluxes for the mass conservation or refluxing process. Afterwards, the integrator performs 2 recursive calls to itself (RF = 2) on the immediately finer level, followed by the synchronisation step that includes the refluxing and projection operations described in Section 4.9. Finally, if it is time to refine, an error estimator is applied and appropriate patches are flagged for the regridding process.

```
SUBROUTINE INTEGRATE(TIME,LEVEL)

    IMPLICIT NONE
    TYPE(TLEVEL), POINTER :: LEVEL
    REAL(WP),  INTENT(IN) :: TIME

    !---LOCAL VARIABLE
    REAL(WP)   :: DT                          !TIME STEP

    CALL UPDATE_BUFFER(LEVEL)                 !NECESSARY FOR FINER SUBSTEPS
    CALL SET_LEVEL_BOUNDARIES(TIME, LEVEL)

    DT=TAU*LEVEL%DX
    CALL APPLY_NUMERICAL_SCHEME(DT, LEVEL)    !ADVANCE THE VECTOR SOLUTION
    CALL SET_LEVEL_TIME(TIME+DT, LEVEL)

END SUBROUTINE INTEGRATE
```

Figure 4-11: Integration Routine for a Level.

Figure 4-11 describes in a bit more detail the integration or evolution of the grid solution for one level. The algorithm begins by making a copy of grid solution vectors to the buffer vectors via the function "**UPDATE_BUFFER**", and then it collects boundary and interface values. Next, it determines the time step interval for the current level, immediately followed by the application of one of the numerical solvers described in Chapter 2 for all the patches of the current level. After the integration has been completed, the "integrate" function finally increments or updates the time information for the level.

4.11.3 Boundary Collection

Function "**SET_LEVEL_BOUNDARIES**" in Figure 4-12 performs the boundary collection operation. As already mentioned in Section 4.8, the boundary and ghost values are supplied by three mechanisms, namely:

1. Calling user supplied physical boundary conditions wrapped in function "**EXTERNAL_BDRY**"
2. Copying from adjacent grid patches using function "**FINE_FINE_BDRY**"
3. Interpolating from grids at a coarser level. This operation is performed via function "**FINE_COARSE_BDRY**"

```
SUBROUTINE SET_LEVEL_BOUNDARIES(TIME, LEVEL)

    IMPLICIT NONE
    REAL(WP),  INTENT(IN) :: TIME
    TYPE(TLEVEL), POINTER :: LEVEL

    IF (.NOT.ASSOCIATED(LEVEL)) THEN
       CALL ABORT("MISSING LEVEL", "SET_LEVEL_BOUNDARIES")
    ENDIF

    CALL EXTERNAL_BDRY(TIME, LEVEL)      !SET INLET/OUTLET BOUNDARY CONDITION
    CALL FINE_FINE_BDRY(LEVEL)           !SET FINE/FINE DUMMY CELLS
    CALL FINE_COARSE_BDRY(LEVEL)         !SET FINE/COARSE DUMMY CELLS

END SUBROUTINE SET_LEVEL_BOUNDARIES
```

Figure 4-12: Boundary Collection Routine

In his Hierarchical AMR (HAMR) boundary collection algorithm, [Neeman, 1996] advocated calling the three functions mentioned above in the reverse order to the one we adopted here. He argued that in this way, the most accurate value replaces less accurate values: the values injected from the coarser level are replaced by values copied from elsewhere on the local level, and values on the exterior of the problem domain are extrapolated.

In our algorithm, the order in which we call the boundary functions does not really matter, a flag index identifies the appropriate type of boundary and any of the three boundary functions implemented can be called interchangeably.

4.11.4 Regridding

```
SUBROUTINE REGRID()

    IMPLICIT NONE
    TYPE(TLEVEL), POINTER :: LEVEL

    CALL ENSURE_PROPER_MESH_RATIO()     !FORCE REFINEMENT (KEEP 2:1 RATIO)

    LEVEL=>LVL_HANDLE
    DO WHILE(ASSOCIATED(LEVEL))
       CALL REFINE_LEVEL(LEVEL)
       LEVEL=>LEVEL%NEXT
    ENDDO

    LEVEL=>GET_LEVEL(LVLMAX)
    DO WHILE(ASSOCIATED(LEVEL))
       CALL CLEAN_LEVEL(LEVEL)          !DELETE UNUSED PATCHES
       LEVEL=>LEVEL%PREVIOUS
    ENDDO
END SUBROUTINE REGRID
```

Figure 4-13: EMAPS Regridding Routine

Like most structured AMR schemes, the EMAPS regridding algorithm (Figure 4-13) replaces a set of grids with a new set that covers more properly the phenomena of interest. However, unlike other schemes, the process is not recursive in itself, allowing regridding to occur at finer levels during a coarse time step cycle. Instead, we restrict the rebuilding of the grid hierarchy to the coarsest level only i.e. at the beginning of each coarse time step iteration. Hence, we avoid the problems associated with sub-cycling the regridding process, notably during the refluxing or mass conservation step.

The algorithm begins by ensuring that a refinement ratio of 2:1 is respected for all the patches flagged for refinement or deletion. If this is not the case, then the function "**ENSURE_PROPER_MESH_RATIO**" will flag extra patches for refinement or cancel the deletion flag for some patches. Next, if there are new grids to replace the old grids, then they are created using function "**REFINE_LEVEL**", and their grid solution values are injected from their parents using an interpolation operation (4.2).

Finally, if old patches need to be deleted, they are removed from the grid structure using the function "**CLEAN_LEVEL**". It should be noted after the refinement and cleaning processes at each level, the boundary relationships between the fine patches, their siblings and their parents is re-evaluated or updated appropriately.

4.11.5 Error Estimation

In previous structured AMR schemes [Berger & Colella, 1989; Neeman, 1996] a Richardson extrapolation was used to estimate the truncation error estimation, and provided a selection criterion for cell or patch refinement. However, this method, while both intuitive and mathematically simple, is complicated in algorithmic implementation and cannot be generalized for an arbitrary numerical solver. Therefore, a gradient-based approach, based on the work of Lezeau & Thompson (1998) was adopted as error estimator. Its formulation was described in detail in Section 4.7.2.1 and Figure 4-14 provides the actual implementation of equations (4.3) and (4.4) that are used to compute the average gradient or error for each half of every patch of the input level.

Once these average gradients are estimated using the function "**ERROR_ESTIMATOR**" of Figure 4-14, an extra function named "**THRESHOLD**" is used to provide the automatic selection criteria defined by formula (4.5). Because this thesis is not a full description of all the Fortran subroutines implemented in the framework EMAPS, the function "threshold" is not shown here, but can be found in the source file "adapt.f90" containing all the necessary mesh refinement functions.

For the reader interested in the structure of the EMAPS framework, a brief description of the key modules and files of the code can be found in Appendix A.

```
SUBROUTINE ERROR_ESTIMATOR(LEVEL)

    IMPLICIT NONE
    TYPE(TLEVEL), POINTER :: LEVEL

    !---LOCAL VARIABLES
    INTEGER       :: I, J, NCELL
    REAL(WP)      :: NORM, GRAD, DX
    REAL(WP),     POINTER :: U(:,:)
    TYPE(TPATCH), POINTER :: CURRENT

    IF (.NOT.ASSOCIATED(LEVEL)) THEN
       CALL ABORT("INVALID LEVEL", "ERROR_ESTIMATOR")
    ENDIF

    CURRENT=>LEVEL%FIRST_GRID
    DO WHILE(ASSOCIATED(CURRENT))

       DX = LEVEL%DX
       U=>CURRENT%BUFFER
       NCELL = CURRENT%NCELL

       NORM=0.0_WP
       DO I=1, NCELL/2                  !PATCH FIRST HALF (LEFT PART)
          DO J=1, NEQ
             IF (I == 1) THEN
                GRAD=(U(I+1,J)-U(I,J))/DX
             ELSE
                GRAD=(U(I+1,J)-U(I-1,J))/DX
             ENDIF

             NORM = NORM + GRAD*GRAD
          ENDDO
       ENDDO
       CURRENT%ERROR(1)=SQRT(NORM/(NEQ*NCELL/2))

       NORM=0.0_WP
       DO I=NCELL/2+1, NCELL            !PATCH SECOND HALF (RIGHT PART)
          DO J=1, NEQ
             IF (I == NCELL) THEN
                GRAD=(U(I,J)-U(I-1,J))/DX
             ELSE
                GRAD=(U(I+1,J)-U(I-1,J))/DX
             ENDIF

             NORM = NORM + GRAD*GRAD
          ENDDO
       ENDDO
       CURRENT%ERROR(2)=SQRT(NORM/(NEQ*NCELL/2))

       CURRENT=>CURRENT%NEXT
    ENDDO

    ! -- CONFIRMS THAT THE ERROR ESTIMATION HAS BEEN DONE -- !
    IF (ASSOCIATED(LEVEL%FIRST_GRID)) LEVEL%ESTIMATE=.TRUE.

END SUBROUTINE ERROR_ESTIMATOR
```

Figure 4-14: Gradient-Based Error Estimation Routine

4.11.6 Flagging

Figures 3.15 and 3.16 present the flagging algorithms for a level and a patch respectively.

```
SUBROUTINE SET_LEVEL_FLAGS(LEVEL)

    IMPLICIT NONE
    TYPE(TLEVEL), POINTER :: LEVEL      !INPUT LEVEL

    !---LOCAL VARIABLES
    REAL(WP)              :: TOL
    TYPE(TPATCH), POINTER :: CURRENT

    IF (.NOT. ASSOCIATED(LEVEL)) RETURN

    CALL SET_NOREFINE(LEVEL)            !RESET PATCH(ES) REFINEMENT FLAGS
    CALL SET_NOREMOVE(LEVEL)            !RESET PATCH(ES) REMOVAL FLAG

    CALL ERROR_ESTIMATOR(LEVEL)         !COMPUTE TWO ERRORS PER PATCH
    TOL = THRESHOLD(LEVEL)              !TOLERANCE FOR LEVEL REFINEMENT

    CURRENT=>LEVEL%FIRST_GRID
    DO WHILE(ASSOCIATED(CURRENT))
       CALL SET_PATCH_FLAGS(CURRENT, TOL)
       CURRENT=>CURRENT%NEXT
    ENDDO

END SUBROUTINE SET_LEVEL_FLAGS
```

Figure 4-15: Flagging Routine for a Specific Level

```
SUBROUTINE SET_PATCH_FLAGS(GRID, TOL)

    IMPLICIT NONE
    TYPE(TPATCH), POINTER :: GRID
    REAL(WP),  INTENT(IN) :: TOL            !TOLERANCE FOR REFINEMENT

    !---LOCAL VARIABLES
    INTEGER               :: IPART
    TYPE(TPATCH), POINTER :: CHILD

    DO IPART=1,2
       IF (GRID%ERROR(IPART) > TOL) THEN
          GRID%REFINE(IPART) = .TRUE.       !MARK PATCH FOR REFINEMENT
       ELSE                                 !CHECK FOR CHILDREN REMOVAL
          IF (IPART == 1) CHILD=>GRID%LEFT_CHILD
          IF (IPART == 2) CHILD=>GRID%RIGHT_CHILD

          IF (ASSOCIATED(CHILD) .AND. (.NOT.GRID%REFINE(IPART))) THEN
             CHILD%REMOVE = .TRUE.          !MARK PATCH FOR DELETION
          ENDIF
       ENDIF
    ENDDO
END SUBROUTINE SET_PATCH_FLAGS
```

Figure 4-16: Patch Flagging Routine

The level flagging routine is fairly simple to understand; the algorithm starts by setting all the refinement and removal flags to "false" via the routines "**SET_NOREFINE**" and "**SET_NOREMOVE**". Then, it computes the average gradient and the overall tolerance or selection criteria for the level. Finally, it flags all the patches in the level using the function "**SET_PATCH_FLAGS**", which actually sets the left or right flags of the input patch for either refinement or deletion as well its children if necessary.

4.11.7 Flux Correction

```
SUBROUTINE CORRECT_COARSE_FLUXES(LEVEL)
    IMPLICIT NONE
    TYPE(TLEVEL), POINTER :: LEVEL

    !---LOCAL VAVRIABLES
    TYPE(TPATCH), POINTER :: CURRENT
    INTEGER               :: IC, NL, NR
    INTEGER               :: NCHILD, NEPHEW

    IF (.NOT.ASSOCIATED(LEVEL)) RETURN
    IF (.NOT.ASSOCIATED(LEVEL%PREVIOUS)) RETURN

    CURRENT=>LEVEL%PREVIOUS%FIRST_GRID
    DO WHILE(ASSOCIATED(CURRENT))

       NCHILD = TYPEOF_CHILD(CURRENT)
       NEPHEW = TYPEOF_NEPHEW(CURRENT)
       CALL GET_INDEX(CURRENT, NCHILD, NL, NR)

       IF (NCHILD == 1) THEN            !ONLY THE LEFT CHILD EXIST.
          IC = NL                       !NL = NCELL/2 + 1
          CURRENT%DATA(IC,:)=CURRENT%DATA(IC,:) - TAU*CURRENT%FIN(:)
       ELSE IF (NCHILD == 2) THEN       !ONLY THE RIGHT CHILD EXIST.
          IC = NR                       !NR = NCELL/2
          CURRENT%DATA(IC,:)=CURRENT%DATA(IC,:) + TAU*CURRENT%FOUT(:)
       ENDIF

       IF (NEPHEW == 1) THEN            !ONLY THE LEFT NEPHEW EXIST.
          IC = NL                       !NL = 1
          CURRENT%DATA(IC,:)=CURRENT%DATA(IC,:) - TAU*CURRENT%FIN(:)

       ELSE IF (NEPHEW == 2) THEN       !ONLY THE RIGHT NEPHEW EXIST.
          IC = NR                       !NR = NCELL
          CURRENT%DATA(IC,:)=CURRENT%DATA(IC,:) + TAU*CURRENT%FOUT(:)

       ELSE IF (NEPHEW == 3) THEN       !BOTH LEFT & RIGHT NEPHEWS EXIST

          CURRENT%DATA(NL,:)=CURRENT%DATA(NL,:) - TAU*CURRENT%FIN(:)
          CURRENT%DATA(NR,:)=CURRENT%DATA(NR,:) + TAU*CURRENT%FOUT(:)
       ENDIF

       CURRENT=>CURRENT%NEXT
    ENDDO

END SUBROUTINE CORRECT COARSE FLUXES
```

Figure 4-17: Flux Correction Routine

Figure 4-17 depicts the flux correction function "**CORRECT_COARSE_FLUXES**" that is based on Section 4.9.2 equations. The algorithm is relatively simple, but it involves a variety of operations that demonstrate the importance of functional data attributes.

The algorithm begins by identifying the type coarse-fine interface boundary that requires refluxing, as well as the boundary relationships between the fine input grid and its parent or "aunt" (previous or next patch to the parent one). Then, the correction values are updated or corrected appropriately following the description given in Section 4.9.2.

It should be noted that for the algorithm to work properly, it requires an additional function "**INIT_CONSERVATIVE_REFLUX**", which actually computes the amount of correction necessary for the flux data, or the difference between the coarse fluxes and their corresponding fine ones.

4.11.8 Projection

Projection from fine to coarse grids is the process of updating a coarser level, using more accurate values of the cells at the fine level to replace the covering cells on immediately coarser level. Figure 4-18 depicts the EMAPS implementation of the algorithm as described by the transfer equation (4.1).

```
SUBROUTINE INTERPOLATE_COARSE_GRID(GRID)

    IMPLICIT NONE
    TYPE(TPATCH), POINTER :: GRID
    INTEGER       :: JCR, JF, JC       !LOCAL VARIABLES

    IF (.NOT.ASSOCIATED(GRID)) THEN
       CALL ABORT("MISSING GRID", "INTERPOLATE_COARSE_GRID")
    ENDIF

    IF (ASSOCIATED(GRID%LEFT_CHILD)) THEN
       DO JC=1,GRID%NCELL/2
          JF=2*JC
          GRID%DATA(JC,:)=0.5_WP*(GRID%LEFT_CHILD%DATA(JF,:)+ &
                                  GRID%LEFT_CHILD%DATA(JF-1,:))
       ENDDO
    ENDIF

    IF (ASSOCIATED(GRID%RIGHT_CHILD)) THEN
       DO JCR=1,GRID%NCELL/2
          JC=JCR+GRID%NCELL/2
          JF=2*JCR
          GRID%DATA(JC,:)=0.5_WP*(GRID%RIGHT_CHILD%DATA(JF,:)+ &
                                  GRID%RIGHT_CHILD%DATA(JF-1,:))
       ENDDO
    ENDIF

END SUBROUTINE INTERPOLATE_COARSE_GRID
```

Figure 4-18: Projection Routine from Fine to Coarse Grid

4.12 Numerical Validation of AMR Scheme

In previous sections, we have laid down the conceptual constructs and design of the AMR scheme that we have developed. We have also shown that the Fortran 90 implementation of its functional algorithms is both flexible and laborious and above all requires careful coordination.

Therefore, we present in this section the AMR scheme with various numerical test cases, and show that the massive effort spent to complete this general-purpose structured mesh refinement scheme was worthwhile.

4.12.1 Burgers test case

The first non-linear example selected is based on the inviscid Burgers equation (2.20) presented in Chapter 2. This scalar equation is used here as a test bed since its exact solution is known for some specific conditions. For the test case investigated, the initial condition is a square discontinuity velocity defined in a 5m pipe as:

$$u(x,0) = 1 \text{ if } 0.5 < x < 1.5$$
$$= 0 \text{ elsewhere}$$

This problem contains a complicated interaction of shock and rarefaction waves and it is a very hard test for mesh refinement algorithm because a large fraction of the computational domain is refined. Figure 4-19 shows good agreement with the analytical result at t = 1 s.

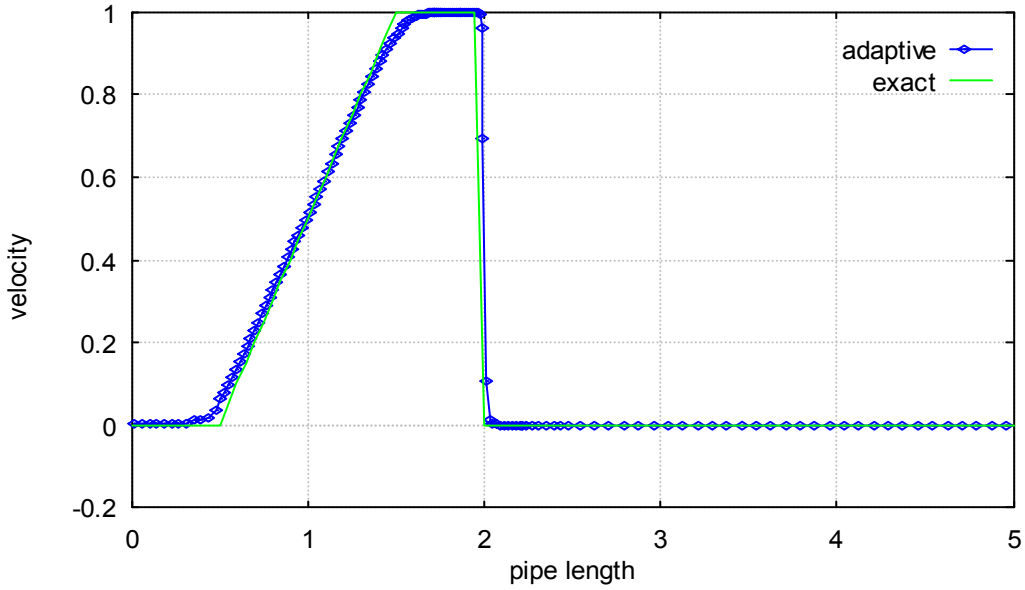

Figure 4-19: Comparison of exact solution and adaptive computation for 50 cells and 4 levels of refinement.

4.12.2 IFP Test Case

The second test case analyses a horizontal two-phase flow line of constant diameter and was studied in Section 3.8.1 of the third chapter for a uniform grid. As already mentioned, the mathematical model used is the HEM-3 described in the second chapter, and the full specifications of the problem are as follows:

- Pipeline: length = 10 km, diameter = 0.146 m
- Operating fluids: air and water (ρ_G variable, $\rho_L = 1000 kg/m^3$)
- Flow temperature: T = 5 °C
- Outlet pressure: 10 bar

The liquid mass flow rate is kept constant and equal to 20 kg/s. The gas mass flow is initially equal to 0.2 kg/s and between t = 1000s and t = 1010s, it is doubled to 0.4 kg/s. All numerical computations use the FCT explicit solver with a CFL value of 0.5.

Flow Evolution

Figures 4.20 and 4.21 present the evolution of the liquid hold-up and superficial velocity at different times. As expected the air expands under the influence of the pressure gradient, forcing a decrease in the liquid volume fraction since the two phases flow with the same velocity. These computations use adaptive gridding with one initial patch of 50 coarse cells and 4 levels of refinement.

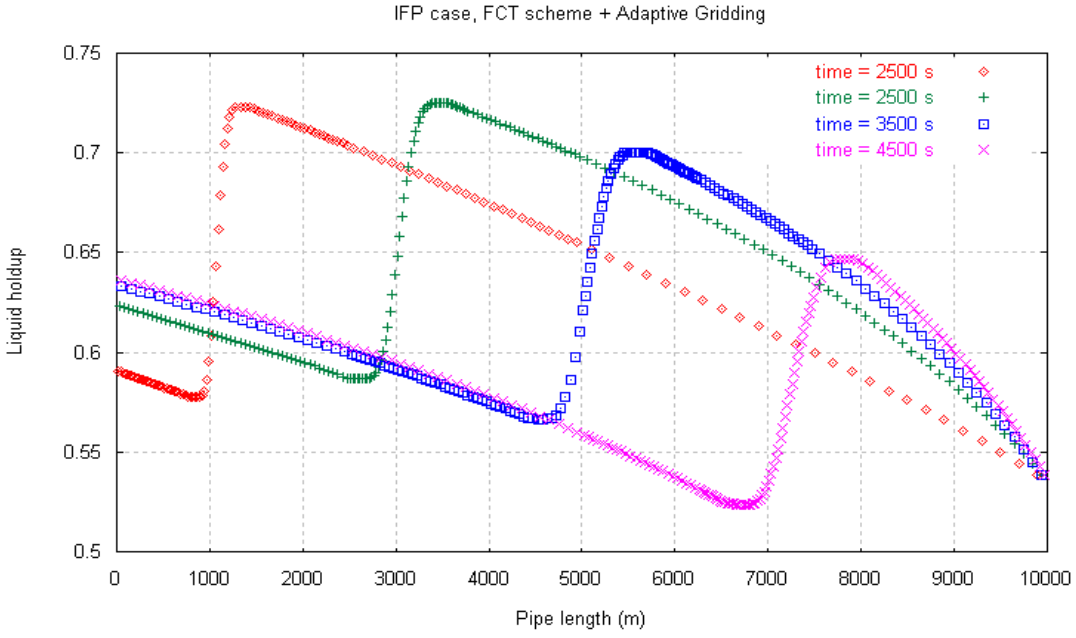

Figure 4-20: HEM-3 [IFP Case]. Time evolution of the liquid hold-up with adaptive grid (50 coarse cells and 4 levels of refinement)

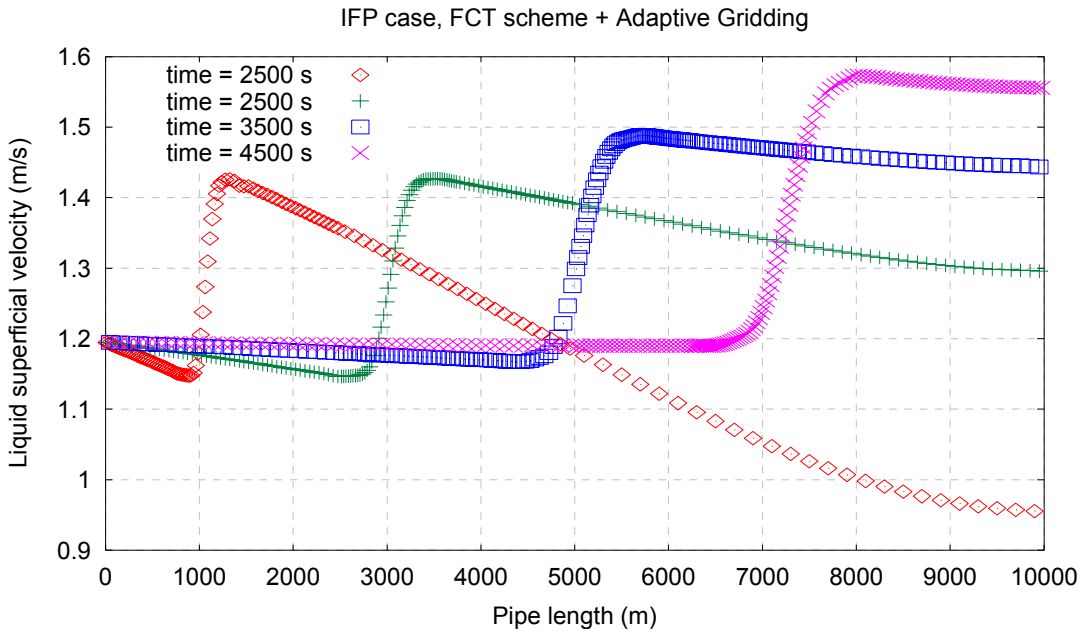

Figure 4-21: HEM-3 [IFP Case]. Time evolution of the liquid superficial velocity with adaptive grid (50 coarse cells and 4 levels of refinement)

The figures clearly show the robustness and effectiveness of the AMR algorithm as the mesh distribution along the pipe automatically evolves with the flow, with fine meshes concentrated near discontinuities where they are needed.

It should be noted that the number of refinement levels in graphs 4.20 and 4.21 is the maximum number of levels input by the user of the AMR code. However, the initial coarse level in the code is indexed 1, and therefore the 4 levels of refinement indicated in the graphs actually correspond to 3 levels of effective refinement in the code. In this thesis, the number of refinement levels will always refer to the one input by the user.

Distribution of Refinement Levels

Figure 4-22 presents the distribution of refinement levels and the holdup profile at time = 3600 seconds. The simulation for this graph was performed using and adaptive gridding with two initial patches of 24 coarse cells and 4 levels of refinement.

The graph confirms the observations mentioned above, and clearly demonstrates the effective concentration of fine cells near the holdup discontinuity, while coarse cells are used far away from the discontinuity.

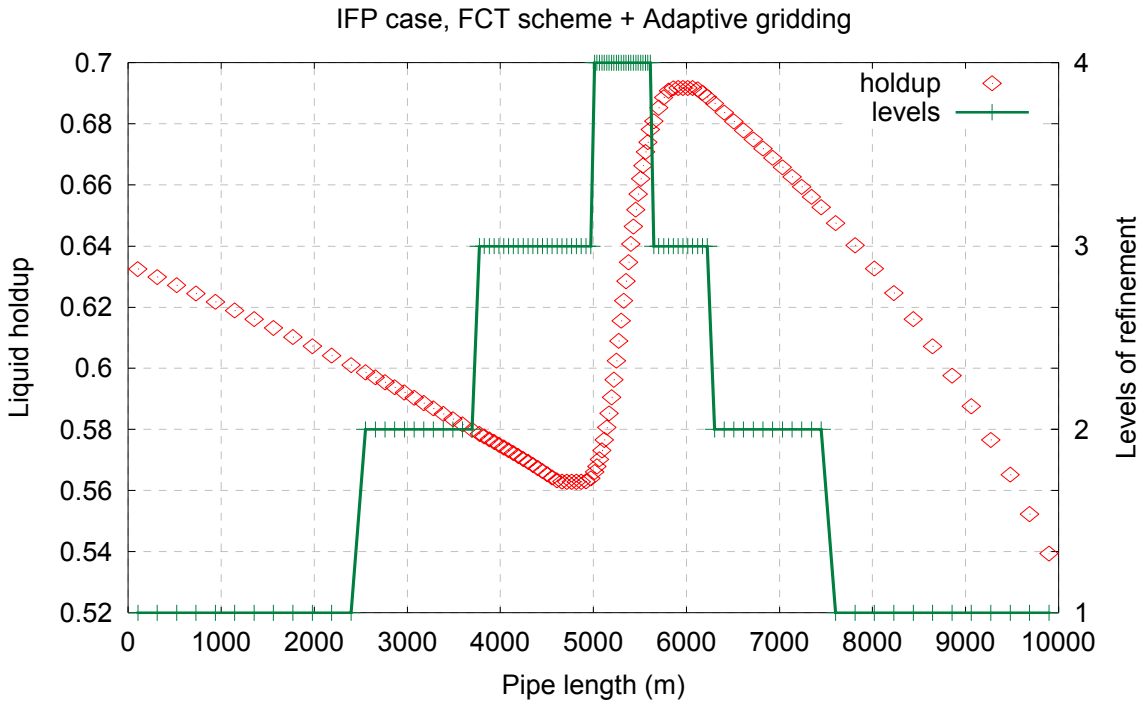

Figure 4-22: HEM-3 [IIFP Case]. Distribution of refinement levels and holdup profile at time = 3600 s.

Comparison Uniform and Adaptive Gridding

Figure 4-23 shows the time evolution of the liquid holdup with 50 uniform cells. We remark the poor quality of results compared to Figure 4-20. This fact is also observed in Figure 4-24, which compares the liquid holdup results obtained using the uniform and adaptive gridding simulations with one initial patch of 50 coarse cells.

Figure 4-24 also compares the adaptive gridding simulation using 50 coarse cells and 4 levels of refinement with the equivalent uniform grid (400 cells), and it can be seen that the two results are very similar. This finding make the AMR scheme very attractive, as a similar convergent solution can be achieved for a fractional computational time compared to the uniform grid code (see Table 4.1).

It is however difficult to evaluate the error or difference between the two solutions, because the adaptive gridding code do not use a fixed number of cells like the uniform grid, and calculation of the error may only be possible in a tiny part of the holdup profile, near the discontinuity, where the fourth and final level of refinement is used by the adaptive gridding code, and the cell locations are identical to the ones used by the uniform grid code.

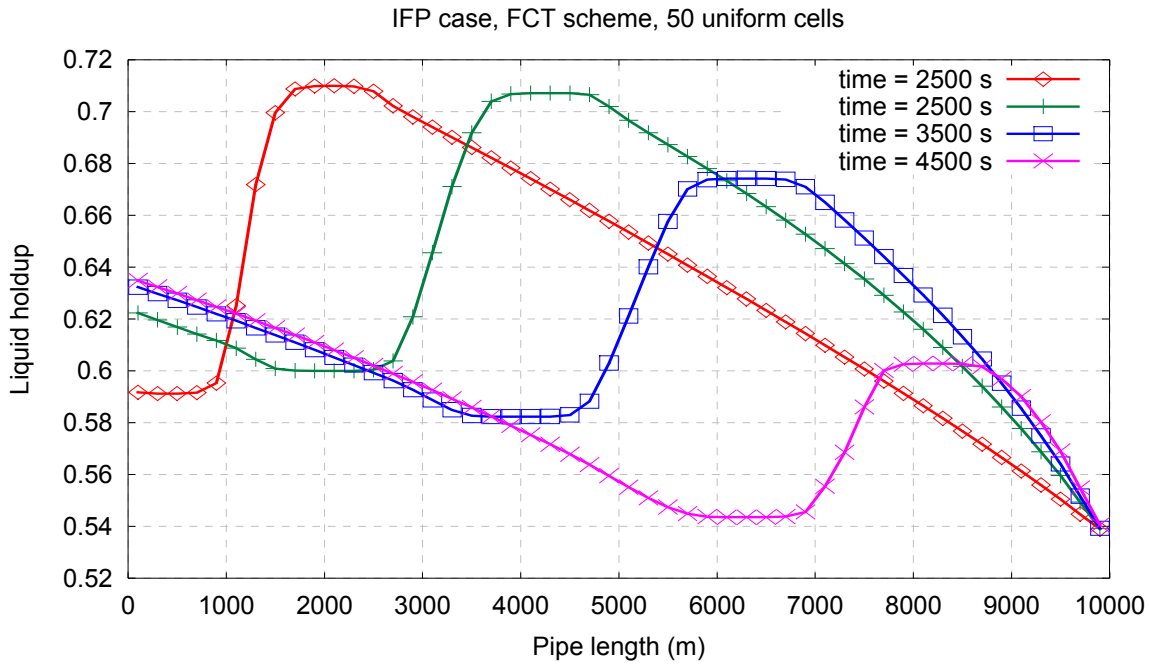

Figure 4-23: HEM-3 [IFP Case]. Time evolution of the liquid hold-up with uniform grid.

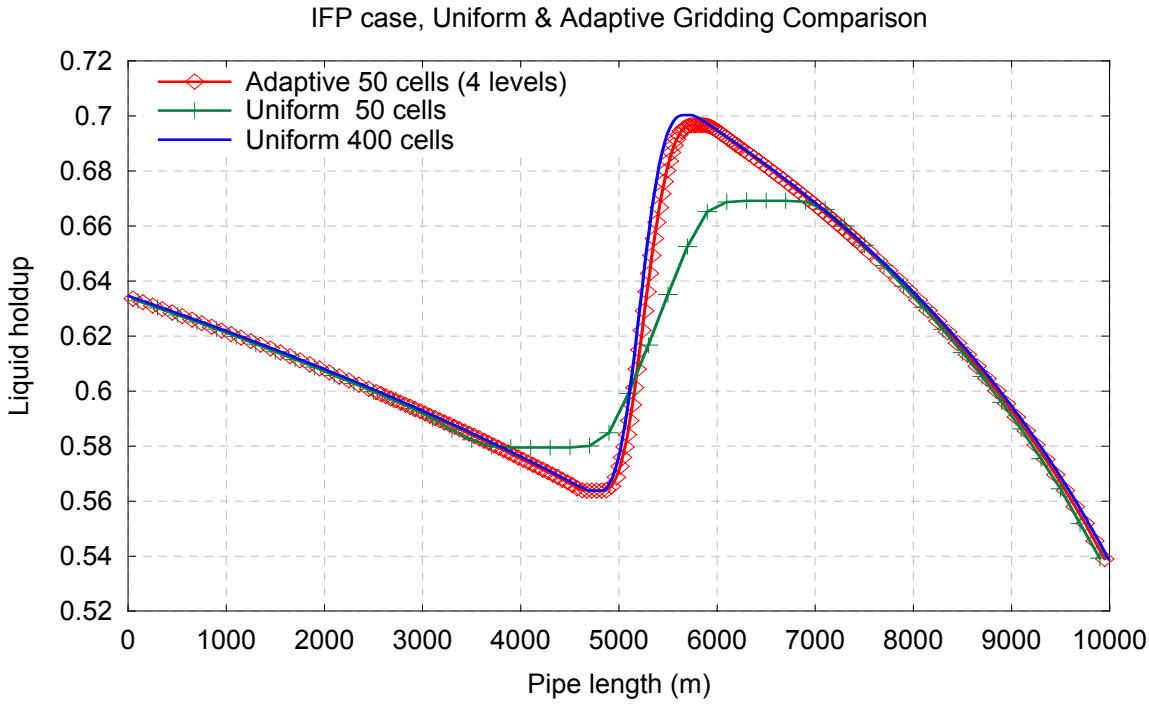

Figure 4-24: HEM-3 [IFP Case]. Comparison between uniform & adaptive grid at 3600 s.

4.12.3 Timings

Table 4-1 shows the execution time recorded for the integration of the IFP test case after 4500 seconds using a DEC Alpha computer. As we can see, the AMR method significantly accelerates the computation compared to uniform grid.

Levels of refinement	Timings (s)			Speed-up	
	Uniform (actual)	Uniform (max-amr)	Adaptive	Uniform (actual)	Uniform (max-amr)
1	4.7 (50)	4.7 (50)	-	-	-
2	16.9 (100)	36.9 (150)	11.0	1.54	3.35
3	64.8 (200)	195.7 (350)	27.0	2.40	7.25
4	259.5 (400)	887.8 (750)	65.3	3.97	13.60
5	1028.6 (800)	3779.9 (1550)	156.6	6.57	24.14

Table 4-1: Running time for different grid types and levels

In Table 4.1, the number in brackets in column 2 and 3 correspond to the total number of cells used by the uniform grid code. More precisely, the adaptive grid code uses 50 coarse cells, which are equivalent to 100 cells for two levels of refinement and a maximum of 150 uniform cells can coexist in the AMR code. Similarly, 3 levels of refinement are equivalent to 200 uniform cells (or a maximum of 350 uniform cells in the AMR code) while 5 levels of refinement are equivalent to 800 uniform cells.

4.13 Conclusion

The algorithm presented in this chapter uses a new automatic grid refinement algorithm to simulate time dependent problems. Although it is composed of many co-ordinated elements, two key features make it possible. An automatic procedure, which estimates the solution average error and selects the appropriate zones to be refined in the computational grid. The other important feature of this algorithm is the flexible data structure that actually supports its implementation. This has immediate impact on the practical utility of the approach since it influences the storage and computation overhead to manage the refinement strategy. It also has a strong bearing on the actual complexity of the code. By using Fortran 90 as the implementation language, we contributed to a fully integrated AMR scheme and designed a data structure that provides the best balance between storage and computational cost without significantly increasing the code complexity.

We have validated our algorithm with several numerical examples and demonstrated that the AMR algorithm achieves the same accuracy for a fraction of the cost of a calculation on a conventional uniform grid. More precisely, we have shown that this algorithmic technique can save as much as an order of magnitude in computational time for two-phase flow problems. However, it should be noted that there are some areas where our mesh refinement scheme still needs research and improvement. Considering that the best initial grid generation procedure is still an important open question, the use of implicit finite difference methods with the EMAPS data structure needs to be developed further, as well as the validation of the scheme for non-conservative mathematical models.

It is also worth mentioning that the design, implementation and testing of AMR in the EMAPS framework was a long and laborious process, the extent of which was not anticipated at the outset. During the overwhelming majority of this process, no aspect of the components had any significant value beyond its anticipated future role within the overall environment. Furthermore, AMR's many functional layers are so completely integrated that it was impossible to employ it for anything useful prior to completion, and this facet of its development proved intensely frustrating. Therefore, we do hope that the conceptual constructs laid out in this chapter will provide an aid to designing, and help the reader in better understanding the structured AMR strategy that we have developed.

In the end, we succeeded in implementing a robust and efficient AMR scheme for conservative one-dimensional models in the EMAPS framework, which proved itself in execution. However, this scheme is not valid for multi-dimensional problems and we do not recommend anyone to embark in the tedious operation of extending the scheme for this class of problems. Instead, we advocate using cross-language implementation for Fortran developers of numerical solvers, and opt for the general-purpose C++ implementation provided by Neeman (1996) in his fully detailed PhD thesis.

4.14 References - 4

- **Arney D. C., (1989)** "An adaptive method with mesh moving and mesh refinement for solving the Euler equations", *AIAA Journal,* **72**.

- **Bell J., Berger M., Saltzman J. & Welcome M., (1994)** "Three-Dimensional Adaptive Mesh Refinement for Hyperbolic Conservation Laws". *SIAM J. Sci. Stat.*, **15(1)**, 127-138.

- **Berger M. J. & Oliger J., (1984)** "Adaptive Mesh Refinement for Hyperbolic Partial Differential Equations". *Journal Computational Physics*, **53**, 484-512.

- **Berger M. J. & Colella P., (1989)** "Local Adaptive Mesh Refinement for Shock Hydrodynamics". *Journal Computational Physics*, **82**, 64-84.

- **Berger M., (1987)** "On Conservation at grid interfaces." *SIAM Journal on Numerical Analysis*, **24**, 967-984.

- **Boden E. P., (1997)** "An Adaptive Gridding Technique for Conservation Laws on Complex Domains". *PhD Thesis*, Cranfield Institute of Technology**,** UK**.**

- **Brandt A., (1977)** "A Multi-level adaptive solutions to boundary-value problems", *Mathematics Of Computation*, **31 (138),** 333-390.

- **Hornung R. & Trangenstein J., (1997)** "Adaptive Mesh Refinement and Multilevel Iteration for Flow in Porous Media", *Journal Computational Physics*, **136**, 522-545.

- **Lezeau P. & Thompson, C. P., (1998)** "Numerical Simulation of Multi-Phase Flow: Speed, Error Control & Robustness", *Cranfield University Technical Report*.

- **Li S. & Petzold L., (1997)** "Moving mesh methods with upwinding schemes for time-dependent PDEs". *Journal Computational Physics*, **131**, 368-377.

- **Lohner R., (1998)** "Finite element methods in CFD: Grid generation, adaptivity and parallelization". Algorithms and data structures for structured and unstructured grid generation, *Selected Special Topics from Previous VKI Lectures Series,* Editor: H. Deconinck. Reprinted from AGARD-R-787, 1992.

- **Mavriplis D. J., (1990)** "Adaptive mesh generation for viscous flows using Delaunay triangulation". *Journal of Computational Physics*, **90(2)**, 271-291.

- **Mavriplis D. J., (1998)** "Unstructured mesh generation and adaptivity". Algorithms and data structures for structured and unstructured grid generation, *Selected Special Topics from Previous VKI Lectures Series,* Editor: H. Deconinck. Reprinted from VKI LS 1995-02.

- **Neeman H. J., (1996)** "Autonomous Hierarchical Adaptive Mesh Refinement For Multiscale Simulations", *PhD Thesis*, University of Illinois.

- **Omgba C., Hanich L., Thompson C., and Lezeau P., (2000)** "Adaptive Grid Refinement for Transient Two-Phase Flows". In *Proceedings of the AMIF-ESF Workshop "Computing Methods in Two-Phase Flow",* Aussois, France, 12-14th January, **Paper 9**.

- **Parashar M., & Browne J., (199?)** "DAGH: A Data-Management infrastructure for Parallel adaptive Mesh refinement Techniques: Preliminary Users Guide", *Department of Computer Science, University of Texas at Austin*, Draft Report.

- **Pember R., Bell J., Colella P., Crutchfield W., and Welcome M., (1995)** "An Adaptive Cartesian Grid Method for Unsteady Compressible Flow in Irregular Regions." *Journal Computational Physics*, **120**, 278-304.

- **Quirk J. J., (1991)** "An Adaptive Grid Algorithm for Computational Shock Hydrodynamics". *PhD Thesis*, Cranfield Institute of Technology**,** UK**.**

- **Skamarock W., Oliger J., and Street R., (1989)** "Adaptive Grid Refinement for Numerical Weather Prediction". *Journal Computational Physics*, **80**, 27-60.

- **Stockie J. M., Mackenzie J. A., and Russel R. D., (2001)** "A moving mesh method for one-dimensional hyperbolic conservation laws". *SIAM J. Sci. Comput.*, **22**, 1791-1813.

- **Tang H., & Tang T., (2003)** "Moving mesh methods for one- and two-dimensional hyperbolic conservation laws". *SIAM Journal on Numerical Analysis*, **41/2**, 487-515.

- **Thompson C. P., Leaf G. K., and van Rosendale J., (1992)** "A dynamically-adaptive parallelizable multigrid algorithm for the incompressible Navier-Stokes equations". *Applied Numerical Mathematics*, **9**, 511-532.

5 Chapter 5 - Stratified Flow Modelling

5.1 Introduction

This chapter deals with issues associated with the accurate modelling of stratified gas-liquid flow in horizontal pipes, in particular the correct description of the momentum transfer for each phase at the wall and between the two phases at the interface. The two main reasons, for looking at this specific flow pattern, are:

- Firstly, because it is the simplest interface configuration encountered in two-phase flows, and there is available and reliable experimental data for validating stratified flow patterns, and we believe that any attempt to model more complex features occurring in two-phase intermittent flows will be achieved with a better understanding and an accurate prediction of stratified flows.

- Secondly and more importantly, because it plays a major role in slug flow configuration, which is the one of the prime objectives of this study. Indeed, most slug units are composed of two regions, a dispersed bubble region (or the liquid slug) and a long bubble region, also known as the stratified film region. In this latter section, the stratified flow theory presented in this chapter is applied.

Unfortunately, being the simplest flow pattern does not mean that stratified flow is easy to model, and there is still intensive ongoing research in two-phase stratified gas-liquid flow with the focus being the improvement of mathematical models to accurately predict key design parameters, such as the pressure drop of a pipeline system, and to understand two-phase flow characteristics such as heat and mass transfer, or friction factors.

5.2 Chapter Outline

Figure 5-1 shows the configuration of stratified flow pattern that we attempt to predict using the incompressible two-fluid model PFM-2 presented in the first chapter of this thesis. As already mentioned, this model assumes:

- No heat transfer between the two phases.
- No mass transfer between the two phases.
- And that the two fluids are taken incompressible.

With those assumptions, the main uncertainties for this one-dimensional stratified flow model are the closure laws for wall and interfacial shear stresses. Therefore, a review and a validation study of these terms constitute the major part of this chapter and are covered in the next sections.

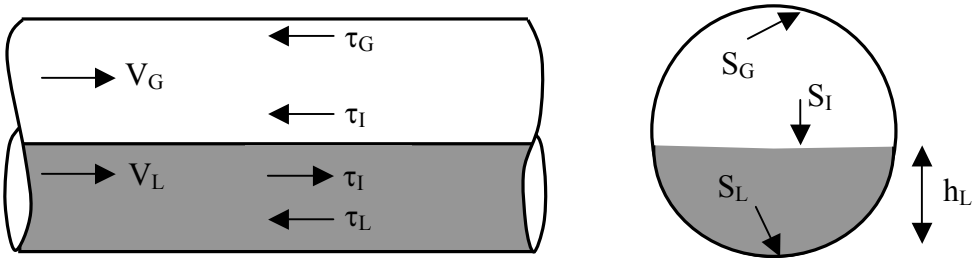

Figure 5-1: Stratified flow in a horizontal pipe

5.3 Characterization of the Interface

A stratified flow pattern is characterized by the separation of the liquid and gas flows, with the liquid moving downstream along the bottom of the horizontal pipe and the gas flowing concurrently above it (Figure 5-1). At low gas velocity, the gas-liquid interface appears undisturbed or smooth. However, as the gas velocity is increased, waves appear on the interface and the flow pattern is referred to as stratified wavy.

(a) Stratified smooth (b) Stratified wavy

Figure 5-2: Stratified flow patterns (from http://www.pe.utexas.edu/2phaseweb/flowhoriz.html, visited on 03/12/2003)

Hence, the simplest classification of the stratified flow patterns is into two sub-regimes, stratified-smooth and stratified-wavy (Figure 5-2) as suggested by Baker (1954). However, several authors [Andreussi & Persen, 1987; Chen et al., 1997; and Espedal, 1998] have further subdivided the stratified-wavy flow into different categories or sub-regimes according to the various types of waves observed at the gas-liquid interface.

The process of interfacial wave formation is not well understood and it is the ability of the interface to deform with the flow, which still makes modelling stratified flow a difficult endeavour. The structure of this deformable interface is very important for mathematical models, as it will dominate the drag between the phases. In 1D models, the drag at the gas-

liquid interface is expressed in terms of an interfacial friction factor, which is considered as the most relevant parameter to predicting two-phase flow. Therefore, a large number of empirical relationships have been suggested for interfacial friction factor.

For this study, we only consider two flow sub-regimes in the stratified region as suggested by Baker (1954), but the key modelling question of this work is to find which interface friction factor is better for each stratified flow regime, and if different correlations must be used for each pattern, when to switch from one to another. We will attempt to answer these two questions in Section 5.6.

5.4 Literature Review – Steady State Parameters

The pressure drop and the phase distribution content (holdup) are the two most important design parameters for petroleum engineers, and therefore many methods have been derived to predict them accurately. In this section we review some of these empirical methods for fully developed (steady-state) stratified flow.

Though, our primary interest lies in predicting the behaviour of unsteady flows, an accurate estimate of these fully developed parameters is generally required in most two-fluid models, as initial conditions for transient simulations. It is therefore crucial that we evaluate properly these two key parameters for a rapid convergence of the mathematical models and numerical schemes described in previous chapters.

5.4.1 Pressure Drop

The overall two-phase pressure drop generally contains three components, namely, the frictional, gravitational and acceleration terms and it is given as:

$$\left(\frac{dP}{dx}\right)_{TP} = \left(\frac{dP}{dx}\right)_{fric} + \left(\frac{dP}{dx}\right)_{grav} + \left(\frac{dP}{dx}\right)_{acc} \qquad (5.1)$$

However, for horizontal flow the gravitational or hydrostatic pressure drop is zero, and Ferguson & Spedding (1995) stated that when the total mass velocity G_T is less than 2700 kg / (m^2 s), only the frictional term is of importance. As most prediction methods are concerned with this case, we only review here the frictional term of the overall pressure drop.

Depending on the two-phase flow behaviour assumption, the methods available in the literature can be classified into two groups, namely the **homogeneous** flow models and **separated** flow models, and they are briefly summarized in the next two sub-sections. For a complete description of many of these models, we refer to the thesis by Pan (1996).

5.4.1.1 Correlations from the "Homogeneous Flow" Approach

This simplified model is generally used to estimate the frictional pressure drop for dispersed flow regime (churn, bubbly) and sometimes for slug flow as well, but it is not recommended for stratified or annular flow regimes. It adopts an opposite approach to the separated flow model described below, and is based on the assumption that the two-phase flow can be treated as a hypothetical single-phase flow having some kind of average properties.

Therefore, for a given gas and liquid mass fluxes (G_G and G_L), McAdams et al. (1942) modified the single-phase equation and proposed an easy way to calculate the two-phase frictional pressure drop; their expression is given by:

$$\left(\frac{dP}{dx}\right)_{fric}^{hom} = \frac{2f_M\left(G_G + G_L\right)^2}{D\rho_H} \tag{5.2}$$

where ρ_H is the homogeneous density and f_M is the single-phase friction factor based on the mixture fluid properties (density and viscosity). Any of the single-phase friction factor correlations presented in Section 5.5.1.1 can be used to evaluate f_M, for example:

$$f_M = \max\left(\frac{16}{Re_M} \quad , \quad \frac{0.079}{Re_M^{0.25}}\right) \tag{5.3}$$

The mixture Reynolds number Re_M is based on the mixture viscosity and it is defined as:

$$Re_M = \frac{\left(G_G + G_L\right)D}{\mu_M} \tag{5.4}$$

Hence, the main issue for the frictional pressure drop prediction with the homogeneous model (5.2) is in evaluating accurately the mixture density and viscosity. There is an agreement in the literature for the homogeneous mixture density, and its expression is usually given by:

$$\frac{1}{\rho_H} = \frac{x_G}{\rho_G} + \frac{1 - x_G}{\rho_L} \tag{5.5a}$$

which leads to:

$$\rho_H = \left(1 - \lambda_L\right)\rho_G + \lambda_L\rho_L \tag{5.5b}$$

The terms x_G and λ_L are respectively known as the (gas) quality and the non-slip (liquid) holdup and are defined as:

$$x_G = \frac{G_G}{G_G + G_L} = \frac{\rho_G J_G}{\rho_G J_G + \rho_L J_L} \tag{5.6}$$

and

$$\lambda_L = \frac{J_L}{J_G + J_L} = \frac{\rho_G (1 - x_G)}{\rho_L x_G + \rho_G (1 - x_G)} \tag{5.7}$$

where J_G and J_L are respectively the gas and liquid superficial velocities.

References	Mixture Viscosity (μ_M)
McAdams et al. (1942)	$\frac{1}{\mu_M} = \frac{x_G}{\mu_G} + \frac{1 - x_G}{\mu_L}$
Cicchiti et al. (1960)	$\mu_M = x_G \mu_G + (1 - x_G)\mu_L$
Dukler et al. (1964)	$\mu_M = (1 - \lambda_L)\mu_G + \lambda_L \mu_L$
Ishii & Zuber (1979) [bubbly flow]	$\mu_M = \mu_L \lambda_L^{\left(-2.5\left[\frac{\mu_G + 0.4\mu_L}{\mu_G + \mu_L}\right]\right)}$
Beattie & Whalley (1982)	$\mu_M = (1 - \lambda_L)\mu_G + \lambda_L \mu_L [1 + 2.5(1 - \lambda_L)]$
Olujic(1985)	$\mu_M = \mu_L \left(1 - x_G \left[1 - \frac{\mu_L}{\mu_G}\right]\right)$
Lin et al. (1991)	$\mu_M = \frac{\mu_L \mu_G}{\mu_G + x_G^{1.4}(\mu_L - \mu_G)}$

Table 5-1: Correlations for the mixture viscosity

As for the homogeneous mixture viscosity, its concept as well as its determination is less obvious, therefore, various expressions have been suggested in the literature and some of them are reported in Table 5-1. These numerous models often lead to a completely different estimate of the mixture viscosity for various operational conditions, and this fact is the main reason why the homogeneous flow model is less in favour as a predictive tool for the pressure drop calculation compared to the separated flow model described below.

5.4.1.2 Correlations from the "Separated Flow" Approach

This model can be used for any type of flow regime, and assumes that distinct parts of the flow cross-section can be assigned to the two phases, reflecting to a large extent what

occurs in stratified or annular flow regimes. It involves the use of a coefficient term also known as a two-phase multiplier and it is defined by:

$$\left(\frac{dP}{dx}\right)_{fric}^{sep} = \phi_R^2 \left(\frac{dP}{dx}\right)_R \tag{5.8}$$

That is, the two-phase frictional pressure gradient is calculated from a reference single-phase frictional pressure gradient $(dP/dx)_R$ multiplied by the two-phase multiplier, the value of which is determined from empirical correlations.

In equation (5.8) the two-phase multiplier is written as ϕ_R^2 to denote that it corresponds to the reference single-phase flow denoted by the subscript R. For gas-liquid two-phase flow, there are four possible reference flows:

1. whole flow liquid, denoted by subscripts LO
2. whole flow gas denoted by subscripts GO
3. only the liquid in the two-phase flow, denoted by subscript L
4. only the gas in the two-phase flow, denoted by subscript G

As pointed out by Levy (1999), there are two aspects of the notation that may lead to confusion and error. First, note that LO and GO do not denote "liquid only" and "gas only" reference flows, as might be expected. On the contrary, they denote flows in which the whole of the flow rate is liquid or gas. It may help to remember them as "liquid overall" and "gas overall". The second point to note is that ϕ^2 denotes the two-phase multiplier, and not its square root value ϕ.

As already mentioned, a very large number of separated pressure drop models are available, and it will be impractical and probably counter-productive to list them all here. In addition, many critical evaluations of the existing pressure drop prediction methods have been performed and we refer the reader to these references.

However, from the early studies of Hughmark (1963) that compared four pressure drops against air-water test data, to the recent study of Ferguson & Spedding (1995) comparing 70 pressure drop models using various test fluids, the numerous comparative studies [Weisman & Choe, 1976; Mandhane et al., 1977; Friedel, 1980; Beattie & Whalley, 1982; Gregory & Fogarasi, 1985; Cawkwell & Charles, 1985; Simpson et al., 1987; and Baker et al., 1988] reported in the literature do not really agree on the recommended frictional pressure drop model.

Therefore, we only present here the models recommended recently by Corradini (1997) who noted that some correlations described in the literature performed better than other for certain flow conditions and pipe topographies, and to obtain an optimal model, he suggested combining three existing models as follows:

1. The Lockhart-Martinelli (1949) correlation for flow where the viscosity ratio $\mu_L/\mu_G > 1000$ and the total flowrate $G_T > 100\ kg/m^2.s$
2. The Chisholm-Baroczy (1973) correlation for flow where $\mu_L/\mu_G > 1000$ and $G_T < 100\ kg/m^2.s$
3. The Friedel (1979) correlation for $\mu_L/\mu_G << 1000$

These three models, which were also recently recommended by Haraburda & Chafin (2000), are detailed a bit more in the following paragraphs, plus an extra phenomenological model that we have adopted for practical applications.

Lockhart & Martinelli (1949) introduced the concept of multiplier mentioned above by proposing a correlation for the frictional pressure drop using the liquid single-phase pressure gradient (R = L) as a reference in Equation (5.8), so that

$$\left(\frac{dP}{dx}\right)_{fric}^{LM} = \phi_L^2 \left(\frac{dP}{dx}\right)_L \tag{5.9}$$

However, the relationship between their two-phase multiplier ϕ_L^2 and the Martinelli parameter X^2 defined by equation (5.11) was originally given in graphical form, but Chisholm (1967) accurately approximated this graphical relationship by a simple expression based on a tabular constant C which depends on whether the gas and liquid are laminar or turbulent. The proposed correlation is:

$$\phi_L^2 = 1 + \frac{C}{X} + \frac{1}{X^2} \tag{5.10}$$

$$X^2 = \frac{\left(\frac{dP}{dx}\right)_L}{\left(\frac{dP}{dx}\right)_G} \tag{5.11}$$

$$\left(\frac{dP}{dx}\right)_k = \frac{2 f_k G_k^2}{D \rho_k}, \qquad k = G, L \tag{5.12}$$

$$f_k = \max\left(\frac{16}{Re_k}\ ,\ \frac{0.046}{Re_k^{0.2}}\right) \tag{5.13}$$

$$Re_k = \frac{G_k D}{\mu_k} \tag{5.14}$$

The coefficient C in relation (5.10) depends on whether the gas and liquid are laminar or turbulent (see Table 5-2).

Gas	Liquid	C
Laminar	Laminar	5
Laminar	Turbulent	10
Turbulent	Laminar	12
Turbulent	Turbulent	20

Table 5-2: Chisholm coefficient C for the Lockhart & Martinelli pressure drop

Using the "liquid overall" flow (R = LO) as a reference, Baroczy (1966) also proposed a frictional pressure drop calculation in graphical form, which Hewitt (1982) recommended as the most widely used and advanced empirical correlation. This graphical relationship was curve-fitted by Chisholm (1973) with the formula:

$$\phi_{LO}^2 = 1 + \left(Z^2 - 1\right)\left(B\left[x_G\left(1 - x_G\right)\right]^{0.9} + x_G^{1.8}\right) \tag{5.15}$$

which extends the range of the graphical relationship. Here, x_G is the quality defined by Equation (5.6) and B is given by:

$$B = \begin{cases} \dfrac{55}{\left(G_G + G_L\right)^{0.5}} & \text{for } 0 <= Z <= 9.5 \\ \dfrac{520}{Z\left(G_G + G_L\right)^{0.5}} & \text{for } 9.5 < Z < 28 \\ \dfrac{15000}{Z^2\left(G_G + G_L\right)^{0.5}} & \text{for } 28 <= Z \end{cases} \tag{5.16}$$

where

$$Z^2 = \left(\frac{dP}{dx}\right)_{GO} \Big/ \left(\frac{dP}{dx}\right)_{LO} \tag{5.17}$$

$$\left(\frac{dP}{dx}\right)_{kO} = \frac{2f_{kO}\left(G_G + G_L\right)^2}{D\rho_k}, \qquad k = G, L \tag{5.18}$$

$$f_{kO} = \max\left(\frac{16}{Re_{kO}} \quad , \quad \frac{0.046}{Re_{kO}^{0.2}}\right) \tag{5.19}$$

$$Re_{kO} = \frac{(G_G + G_L)D}{\mu_k} \tag{5.20}$$

Finally, the Chisholm-Baroczy [Chisholm, 1973] pressure drop for two-phase flows is calculated by:

$$\left(\frac{dP}{dx}\right)_{fric}^{CB} = \phi_{LO}^2 \left(\frac{dP}{dx}\right)_{LO} \tag{5.21}$$

Based on a data bank of 25, 000 data points from the literature, Friedel (1979) also proposed a generalized correlation using the "liquid overall" two-phase multiplier as a reference similarly to relation (5.21). His multiplier can be expressed as:

$$\phi_{LO}^2 = C_1 + \frac{3.24 C_2 C_3}{\overline{Fr}_M^{0.045} We_M^{0.035}} \tag{5.22}$$

where the coefficients C_1, C_2, C_3, and the square mixture Froude number and the Weber number are respectively defined by:

$$C_1 = (1 - x_G)^2 + x_G^2 \frac{\rho_L}{\rho_G}\left(\frac{f_{GO}}{f_{LO}}\right) \tag{5.23a}$$

$$C_2 = x_G^{0.78}(1 - x_G)^{0.24} \tag{5.23b}$$

$$C_3 = \left(\frac{\rho_L}{\rho_G}\right)^{0.91}\left(\frac{\mu_G}{\mu_L}\right)^{0.19}\left(1 - \frac{\mu_G}{\mu_L}\right)^{0.7} \tag{5.23c}$$

$$\overline{Fr}_M = \frac{V_M^2}{gD} = \frac{(J_G + J_L)^2}{gD} \tag{5.24}$$

$$We_M = \frac{(G_G + G_L)^2 D}{\sigma \rho_H} \tag{5.25}$$

The friction factors f_{LO} and f_{GO} should be calculated using equations (5.19)-(5.20) and finally the pressure drop should be calculated using equations (5.21), (5.22) and (5.18).

Muller-Steinhagen & Heck (1986) proposed a simple phenomenological frictional pressure drop correlation, which is applicable for all gas-liquid flow patterns. The model is essentially an empirical two-phase extrapolation between all liquid flow and all vapour flow such that is applicable for $0 \le x_G \le 1$. Recently, Tribble & Muller-Steinhagen (2000) have shown that this method gave the best results from a comparison of competing methods against a database covering air-oil, air-water, steam-water and several refrigerants. This pressure gradient correlation is:

$$\left(\frac{dP}{dx}\right)_{fric}^{MH} = G(1-x_G)^{1/3} + bx_G^3 \tag{5.26}$$

The factor G is given by:

$$G = a + 2(b-a)x_G \tag{5.27}$$

The variables a and b represent the frictional pressure drop gradients for all the flow liquid $(dP/dx)_{LO}$ and all the flow gas $(dP/dx)_{GO}$ obtained from equation (5.18). It is this simple correlation that has been implemented in the EMAPS code for initial condition purposes in the case where the two-phase pressure based models (HEM-3 or SPM-4) are selected for practical flow conditions including the stratified flow regime.

5.4.2 Liquid Holdup

As already mentioned, an estimate of the liquid holdup is often required as initial condition for two-phase flow simulations, and similarly to the pressure drop, many correlations have been proposed in the literature. They are generally flow regime-dependent and therefore not applicable to all flow situations.

In the next paragraph, we only describe six empirical correlations, which were critically evaluated and recommended in review papers by Dukler et al. (1964), Mandhane et al. (1975), and Payne et al. (1979). All these correlations, although derived for general-purpose applications and for all flow patterns, do not always constitute an initial guess for the liquid holdup in the stratified flow case. Therefore, we also present the semi-theoretical correlation presented by Taitel & Dukler (1976) and which is generally selected as a default value for the initial liquid holdup in the EMAPS code.

5.4.2.1 Empirical Correlations

Lockhart & Martinelli (1949) presented an empirical liquid holdup correlation that was later recommended by Mandhane et al. (1975) for the annular flow regime only. This

correlation only depends upon of the dimensionless parameter X defined by Equation (5.11) as the ratio between the liquid and gas frictional pressure drops, and was given in graphical form. It was later fitted by Pan (1996) with the following formula:

$$R_L = 0.228255 + 0.111327 \ln X + 0.012566[\ln X]^2 - 0.001085[\ln X]^3 \qquad (5.28)$$

Hughmark (1962) presented a generalized two-phase liquid holdup correlation using a graphical relationship between two parameters K and Z and claimed it to be applicable to horizontal as well as vertical upward flow. His implicit correlation can be expressed as:

$$R_L = 1 - K(1 - \lambda_L) \qquad (5.29)$$

where K is function of the parameter Z defined by:

$$Z = Re_M^{1/6}\left[\frac{Fr_M}{\lambda_L}\right]^{1/4} \qquad (5.30)$$

The non-slip liquid holdup λ_L and the mixture Froude number Fr_M are defined by Equations (5.7) and (5.24) respectively and the mixture Reynolds number Re_M is given by relation (5.4) where the mixture viscosity is a linear function of the calculated holdup, defined as:

$$\mu_M = R_G \mu_G + R_L \mu_L \qquad (5.31)$$

The relation between K and Z was given in tabular form by the author, but was later expressed in algebraic form by Pan (1996) as:

$$K = \begin{cases} -0.16367 + 0.31037Z - 0.03525Z^2 + 0.0013667Z^3 & Z < 10 \\ 0.75545 + 0.0358Z - 0.146 \cdot 10^{-4} Z^2 & \text{otherwise} \end{cases} \qquad (5.32)$$

Guzhov et al. (1967) proposed a simple liquid holdup correlation that only depends upon two parameters: the no-slip liquid fraction λ_L and the mixture Froude number Fr_M. Payne et al. (1979) recommended this simple relation for stratified flow, and it is given as:

$$R_L = 1 - 0.81(1 - \lambda_L)(1 - \exp(-2.2Fr_M)) \qquad (5.33)$$

where λ_L and Fr_M have already been defined in Equations (5.7) and (5.24).

Rouhani & Axelsson (1969) derived a mean liquid holdup correlation based on the drift flux model of Zuber & Findlay (1965), and proposed the following relation:

$$R_L = 1 - \left(\frac{x_G}{\rho_G}\right) \Bigg/ \left[\frac{1 + 0.12(1 - x_G)}{\rho_H} + \frac{1.18}{(G_G + G_L)}\left[\frac{g\sigma(\rho_L - \rho_G)}{\rho_L^2}\right]^{0.25}\right] \tag{5.34}$$

where x_G is the gas flow quality, ρ_H the homogeneous mixture density defined by relation (5.5) and σ is the gas-liquid surface tension.

Premoli et al. (1970) proposed a two-phase flow correlation that was later recommended by Hewitt (1982) and Whalley (1987) as the best method available for calculating the average liquid holdup. Their relation is expressed as:

$$R_L = \frac{1}{1 + \dfrac{x_G}{S(1 - x_G)}\dfrac{\rho_L}{\rho_G}} \tag{5.35}$$

where x_G is the flow quality, S the slip or velocity ratio defined as:

$$S = 1 + E_1\sqrt{\frac{y}{1 + yE_2} - yE_2} \tag{5.36}$$

The superficial velocity ratio y is defined by $y = J_G / J_L$, while the coefficients E_1 and E_2 are given by:

$$E_1 = 1.578\,Re_{LO}^{-0.19}\left(\frac{\rho_L}{\rho_G}\right)^{0.22}, \quad E_2 = 0.0273\,We_{LO}\,Re_{LO}^{-0.51}\left(\frac{\rho_L}{\rho_G}\right)^{-0.08} \tag{5.37}$$

The terms Re_{LO} and We_{LO} represent the Reynolds and Weber numbers respectively, when all fluid is liquid, and they are defined using the pipe diameter D, the mass flux of the mixture and the liquid properties as:

$$Re_{LO} = \frac{(G_G + G_L)D}{\mu_L} \tag{5.38}$$

$$We_{LO} = \frac{(G_G + G_L)^2 D}{\sigma\rho_L} \tag{5.39}$$

Beggs & Brill (1973) developed a flow pattern-dependent liquid holdup correlation based on air-water data from two pipelines with diameter of 25 and 28 mm at a system pressure of 2.4 to 6.55 bara. Various pipe inclinations ranging from –90° to 90° from horizontal were investigated and the correlation proposed was given as:

$$R_L = \phi R_{L0} \tag{5.40}$$

where the pipe inclination correction ϕ is defined by:

$$\phi = 1 + C(1 - \lambda_L)\left[\sin(1.8\beta) - \frac{\sin^3(1.8\beta)}{3}\right] \tag{5.41}$$

The horizontal liquid holdup R_{L0} ($\beta = 0$) and the inclination correction factor C are flow regime dependent and are defined in Table 5-3.

Horizontal flow pattern	Horizontal holdup R_{L0}	Upward flow C	Downward flow C
Segregated	$\frac{0.98\lambda_L^{0.4846}}{Fr_M^{0.0868}}$	$Ln\left[\frac{0.011N_{LV}^{3.539}}{\lambda_L^{3.768}Fr_M^{1.614}}\right]$	$Ln\left[\frac{4.7N_{LV}^{0.1244}}{\lambda_L^{0.3692}Fr_M^{0.5056}}\right]$
Intermittent	$\frac{0.845\lambda_L^{0.5351}}{Fr_M^{0.0173}}$	$Ln\left[\frac{2.96\lambda_L^{0.305}Fr_M^{0.0978}}{N_{LV}^{0.4473}}\right]$	Same as above
Distributed	$\frac{1.065\lambda_L^{0.5824}}{Fr_M^{0.0609}}$	0	Same as above

Table 5-3: Correlations for calculating R_{L0} and C. [Beggs & Brill, 1973]

The non-slip liquid holdup λ_L and the mixture Froude number Fr_M are given by Equations (5.7) and (5.24) respectively, while the liquid velocity number N_{LV} is defined by:

$$N_{LV} = J_L\left(\frac{\rho_L}{g\sigma}\right)^{0.25} \tag{5.42}$$

To predict the flow patterns, Beggs & Brill (1973) simplified their transition map by considering only three types of flow patterns, and proposed the following criteria:

$$\begin{cases} \text{Segregated} & Fr_M < L_1 \\ \text{Intermittent} & L_1 < Fr_M < L_2 \\ \text{Distributed} & Fr_M > L_1 \quad \& \quad Fr_M > L_2 \end{cases} \tag{5.43}$$

where the parameters L_1 and L_2 are given as a function of $y = \ln(\lambda_L)$ as follows:

$$L_1 = \exp(-4.62 - 3.757y - 0.481y^2 - 0.0207y^3) \tag{5.44}$$

$$L_2 = \exp\left(1.061 - 4.602y - 1.609y^2 - 0.179y^3 + 0.635 \cdot 10^{-3} y^5\right) \qquad (5.45)$$

5.4.2.2 Taitel & Dukler Equilibrium Value

Using a one-dimensional steady state separated flow model, Taitel & Duckler (1976) proposed the first analytical solution for the liquid holdup value. They combined separate momentum balances for the gas and liquid by eliminating the pressure gradient terms. Assuming that the liquid layer is of constant height, with a smooth gas-liquid interface, and that the interfacial shear term is equal to the gas-wall shear term, they derived a non-dimensional form of this combined momentum balance as:

$$X^2\left[\left(\tilde{V}_L \tilde{D}_L\right)^{-n} \tilde{V}_L{}^2 \frac{\tilde{S}_L}{\tilde{A}_L}\right] - \left[\left(\tilde{V}_G \tilde{D}_G\right)^{-m} \tilde{V}_G{}^2 \left(\frac{\tilde{S}_G}{\tilde{A}_G} + \frac{\tilde{S}_L}{\tilde{A}_L} + \frac{\tilde{S}_I}{\tilde{A}_G}\right)\right] - 4Y = 0 \qquad (5.46)$$

For given gas and liquid flowrates and fluid properties (density and viscosity), the Martinelli parameter X^2 is constant and defined by relation (5.11), while the inclination parameter Y in Equation (5.46) is also constant and given by the following expression:

$$Y = \frac{(\rho_L - \rho_G) g \sin\beta}{\left(\frac{dP}{dx}\right)_G} \qquad (5.47)$$

where the gas pressure gradient $(dP/dx)_G$ is computed using relation (5.12). Hence, the momentum balance (5.46) depends upon only one dimensionless variable $\left(\tilde{h}_L = h_L/D\right)$, where h_L is the liquid film height and D the pipe diameter. The remaining unknowns in the equilibrium height relation are therefore defined as:

$$\tilde{A}_L = A_L/D^2 = 0.25\left\{\pi - \cos^{-1}\left[2\tilde{h}_L - 1\right] + \left[2\tilde{h}_L - 1\right]\sqrt{\left(1 - \left[2\tilde{h}_L - 1\right]^2\right)}\right\} \qquad (5.48a)$$

$$\tilde{A} = A/D^2 = \pi/4 \qquad (5.48b)$$

$$\tilde{A}_G = \tilde{A} - \tilde{A}_L \qquad (5.48c)$$

$$\tilde{S}_G = S_G/D = \cos^{-1}\left(2\tilde{h}_L - 1\right) \qquad (5.48d)$$

$$\widetilde{S}_L = S_L / D = \pi - \widetilde{S}_G \tag{5.48e}$$

$$\widetilde{S}_I = S_I / D = d\widetilde{A}_L / d\widetilde{h}_L = \sqrt{1 - \left(2\widetilde{h}_L - 1\right)^2} \tag{5.48f}$$

$$\widetilde{V}_L = V_L / J_L = \widetilde{A} / \widetilde{A}_L = \pi / \left(4\widetilde{A}_L\right) \tag{5.48g}$$

$$\widetilde{V}_G = V_L / J_G = \widetilde{A} / \widetilde{A}_G = \pi / \left(4\widetilde{A}_G\right) \tag{5.48h}$$

$$\widetilde{h}_L = h_L / D \tag{5.48i}$$

$$\widetilde{D}_L = 4\widetilde{A}_L / \widetilde{S}_L \tag{5.48j}$$

$$\widetilde{D}_G = 4\widetilde{A}_G / \left(\widetilde{S}_G + \widetilde{S}_I\right) \tag{5.48k}$$

The equilibrium equation (5.46) coupled with relationships (5.48a-k) is an implicit function of the liquid height. Therefore, an iterative root finding scheme, such as Newton's method, can be used to solve it and provide an accurate estimate not only for the stratified liquid height, but also for the equilibrium gas and liquid volume fractions and velocities. A simple **Fortran 90** programme has been written to perform this task.

5.4.3 Stability Criteria – Stratified to Slug Transition

The transition from stratified to slug flow is a complex phenomenon that has been widely studied over the past thirty years. And besides the early empirical relations [Beggs & Brill, 1973; Mandhane et al., 1974], three theoretical relations have been often used to predict the transition criterion. These include the inviscid Kelvin-Helmholtz (IKH) theory, the viscous long waves (VLW) also known as viscous Kelvin-Helmholtz (VKH) theory and the slug stability theory.

However, early theoretical models [Kordyban & Ranov, 1970; Taitel & Dukler, 1976] considered the process leading to the transition to be solely linked to the Kelvin-Helmholtz instability [Milne-Thompson, 1968] which occurs when the suction effect due to pressure

variation over a wave overcomes the stabilising effect of gravity, enabling small interfacial disturbances to grow into waves that may be potentially large enough to bridge the pipe and form slugs. But nowadays, many researchers [Scott et al., 1990; Bendiksen & Espedal, 1992; Woods & Hanratty, 1996] often used the stability of an existing slug to explain the transition from stratified flow.

It is still not clear which theoretical method is best as predictive tool for the transition from stratified flow, and we refer the reader to paper by Mata et al. (2002) which compared different stability limit methods, and the thesis by Hale (2000) which reviewed the various models dealing with the growth of disturbances into large amplitude waves and potentially slug flow. But, as a guide for selecting a transition mechanism, we advocate the recent article by Hurlburt & Hanratty (2002) who combined the use of the three existing theoretical methods depending on the gas superficial velocity. However, in this thesis, we only describe the Taitel & Dukler (1976) transition model, because it is most widely used in the literature.

Starting from a solitary wave of finite amplitude, Taitel & Duckler (1976) studied its growth on a smooth stratified layer in horizontal channel, and derived a stability criterion to pinpoint the transition between stratified and slug flow. Neglecting the wave motion, they wrote a balance equation between the pressure variation and the acceleration of the gas phase. This results in a condition of instability for a rectangular channel, which was further modified for circular geometries as:

$$V_G > K\sqrt{\frac{(\rho_L - \rho_G)g\cos\beta}{\rho_G}\frac{A_G}{dA_L/dh_L}}, \qquad (5.49)$$

The coefficient K = 1 corresponds to a slightly modified version of the inviscid Kelvin-Helmholtz criteria given by relation (1.57). However, the authors realised that this IKH criteria over-predicted the transition limit, and recommended the following expression:

$$K = K^{TD} = 1 - \frac{h_L}{D} \qquad (5.50)$$

The Taitel & Dukler (1976) model (5.49)-(5.50) works reasonably well for horizontal pipes and its transition line is illustrated in Figure 5-3 for air-water flow at atmospheric conditions.

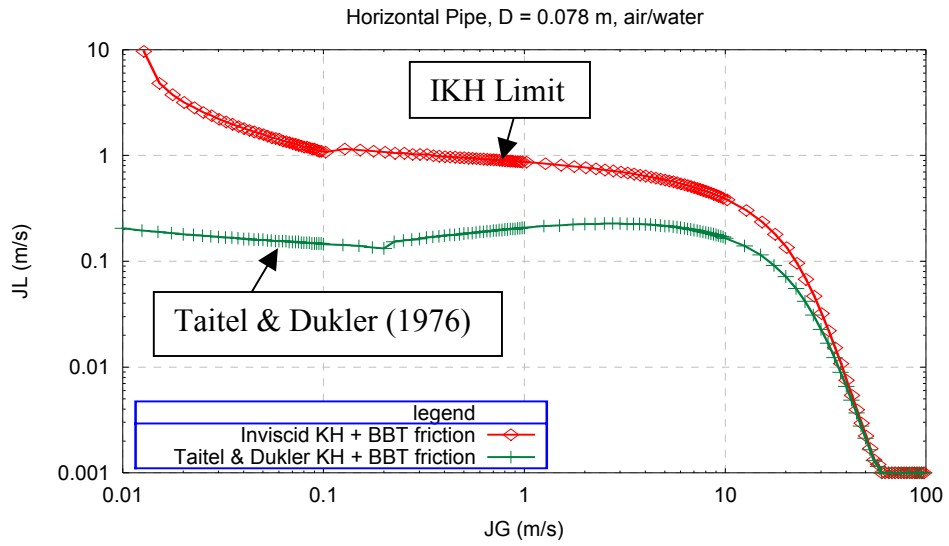

Figure 5-3: Taitel & Dukler (1976), and Inviscid Kelvin-Helmholtz (IKH) transition lines from stratified flow.

5.5 Friction Factors

One of the weakest links in the formulation of two-fluid models is the closure equation for friction factors. Despite numerous theoretical [Taitel & Dukler, 1976] and experimental [Andritsos & Hanratty, 1987] investigations into gas liquid pipe flow, no general friction models are available that reliably predict frictional pressure drop and liquid holdup for all horizontal flow situations. However, some successful models exist in the literature; they are flow regime dependent and sometimes pipe sizes and fluid dependent.

Hence, because there is no established standard friction correlations, we designed the EMAPS code – which contains each of the mathematical models used in the present study – in such a way that it can accommodate a wide range of friction factors, allowing the implemented 1D models to be flexible in investigating the applicability of friction terms for stratified flow predictions. Therefore, we summarize in Table 5-4 the wall and interface friction factor correlations that have been implemented in the code.

The friction factors are related to the shear stresses in two different ways in the fluid dynamic literature. It is therefore important to be clear about the exact definition of the friction factor when using this term. In this study, the liquid and gas wall shear stresses τ_L, τ_G and the interfacial shear stress τ_I were defined in a generic way as follows:

$$\tau_L = f_L \frac{\rho_L V_L |V_L|}{2} \qquad \tau_G = f_G \frac{\rho_G V_G |V_G|}{2} \tag{5.51}$$

$$\tau_I = f_I \frac{\rho_G V_r |V_r|}{2} \qquad \text{with} \qquad V_r = V_G - V_L \tag{5.52}$$

The coefficients f_G, f_L, and f_I are defined as the Darcy or Fanning friction factor [Perry & Green, 1984] and $\mathbf{V}_r$ the relative or slip velocity between the gas and the liquid.

A detailed presentation of different models for stratified flow can be found in the thesis by Espedal (1998) and Khor (1998). In what follows, we briefly describe some of those mentioned in Table 5-4.

5.5.1 Wall Friction Factors

In two-phase flow computations, it is common practice to model the fluids wall friction factors using single-phase pipe flow formulas. Therefore, we firstly present some useful formulas validated for single-phase pipe flow.

5.5.1.1 Single-Phase Flow Correlations

The oldest, simple and widely used formula for friction factors in single phase turbulent flow is the Blasius equation. This formula, which is only valid for smooth walls and for Reynolds number (Re) ranging between 2.5 $\bullet 10^{-3}$ and 10^{-5}, can be found in most fluid dynamics textbooks and is given by:

$$f = 0.0792 \cdot Re^{-0.25} \tag{5.53}$$

But the most accurate and commonly accepted formulas for friction factors in turbulent pipe flow are the Prandtl or von Karman formula for smooth walls and the Nikuradse formula for fully rough pipes [Perry & Green, 1984]. Prandtl's formula is given by:

$$\frac{1}{\sqrt{f}} = -4.0 \cdot \log_{10}\left(\frac{1.256}{Re\sqrt{f}}\right) \tag{5.54}$$

while the Nikuradse formula for rough pipes is given by:

$$\frac{1}{\sqrt{f}} = -4.0 \cdot \log_{10}\left(\frac{\varepsilon}{3.715 \cdot D}\right) \tag{5.55}$$

where f is the Darcy friction factor, D is the pipe inner diameter and ε is the pipe roughness.

Colebrook (1939) combined the Prandtl formula (5.54) for smooth pipes and the Nikuradse formula (5.55) for rough pipes, and proposed an implicit formula for the wall friction factor, which is now universal in engineering, as it covers the full range of smooth and rough pipes. This formula is expressed as:

$$\frac{1}{\sqrt{f}} = -4.0 \cdot \log_{10}\left(\frac{1.256}{Re\sqrt{f}} + \frac{\varepsilon}{3.715 \cdot D}\right) \tag{5.56}$$

Equation (5.56) agrees well with commercial pipe friction data in the transition region between hydraulically rough and smooth flow, and it also contains equations (5.54) and (5.5) as limiting cases when $\varepsilon/D \to 0$ and $Re \to \infty$, respectively

Friction factor tables based on Colebrook's equation are widely used in the industry, however, the implicit nature the correlation makes it inconvenient for practical modelling applications and simulations, and hence several explicit approximations have been proposed in the literature. The earliest of those approximations is due to Moody (1947) and it was given as:

$$f = 0.001375\left[1 + \left[2.10^4\left(\frac{\varepsilon}{D}\right) + \frac{10^6}{Re}\right]^{1/3}\right] \tag{5.57}$$

Since, the first expression proposed by Moody in 1947, a series of increasingly more accurate and complex explicit approximations have been published. Since this document is not a review report on single-phase wall friction factors, in what follows, we only mention two additional explicit approximations, and refer the interested reader to the review paper by Zigrang & Sylvester (1985) on explicit friction factor equations.

Eck (1973) presented an explicit wall friction correlation, which is often used in two-phase flow modelling; this popular relation is expressed as:

$$f = \frac{0.0625}{\left[\log_{10}\left(\frac{15}{Re} + \frac{\varepsilon}{3.715 \cdot D}\right)\right]^2} \tag{5.58}$$

But if looking for an expression, which is both simple and accurate, Espedal (1998) stated that the best choice is probably the approximation given by Haaland (1983).

$$f = \frac{0.07716}{\left[\log_{10}\left(\frac{6.9}{Re} + \left(\frac{\varepsilon}{3.7 \cdot D}\right)^{1.11}\right)\right]^2} \tag{5.59}$$

Haaland (1983) found that the explicit equation (5.59) is in good agreement with the Colebrook implicit equation (5.6) with less than ± 1.5% difference in the range $4.10^3 \leq Re \leq 5.10^8$ and $0 \leq \varepsilon/D \leq 5.10^{-2}$.

It should be noted that all the wall friction correlations mentioned above are valid for turbulent flow, but for fully developed laminar flow in a round tube, a simple formula derived by Hagen and Poiseuille [Perry & Green, 1984] is generally used for practical applications, and it is given as:

$$f = \frac{16}{Re} \tag{5.60}$$

5.5.1.2 Two-Phase Flow Correlations

Gas and liquid two-phase friction terms are almost always calculated using correlations developed for smooth or rough wall single-phase pipe flow in which the pipe inner diameter is replaced by the appropriate fluid hydraulic diameter and the Reynolds number is calculated using the same hydraulic diameter. For completeness, these fluid parameters are defined as follows:

$$D_{hG} = \frac{4A_G}{S_G + S_I} \qquad D_{hL} = \frac{4A_L}{S_L} \tag{5.61}$$

and

$$Re_G = \frac{\rho_G D_{hG} |V_G|}{\mu_G} \qquad Re_L = \frac{\rho_L D_{hL} |V_L|}{\mu_L} \tag{5.62}$$

where A_G and A_L are the gas and liquid pipe cross section areas. S_G, S_L, and S_I are the gas, liquid and interfacial wetted perimeters, and D_{hG} and D_{hL} are the hydraulic diameters for the gas and liquid, respectively. ρ_G and ρ_L are the gas and liquid densities, and μ_G and μ_L are the dynamic viscosities for the gas and liquid.

However, new correlations have been derived from two-phase flow studies, and a slightly different expression of the Blasius equation (5.53) has been used in the works of Taitel & Dukler (1976) and Andreussi & Persen (1987). This expression is given by:

$$f_k = 0.046 \cdot Re_k^{-0.2} \qquad k = G, L \tag{5.63}$$

Similarly to the original expression, this modified Blasius equation (5.63) is only valid for smooth pipes. Hence, to account for the effects of the pipe roughness, the wall friction factors are often evaluated by single-phase explicit formula (5.57), (5.58) or (5.59).

Kowalski (1987) demonstrated that measurements of gas friction f_G were accurately predicted by the Blasius equation defined in relation (5.63), but the liquid wall friction factor did not follow the Blasius equation, but a correlation of the type:

$$f_L = c_1 \left(R_L \, Re_{LS} \right)^{c_2} \tag{5.64}$$

where c_1 and c_2 are correlated coefficients, R_L is the liquid volume fraction, and Re_{LS} is a Reynolds number based on the liquid superficial velocity and the pipe inner diameter.

Based on his experimental data, Kowalski (1987) proposed to use the values $c_1 = 0.263$, and $c_2 = -0.5$. However, Hand (1991) found that these coefficients do not agree with his experimental data, so he suggested using $c_1 = 0.0262$ and $c_2 = -0.139$, while Srichai (1994) later proposed the values of 0.762 and -0.562 for c_1 and c_2 respectively.

Many models have been proposed to calculate the gas or liquid wall friction factors, but for turbulent flow, most of the recent models seem to use the modified Blasius equation (5.13) for gases and the Kowalski type of equation (5.64) for liquids. In the laminar region, the Hagen-Poiseuille equation (5.60) is still preferred.

5.5.2 Interfacial Friction Factor

Many authors [Andritsos & Hanratty, 1987; Xiao & Shoham, 1990; Spedding & Hand, 1997; Espedal, 1998] have shown that the relation assigned to the interfacial shear stress was of crucial importance in modelling two-phase stratified flow. They have discussed the various approaches and models, which have been used in the past to evaluate the interfacial shear stress. Some of those, which were reported to be useful, were implemented in the EMAPS code, and will be mentioned below.

The simplest relation for interfacial friction factor is the one used by Taitel & Dukler (1976). They proposed to take the interfacial shear stress equal to the gas shear stress for smooth and wavy stratified flow.

$$f_I = f_G \tag{5.65}$$

Based on results of different studies, the PLAC code [AEA technology, 1996] found that the correlation proposed by Sinai (1983) gives realistic values for interfacial friction factor in high pressure, large diameter pipelines. This friction factor is calculated as:

$$f_I = 2 \left(\frac{\mathbf{v}_T}{\mathbf{v}_G} \right)^2 \tag{5.66}$$

where
$$\frac{\mathbf{v}_G}{\mathbf{v}_T} = 5.75 \log_{10}\left(\frac{D_{hG}}{2\varepsilon_i}\right) + 4.73 \tag{5.67}$$

and
$$\varepsilon_i = 180 \frac{S_I}{S_G + S_I} \frac{\mathbf{v}_T^2}{g} \frac{\rho_G}{(\rho_L - \rho_G)} \tag{5.68}$$

The interfacial friction factor (5.66) is limited to a maximum of 6 times the gas wall friction factor. Srichai (1994) adopted a similar approach in his study, and the friction factor that he developed is given in Table 5-4. But, contrary to Srichai (1994) interface friction relation, [Sinai, 1983] correlation was not implemented in EMAPS because it is defined implicitly and its related interface shear stress τ_I is not expressed in the generic way given by Equation (5.57).

Andritsos & Hanratty (1987) investigated the behaviour of interfacial waves in stratified flow, while Andristsos et al. (1989) studied the effect of the liquid viscosity on these waves for horizontal pipelines of diameters from 2.52 cm to 95.25 cm. They proposed a novel correlation for interfacial friction factor f_I, when the superficial gas velocity was larger than the critical velocity (J_G = 5 m/s) necessary to initiate large amplitude roll waves. Their correlation is given as:

$$\begin{cases} f_I = f_G & \text{for} \quad J_G < 5 \text{ m/s} \\ f_I = f_G \left[1 + 15 \cdot \left(\frac{J_G}{5} - 1\right) \sqrt{\left(\frac{h_L}{D}\right)}\right] & \text{for} \quad J_G \geq 5 \text{ m/s} \end{cases} \tag{5.69}$$

Spedding & Hand (1997) showed that the model predicted pressure loss satisfactorily in the stratified long and short roll wave and droplet regimes using the Taitel & Duckler (1976) correlation for gas and liquid friction factors. In their comparative study, evaluating the performance of several interfacial friction factors, Xiao & Shoham (1990) suggested using the model by Andritsos & Hanratty (1987) for pipes below 0.127 m (5 inches), and the one by Baker et al. (1988) for large diameter pipes. The Baker et al. (1988) model is not described here because the complexity of its formulation makes it less attractive for computer codes.

Hart et al. (1989) investigated stratified flow with small liquid holdup (R_L < 0.06). A complex interfacial relationship, presented in Table 5-4, was proposed which accounted for the distortion of the gas-liquid interface into a crescent-shaped film. Spedding & Hand (1997) have shown that excellent agreement existed between the Hart et al. (1989) model and experiments (< ±15%), with successful prediction of the holdup and the pressure drop for the stratified, annular and the droplet type flow regimes.

Espedal (1998) reported that the model by Andreussi & Persen (1987) gives reasonable predictions for R_L> 0.1, while for lower values, it under-predicts the liquid holdup. This model, which depends on the dimensionless film height, h_L/D, and the difference between a

modified gas Froude number, and its value at the onset of two-dimensional waves, leads to the following expression:

$$\begin{cases} f_I = f_G \quad \text{for} \quad Fr_G \le 0.36 \quad \text{(stratified smooth)} \\ f_I = f_G \left[1 + 29.7 \cdot \left(Fr_G - 0.36 \right)^{0.67} \left(\frac{h_L}{D} \right)^{0.2} \right] \text{for } Fr_G > 0.36 \quad \text{(stratified wavy)} \end{cases} \tag{5.70}$$

where the expression of the Froude number Fr_G is given in Table 5-4.

The model proposed by Spedding & Hand (1997) predicts both the pressure drop and the liquid hold-up within ±15%. This model also shows good agreement with the independent air-water data of Andritsos. It uses a volumetric fraction $(\beta_L)_r$ which seems to be fluid dependent. This model is fully described in the following table as well as the Kowalski (1987) model for interface friction and which is not mentioned in the above discussion.

Correlation	Fluids	D_h & Re	Gas-Liquid Wall Shear Stresses τ_G, τ_L	Gas-Liquid Interfacial Shear Stress τ_I
Taitel & Dukler (1976)	Air-water		$f_k = 0.046\,\mathrm{Re}_k^{-0.2}$ if turbulent flow $f_k = \dfrac{16}{\mathrm{Re}_k}$ if laminar flow $(k = G, L)$	$f_I = f_G$
Andritsos & his co-workers (1985, 87)	Air-water		$f_G = 0.046\,\mathrm{Re}_G^{-0.2}$	$\begin{cases} J_G \le 5\,\mathrm{m/s} & f_I = f_G \\ J_G > 5\,\mathrm{m/s} & \dfrac{f_I}{f_G} = 1 + 15 \cdot \left(\dfrac{J_G}{5} - 1\right)\sqrt{\left(\dfrac{h_L}{D}\right)} \end{cases}$
Andreussi & Persen (1987)	Air-water		$f_G = 0.046\,\mathrm{Re}_G^{-0.2}$ $f_L = 0.046\,\mathrm{Re}_L^{-0.2}$	$\begin{cases} f_I = f_G & \text{if } \mathrm{Fr}_G \le 0.36 \text{ else} \\ f_I = f_G\left[1 + 29.7 \cdot (\mathrm{Fr}_G - 0.36)^{0.67}\left(\dfrac{h_L}{D}\right)^{0.2}\right] \end{cases}$ $\mathrm{Fr}_G = V_G \cdot \sqrt{\left[\left(\dfrac{\rho_G}{\rho_L - \rho_G}\right)\left(\dfrac{dA_L/dh_L}{A_G}\right)\left(\dfrac{1}{g\cos\beta}\right)\right]}$
Kowalski (1987)	Air-water	$\mathrm{Re}_{GS} = \dfrac{J_G D}{\nu_G}$ $\mathrm{Re}_{LS} = \dfrac{J_L D}{\nu_L}$	$f_G = 0.046\,\mathrm{Re}_G^{-0.2}$ $f_L = 0.263(R_L\,\mathrm{Re}_{LS})^{-0.5}$	$f_I = 0.96\,\mathrm{Re}_{GS}^{-0.52}$ smooth stratified $f_I = 7.5 \cdot 10^{-5} R_L^{-0.25}\,\mathrm{Re}_G^{-0.3}\,\mathrm{Re}_L^{0.83}$ wavy stratified

Table 5-4: Summary of recent friction factors for stratified flow (Part 1/3)

Correlation	Fluids	D_h & Re	Gas-Liquid Wall Shear Stresses τ_G, τ_L	Gas-Liquid Interfacial Shear Stress τ_I
Hart et al. (1989)	Air-water	$\mathrm{Re_G} = \dfrac{\mathrm{V_G D}}{\nu_G}$ $\mathrm{Re_{LS}} = \dfrac{\mathrm{J_L D}}{\nu_L}$	$f_G = \dfrac{0.07725}{\left[\log_{10}\left(\dfrac{\mathrm{Re}_G}{7}\right)\right]^2}$ $\dfrac{f_L}{f_I} = 108\left(\mathrm{Re}_{LS}\right)^{-0.726}$	$\mathrm{f_I} = \dfrac{0.0625}{\left[\log_{10}\left\{\dfrac{15}{\mathrm{Re_G}} + \dfrac{\mathrm{k_I}/\mathrm{D}}{3.715}\right\}\right]^2}$ $\dfrac{\mathrm{k_I}}{\mathrm{D}} \approx 2.3\dfrac{\mathrm{R_L}}{4\phi}; \qquad \mathrm{Fr_L} = \dfrac{\rho_L \mathrm{V_L^2}}{\mathrm{gD}\left(\rho_L - \rho_G\right)}$ $\phi = 0.52\left(\mathrm{R_L}\right)^{0.374} + 0.26\mathrm{Fr_L^{0.58}}$
Hand & his co-workers (1991, 1997)	Air-water	$\mathrm{Re_{LS}} = \dfrac{\mathrm{J_L D}}{\nu_L}$ $\mathrm{Re_{GS}} = \dfrac{\mathrm{J_G D}}{\nu_G}$	$\begin{cases} \mathrm{Re_G} < 2100 & \mathrm{f_G} = \dfrac{16}{\mathrm{Re_G}}, \quad \mathrm{f_{GS}} = \dfrac{16}{\mathrm{Re_{GS}}} \\ \mathrm{Re_G} \geq 2100 & \begin{bmatrix} \mathrm{f_G} = 0.046\,\mathrm{Re_G^{-0.2}} \\ \mathrm{f_{GS}} = 0.046\,\mathrm{Re_{GS}^{-02}} \end{bmatrix} \end{cases}$ $\begin{cases} \mathrm{Re_L} < 2100 & \mathrm{f_L} = \dfrac{24}{\mathrm{Re_L}} \\ \mathrm{Re_L} \geq 2100 & \mathrm{f_L} = 0.0262\left(\mathrm{R_L\,Re_{LS}}\right)^{-0.139} \end{cases}$	$\mathrm{f_I} = \mathrm{f_{GS}} \cdot \left[1.76\left(\dfrac{\mathrm{J_G}}{6}\right) + \mathrm{k_i}\right]$ $\mathrm{k_i} = 2.7847\log_{10}\left(\beta_L\right)_r + 7.8035$ $\left(\beta_L\right)_r = \dfrac{\mathrm{J_G}}{\mathrm{J_G} + 6}$

Table 5-4: Summary of recent friction factors for stratified flow (Part 2/3)

Correlation	Fluids	D_h & Re	Gas-Liquid Wall Shear Stresses τ_G, τ_L	Gas-Liquid Interfacial Shear Stress τ_I
Srichai (1994)	Air-water & Air-oil	$Re_{LS} = \frac{J_L D}{\nu_L}$	$f_G = \frac{0.0625}{\left[\log_{10}\left\{\frac{15}{Re_G} + \frac{\varepsilon_s / D}{3.715}\right\}\right]^2}$ $f_L = 0.765\left(R_L\, Re_{LS}\right)^{-0.562}$	$\tau_I = \frac{1}{2} f_I \rho_G V_G^2; \qquad f_I = 2\left(\frac{V_G}{V_I^*}\right)^{-2}$ $\frac{V_G}{V_I^*} = 5.75 \log_{10}\left(\frac{D_G}{2k_I}\right) + 4.73$ $\frac{D_G}{k_I} = 0.1985\left(\frac{h_L'}{D}\right)^{0.0825}$ $\frac{h_L'}{D} = a + b\left(R_L\, Re_G\right) + c\left(R_L\, Re_G\right)^2$ where $\begin{cases} a = 2.65 \cdot 10^4 \left(\frac{\rho_G}{\rho_L - \rho_G}\right)^{4.517} \\ b = 8.995 \cdot 10^{-10} \left(\frac{\rho_G}{\rho_L - \rho_G}\right)^{-1.227} \\ c = 1.987 \cdot 10^{-13} \left(\frac{\rho_G}{\rho_L - \rho_G}\right)^{-0.925} \end{cases}$

Table 5-4: Summary of recent friction factors for stratified flow (Part 3/3)

5.6 Validation of Friction Factor Correlations

It is important to back up modelling work with experiments for two reasons. Firstly, it is not possible to describe stratified flow analytically, because of the complexity of the combined effects of the turbulence and the generation of interfacial waves, therefore experimental data are needed to validate numerical and mathematical models that are developed. Secondly, and more importantly, the mathematical models have to represent the physical nature of the two-phase system, and a major understanding of the physics of the system can only be achieved through experiments.

In the previous sections, we have presented most of the recommended friction models, currently used in two-phase stratified flow. They have all been developed for steady flow and their applications to transient flows and the full range of stratified patterns (smooth & wavy) is still an open debate.

In the next sections, we explain our choice of friction factors through an experimental test case.

5.6.1 Shaha Test Case

Shaha (1999) performed a series of test cases to study the interfacial structure of transient stratified flow. One of those tests was presented in a Transient Multiphase Flows (TMF) Meeting [Hewitt, 2002] and it has been selected in this study, because it highlighted the incapacity of the current commercial pipeline codes Olga, Plac, and Tacite to accurately predict this simple stratified transient flow case.

The test case is characterized by an increase of the inlet gas flowrate after 30 seconds of an initial steady state, while keeping the liquid flowrate constant (Figure 5-4). The crucial point about this test is that, before the increase of the gas flowrate, the flow conditions are in the smooth interface region, while those after the increase, may be considered as being in the stratified wavy region.

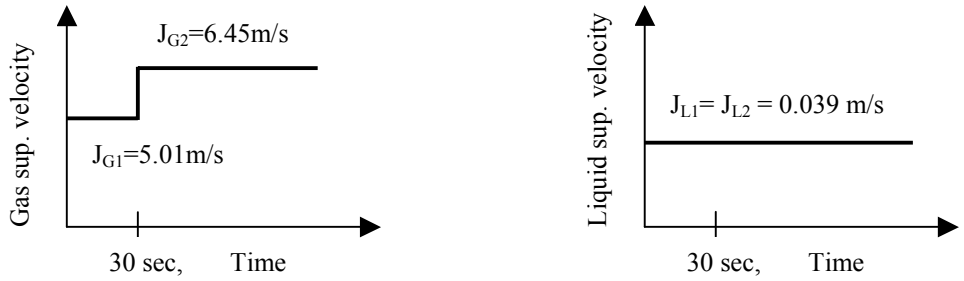

Figure 5-4: Shaha test case, variation of the gas and liquid superficial velocities.

5.6.2 Validation of the Wall Friction

5.6.2.1 Stratified-Smooth Pattern

Several authors [Andreussi & Persen, 1987; Kowalski, 1987] have reported that the experimental gas and liquid wall friction factor measurements were consistent and accurately predicted with the modified Blasius equation (5.63), or the original expression (5.53) for stratified-smooth flows.

Thus, for smooth pipes or when the pipe roughness is not known, we advocate using expression (5.63) for turbulent flow and expression (5.60) for laminar flow. So the combined expression for the wall friction is given by:

$$f_{wk} = \max\left[\frac{16}{Re_k}, \frac{0.046}{Re_k^{0.2}}\right] \tag{5.71}$$

where k is either the gas or liquid phase, and the Reynolds number Re_k is defined by expression (5.62).

It can be seen from equation (5.71) that there is no explicit use of critical Reynolds number for the transition from laminar to turbulent flow. The reason is that if the critical Reynolds number of roughly 2000 is used, as suggested by many investigators, then from the Fanning diagram [Perry & Green, 1984] or Figure 5-5, the friction factor obtained by the using the turbulent Blasius equation (5.63) is almost twice the value obtained by the laminar Hagen-Poiseuille expression (5.60).

This massive difference in the transitional flow can create a big jump in the solution for a tiny variation of the Reynolds number, and lead to numerical instabilities. To avoid that problem, some investigators [De Henau, 1995; Masella, 1998] have used a critical zone of $2000 < Re_k < 3000$ and interpolated the friction from the laminar to the turbulent expression in this critical transition zone. We prefer using the maximum approach to smooth the friction expression, because it is a simple and fast numerical solution without lost of accuracy. Equation (5.71) means however that the transition occurs at a much lower critical value of the Reynolds number $Re_c = (16/0.046)^{5/4} \cong 1500$, but because the transition from laminar to turbulent is still not well defined, even in single phase flow, errors created by this approach are seen to be minimal.

Equation (5.71) is only valid for smooth pipes, when the pipe roughness is considered, then we have to choose among the many explicit expressions available in the literature. To help us choose an appropriate correlation, we have reduced the list of explicit expressions to the three mentioned in Section 5.5.1.1, and plot their values for a range of Reynolds numbers with a pipe roughness of $4.6\ 10^{-5}$ m (see Figure 5-5), which the value used for the Shaha test case.

As can be seen from Figure 5-5, there is very little variation among the expressions in the Reynolds number range [2. 10^4, 1. 10^8], making it hard to choose among the various expressions. But, because those expressions are valid for smooth and rough pipes, the choice was decided when the roughness tends to zero, in that case, the Eck expression (5.58) and the Haaland expression (5.59) will create singularities in the solution when the Reynolds number tends to 15 and 6.9 respectively, and the maximum approach is no longer valid, so we decide to choose the earliest explicit expression, which is the Moody equation (5.57).

Thus, for rough pipes in the stratified-smooth region, we advocate using the following wall friction expression:

$$f_{wk} = \max\left\{\frac{16}{Re_k}, 0.001375\left[1+\left[2.10^4\left(\frac{\varepsilon}{D_{hk}}\right)+\frac{10^6}{Re_k}\right]^{1/3}\right]\right\} \qquad (5.72)$$

where k refers to either the gas or liquid phase, ε is the pipe roughness, D_{hk} is the phase or fluid hydraulic diameter given by expression (5.61) and Re_k is the Reynolds number defined by expression (5.62).

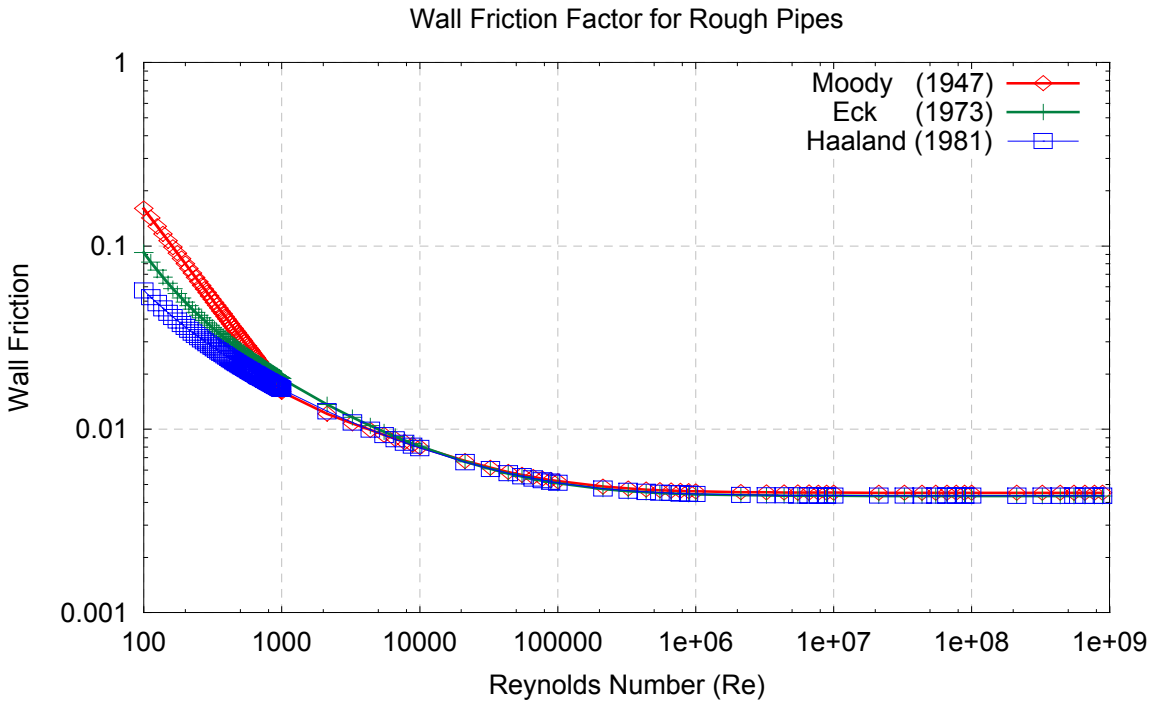

Figure 5-5: Variation of explicit single-phase wall friction for rough pipes with Reynolds number Re (Pipe roughness = 4.6 10^{-3} m).

5.6.2.2 Stratified-Wavy Pattern

It is recognised that the gas wall friction can still be evaluated either by expression (5.71) or (5.72) in the stratified-wavy region, but it is no longer true for the liquid wall friction. Andreussi & Persen (1987) found that the smooth pipe equation (5.71) underestimated the liquid wall friction for wavy stratified flow patterns, with deviation between the data and the prediction increasing with increasing gas velocity. Their experimental results showed that, at the onset of interfacial waves, an increase in turbulent mixing in the stratified film creates a sharp increase in the liquid wall friction, which is not predicted by the stratified smooth expression (5.71). Those results were confirmed the same year by Kowalski (1987) who proposed a generic expression of the liquid wall friction, whose coefficients were later modified by various authors [Srichai, 1994; and Spedding & Hand, 1997].

To see which one of these expressions gives the best predictions, we compare the results for the liquid holdup using two different interface friction factors, the classic smooth expression ($f_i = f_{wg}$) used for stratified-smooth flow, and the expression by Andritsos & Hanratty (1987), which was reported by Xiao & Shoham (1990) to produce the best predictions.

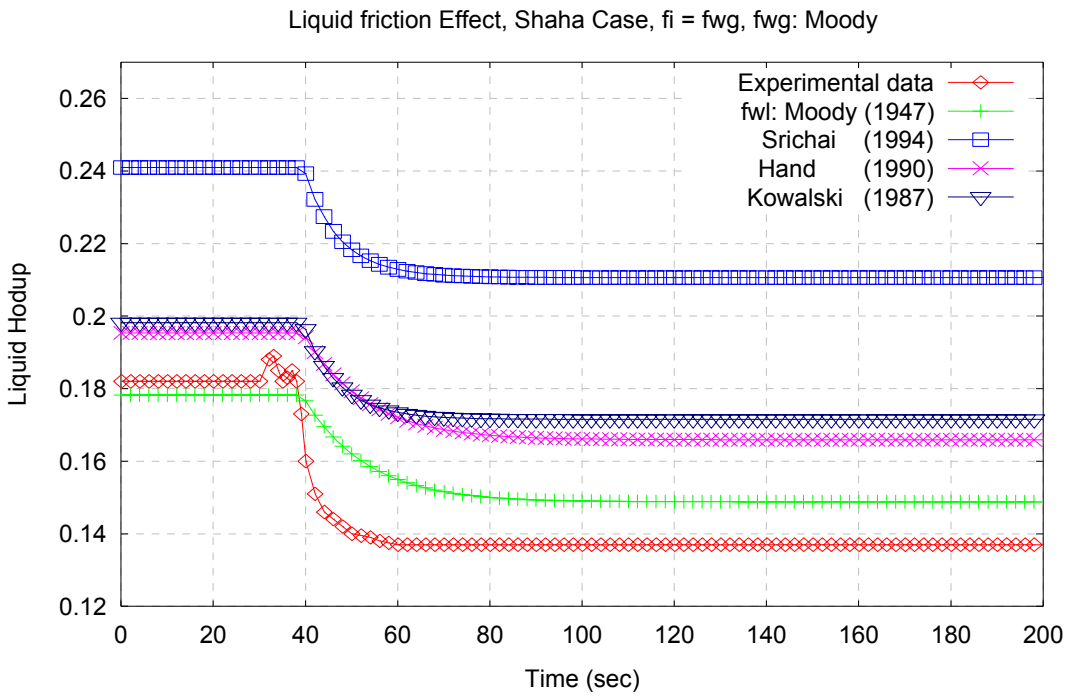

Figure 5-6: PFM-2 [Shaha Case]. Liquid holdup variation with time for different liquid wall friction and the smooth interface expression ($f_i = f_{wg}$).

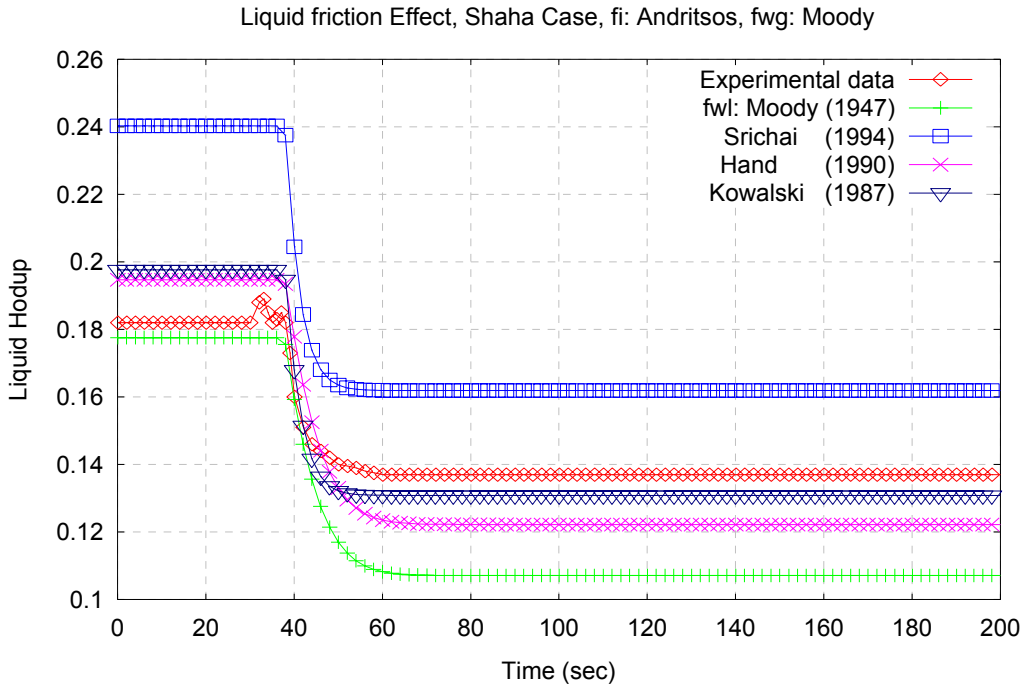

Figure 5-7: PFM-2 [Shaha Case]. Liquid holdup variation with time for different liquid wall friction and the [Andritsos & Hanratty, 1987] interface friction.

The results are given respectively in Figure 5-6 for the smooth interface expression (5.65), and in Figure 5-7 for the Andritsos & Hanratty (1987) equation (5.69).

When using the smooth interface expression (5.65), which is not appropriate for the stratified-wavy region, we can see that only the Moody liquid wall friction predicts with a 20% margin the final steady state value of the liquid holdup. But when using the Andritsos & Hanratty (1987) equation (5.69), then the expressions by Kowalski (1987) and Hand (1991) accurately predict the liquid holdup value. From Figure 5-7, it can be seen that the Moody wall friction now underestimates the liquid holdup value, and predicts a final holdup value of around 0.107, which more than 20% lower than the experimental value of 0.137 (see Table 11.3).

It can also be seen from Figures 4.6 and 4.7 that the Srichai (1994) expression overestimates the final steady state value of the liquid holdup. So we have decided to discard this expression, as well as the Moody expression. We, therefore, retain the expressions by Kowalski (1987) and Hand (1991) for the liquid wall friction. The final choice will be made after assessing and validating the interface friction factor, which is made in the following section.

5.6.3 Validation of the Interface Friction

In the same way that the wall friction mainly depends on the pipe roughness for turbulent rough pipes, we may argue that the interfacial friction factor mainly depends on the interfacial wave characteristics such as the wave amplitude and the wavelength. Unfortunately, as was noted by Chen et al. (1997) very little work has been devoted to improve the understanding of interfacial wave phenomenon in gas-liquid stratified flow [Andritsos & Hanratty, 1987; Line & Lopez, 1995].

However, many steady state correlations have been suggested for modelling the interface friction factor. In this section we evaluate the proposed models for the transient test case of Shaha (see Section 5.4.1).

In Figure 5-8, we plot the evolution of the liquid holdup for different interface friction factors, using the Moody based correlation (5.72) for the gas and liquid wall frictions. We can see that the simplest interface friction ($f_i = f_{wg}$), which is also embodied in the Andritsos & Hanratty (1987) expression, accurately predicts, with 2.2% error the initial steady value of the liquid holdup. The next accurate result for the initial holdup value is the correlation used by Tronconi (1990), which gives a holdup value of 0.146, therefore underestimates this value for about 19.8% compared to the experimental value of 0.182. all the other interface friction correlations underestimate the initial holdup value with more than 20% and should not be considered for stratified-smooth flow.

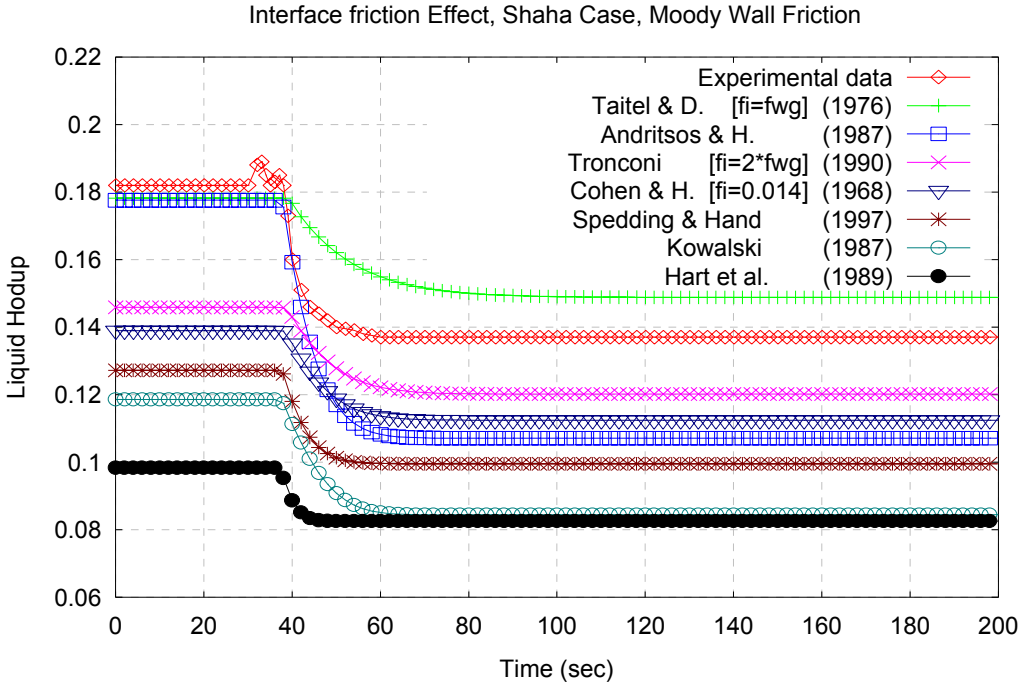

Figure 5-8: PFM-2 [Shaha Case]. Time evolution of the liquid holdup for different interface friction factors.

The same analysis as above should be considered for stratified-wavy flows using the Moody based relation (5.72) for the gas wall friction and either the Kowalski (1987) expression for the liquid wall friction or the Hand (1991) liquid wall friction factor. But instead, we compile the best-predicted values (with less than 10% error) for the final steady state value of the liquid holdup.

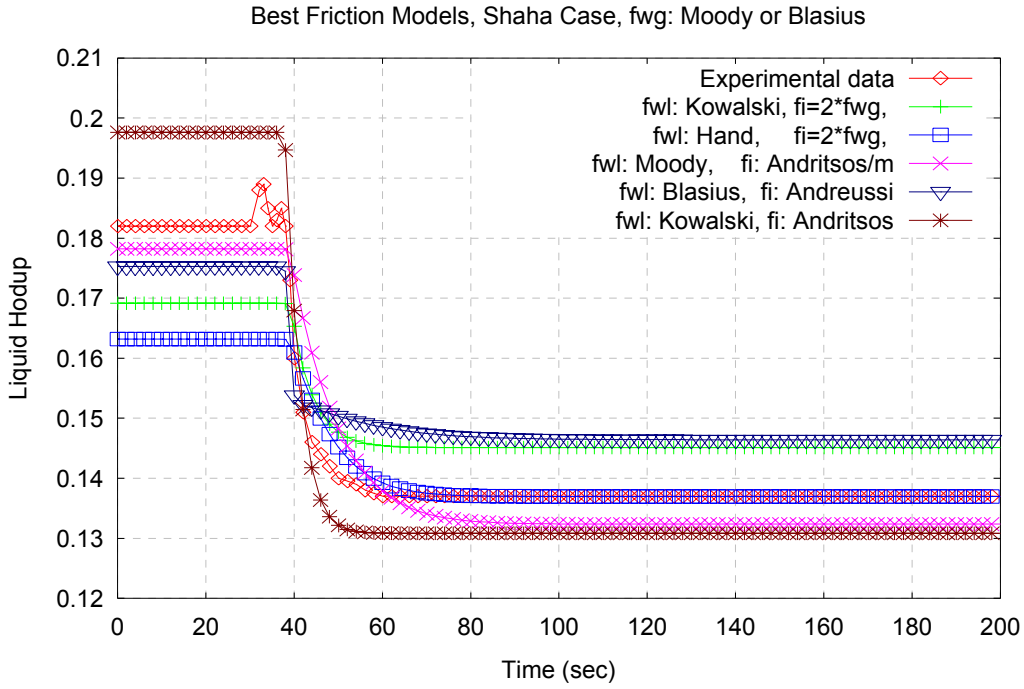

Figure 5-9: PFM-2 [Shaha Case]. Best predicted final holdup value, for various interface and liquid wall frictions, using the Moody expression (5.52) for the gas wall friction.

For stratified-wavy flow, we have found that the interfacial friction correlations proposed by Kowalski (1987) and Hand (1991) did not perform well when using their respective liquid wall friction. But instead, as shown in Figure 5-9, the Kowalski (1987) liquid wall friction (5.64) works well with the Andritsos & Hanratty (1987) interface friction expression (5.69), while the best (exact) result for this test case is given by the combination of the Hand (1991) expression (5.64) for the liquid wall friction and the Tronconi (1990) linear expression ($f_i = 2f_{wg}$) for the interface friction.

We believe that the reason why the Hand (1991) liquid wall and the Tronconi (1990) interface frictions predict the "exact" final steady state value of the liquid holdup is because the value of the superficial gas velocity is close to the transition to roll waves, and from the study of Andreussi & Persen (1987), the interface friction factor can be estimated to twice the value of the gas wall friction at those superficial gas velocities. So there is no guaranteeing that this combination of friction factors will work well for stratified-wavy flows at higher gas flowrates where the interface friction becomes more important.

Thus, we have decided to adopt the combination of models (5.64) and (5.69) proposed respectively by Kowalski (1987) and Andritsos & Hanratty (1987) for the liquid wall and interface friction factors.

Andritsos & Hanratty (1987) stated that the transition to roll waves or stratified wavy flow roughly occurs at a superficial gas velocity of 5.0 m/s. They then used this transition value in their interfacial friction model, adding that it over predicted the friction factors in a range of superficial gas velocity from $J_{G,T}$ = 5.0 m/s to the actual critical gas velocity needed to generate large amplitude waves. Spedding & Hand (1997) later suggested that the transition to roll waves occurs at a higher superficial gas velocity of 6 m/s, so we propose to use the Andritsos & Hanratty (1987) expression with a modified transition value of $J_{G,T}$ =5.5 m/s for the gas superficial velocity, which is an average between the value given by Andritsos & Hanratty (1987) and the value given by Spedding & Hand (1997).

Therefore the liquid wall f_L and interface friction f_I models that we suggested using for stratified smooth and wavy flows can be summarized as follows:

$$\begin{cases} f_L = \max\left\{\dfrac{24}{Re_L}, \dfrac{0.263}{\alpha_L}\sqrt{\dfrac{D_{hL}}{Re_L\, D}}\right\} & \text{if} \quad J_G > J_{G,T} = 5.5\text{m/s} \\ f_L = \max\left\{\dfrac{16}{Re_L}, 0.001375\left[1+\left[2.10^4\left(\dfrac{\varepsilon}{D_{hL}}\right)+\dfrac{10^6}{Re_L}\right]^{1/3}\right]\right\} & \text{otherwise} \end{cases} \tag{5.73}$$

and

$$f_I = f_G\left\{1+\max\left[0, 15\left(\frac{J_G}{J_{G,T}}-1\right)\sqrt{\frac{h_L}{D}}\right]\right\} \quad \text{where} \quad J_{G,T} = 5.5\text{m/s} \tag{5.74}$$

where f_G is the gas wall friction factor, and it is defined by equation (5.72), R_L is the liquid holdup, h_L the liquid height, D_{hL} the liquid hydraulic diameter, D the pipe inner diameter, Re_L the liquid Reynolds number.

5.7 Conclusion

To formulate an accurate mathematical model for stratified flows with the assumptions mentioned in the introduction of this chapter, we need an accurate estimation of gas and liquid wall friction factors as well as the gas-liquid interfacial friction factor. Therefore, we first reviewed in this chapter the best available models in the literature for those terms, and

then studied the combined effect of the liquid wall friction and the interface friction, which are the most uncertain parameters in the modelling of stratified flows.

The uncertainties come from the structure of the stratified interface, which can either be flat or with large amplitude waves at the interface. The existence of these two sub- patterns (smooth and wavy) of the stratified flow make most available models for wall friction and interface friction to be valid only for one stratified sub-pattern.

To remedy to this problem, we proposed in this chapter a set of wall and interface friction models, which are valid for the full range of stratified flows (smooth and wavy). These models are defined by the Moody (1947) based equation (5.72) for the gas wall friction, the combined Moody (1947) and Kowalski (1987) based equation (5.73) for the liquid wall friction, and the modified Andritsos & Hanratty (1987) equation (5.74) for the interface friction factor.

A simple transition value, based on the gas superficial velocity, has also been proposed, for the transition from stratified-smooth to stratified-wavy flows, and the new friction models (5.73) & (5.74) can be easily updated when a better value for the transition to roll waves become available.

A good agreement of liquid holdup values between a selected experimental test (also called the Shaha case), which exhibits both stratified smooth and stratified wavy regions, and numerical predicted data with the new set of friction models is shown in Figure 5-10.

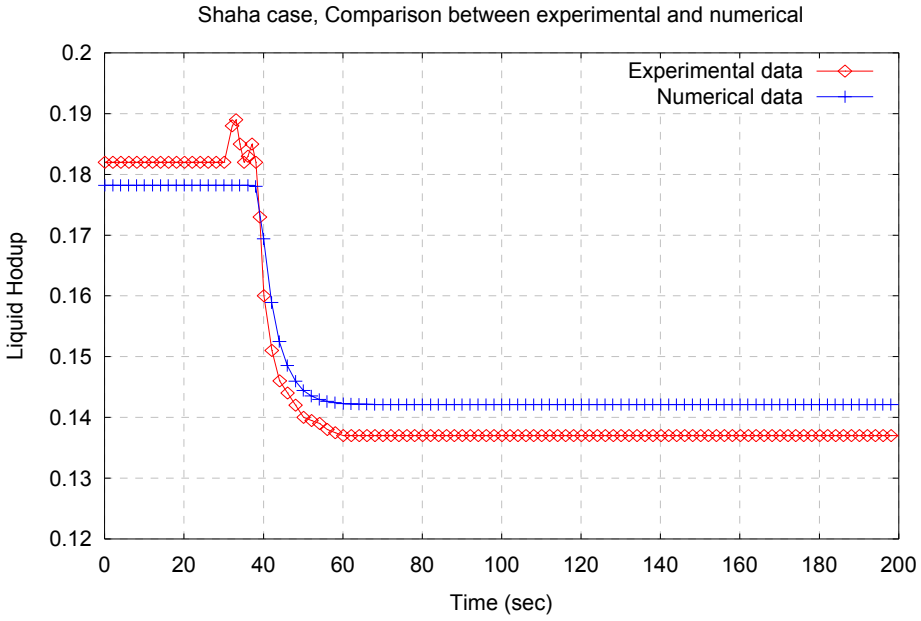

Figure 5-10: PFM-2 [Shaha Case]. Liquid holdup evolution, comparison between experimental and numerical for the proposed set of friction models.

5.8 References - 5

- **AEA Technology (1996).** "PLAC User Guide and Technical Manual", PC version 5.3, (January 1996)

- **Andreussi P., & Persen L. N., (1987)** "Stratified Gas-Liquid Flow in Downwardly Inclined Pipes". *Int. J. Multiphase Flow*, **13 (5)**, 565-575.

- **Andritsos N., & Hanratty T. J., (1987)** "Influence of interfacial waves in stratified gas-liquid flows". *AIChE Journal*, **33 (3)**, 444-454.

- **Andritsos N., Williams L., and Hanratty T. J., (1989)** "Effect of liquid viscosity on the stratified-slug transition in horizontal pipe flow". *Int. J. Multiphase Flow*, **15**, 877–892.

- **Baker A., Nielsen K., and Gabb A., (1988a)** "Pressure Loss, Liquid Hold-up Calculations Developed", *Oil & Gas Journal*, 55-59, March 14th 1988.

- **Baker A., Nielsen K., and Gabb A., (1988b)** "Field Data Test New Hold-up, Pressure Loss Calculations for Gas, Condensate Pipelines", *Oil & Gas Journal*, 79-87, March 21st 1988.

- **Baker O., (1954)** "Simultaneous Flow of Oil and Gas". *Oil & Gas Journal,* **53**, 185-195.

- **Baroczy C. J., (1966)** "A systematic correlation for two-phase pressure drop". *Chem. Eng. Prog. Symp. Ser.*, **62 (64)**, 232-249.

- **Beattie D. R. H., & Whalley P. B., (1982)** "A simple two-phase frictional pressure drop calculation method". *Int. J. Multiphase Flow*, **8**, 83.

- **Beggs H. D., & Brill J. P., (1973),** "A study of two-phase flow in inclined pipes". *Journal of Petroleum Technology, Transactions*, **25**, 607-617, May 1973.

- **Bendiksen K. H., & Espedal M., (1992)** "Onset of slugging in horizontal gas–liquid pipe flow". *Int. J. Multiphase Flow*, **18**, 234–247.

- **Cawkwell M. G., & Charles M. E., (1985)** "Pressures, temperatures predicted for two-phase pipelines". *Oil & Gas J. Tech.,* 101, May 1985

- **Chen X. T., Cai X. D., and Brill J. P., (1997)** "Gas-Liquid Stratified Wavy Flow in Horizontal Pipelines". *Journal of Energy Resources Technology*, **119**, 209-216.

- **Chisholm D., (1967)** "A theoretical basis for the Lockhart-Martinelli correlation for two-phase flow". *Int. J. Heat Mass Transfer*, **10**, 1767-78.

- **Chisholm D., (1973)** "Pressure gradients due to friction during the flow of evaporating two-phase mixtures in smooth tubes and channels". *Int. J. Heat Mass Transfer*, **16**, 347-358.

- **Cicchitti A., Lombardi C., Silvestri M., Solddaini G., and Zavalluilli R., (1960)** "Two-phase cooling experiments–Pressure drop, heat transfer and burnout measurement". *Energia Nucl.*, **7 (6)**, 407–425.

- **Colebrook C. F., (1939)** "Turbulent Flow in Pipes, With Particular Reference to the Transition between the Smooth and Rough Pipe Laws". *J. Inst. Civ. Eng.,* **11**, 133-156, London, 1939.

- **Corradini M. L., (1997)** "Fundamental of Multiphase Flows". Department of Engineering Physics, University of Wiscosin. **N.B.** The Internet link for this book is no longer valid, but do check http://silver.neep.wisc.edu/~WINS/publications.html.

- **Dukler A. E., Wicks M., and Cleveland R. G., (1964)** "Frictional pressure drop in two-phase flow: An approach through similarity analysis". *AIChE J.*, **10**, 38-43.

- **Eck B., (1973)** "Technische Stromungslehre", Springer, New York, 1973.

- **Espedal M., (1998)** "An Experimental Investigation of Stratified Two-Phase Pipe Flow at Small Inclinations", PhD thesis, Department of Applied Mechanics, Norwegian University of Science and Technology (NTNU), Trondheim, Norway.

- **Ferguson M. E. G., & Spedding P. L., (1995)** "Measurement and predication of pressure drop in two-phase flow". *J. Chem. Tech. Biotechnol.*, **62**, 262.

- **Friedel L., (1979)** "Improved friction pressure drop correlations for horizontal and vertical two-phase pipe flow". *European Two Phase Flow Group Meeting*, **Paper E2**, Ispra, Italy, June 1979.

- **Friedel L., (1980)** "Pressure drop during gas/vapour-liquid flow in pipes". *Int. Chem. Eng.*, **20**, 253.

- **Gregory G. A., & Fogarasi M., (1985)** "A critical evaluation of multiphase gas-liquid pipeline calculation methods". *Int. Conf. Multiphase Flow*, **2**, 93-108.

- **Guzhov A. L., Mamayev V. A., and Odishariya G. E., (1967)** "A Study of Transportation in Gas-Liquid Systems". *10th Int. Gas Union Conference*, Hamburg, Germany, June 1967.

- **Haaland S. E., (1983)** "Simple and Explicit Formulas for the Friction Factor in Turbulent Pipe Flow". *Journal of Fluids Engineering*, **105**, 89-90.

- **Hale C. P., (2000)** "Slug formation, growth and decay in gas-liquid flows". *PhD thesis*, Department of Chemical Engineering, Imperial College, London, UK.

- **Hand N. P., (1991)** "Gas-Liquid Co-Current Flow in a Horizontal Pipe". *PhD thesis*, Faculty of Engineering, The Queen's University of Belfast.

- **Hart J., Hamersma P. J., and Fortuin J. M., (1989)** "Correlations predicting frictional pressure drop and liquid hold-up during horizontal gas-liquid pipe flow with a small liquid hold-up". *Int. J. Multiphase Flow*, **15 (6)**, 947-964.

- **Haraburda S. S., & Chafin S., (2000)** "Calculating Two-Phase Pressure Drop". *Chemical Processing*, 2000 Fluid Flow Annual, 1-8.

- **Hewitt G. F., (1982)** "Gas-liquid two-phase flow". **Chapter 2**, *Handbook of Multiphase Systems,* edited by G. Hetsroni, Hemisphere Publishing Corp.

- **Hewitt G. F., (2002)** "Joint Project on Transient Multiphase Flows (TMF3)". *http://www.cranfield.ac.uk/sme/amac/tmf/tmf3_prospectus_final_version_may_2nd_2002.pdf* (visited on the 02/12/2003)

- **Hughmark G. A., (1962)** "Holdup in gas-liquid flow". *Chem. Eng. Prog.,* **58 (4)**, 62-65.

- **Hughmark G. A., (1963)** "Pressure drop in horizontal and vertical co-current gas-liquid flow". *IEC Fund.,* **2**,. 315-321.

- **Ishii M., & Zuber N., (1979)** "Drag Coefficient and Relative Velocity in Bubbly, Droplet or Particulate Flows". *AIChE Journal*, **25 (5)**, 843-854.

- **Issa R. I., & Woodburn P. J., (1998)** "Numerical prediction of instabilities and slug formation in horizontal two-phase flows". *Proc. 3rd Int. Conf. Multiphase Flow*, Lyon, France, June 8-12.

- **Khor S. H., (1998)** "Three-Phase Liquid-Liquid-Gas Stratified Flow in Pipelines", *PhD thesis*, Department of Chemical Engineering and Chemical Technology, Imperial College of Science, Technology & Medicine, London, UK.

- **Kordyban E. S., & Ranov T., (1970)** "Mechanism of slug formation in horizontal two-phase flow". *Journal of Basic Engineering, T.A.S.M.E.,* **Dec 1970**, 857-864.

- **Kouba G. E., & Jepson W. P., (1990)** "The flow of slugs in horizontal two-phase pipelines". *Trans. ASME*, **112**, 20-25.

- **Kowalski J. E., (1987)** "Wall and Interfacial Shear Stress in Stratified Flow in a Horizontal Pipe". *AIChE Journal*, **33** (2), 274-281.

- **Levy S., (1999)** "Two-Phase Flow in Complex Systems". *John Wiley & Sons, Inc*.

- **Lin S., Kwok C. C. K., Li R.Y., Chen Z. H., and Chen Z. Y., (1991)** "Local frictional pressure drop during vaporization for R-12 through capillary tubes". *Int. J. Multiphase Flow*, **17**, 95–102.

- **Liné A., & Lopez D., (1995)** "Wavy stratified flow with low liquid hold up: simulation & modelling". *7th International Conference Multiphase*, 7-9 June, Cannes, France, Bhr Group Publications, 357-377.

- **Lockhart R. W., & Martinelli R. C., (1949)** "Proposed correlation of data for isothermal two-phase, two component flow in pipes". *Chem. Engng. Prog.*, **45 (1)**, 39-48.

- **Mandhane J. M., Gregory G. A., and Aziz K., (1974)** "A flow pattern map for gas-liquid flow in horizontal pipes". *Int. J. Multiphase Flow*, **1**, 537-553.

- **Mandhane J. M., Gregory G. A., and Aziz K., (1975)** "Critical Evaluation of Holdup Prediction Methods for Gas-Liquid Flow in Horizontal Pipes". *J. Pet. Tech.*, **27**, 1017-1026.

- **Mandhane J. M., Gregory G. A., and Aziz K., (1977)** "Critical Evaluation of Friction Pressure-Drop Prediction Methods for Gas-Liquid Flow in Horizontal Pipes". *J. Pet. Tech.*, **29**, 1348-1358

- **Mata C., Peyrera E., Trallero J. L., and Joseph D. D., (2002)** "Stability of stratified gas-liquid flows". *Int. J. Multiphase Flow*, **28**, 1249-1268.

- **McAdams W. H., Woods W. K., & Heroman L. C., (1942)** "Vaporisation inside horizontal tubes, 2: Benzene-Oil mixtures". *Trans. A.S.M.E*, **64**,193-200.

- **Milne-Thomson L. M., (1968)** "Theoretical Hydrodynamics". Fifth ed., The MacMillan Press, London.

- **Moody L. F., (1947)** "An Approximate Formula for Pipe Friction Factors". *Transactions ASME*, **69**, 1005.

- **Muller-Steinhagen H., & Heck K., (1986)** "A simple Friction Pressure Drop Correlation for Two-Phase Flow in Pipes". *Chemical Engineering and Processing*, **20**, 297-308.

- **Olujic Z., (1985)** "Predicting two-phase flow friction loss in horizontal pipelines". *Chemical Engineering*, **June 24**, 45-50.

- **Pan L., (1996)** "High pressure three-phase (gas/liquid/liquid) flow". *PhD Thesis,* Department of Chemical Engineering and Chemical Technology, Imperial College of Science, Technology & Medicine, London, England, 1996.

- **Payne G. A., Palmer C. M., Brill J. P., & Beggs H. D., (1979)** "Evaluation of inclined-pipe, two-phase liquid holdup and pressure-loss correlations using experimental data". *Journal of Petroleum Technology, September 1979*, 1198-1208.

- **Perry R. H., & Green D. W., (Eds) (1984)** "Perrys Chemical Engineers Handbook" 6th Edn, McGraw Hill, New York.

- **Premoli A., Francesco D., & Prina A., (1971)** "A dimensionless correlation for determining the density of two-phase mixtures". *Thermotecnica*, **25**, 17-26.

- **Rouhani S. Z., & Axelsson E., (1970)** "Calculation of void volume fraction in the subcooled and quality boiling regions". *Int. J. Heat Mass Transfer*, **13**, 383-393.

- **Scott S. L., & Kouba G. E., (1990)** "Advances in Slug Flow Characterization for Horizontal and Slightly Inclined Pipelines". *65th SPE Annual Technical Conference and Exhibition*, New Orleans, September 23-26, **SPE 20628**, 125-140.

- **Shaha J., (1999)** "Phase Interactions in Transient Stratified Flow". *PhD thesis*, Department of Chemical Engineering, Imperial College, London, UK.

- **Simpson H. L., Rooney D. H., Gilchrist A., Grattan E., and Callender T. M. S., (1987)** "An assessment of some two-phase pressure gradient, holdup and flow pattern prediction methods in current use". *3rd International Conference on Multiphase Flow*, The Hague 18-20 May, **Paper A3**, 23-30.

- **Sinai Y. L., (1983)** "A Charnock-Based Estimate of Interfacial Resistance and Roughness for Internal, Fully-Developed, Stratified, Two-Phase Horizontal Flow". *Int. J. Multiphase Flow*, **9 (1)**, 13-19.

- **Spedding P. L., & Hand N. P., (1997)** "Prediction in Stratified Gas-Liquid Co-Current Flow in Horizontal Pipelines". *Int. J. Heat Mass Transfe*r, **40** (8), 1923-1935.

- **Srichai S., (1994)** "High Pressure Separated Two-Phase Flow", *PhD thesis*, Department of Chemical Engineering, Imperial College, London, UK.

- **Strand O., (1993)** "An Experimental Investigation of Stratified Two-Phase Flow in Horizontal Pipes", *PhD thesis*, Department of Mathematics, University of Oslo, Norway.

- **Taitel Y., & Duckler A. E., (1976)** "A Model For Predicting Flow Regime Transitions in Horizontal and Near-Horizontal Gas-Liquid Flow". *AIChE Journal*, **22 (1)**, 47-55.

- **Tronconi E., (1990)** "Prediction of slug frequency in horizontal two-phase flow". *AIChE Journal*, **36 (5)**, 701-709.

- **Vigneron F., Sarica C., & Brill J. P., (1995)** "Experimental Analysis of Imposed Two-Phase Flow Transient in Horizontal Pipelines". *Proceedings of the 7th International Conference on Multiphase Production*, Multiphase 95 edited by Wilson A., 199-217, Cannes, France, 7-9 June.

- **Weisman J., & Choe W. G., (1978)** "Methods for calculation of pressure drop in co-current gas-liquid flow". In *Two-Phase Transport and Reactor Safety*, ed. T. N. Veziroglu and Kakac, Hemisphere, WA, 1224-31.

- **Whalley P. B., (1987)** "Boiling, Condensation and Gas-Liquid Flow". *Clarendon Press, Oxford*.

- **Woods D. B., & Hanratty T J., (1996)** "Relation of slug stability to shedding rate". *Int. J. Multiphase Flow*, **22**, 809-828.

- **Xiao J. J., & Shoham O., (1991)** "Evaluation of Interfacial Friction Factor Prediction Methods for Gas/Liquid Stratified Flow". *SPE 22765*, 66th Annual Technical Conference and Exhibition, Dallas, Texas, 1991.

- **Zigrang D. J., & Sylvester N. D., (1985)** "A Review of Explicit Friction Factor Equations". *Journal of Energy Resources Technology*, **107**, 280-283.

6 Chapter 6 - Slug Flow Modelling

6.1 Introduction

Oil produced offshore is transported through pipelines as a complex mixture of gas, oil, water and sand. One common flow regime is known as slug flow, in which the liquid intermittently flows along the pipes in concentrated masses called slugs.

This complex and multi-dimensional type of flow exists for the whole range of pipe inclinations and over a wide range of gas and liquid flowrates, and its inherently unsteady nature means that even when the gas and liquid flowrates are maintained at a steady value the component mass flowrates, phase velocities and pressure at any cross-section normal to the pipe axis exhibit large variations with respect to time.

As a result, processes such as heat and mass transfer are unsteady, with substantial variation of the system temperature and concentration profiles occurring. Other potential consequences include increased erosion-corrosion of the pipe and the onset of damaging resonant vibrations within the pipeline system. Further downstream, the combination of flow-induced pressure fluctuations with an intermittent flow of gas and liquid may cause problems for control of separation equipment; necessitating large separation stage vessels called “slug catchers” to safely collect the slugs so that some of the inherent unsteadiness may be reduced.

Pipeline systems must therefore be able to safely withstand the fluctuating nature of the slug flow, whilst accommodating pressure drops up to an order of magnitude larger than those encountered in stratified flow and hence much larger than those found in single-phase flow. The increased pressure drop may make a well economically unviable. Consequently, in order to produce the most effective designs, it is essential to obtain accurate predictions of system properties based on an understanding of the mechanisms responsible for slug flow.

Unfortunately, despite five decades of intensive study of this complex flow, both experimentally and theoretically, a full understanding of its mechanisms is still not completed even though various approximate methods have been developed for calculating slug hydrodynamics. In the past, these have relied on correlation with experimental data, but more recently modelling has been used to simulate the flow behaviour. However, numerical calculation of some flow characteristics, such slug frequency or maximum slug

length, is still subjected to margins of error way beyond acceptable tolerance. In this project, we attempt to understand why the classic two-fluid model sometimes fails to represent this type of two-phase flow regime.

6.2 Chapter Outline

To achieve our objective, we start by explaining the mechanisms of slug flow formation following experimental observations. Then, we present a literature review of the key parameters for an accurate prediction of slug flow, followed by a brief description of the various approaches used in the literature to numerically model this complex flow regime.

The chapter continues with the analysis of the numerical simulations of a slug flow test case, obtained using the validated stratified flow model described in the previous chapter. Finally, we conclude with some suggestions in order to improve the predictions of our incompressible code as well as the current commercial codes.

6.3 Mechanisms of Slug Flow

Following the experimental observations of Hale (1994) and Manolis (1995), the five steps leading to the formation of stable slugs in the WASP rig can be summarized as follows:

1. **Interface wave formation:**
   Initially, gas and liquid flow co-currently into the pipeline, so that near the entrance point the gas flows above a moving stratified liquid layer. However, due to the shear force created at the wall, the liquid layer decelerates as it moves along the pipe and its level rises. Meanwhile, small disturbances on the stratified layer grow into rising waves due to the "suction" effect caused by the increased gas velocity over the liquid bumps.
2. **Wave growth & Pipe bridging event:**
   As a result of the interphase energy transfer, one of these waves eventually grows to a sufficient size to momentarily bridge the pipe, blocking the flow of the gas, so that pressure builds up behind it, hence causing the blockage to be accelerated to the gas velocity.
3. **Slug growth**
   This blockage appears to be accelerated uniformly across its cross-section, scooping up and accelerating all the slow moving liquid ahead of it, and so it begins to grow in volume to become a slug.
4. **gas entrainment:**
   As this occurs, a mixing vortex (Figure 6-1) forms near the slug front due to the presentation of the slower moving film into the slug body. Simultaneously, gas may be entrained in the form of small bubbles, which are deformed by the combined effect of buoyancy forces and the turbulent shear forces caused by velocity

differences between the slug front and the liquid film. As a result, a dispersion of small bubbles is produced which may be transported through the body of the liquid slug.

5. **Stratified layer formation:**
   Meanwhile, the liquid and the previously entrained gas are shed from the slug tail. The shed liquid decelerates to a velocity determined by the shear stresses at the wall and the interface and becomes a stratified layer. The shed gas mainly enters the elongated bubble.

As long as the volumetric pick-up rate is larger than the shedding rate, the slug continues to grow. However eventually the pick-up rate may become equal to the shedding rate, so that the slug becomes fully developed and the slug length stabilises

Subsequent slug formation may occur in a similar manner, except that this time the new slug picks-up the slow moving liquid shed from the tail of the slug in front. As a result the process of slug formation, growth and stabilisation may once again repeat.

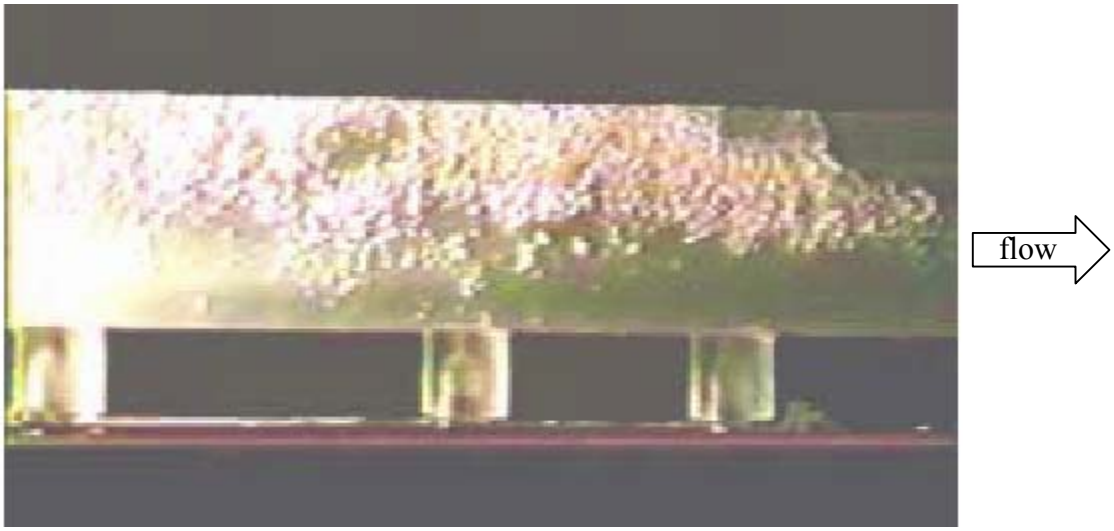

Figure 6-1: Image of mixing zone in the liquid slug (from http://www.cortest.com/multiphase.htm).

6.4 Literature Review - Slug Flow Parameters

6.4.1 Translational Velocity & Dynamics of Long Bubbles

Gas-liquid slug flow is characterised by large elongated bubbles separated quasi-periodically by liquid slugs that may contain small dispersed bubbles (Figure 6-1). As the elongated bubbles convey most of the gas, a complete model for slug flow requires information about these long bubbles and, in particular, their propagation or translational

velocity (V_T). Numerous researchers have therefore studied this key flow parameter theoretically and experimentally, and a considerable amount of slug motion data has been obtained for various flow conditions, fluid properties and pipe diameters and inclinations.

It is now generally assumed that the translational velocity of elongated bubbles V_T in a flowing liquid, which results from the complex influence of both buoyancy and mean motion of the liquid, is a superposition of the bubble propagation velocity in a stagnant liquid, i.e. the drift velocity V_D, and a contribution due to the mixture gas and liquid velocity V_M. Nicklin et al. (1962) proposed the expression that is commonly used in the literature as follows:

$$V_T = C_0 V_M + V_D \tag{6.1}$$

The values of the coefficient C_0 and the drift velocity V_D strongly depend upon the pipe or tube inclination, and the current research on long bubble motion usually treats separately the vertical, horizontal and inclined cases. In what follows, we mainly describe the horizontal case values, and for a complete presentation of all pipe inclination cases, we refer to recent review papers [Taitel & Barnea, 1990b; Fabre & Liné, 1992; Dukler & Fabre, 1994; Bendiksen et al., 1996] on slug flow.

6.4.1.1 Drift Velocity Coefficient

Early studies on long bubble drift velocity were concentrated on vertical stagnant liquid [Davies & Taylor, 1950; Griffith & Wallis, 1961; Nicklin et al., 1962]. Looking at air bubbles confined inside circular tubes, one of the questions that puzzled researchers was summarised by Davies & Taylor (1950) as:

> "How fast will the air column rise in a vertical tube with a closed top when the bottom is opened? Or, alternatively, how fast will a vertical tube with a closed top empty itself when the bottom is opened?"

To answer this question, Davies & Taylor (1950) performed a potential flow analysis around the nose of the elongated bubble and they obtained the following expression for the drift velocity:

$$V_D = C_1 \sqrt{gD} \tag{6.2}$$

A constant value of 0.328 for C_1 was obtained theoretically using approximate relaxation methods. This value was later refined to 0.351 and validated using confirmed air/water experimental data [Nicklin et al., 1962].

The drift velocity of long bubbles moving in a liquid at rest depends primarily on the force that creates the drift, i.e. gravity. However other forces such as viscous or surface tension may have some secondary effects; therefore many authors have studied the influence of the physical properties of the operating fluids and the pipe inclination to the drift coefficient

C_1. The dependency found is expressed through the general relationship given by Zukoski (1966) as:

$$V_D = C_1(N_f, Eo, \beta)\sqrt{\hat{g}D} \tag{6.3}$$

where the gravitational acceleration g has been replaced for convenience by $\hat{g} = g\Delta\rho/\rho_L$, N_f is the dimensionless inverse viscosity defined by $N_f = D^{3/2}\sqrt{\rho_L \Delta\rho g}/\mu_L$, β is the pipe inclination, and Eo is the Eotvös number, which is ratio between gravitational and surface tension forces, and expressed as:

$$Eo = \frac{\Delta\rho g D^2}{\sigma} \tag{6.4}$$

In the absence of surface tension and viscosity, the rate of propagation of a large bubble in a horizontal pipe can also be calculated using the inviscid flow theory, and the analytical value of the drift coefficient C_1, given by Benjamin (1968), is 0.542.

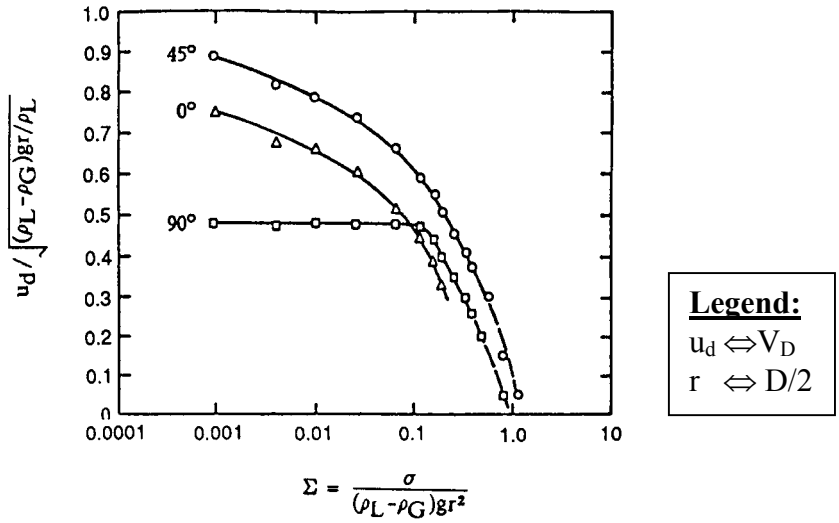

Figure 6-2: Variation of the normalised drift velocity with surface tension parameter for pipe inclination β = 0º, 45º, 90º. (After Zukoski [1966])

For small diameter pipes, Weber (1981) showed that the surface tension is important, as its increase considerably decreases the drift velocity (Figure 6-2). Therefore, he correlated Zukoski (1966) data using the following relation:

$$C_1 = 0.54 - \frac{1.76}{Eo^{0.56}} \tag{6.5}$$

It should be noted that the concept of a horizontal drift velocity was long a subject of controversy in the 1960s and 70s; some authors claimed that the drift velocity is zero [Wallis, 1969; Gregory & Scott, 1969; Dukler & Hubbard, 1975] on the basis that gravity cannot act in the horizontal direction, but this contradicted the experimental results of Zukoski (1966) as well as the theory of Benjamin (1968).

However, the recent studies of Nicholson et al. (1978), Ferré (1979), Weber (1981), Bendiksen (1984), Théron (1989), Manolis (1995), and Woods & Hanratty (1996) clearly show that a drift velocity does exist for the horizontal case due to hydrostatic pressure difference between the top and the bottom of the bubble nose, and it may even exceed the vertical case value.

The work of Ferré (1979) was particularly helpful in clarifying the horizontal case controversy. Whilst studying large bubble motion in a 45 mm diameter air-water flow loop, he noted that they were two critical velocities or Froude numbers for which the drift velocity abruptly changed in value, and he proposed the following correlation:

$$C_1 = \begin{cases} 0.44 & Fr_M \le 2.26 \\ 0 & 2.26 < Fr_M < 8.28 \\ 3 & Fr_M \ge 8.28 \end{cases} \tag{6.6}$$

Ferré (1979) experiments confirmed the existence of a drift velocity at low and very high mixture velocities, but also showed that at intermediate mixture velocities, the drift velocity is zero. The mixture Froude number Fr_M in the above relation is given by the following expression:

$$Fr_M = \frac{V_M}{\sqrt{gD}} = \frac{J_G + J_L}{\sqrt{gD}} \tag{6.7}$$

During his investigations of large bubbles in inclined tubes, Bendiksen (1984) put in evidence two different regimes of bubble motion, and therefore confirmed the existence of Ferré (1979) first transition criteria. However, using a liquid Froude number based on the superficial velocity $\left(Fr_L = J_L / \sqrt{gD}\right)$, he suggested that this transition might occur at a critical value of 3.5. His relation was validated for all pipe inclinations and is given as:

$$C_1 = \begin{cases} 0.54\cos\beta + 0.35\sin\beta & Fr_L < 3.5 \\ 0.35\sin\beta & Fr_L \ge 3.5 \end{cases} \tag{6.8}$$

Bendiksen (1984) suggested that the change in value at higher mixture velocities reflects the behaviour of the tip of the large bubble nose, which moves from a position near the top of the pipe to a point closer to the axial centreline of the pipe, as the inertia effect overcomes the buoyancy.

The drift velocity resulting from the above equation [Bendiksen, 1984] is discontinuous at the transitional Froude number, and that can lead to unstable solutions during numerical calculations. To overcome this difficulty, Théron (1989) proposed a continuous relation for the drift coefficient that is also valid for all pipe inclinations. His relation was expressed as:

$$C_1 = \left(-0.5 + \frac{0.8}{\Gamma} \right) \cos\beta + 0.35 \sin\beta \qquad (6.9)$$

The pipe inclination β is given from the horizontal. To define the parameter Γ, Théron (1989) used the same critical Froude value as Bendiksen (1984), and the mixture Froude number given by relation (6.7) instead of liquid Froude number used by Bendiksen (1984). This parameter was expressed as:

$$\Gamma = 1 + \left(\frac{Fr_M}{Fr_C} \cos\beta \right)^{10} \qquad \text{and} \qquad Fr_C = 3.5 \qquad (6.10)$$

It is still not clear what the value of the transitional Froude number is for the existence of a horizontal drift velocity, as various researchers have used different values. This critical value seems to be related to the slug flow sub-regimes, and understanding the transitions between these sub-regions is still ongoing research [Paglianti et al., 1996; Bertola, 2002].

Manolis (1995) studied the translational velocity of a slug tail for carefully controlled non-aerated liquid slugs in a 78 mm diameter pipe using air/water and air/oil as test fluids. In his "push-out" experiments, gas was injected at a predetermined rate at the inlet of a pipe, which was initially full of liquid. This resulted in the growth of a long gas bubble that pushed out the liquid to the pipe outlet. The bubble front velocity, equivalent to the slug tail velocity, was measured for various mixture velocity conditions and the obtained data were correlated to give an expression similar to that of Bendiksen (1984):

$$C_1 = \begin{cases} 0.477 & Fr_M < 2.86 \\ 0 & Fr_M \geq 2.86 \end{cases} \qquad (6.11)$$

The drift coefficient given by Manolis (1995) for low Froude numbers has been adjusted to make it dimensionally consistent with Zukoski (1966) equation (6.3).

In their studies of slug initiation at high gas velocities, Woods & Hanratty (1996) also measured the bubble translational velocity in a 95 mm diameter pipe using air and water, and they obtained the following result:

$$C_1 = \begin{cases} 0.52 & Fr_M < 3.1 \\ 0 & Fr_M \geq 3.1 \end{cases} \qquad (6.12)$$

This expression was given using the mixture velocity 3 m/s as the transitional velocity, but it is reported here using the mixture Froude number for consistency with other correlations.

6.4.1.2 Mean Bubble Motion Coefficient

The parameter C_0 in the translational velocity equation (6.1) is a distribution coefficient related to the velocity profiles in dispersed systems. It may be closely approximated by the ratio of the maximum to the mean velocity in the liquid ahead of the bubble. From their experimental data, Nicklin et al. (1962) suggested a constant value of 1.2 for fully developed turbulent flow, but noticed the variation of this coefficient at low slug Reynolds numbers (< 8000). From various expressions found in the literature, the parameter C_0 can be expressed through the following general expression:

$$C_0 = C_0\left(Fr_M, Re_S, \beta\right) \tag{6.13}$$

where β is the pipe inclination, Fr_M is a Froude number given as $Fr_M = V_M \big/ \sqrt{gD}$, and Re_S is the slug Reynolds number defined by:

$$Re_S = \frac{\rho_L V_M D}{\mu_L} \tag{6.14}$$

Compared to vertical flows, the distribution coefficient C_0 has been less studied theoretically for horizontal slug flows. To our knowledge, Dukler et al. (1985) reported the only analytical expression using a boundary layer analysis and a power law model. Their relation was given as:

$$C_0 = \frac{(2n+1)(n+1)}{2n^2} \xrightarrow{n=7} 1.225 \tag{6.15}$$

where n = 7 corresponds to the $1/7^{th}$ power law velocity profile for turbulent flow.

The above expression is in agreement with the experimental value suggested by Nicklin et al. (1962). However, the exact value of C_0 is still not clear for all flow conditions and reported experimental values spread considerably from 1.02 to 1.35 (Table 6-1). Hale (1994) attributed this to the fact that the plot of translational velocity V_T versus the mixture velocity V_M is not perfectly linear, but instead bends very slightly upwards [Bendiksen, 1984]. As a result, investigators that have calculated a line of best fit to their experimental data, and then extrapolated to $V_M = 0$ to obtain the drift velocity, are likely to provide one set of values whereas those that have first specified the drift velocity and then plotted the line of best fit originating from the point $V_M = 0$, $V_T = V_D$ will provide another. Further discrepancies may be caused by the fact that many of the earlier papers neglected the

contribution of the drift velocity [e.g. Hughmark, 1965; Dukler & Hubbard, 1975] and assumed that the relationship is given in the simpler form:

$$V_T = (1 + K)V_M = C_0 V_M \tag{6.16}$$

where K was defined as the rate of shedding to the rate of flow in the liquid slug. Assuming a fully established pipe flow in the front of the bubble nose, and a logarithmic velocity profile, Dukler & Hubbard (1975) proposed the following correlation for C_0:

$$C_0 = 1.022 + 0.021 \ln Re_M \tag{6.17}$$

where the mixture Reynolds number Re_M ranges from 3.10^4 to 4.10^5 and is defined as:

$$Re_M = \frac{\rho_M V_M D}{\mu_M} \tag{6.18}$$

The mixture density ρ_M and viscosity μ_M were defined as linear average of fluids properties using the liquid slug holdup as the coefficient of proportionality. However, because of the uncertainty in defining the viscosity of a mixture, these mixture quantities are sometimes replaced by the liquid values in the literature, and the mixture Reynolds number is replaced by the slug Reynolds number given by relation (6.14).

The experimental results of Ferré (1979) suggested that the discrepancies in the coefficient C_0 might be due to the occurrence of a flow transition. As reported previously, he found two different critical Froude numbers at which the values of the drift velocity change, and proposed the following expression:

$$C_0 = \begin{cases} 1.10 & Fr_M \le 2.26 \\ 1.30 & 2.26 < Fr_M < 8.28 \\ 1.02 & Fr_M \ge 8.28 \end{cases} \tag{6.19}$$

Similarly, whilst investigating the motion of single bubbles in pipes, Bendiksen (1984) noticed that there was a critical Froude number at which the values suddenly changed. As a result, he suggested that the following criteria should be used for all pipe inclinations:

$$C_0 = \begin{cases} 1.05 + 0.15 \sin^2(\beta) & Fr_L < 3.5 \\ 1.20 & Fr_L \ge 3.5 \end{cases} \tag{6.20}$$

Théron (1989) included the effect of the Froude number on the distribution coefficient C_0, and presented a simple continuous correlation that is valid for all pipe inclinations. His relation can be written as:

$$C_0 = 1.3 - \frac{0.23}{\Gamma} + 0.13\sin^2\beta \qquad (6.21)$$

where Γ is defined in the same way as in the drift coefficient and is given by relation (6.10).

From his "push-out" experimental data, Manolis (1995) correlated the parameter C_0 with the following expression:

$$C_0 = \begin{cases} 1.033 & Fr_M < 2.86 \\ 1.216 & Fr_M \geq 2.86 \end{cases} \qquad (6.22)$$

King (1998) compared the experimental data of Manolis (1995) with the predictions of five other correlations from the literature and found that the best two relations are the one of Bendikson (1984) presented earlier, and the one of Manolis (1995) described above.

Woods & Hanratty (1996) reported a similar expression to the one of Manolis (1995) and their correlation is given as:

$$C_0 = \begin{cases} 1.1 & Fr_M < 3.1 \\ 1.2 & Fr_M \geq 3.1 \end{cases} \qquad (6.23)$$

Recently, Petalas & Aziz (1998) used the Stanford Multiphase Flow Database to account for the effect of the slug Reynolds number on the coefficient C_0, and empirically derived the following correlation:

$$C_0 = \frac{1.64 + 0.12\sin\beta}{Re_S^{0.031}} \qquad (6.24)$$

where β is the pipe inclination and Re_S is the liquid slug Reynolds number defined by Equation (6.15). The above relation is valid for all pipe inclinations.

A summary of the mean motion coefficient C_0 and the drift velocity coefficient C_1 is presented in Table 6-1

Reference	D (mm)	Translational Velocity $V_T = C_0 V_M + C_1\sqrt{\hat{g}D}$	
		C_0	C_1
Benjamin (1968)	-	-	0.542 (Theory)
Gregory & Scott (1969)	19	1.35	0.0

Dukler & Hubbard (1975)	38	$1.022 + 0.021 \ln \mathrm{Re_S}$ $3.10^4 \le \mathrm{Re_S} \le 4.10^5$	0.0
Nicholson et al. (1978)	25, 51	1.196 (25 mm) 1.128 (51 mm)	0.538 (25 mm) 0.396 (51 mm)
Ferré (1979)	45	$\begin{cases} 1.1 & \mathrm{Fr_M} \le 2.26 \\ 1.3 & 2.26 < \mathrm{Fr_M} < 8.28 \\ 1.02 & \mathrm{Fr_M} \ge 8.28 \end{cases}$	$\begin{cases} 1.1 & \mathrm{Fr_M} \le 2.26 \\ 1.3 & 2.26 < \mathrm{Fr_M} < 8.28 \\ 1.02 & \mathrm{Fr_M} \ge 8.28 \end{cases}$
Weber (1981)	5 - 178	-	$0.54 - \frac{1.76}{\mathrm{Eo}^{0.56}}$
Bendikson (1984)	50	$\begin{cases} 1.05 & \mathrm{Fr_L} < 3.5 \\ 1.2 & \mathrm{Fr_L} \ge 3.5 \end{cases}$	$\begin{cases} 0.54 & \mathrm{Fr_L} < 3.5 \\ 0 & \mathrm{Fr_L} \ge 3.5 \end{cases}$
Dukler et al. (1985)	-	1.225 (Theory)	-
Théron (1989)	53	$1.3 - \frac{0.23}{1 + (\mathrm{Fr_M}/3.5)^{10}}$	$-0.5 + \frac{0.8}{1 + (\mathrm{Fr_M}/3.5)^{10}}$
Manolis (1995)	78	$\begin{cases} 1.033 & \mathrm{Fr_M} < 2.86 \\ 1.216 & \mathrm{Fr_M} \ge 2.86 \end{cases}$	$\begin{cases} 0.477 & \mathrm{Fr_M} < 2.86 \\ 0 & \mathrm{Fr_M} \ge 2.86 \end{cases}$
Woods & Hanratty (1996)	95	$\begin{cases} 1.1 & \mathrm{Fr_M} < 3.1 \\ 1.2 & \mathrm{Fr_M} \ge 3.1 \end{cases}$	$\begin{cases} 0.52 & \mathrm{Fr_M} < 3.1 \\ 0 & \mathrm{Fr_M} \ge 3.1 \end{cases}$
Petalas & Aziz (1998)	-	$\mathrm{C_0} = \frac{1.64}{\mathrm{Re_S}^{0.031}}$	$\mathrm{C_1} = 0.54 - \frac{1.76}{\mathrm{Eo}^{0.56}}$

Table 6-1: Values of the translational velocity coefficients C_0 & C_1 for horizontal slug flow ($\beta = 0$)

6.4.2 Slug Body Holdup

The slug body holdup, i.e. the volume fraction of the liquid in the slug body, is also required in slug models as a closure relationship. The process in which gas bubbles are entrained in the slug body is very complex and few theoretical methods have been proposed for the prediction of the average liquid holdup $\mathbf{R_{LS}}$ within the slug. Instead, graphical or empirical relations based on limited data sets are used, and they are reviewed in this section. It is worth mentioning that whenever it is possible, we re-write existing empirical correlations using dimensionless numbers.

Gregory et al. (1978) measured the slug body holdup for air and light refined oil flow in horizontal pipe with diameters of 25.8 mm and 51.2 mm, and they proposed an empirical correlation that only depends upon the mixture velocity and it is given by:

$$R_{LS} = \frac{1}{1 + \left(\frac{V_M}{8.66} \right)^{1.39}} \tag{6.25}$$

This equation is widely used in the literature because of its simplicity even though it fails to account for the effect of the fluids physical properties.

Using the same experimental data as Gregory et al. (1978), Malnes (1982) accounted for the gravitational and surface tension effects, and proposed an alternative correlation, which can be written as follows:

$$R_{LS} = 1 - \frac{1}{1 + \left(\frac{83}{Fr_M Bo_L^{0.25}} \right)} \tag{6.26a}$$

The mixture Froude number Fr_M in above relation is given by equation (6.7), while the liquid Bond number is defined as:

$$Bo_L = \frac{gD^2 \rho_L}{\sigma} \tag{6.26b}$$

Ferschneider (1983) proposed a slug body correlation, based on experiments carried out at the Boussens flow loop in France, which is 120 m long and has a diameter of 152.4 mm. The data were obtained using natural gas and light hydrocarbon oil at high pressures between 10 and 50 bars. The reported correlation is:

$$R_{LS} = \frac{1}{\left[1 + \left(\frac{V_M}{\sqrt{gD(\Delta\rho/\rho_L)}} \right)^2 \Big/ \left(\frac{A}{Bo^{\beta}} \right)^2 \right]^2} \tag{6.27}$$

where the Bond number Bo, which is the ration between gravitational and surface tension force, is defined as:

$$Bo = \frac{gD^2 \Delta\rho}{\sigma} \tag{6.28}$$

No information was given on the value of the coefficients A and β, but in later references [Théron (1989), Paglianti et al. (1993)] this correlation was written as follows:

$$R_{LS} = \frac{1}{\left(1 + \frac{\hat{Fr}_M^2 Bo^{0.2}}{625}\right)^2} \tag{6.29}$$

thereby implying the values of 25 and 0.1 for A and β respectively. The modified mixture Froude number in the above expression is defined as:

$$\hat{Fr}_M = \frac{V_M}{\sqrt{gD(\Delta\rho/\rho_L)}} \tag{6.30}$$

Barnea & Brauner (1985) proposed a method for predicting the liquid holdup in the slug body. The method was based on the assumption that the gas holdup in the slug body is determined by a balance between breakage forces, acting on the bubbles due to turbulence, and coalescence forces resulting from the effect of gravity and surface tension. They related this concept to the slug/dispersed bubble flow transition, and derived a correlation that was expressed by Taitel & Barnea (1990b) as follows:

$$R_{LS} = 1 - 0.058\left[2\left(\frac{0.4\sigma}{\Delta\rho g}\right)^{0.5}\left(\frac{2f_s V_M^3}{D}\right)^{0.4}\left(\frac{\rho_L}{\sigma}\right)^{0.6} - 0.725\right]^2 \tag{6.31}$$

where f_s is the Blasius friction factor based on the liquid slug Reynolds number $(Re_S = \rho_L V_M D/\mu_L)$. If the original Blasius expression $f_s = 0.079\,Re_S^{-0.25}$ is used instead of the modified relation $f_s = 0.046\,Re_S^{-0.2}$ preferred by the Barnea & Brauner (1985), then their original relation can be reformulated using dimensionless numbers to give a simple expression as:

$$R_{LS} = 1 - 0.058\left[0.605\left(\frac{Bo}{Re_S}\right)^{0.1}\hat{Fr}_M^{1.2} - 0.725\right]^2 \tag{6.32}$$

The Bond Bo, slug Reynolds Re_S, and the modified mixture Froude Fr_M numbers are respectively given by relations (6.28), (6.14), and (6.30). The above equation can be concisely written as:

$$R_{LS} = 1 - 0.021\left[\hat{Fr}_M^{1.2}\left(\frac{Bo}{Re_S}\right)^{0.1} - 1.2\right]^2 \tag{6.33}$$

The calculated value of R_{LS} ranges from 1 to 0.48, where 0.48 is a limiting value associated with the maximum volumetric packing of the dispersed bubbles in the liquid slug.

Andreussi & Bendiksen (1989) investigated the effect of pipe diameter and inclination on the slug body void fraction using 48 mm and 89 mm diameter pipes and air/water as test fluids. By balancing the net loss rate of small bubbles at the slug tail to the net entrainment rate at the slug front, they developed two semi-empirical relations for the slug body holdup. Andreussi et al. (1993) later used the following relation in their slug model:

$$R_{LS} = \frac{F_0 + F_1}{Fr_M + F_1} \tag{6.34a}$$

where the mixture Froude number Fr_M is given by relation (6.7) and the coefficients F_0 and F_1 by the following expressions:

$$F_0 = \max\left[0,\ 2.6\left(1 - 2\left(\frac{D_0}{D}\right)^2\right)\right], \qquad \text{and} \qquad F_1 = 2400\left(1 - \frac{\sin\beta}{3}\right)Bo^{-3/4} \tag{6.34b}$$

with the critical diameter value $D_0 = 2.5$ cm.

Using air-water and air-light oil experimental data, Paglianti et al. (1993) compared the above correlation with the relations of Gregory et al. (1978), Malnes (1982), and Ferschneider (1983), and found that it provides the best prediction for the slug holdup.

Marcano et al. (1998) tested sixty-two slug flow cases over varying combinations of gas and liquid flowrates in a horizontal flow loop of 78 mm diameter and 420 m long. Based on their experimental results, they formulated the following correlation for the slug body holdup:

$$R_{LS} = \frac{1}{1.001 + 0.0179V_M + 0.0011V_M^2} \tag{6.35}$$

They compared this correlation with their experimental data and observed a relative error of 8%. They applied this correlation and the correlation of Gregory et al. (1978) to a combined slug flow data set from the literature and found that their correlation was more accurate and 43% better than that of Gregory et al. (1978).

From an experimental database of numerous slug holdup data, Gomez et al. (2000) recently presented a correlation for upward inclined slug flow. The correlation was given by the following expression:

$$R_{LS} = \exp\left(-\left(0.45\beta + 2.4810^{-6}\,Re_S\right)\right) \qquad 0 \le \beta \le 1.57 \tag{6.36}$$

where β is the pipe inclination angle in radians and Re_S is the slug Reynolds number defined by $Re_S = \rho_L V_M D/\mu_L$.

Abdul-Majeed (2000) recently developed a new empirical equation for estimating the liquid slug holdup based on 316 data points for horizontal flow and 107 data points for slightly inclined flow. His analysis of the experimental data, taken over a wide range of parameters, indicated that the slug holdup is only affected slightly by the pipe diameter and the surface tension, but is strongly influenced by the fluids dynamic viscosity. Therefore, he proposed the following correlation:

$$R_{LS} = (1.009 - CV_M)A \tag{6.37a}$$

where the coefficient C is given by:

$$C = 0.006 + 1.3377 \frac{\mu_G}{\mu_L} \tag{6.37b}$$

The parameter A was included to account for the effect of pipe inclination and it is expressed as:

$$A = \begin{cases} 1 & \text{if} \quad \beta \le 0 \\ 1 - \sin(\beta) & \text{if} \quad \beta > 0 \end{cases} \tag{6.37c}$$

Abdul-Majeed (2000) compared his correlation with the experimental data and found that all the predicted values agree to within 10% of the measured data.

6.4.2.1 Effect of Viscosity

Nadler & Mewes (1995) carried out experiments at 5 bars to study the effect of the liquid viscosity on the phase distribution in horizontal air-liquid slug flow. The liquids used for the experiments were water and oil, and their investigation showed that the increase in liquid viscosity results in increasing liquid holdup in the slug body. Unfortunately, they did not derive a practical empirical correlation, and although, they indicated that trends from their study are only for a limited range of the tested liquid viscosities, it appears that the recent correlation (6.37) from Abdul-Majeed (2000) agrees with their observations.

6.4.2.2 Effect of Pressure

Manolis (1995) measured the average slug body holdup in air-water and air-oil systems. For both flows, he observed that increasing the air superficial velocity led to a decrease in the average slug body holdup for a constant liquid superficial velocity. In addition, he also showed that increasing the system pressure led to a decrease in the average slug body holdup. This pressure effect could be significant in the petroleum industry, where pipelines

sometimes operate at high pressure, unfortunately, he did not derive a practical correlation to account for this effect, and it cannot be included in existing slug models.

Model	D (mm)	Fluids	Slug Body Holdup
Gregory et al. (1978)	25, 51	Air/light oil	$R_{LS} = \frac{1}{1+\left(\frac{V_M}{8.66}\right)^{1.39}}$
Malnes (1982)	25, 51	Air/light oil	$R_{LS} = 1 - \frac{1}{1+\left(\frac{83}{Fr_M Bo_L^{0.25}}\right)}$
Ferschneider (1983)	152	Air/light oil	$R_{LS} = \frac{1}{\left(1+\frac{\hat{Fr}_M^2 Bo^{0.2}}{625}\right)^2}$
Barnea & Brauner (1985)	-	-	$R_{LS} = 1 - 0.021\left[\hat{Fr}_M^{1.2}\left(\frac{Bo}{Re_S}\right)^{0.1} - 1.2\right]^2$
Andreussi & Bendiksen (1989)	48, 89	Air/water	$R_{LS} = 1 - \frac{Fr_M - F_0}{Fr_M - F_1}$
Marcano et al. (1998)	78	Air/kerosene	$R_{LS} = \frac{1}{1.001 + 0.0179V_M + 0.0011V_M^2}$
Gomez et al. (2000)	51 to 203	Air/water Air/oil Freon/water	$R_{LS} = \exp\left(-\left(0.45\beta + 2.4810^{-6}\,Re_S\right)\right)$
Abdul-Majeed (2000)	25 to 203	Air/water Air/light oil Air/kerosene Freon/water Nitrogen/diesel	$R_{LS} = (1.009 - CV_M)A$ $C = 0.006 + 1.3377\frac{\mu_G}{\mu_L}$ $A = \begin{cases} 1 & \text{if } \beta \le 0 \\ 1-\sin(\beta) & \text{if } \beta > 0 \end{cases}$

Table 6-2: Summary of slug body liquid holdup correlations

6.4.3 Slug Frequency

Gregory & Scott (1969) defined the slug frequency ω_s as the average number of slug units passing a given point in the system over a unit of time. And despite many slug frequency data reported in the literature, it is still one of the least reliably modelled parameters. This is due to the statistical nature of the slug flow pattern and the frequency parameter reflects the

intermittency of the flow. However due to its inclusion as a closure relation in many slug flow models, it is important to accurately predict this parameter.

The slug frequency varies depending on the nature of the flow, whether it is developing or fully developed. Thus two types of models appear in the literature: there are a few phenomenological models that give the slug frequencies obtained near the pipe entrance and many empirical correlations based on data collected at downstream pipe locations where the slug flow is known to be fully developed.

6.4.3.1 Empirical Models

Gregory & Scott (1969) proposed one of the first slug frequency correlations based on experimental data for carbon dioxide-water flow in a horizontal pipe with a diameter of 19 mm. Their expression was given as:

$$\omega_s = 0.0226\left[\frac{J_L}{gD}\left(\frac{19.75}{V_M} + V_M\right)\right]^{1.2} \tag{6.38}$$

Greskovich & Shrier (1972) re-arranged this expression using the Froude number to obtain the following relationship:

$$\omega_s = 0.0226\left[\lambda_L\left(\frac{2.02}{D} + Fr_M^2\right)\right]^{1.2} \tag{6.39}$$

where λ_L is the no-slip liquid holdup and Fr_M is the Froude number based on the mixture velocity. But, based on data collected from a 45 mm line, they observed that the effect of diameter is not properly taken into account by this expression. Therefore, they recommended using their graphical correlation for cases involving large diameters.

Using air-water flow in a 42 mm diameter pipe, Heywood & Richardson (1979) determined the Power Spectral Density (PSD) function of the instantaneous liquid holdup measured by a gamma densitometer. They estimated the mean slug frequency by taking the frequency at which the maximum power value was obtained from the PSD function, and proposed an expression similar to the one of Gregory & Scott (1969); it is given as:

$$\omega_s = 0.0434\left[\lambda_L\left(\frac{2.02}{D} + Fr_M^2\right)\right]^{1.02} \tag{6.40}$$

Utilising a larger database of slug flow characteristics in both low-pressure test rigs and field production flowlines, Hill & Wood (1990) suggested that low frequency slugs in large diameter pipes may be better correlated by:

$$\omega_s = 0.275\frac{V_M}{3600D}10^{(2.68R_{LE})} \tag{6.41}$$

where the equilibrium stratified liquid holdup R_{LE} is calculated using the Taitel & Dukler (1976) method. They included the slip velocity into this initial correlation, and proposed a revised and improved slug frequency relation expressed as:

$$\omega_s = 2.74\frac{(V_{GE} - V_{LE})}{3600D}\frac{R_{LE}}{(1 - R_{LE})} \tag{6.42}$$

where V_{GE} and V_{LE} are respectively the gas and liquid velocities and are calculated within the method used to obtain the equilibrium stratified liquid holdup. The Hill & Wood (1990) correlations were given using the inverse of an hour unit, but they are expressed in this thesis in (Hz) for the convenience of consistency.

Tronconi (1990) studied the formation of slugs from their precursor waves and suggested that the slug frequency is inversely proportional to the period of these precursor waves. Based on the work of Dukler et al. (1985) on the coalescence of unstable slugs, he assumed that only half of the waves develop into stable slugs and using the concept of the most dangerous waves proposed by Mishima & Ishii (1980) and a non-linear analysis of the inviscid two-dimensional flow in a rectangular channel, he derived a semi-theoretical slug frequency model for horizontal flow that may be given as:

$$\omega_s = 0.61\left(\frac{\rho_G}{\rho_L}\frac{V_{GE}}{h_{GE}}\right) \tag{6.43}$$

where V_{GE} and h_{GE} are the equilibrium gas velocity and height obtained by using the Taitel & Dukler (1976) type of momentum balance.

Stapelberg & Mewes (1994) derived a slug frequency correlation by curve-fitting the data of Heywood & Richardson (1979), and proposed the following expression:

$$\omega_s = \left[Fr_{min} + A\left(Fr_M^{0.1} - 1.17Fr_L^{0.064}\right)\right]^2\sqrt{\frac{g}{D}} \tag{6.44a}$$

where

$$Fr_L = \frac{J_L}{\sqrt{gD}} \qquad Fr_{min} = 0.048Fr_L^{0.81} \qquad A = 0.73Fr_L^{2.34} \tag{6.44b}$$

This correlation predicts no dependence of the slug frequency on the pipe inclination angle, but Zabaras (1999) found it to give good agreement with air-water slug frequency data measured in an inclined flow loop of 101 mm diameter.

Manolis (1995) studied the effect of pressure on the slug frequency. He conducted an exhaustive set of experiments on a 78 mm diameter pipe at pressure up to 14.5 bars and reported the inadequacy of existing slug frequency models in predicting his data. Therefore, he developed a new slug frequency correlation based on six dimensionless numbers.

$$\omega_s = f\left(X, Z, Fr_L, \hat{Fr}_G, Eo, N_f\right) \tag{6.45}$$

A close look at the model reveals that one dimensionless number appears to be redundant; therefore, the Manolis (1995) correlation is described below with only five dimensionless numbers:

$$\omega_s = \frac{J_G}{D}\left(0.0363\frac{Fr_L}{\hat{Fr}_G}\frac{Z_L}{Eo^{0.2}}\right)^n \tag{6.46a}$$

where the exponent n is a function of the viscosity number and is given by:

$$n = \frac{N_f}{260 + 0.85N_f} \tag{6.46b}$$

The relation (6.4) defines the Eotvös number as $\left(Eo = gD^2\Delta\rho/\sigma\right)$, while the viscosity number N_f is given by the following expression:

$$N_f = \frac{D^{1.5}\sqrt{\rho_L\Delta\rho g}}{\mu_L} \tag{6.46c}$$

The liquid Froude number Fr_L and the modified gas Froude number $\hat{Fr}_G$ are defined as:

$$Fr_L = \frac{J_L}{\sqrt{gD}} \qquad \hat{Fr}_G = \frac{J_G}{\sqrt{gD\left(\rho_L/\Delta\rho\right)}} \tag{6.46d}$$

The parameter Z_L in relation (6.46a) is a combination of two dimensionless numbers X and Z used by Manolis (1995) and it is defined as the ratio of the liquid inertia to the liquid pressure drop. It is given by:

$$Z_L = \left[\frac{\frac{\rho_L J_L^2}{2D}}{\left(\frac{dp}{dx}\right)_L} \right]^{0.5} = \left[\frac{1}{4C_f \, Re_L^{-m}} \right]^{0.5} \qquad (6.46e)$$

The liquid Reynolds number $\left(Re_L = \rho_L J_L D/\mu_L\right)$ is based on the liquid superficial velocity. C_f and m are the friction factor constant coefficient and exponent and they depend on the nature of the flow, whether it is turbulent or laminar (C_f = 0.046, m = 0.2 if Re_L > 2000, otherwise C_f = 16 and m = 1).

Manolis (1995) compared his correlation with published slug frequency data from the literature as well as those obtained from the WASP facility at Imperial College London and concluded that his correlation predicted all the experimental data reasonably well.

Model	D (mm)	Fluids	Slug Frequency (Hz)
Gregory & Scott (1969)	19	CO_2-water	$\omega_s = 0.0226\left[\lambda_L\left(\frac{2.02}{D} + Fr_M^2\right)\right]^{1.2}$
Heywood & Richardson (1979)	42	Air/water	$\omega_s = 0.0434\left[\lambda_L\left(\frac{2.02}{D} + Fr_M^2\right)\right]^{1.02}$
Tronconi (1990)	-	-	$\omega_s = 0.61\left(\frac{\rho_G}{\rho_L}\frac{V_{GE}}{h_{GE}}\right)$
Hill & Woods (1990)	50 to 590	Air/water Air/kerosene	$\omega_s = 0.275\frac{V_M}{3600D}10^{(2.68R_{LE})}$
Hill & Woods (1990)	50 to 590	Air/water Air/kerosene	$\omega_s = 2.74\frac{(V_{GE} - V_{LE})}{3600D}\frac{R_{LE}}{(1-R_{LE})}$
Stapelberg & Mewes (1994)	42, 101	Air/water	$\omega_s = \left[Fr_{min} + A\left(Fr_M^{0.1} - 1.17Fr_L^{0.064}\right)\right]^2\sqrt{\frac{g}{D}}$
Manolis (1995)	78	Air/water Air/oil	$\omega_s = \frac{J_G}{D}\left(0.0363\frac{F_L}{F_G}\frac{Z_L}{Eo^{0.2}}\right)^n$
Zabaras (1999)	25 to 203	Air/water Air/oil	$\omega_s = 0.0226\left[\lambda_L\left(\frac{2.02}{D} + Fr_M^2\right)\right]^{1.2}\phi$ $\phi = 0.836 + 2.75\sin^{0.25}(\beta)$

Table 6-3: Summary of fully developed slug frequency models

Recently, Zabaras (1999) reviewed six empirical and two mechanistic slug frequency correlations for horizontal and inclined flows. He found poor prediction results for inclined slug flow, which is not surprising as none of the models studied was based on inclined pipe data. Therefore, he proposed a correction factor to the relation of Gregory & Scott (1989) which accounted for the pipe inclination effect. The revised correlation is given by:

$$\omega_s = 0.0226\left[\lambda_L\left(\frac{2.02}{D} + Fr_M^2\right)\right]^{1.2}\phi \qquad (6.47a)$$

where the correction factor ϕ is defined as

$$\phi = 0.836 + 2.75\sin^{0.25}(\beta) \qquad (6.47b)$$

A summary of all the slug frequency models mentioned above is given in Table 6-3.

6.4.3.2 Phenomenological Models

Taitel & Dukler (1977) considered the slug formation to be an entrance phenomenon and suggested that the slug frequency is given by the inverse of the time taken for the film to rebuild its level and form a slug. They then solved one-dimensional mass and momentum relations using the shallow channel approximation to calculate the characteristic time for this process. Comparison of the predictions of their model with the data of Dukler & Hubbard (1975) showed good agreement, but the results were less satisfactory when compared with data from Gregory & Scott (1969) and Vermeuleun & Ryan (1971). The model predicts an increase of frequency with increasing liquid superficial velocity at constant gas superficial velocity. It also predicts a minimum in the plot of slug frequency versus gas velocity at constant liquid superficial velocity. However, as pointed out by Hale & Hewitt (1999), a general validation of this model is still lacking.

Hale & Hewitt (1999) reviewed in detail the Taitel & Dukler (1977) frequency model and highlighted its limitations. To overcome the deficiencies, they proposed a non-correlational approach for predicting the slug frequency in which the processes of slug initiation, growth and decay were taken into account. The resulting model is therefore based on the physics of the flow, and appears to be in very good agreement with experiments. However, its implementation details seem complicated and difficult to include in current legacy codes.

6.4.4 Slug Length

The liquid slug length (L_s) is an important design parameter for hydrocarbon pipelines, particularly for sizing downstream separation facilities such as slug catchers. It is closely related to the slug frequency, but appears to be preferred in most slug flow models. In what follows, a brief review of the most common correlations for slug length in the literature is presented.

Dukler & Hubbard (1975) and later Dukler et al. (1985) found that the minimum stable slug length increases with the slug Reynolds number, and from experiments on a 38 mm horizontal pipe, they observed that the slug lengths are approximately 12-30D and appear to be relatively insensitive to the gas and liquid flowrates. Other researchers have confirmed the same observations as indicated in Table 6-4. Hence constant values are generally used for the mean slug length in slug flow models.

Reference	D (mm)	Fluids	Mean slug length
Dukler & Hubbard (1975)	38	Air/water	12-30D
Nicholson et al. (1978)	25, 51	Air/light oil	~30D
Gregory et al. (1978)	25, 51	Air/light oil	~30D (N.B. some slugs reached 375D)
Barnea & Brauner (1985)	Theory	Theory	32D
Andreussi et al. (1988)	50	Air/water	22D
Nydal et al. (1992)	53, 90	Air/water	15-20D (53 mm pipe) 12-16D (90 mm pipe)
Manolis (1995)	78	Air/water Air/oil	10-25D

Table 6-4: Mean slug lengths in horizontal pipes

Although these constant values provide reasonable estimates in pipes of small diameter (25 to 90 mm), they greatly under-predict typical values encountered in large diameter pipes (400 to 600 mm). For example in oil pipelines, Scott et al. (1986) observed that slugs are typically 300D long. In absence of any theory to predict this value satisfactorily, some logarithmic expressions have been suggested and they are reported below.

Based on field data obtained from the Prudhoe Bay oil field in Alaska, Brill et al. (1981) included the effect of the pipe diameter and mixture velocity in the mean slug length and proposed the following correlation:

$$\ln(L_S) = -3.851 + 0.059 \ln\left(\frac{V_M}{0.3048}\right) + 5.445\left[\ln\left(\frac{D}{0.0254}\right)\right]^{0.5} \qquad (6.48)$$

Norris (1982) modified the above expression using further data from the Prudhoe Bay field, and produced the following expression:

$$\ln(L_S) = -3.287 + 4.589\left[\ln\left(\frac{D}{0.0254}\right)\right]^{0.5} \tag{6.49}$$

Scott et al. (1986) attempted an improvement of the above correlation by accounting for two slug growth mechanisms, namely liquid pickup at the slug front and gas expansion within the slug body. They suggested that the mean slug length should be given by the following empirical equation:

$$\ln(L_S) = -26.6 + 28.495\left[\ln\left(\frac{D}{0.0254}\right)\right]^{0.1} \tag{6.50}$$

Gordon & Fairhust (1987) advocated the use of Norris (1982) expression after analysing field data from 0.3 to 0.6 m diameter pipes.

The above logarithmic expressions over-predict the slug length for small diameter pipes as observed by Manolis (1995), and to the author's knowledge, there is no simple empirical expression for mean slug length over a wide range of pipe diameters in the literature. However, slug flow is chaotic in nature, and the slug length should be characterized statistically. To this end, some researchers have attempted to evaluate the mean slug length using probability density functions. King (1998) reviewed these statistical correlations in his thesis.

6.5 Slug Modelling Approaches

As mentioned previously, the most distinctive feature of slug flow is its intermittent nature. Therefore, any attempt to model the flow by a standard time averaging procedure would be extremely restrictive. Instead, a much more detailed analysis is required which take account of the inherent intermittency and distinguishes between the liquid slug region, possibly containing dispersed gas bubbles, and the large gas bubble region that follows.

This means that the phenomenological model of slug flow must, in effect, use characteristics from both the dispersed and the stratified flow models while still accounting for the exchange of fluid between each region. We briefly present in what follows, the three different approaches that were found in the literature and which attempt to describe the main aspects of this extremely complex flow.

6.5.1 "Steady" state models

The easiest and therefore the most popular, approach is to reduce the intermittency to periodicity and to assume fully-developed flow so that the complex structure can be

simplified to an "equivalent cell unit" consisting of a liquid slug and a long bubble. The balance equations can be written in a frame of reference with the unit cell so that the flow appears steady with mass and momentum conserved across the boundary between the liquid slug and the long gas bubble region.

Following the approach of [Taitel & Barnea, 1990a, 1990b], the "equivalent slug unit" is shown below in Figure 6-3.

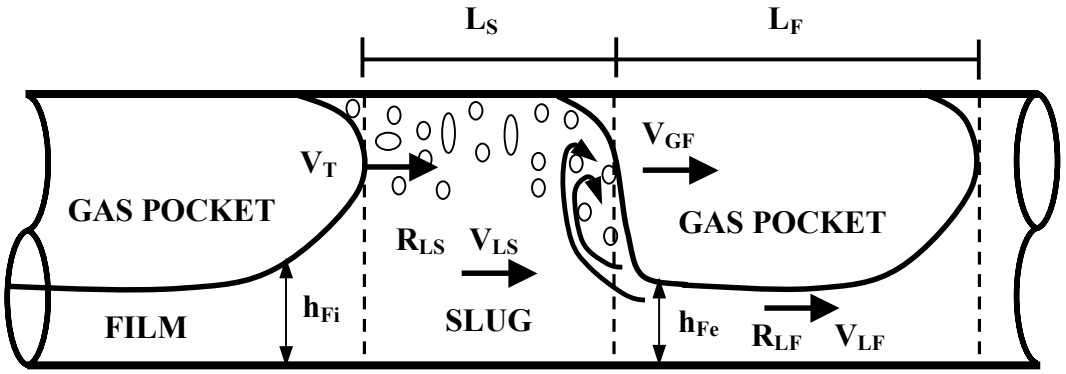

Figure 6-3: The "equivalent slug unit"

The unit consists of a slug region of length L_S and a film region of length L_F. The liquid slug region may be aerated with dispersed gas bubbles but it is still sufficient to bridge the pipe so that it cannot be penetrated by gas. The liquid holdup of this region is denoted R_{LS}. The average liquid velocity in the liquid slug is V_{LS}; it is also the average axial velocity of the dispersed bubbles in this region. These two velocities are not necessarily the same, but are generally considered to be equal in the case of horizontal flow.

The film region contains a liquid film and an elongated or Taylor gas bubble. For the case of horizontal and inclined pipes, the bubble is in the upper part of the pipe. It moves downstream at a translational velocity V_T. The liquid velocity in the film region is V_{LF}, and the gas velocity is V_{GF}. However, the gas and liquid velocities in the film are not axially homogeneous; instead they vary along the pipe due to the changing film thickness, h_F.

In a Lagrangian framework, by moving the system at the translational velocity of the elongated bubble V_T, the slug unit appears to be stationary. This enables the "steady state" mass and momentum balances to be obtained. Combined with several empirical relationships, the momentum balances obtained enable the hydrodynamics of the liquid film in the elongated bubble region to be modelled and lead to the prediction of the liquid holdup profile and an average pressure drop over the full slug unit.

Since the first horizontal "slug unit" model proposed by Dukler & Hubbard (1975), a lot of conceptual variations of the slug unit approach have been suggested, and can be found in a

review by Hale (1994). Here we only mention the "equivalent slug unit" proposed by Taitel & Barnea (1990b) as it was used to calculate the initial holdup profile for the slug flow simulations used in this study.

6.5.1.1 The Taitel & Barnea model (1990b)

Taitel & Barnea (1990b) have presented the most comprehensive study of the "steady state equivalent slug unit". In their analysis three distinct cases were presented, providing increasingly more complex descriptions of the film region. In the simplest case, which we implemented, a constant film thickness is assumed and therefore, the film momentum balance is given by the following simplified equation:

$$\frac{\tau_F S_F}{A_F} - \frac{\tau_G S_G}{A_G} - \tau_i S_i \left(\frac{1}{A_F} + \frac{1}{A_G} \right) + (\rho_L - \rho_G) g \sin\beta = 0 \qquad (6.51)$$

where τ_F and τ_G are the liquid and the gas wall shear stress in the film or elongated bubble region; they are defined in the previous chapter by equation (5.51). The terms S_F, S_G, and S_i are the liquid, the gas and the interfacial wetted perimeters in the film region, and are defined below. A_F and A_G are the liquid and gas cross-sections, ρ_L and ρ_G are the liquid and gas density and β is the pipe inclination.

Thus, for a given pipe geometry of known diameter and inclination, known gas and liquid physical properties, and specified gas and liquid flowrates, the following procedure is employed to calculate the liquid film profile:

1. V_{LS} is calculated assuming that it is equal to the mixture velocity, $V_{LS} = V_M = J_G + J_L$ where J_G and J_L are respectively the input gas and liquid superficial velocities.

2. The auxiliary variables V_T and R_{LS} are calculated respectively by the empirical relations of Bendiksen (1984) and Gregory et al. (1978). Those two expressions are presented in Section 6.4 and repeated here as follows:

$$V_T = 1.2 V_M + 0.54\sqrt{gD} \qquad (6.52)$$

$$R_{LS} = \frac{1}{1 + \left(\frac{V_M}{8.66} \right)^{1.39}} \qquad (6.53)$$

where D is the pipe diameter, and V_M the mixture velocity calculated during the first step of this procedure.

3. An estimate of the film height, h_F is specified. A_F, A_G, S_F, S_G, S_i and R_{LF} are then obtained using the following relations for stratified flow:

$$A_F = AR_{LF} \tag{6.54}$$

$$A_G = A(1 - R_{LF}) \tag{6.55}$$

$$S_F = D\left[\pi - \cos^{-1}\left(2\frac{h_F}{D} - 1\right)\right] \tag{6.56}$$

$$S_G = \pi D - S_F \tag{6.57}$$

$$S_i = D\sqrt{1 - \left(2\frac{h_F}{D} - 1\right)^2} \tag{6.58}$$

$$R_{LF} = \left(\frac{1}{\pi}\right)\left\{\pi - \cos^{-1}\left[2\frac{h_F}{D} - 1\right] + \left[2\frac{h_F}{D} - 1\right]\sqrt{\left(1 - \left[2\frac{h_F}{D} - 1\right]^2\right)}\right\} \tag{6.59}$$

4. V_{LF} and V_{GF} are calculated using the following mass balance equations over the film zone:

$$(V_T - V_{LF})R_{LF} = (V_T - V_{LS})R_{LS} \tag{6.60}$$

$$V_M = V_{LF}R_{LF} + V_{GF}(1 - R_{LF}) \tag{6.61}$$

5. The friction factors f_F, f_G and f_i are evaluated using Equations (5.71) and (5.65). The shear stresses τ_F, τ_G and τ_i are calculated using Equations (5.51) and (5.52), but with V_{GF} and V_{LF}, determined in the previous step, as the gas and liquid velocities.

6. All required variables can now be estimated and so the estimate of h_F can be checked and a new estimate is obtained. Steps (3) - (5) are repeated until convergence of equation (6.51) is satisfied.

A simple **Fortran 90** programme has been written to evaluate the steady state liquid film holdup, using the procedure described above. This simplified model also enables the calculation of the pressure drop over the full slug unit, assuming an empirical correlation for the slug length L_S, but because this value is not required in this study, its expression was not presented.

Steady models as described above give an estimate of averaged flow values, and those values can be used as initial conditions for two-fluid transient models. However, knowledge of those averaged values alone may be inadequate due to the lack of information about the longitudinal distribution of the flow, which is sometimes essential. Slug catchers, which should remove slugs from pipelines, are for example designed on the basis of the maximum slug length value and not the average value. So we did not pursue this approach further.

6.5.2 Slug-tracking models

Slug-tracking techniques provide an alternative way of modelling slug flow. They are distinguished from "unit cell" models (discussed in the previous section) in that they consider each slug individually, and model the propagation of a number of discrete slugs along a pipeline. This technique has a significant advantage over the unit cell approach as the slug length distribution arising from a particular pipeline configuration may be obtained without recourse to statistical correlations. Slug tracking schemes have received considerable interest in recent years. However, they are computationally intensive since a pipeline may contain hundreds of slugs, each of which requires a unique solution to the modelling equations at each time step during a transient simulation. As a result, highly simplified physical models have been implemented in the published slug tracking schemes. A review of those schemes can be found in the recent work by Manfield (2000) and it is not repeated here.

Although some underlying assumptions made in the simplified slug-tracking models are questionable, the advantages of these schemes are that if they are implemented properly, they can result in a great increase in computing efficiency compared to two-fluid models, and more importantly, complex three-dimensional effects (such as the effect of velocity distribution within the slug and the effect of slug length on slug tail velocity) can be easily included the scheme, allowing correct description of the local and global flow. It is worth noting that in the next phase of the TMF programme [Hewitt, 2002], the accuracy, robustness, and efficiency of these schemes will be thoroughly investigated.

Slug-tracking models may generate statistical data about slug flow at a particular set of conditions, giving for example the mean and maximum values of key variables, such as the slug length or frequency, which are likely to be encountered in a real production line, but their implementation appears very tedious and follows a Lagrangian approach, therefore these schemes will not be pursued in our Eulerian framework.

6.5.3 Slug capturing using the two-fluid model

Commercial pipeline transient codes OLGA, PLAC, and to some extent TACITE are all based on two-fluid models, and this approach appears to be the natural way of modelling slug flow, because mechanisms such as interfacial wave formation are naturally embodied

in the model. In addition, it does not rely on empirical closure laws to describe the flow, apart from the appropriate wall and interfacial friction factors, but this is also true for the steady state and the slug-tracking approaches.

However, despite seeming attractive, very few studies have been done using this approach. To our knowledge, only recent works by Issa & Woodburn (1998) and Bonizzi et al. (2001) have shown that the two-fluid model is capable of capturing many of the principal features of slug flows, including interfacial wave formation, development and propagation.

One possible reason for this lack of two-fluid slug flow studies comes from the fact that some researchers [Hewitt, 2002; Manfield, 2000] believe that the phenomena involved in slug flow are inherently multi-dimensional and can not be represented in detail in a one-dimensional two-fluid framework without recourse to additional closure relationships. We do not entirely share this belief, and complex mechanisms such as gas entrainment, which are not naturally included in a classic two-fluid model, have been recently modelled by an additional transport equation for the dispersed gas bubbles [Bonizzi et al., 2001].

The more logical explanation comes from the fact that to achieve their results, Issa & Woodburn (1998) and Bonizzi et al. (2001) have used very small mesh sizes, which are several orders of magnitude below those commonly used in the commercial simulators. Issa & Woodburn (1998) showed that the computation becomes relatively insensitive to the node size when this falls below about 225 mm (roughly a third of their pipe diameter). This large number of nodes required seems impracticable in the context of an industrial scale pipeline, however the continuing increase in computing power may eventually overcome this aspect. Furthermore, although not investigated in this chapter, we will expect the adaptive gridding techniques developed in Chapter 4, to considerably reduce the number of coarse nodes, and improve the efficiency of the numerical solution.

Issa & Woodburn (1998) and Bonizzi et al. (2001) use a two-fluid model with a compressible gas phase, and Taitel & Barnea (1998) have recently studied the effect of gas compressibility on a slug-tracking model, and their results showed that the inclusion of the gas compressibility caused an increase in the slug unit length, but had a minor effect on the growth of the slug body as the slug moved downstream, so we expect our incompressible two-fluid model to represent most of the mechanisms of slug flow described in Section 6.3.

6.6 Validation of the Two-Fluid Model

In this section we study the validity of the incompressible two-fluid model (PFM-2), presented in Chapter 2, for a slug flow test called Case 24. The Blasius correlation (5.71) is used for the gas and liquid wall friction factors, and the stratified-smooth relation of Taitel & Dukler (1976) for the interfacial friction factor, hence the notation BBT in Figure 6.4, for which B and T stand for Blasius and Taitel respectively.

6.6.1 Case 24

This benchmark case was first proposed by Hale & Hewitt (1999) as part of the TMF programme, and from the neutral stability curve plotted in Figure 6-4, it can be seen that Case 24 is within the slug flow region, more precisely it is on the inviscid Kelvin-Helmholtz line for transition from stratified to slug flow, which is also the limit of well-posedness of our two-fluid model [Louaked et al., 2003].

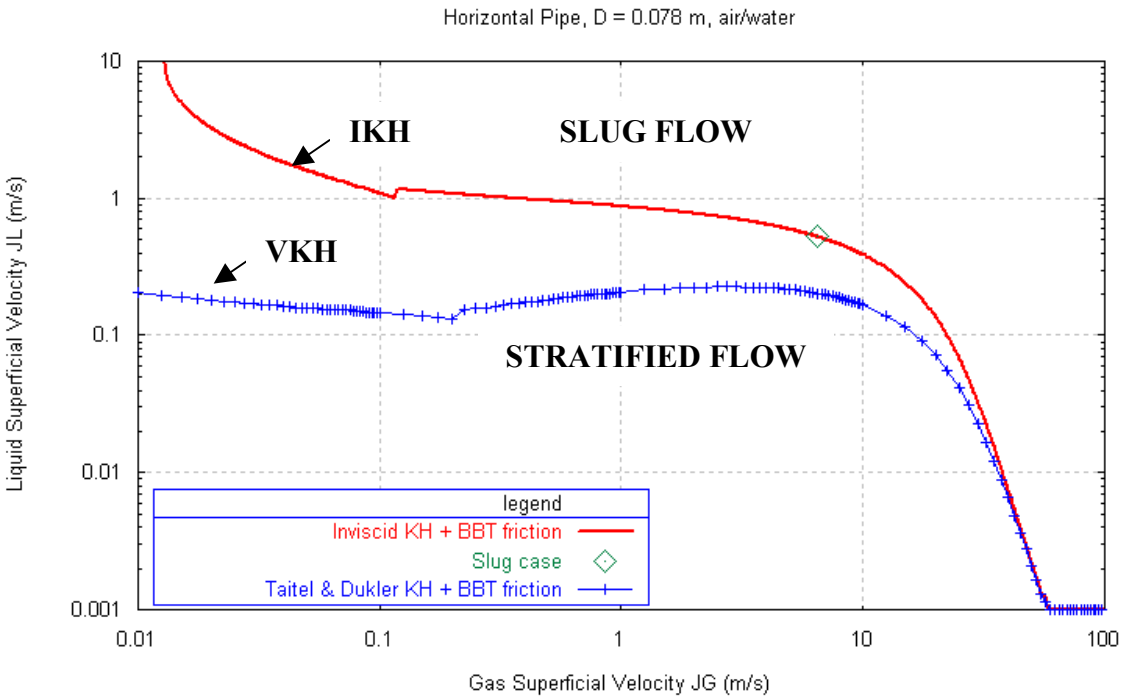

Figure 6-4: Viscous & Inviscid Kelvin Helmholtz transitions from stratified to slug flow.

Experimental measurements using the gas and liquid flow conditions for this particular case have recently been collected as part of the TMF programme [Hewitt, 2002], and they will provide useful data for future comparison.

6.6.2 Simulation parameters

The fluids used for the simulation are air and water at atmospheric conditions. As can be seen from Figure 6-4, the gas superficial velocity is 6.532 m/s, while the liquid superficial velocity is 0.532 m/s. A horizontal pipe of 100m in length and with diameter of 0.078 m is

used. The Rusanov scheme (3.11) is used with a CFL value of 0.1 for all the computations presented here while the mesh size value is generally taken as 0.1 m.

- **Initial condition**

A step initial liquid holdup was used as initial condition (Figure 6-5). The initial upstream film profile is the stratified equilibrium liquid level, which is calculated from the steady state momentum balance equation (6.51), with the gas and liquid velocities obtained from the input superficial velocities.

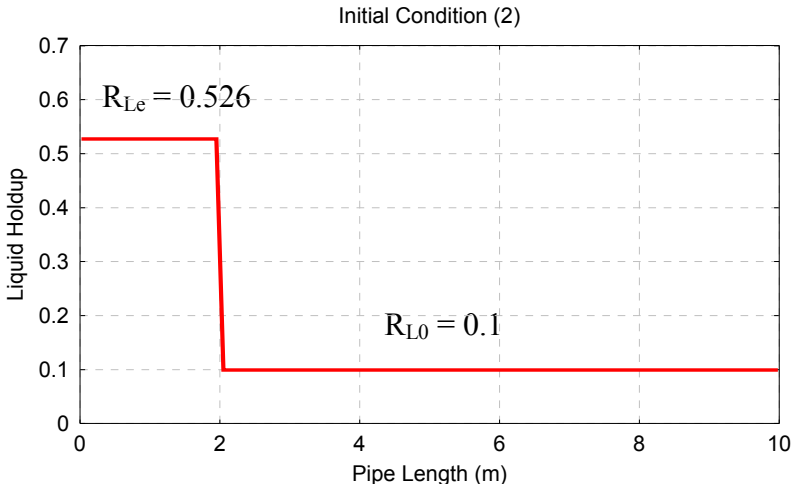

Figure 6-5: Initial Condition

The initial downstream film profile is obtained by using the Taitel & Barnea (1990b) steady state procedure described in Section 6.5.1.1.

- **Boundary condition**

The inlet holdup is fixed to the stratified equilibrium value (initial upstream value), and an open outlet boundary approximation is used.

6.6.3 Simulation results

The results are presented here according to the slug flow mechanisms described in Section 6.3.

6.6.3.1 Slug wave initiation

As can be seen from Figure 6-6, unstable interfacial waves are formed from the first iteration and propagate downstream while growing.

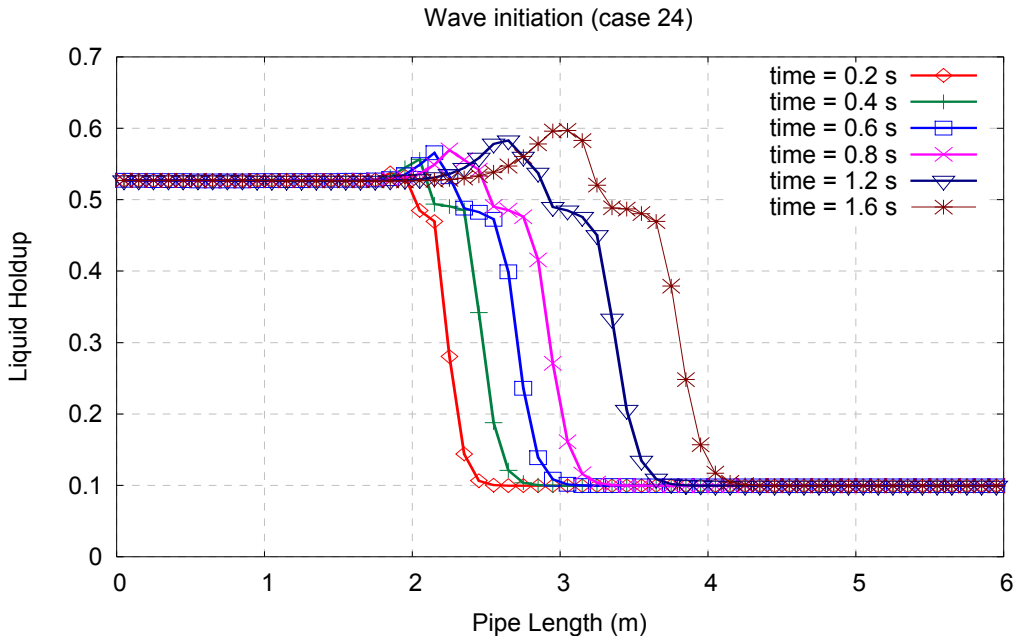

Figure 6-6: Interface wave formation

6.6.3.2 Wave growth & Pipe bridging event

Figure 6-7 presents snapshots of the simulation at different times, showing how the initially formed interfacial wave grows to bridge the pipe and form the slug precursor. A cut-off value of 0.99 is directly imposed in the code if the liquid holdup is greater than or equal to this value.

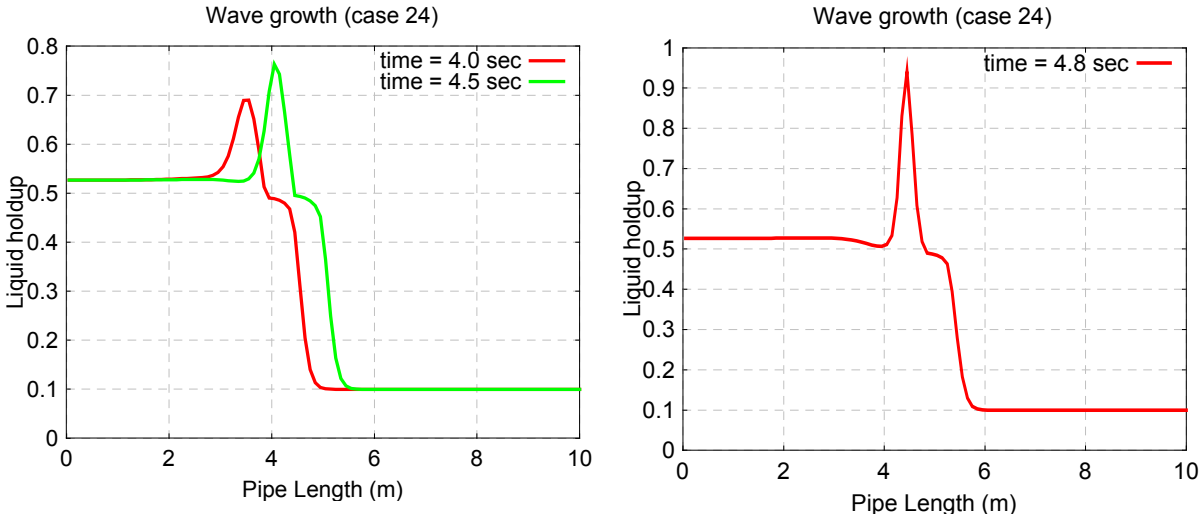

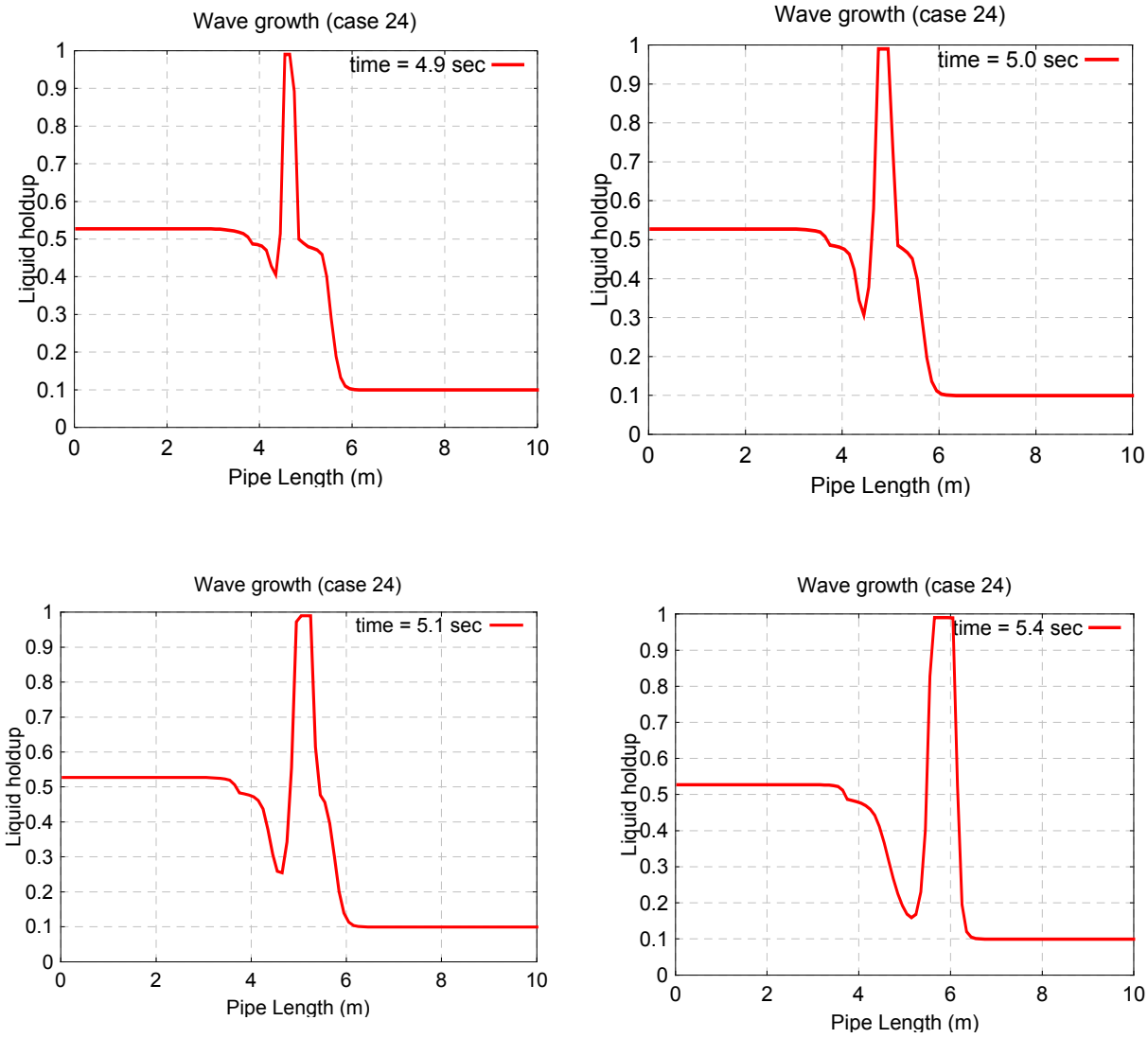

Figure 6-7: Snapshots of wave growth and pipe bridging event.

6.6.3.3 Stratified layer formation, Slug Growth & Propagation

Figure 6-8 clearly shows a liquid slug zone followed by a stratified film layer. It also shows the mechanisms of "stable slug" propagation, as well as the initiation of new slugs on the sloping interface formed after the departure of the previous slug precursor. The values of T_{bk} and X_{bk} in the graphs indicate the time and location at which the wave index-linked "k" bridges the pipe

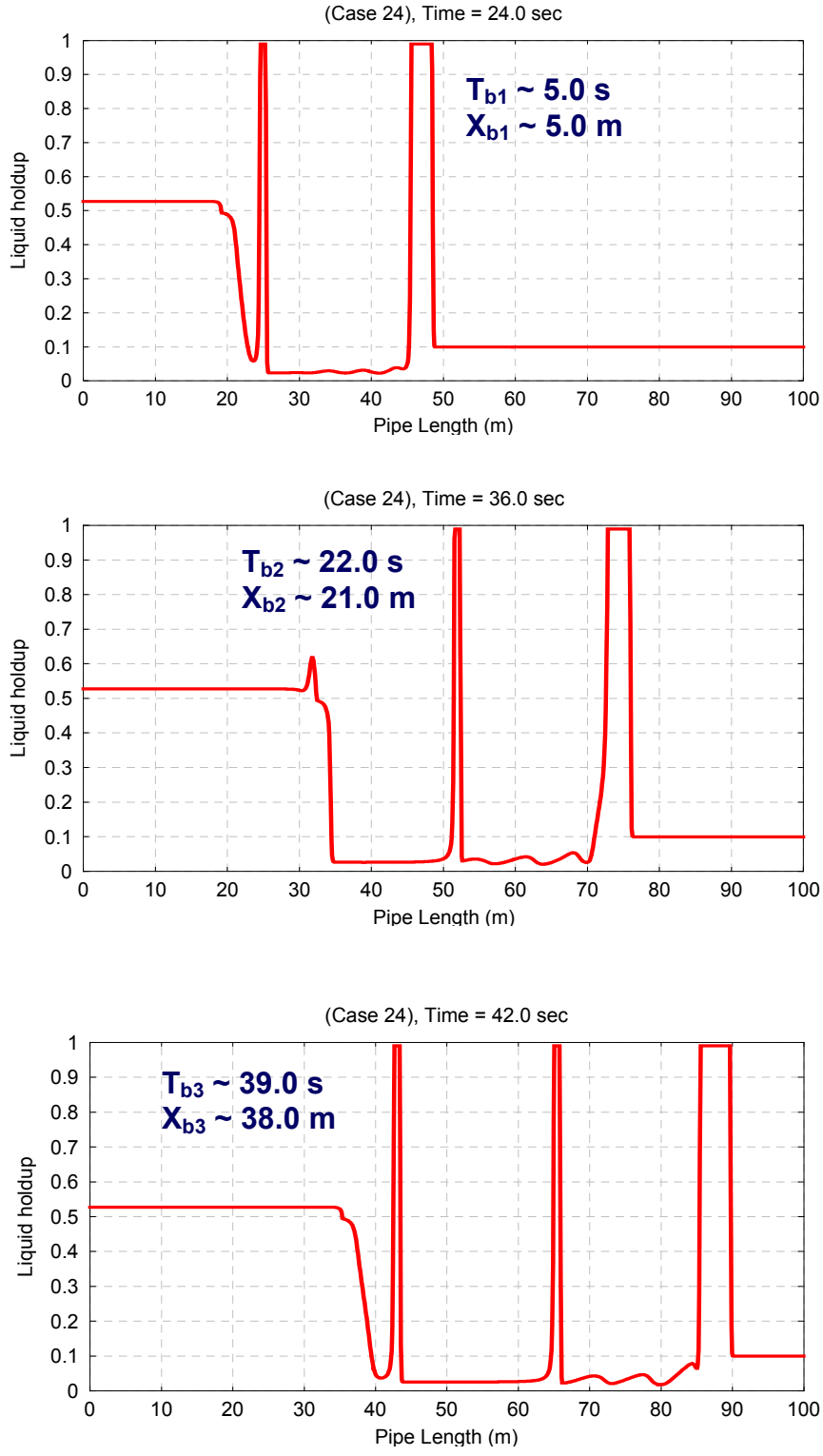

Figure 6-8: Stratified layer formation, Slug Growth & Propagation

6.6.4 Effect of Initial Film Level

The effect of the initial downstream liquid level has been evaluated in this section. Figure 6-9 shows the result of the simulation after 24 seconds for the first slug body length L_{S1}, which is twice the value obtained by the steady state procedure described in Section 6.5.1.1. Although the elongated bubble length remains comparable to the initial value, we can see from the Figure 6-10 that the slug precursor length has doubled and that the stratified film layer appears wavier compared to the original shape.

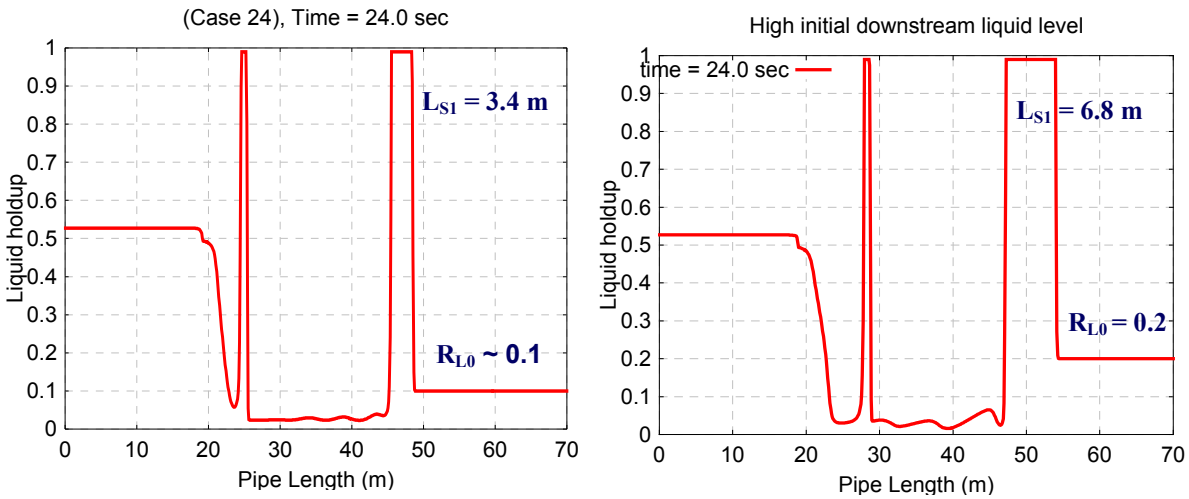

Figure 6-9: Effect of a higher initial downstream liquid level

We have found that there is a critical initial downstream level (film holdup) for which interface waves will grow to form a slug, illustrating the importance of the initial conditions (Figure 6-10). An investigation of this critical liquid level is still under way.

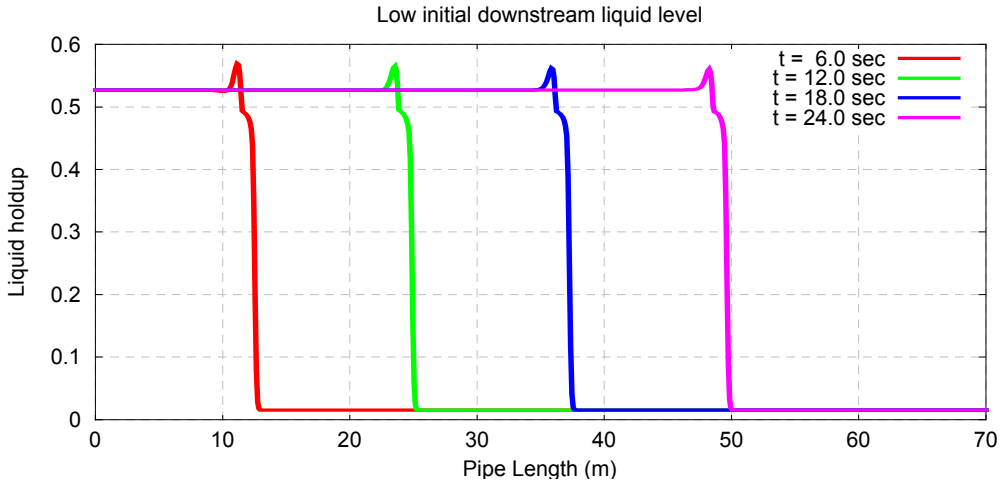

Figure 6-10: Effect of a lower initial downstream liquid level

6.6.5 Mesh Refinement

Because Case 24 is at the IKH transition from stratified to slug, which is also the limit of validity of the incompressible two-fluid model used, it was crucial to study the effect of the mesh size on the numerical results. From Figure 6-11, one can clearly see the major difference between two mesh sizes (one diameter or eight diameters) appears in the slug frequency, illustrated in the figure by the elongated bubble length L_B, which is 10 times larger when using the coarse mesh.

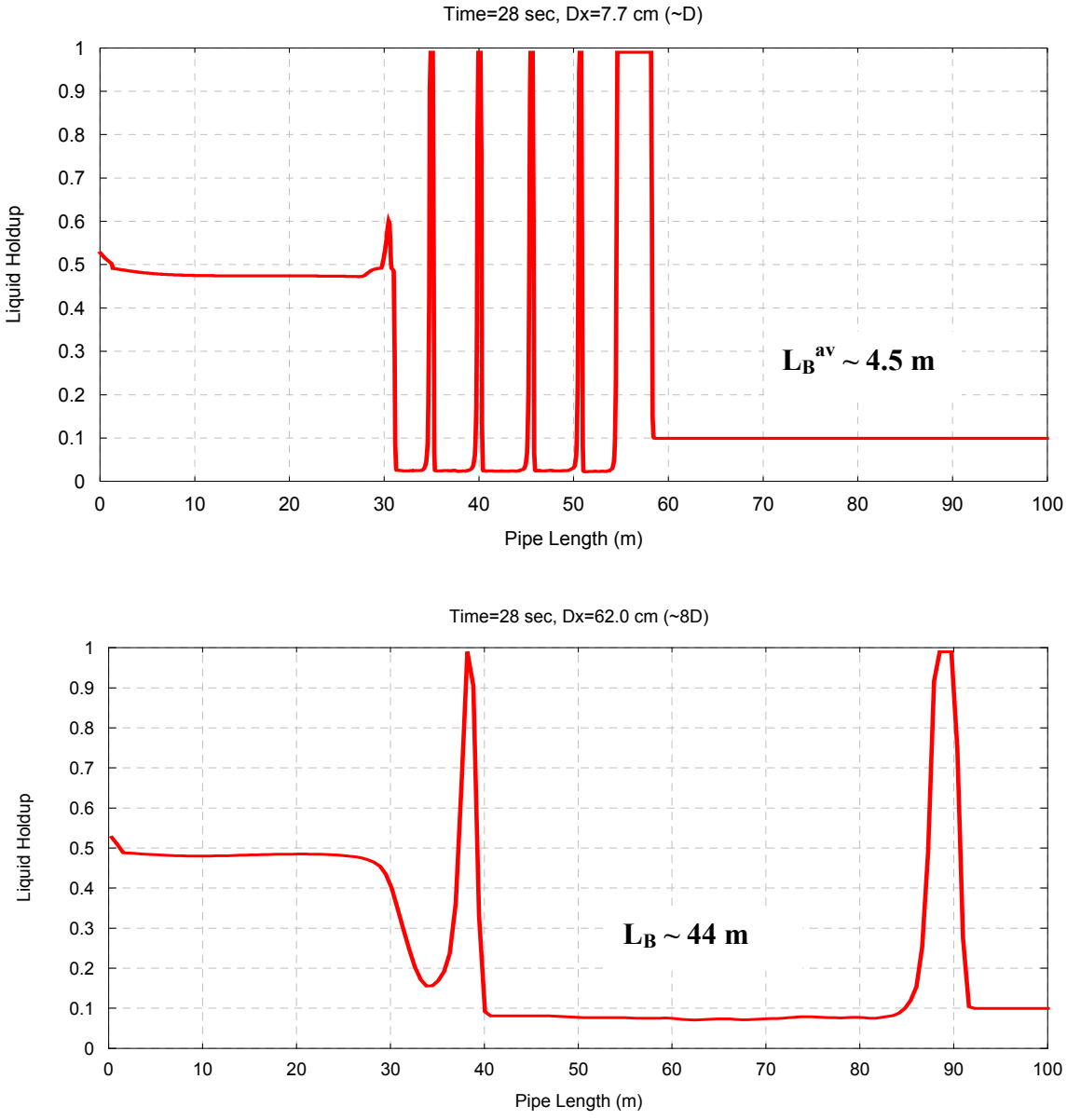

Figure 6-11: Effect of the mesh size

Figure 6-12 and Table 6-5 confirm these results by showing a strong dependency of the slug frequency on the mesh size for different liquid friction factors.

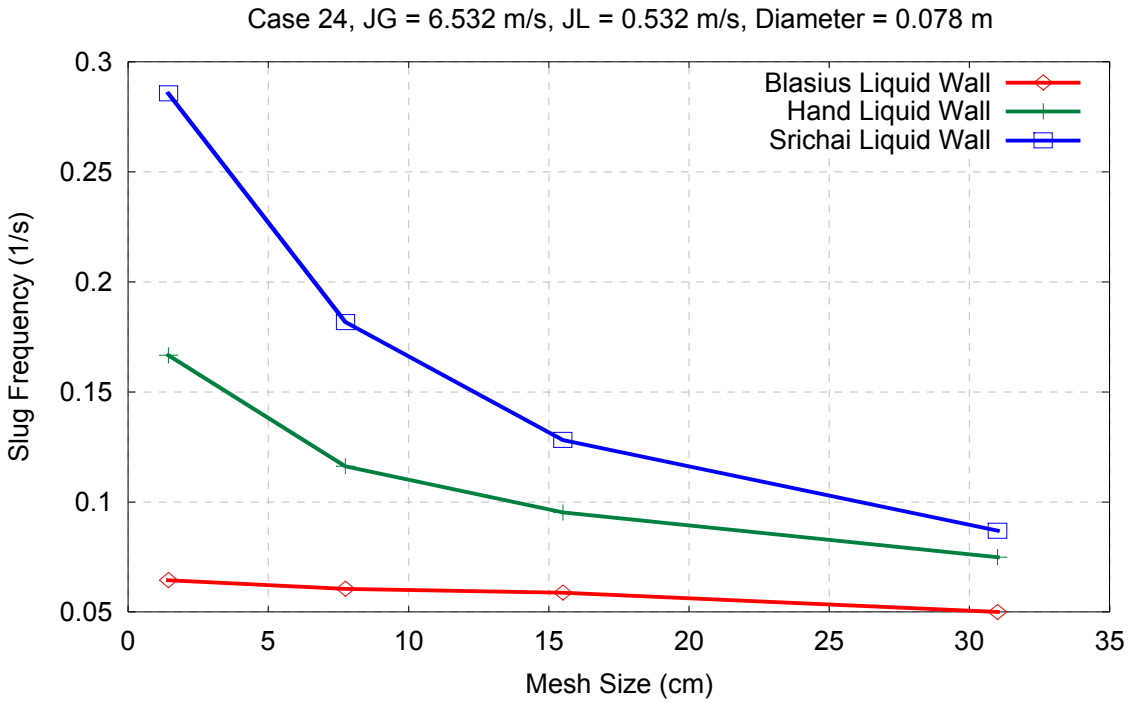

Figure 6-12: Variation of Slug Frequency with Mesh Size

	Blasius	Hand (1991)	Srichai (1994)
Slug Frequency (1/s)	0.06	0.12	0.18
Average bubble length (m)	17.1	9.9	4.5
Average slug length (m)	1.3	1	0.5

Table 6-5: Slug characteristics for mesh size Δx = Diameter

6.7 Conclusion

Numerical results reported in this chapter showed that the incompressible two-fluid model is unable to simulate most of the features of this complex flow regime for the test case selected. Mechanisms such as the interfacial wave formation, the pipe bridging event, the slug growth and propagation can be qualitatively observed, but flow characteristics such the slug length, frequency and velocity are not accurately determined.

Phenomena such as the entrainment of dispersed gas bubbles in the liquid slug are not predicted, which is expected as no mechanism was introduced in the basic equations to account for these turbulent effects. In addition, a team of researchers [Bonizzi et al., 2002] in the Imperial College London is currently investigating this important three-dimensional effect in slug flow, while another team in the same university [Hale & Hewitt, 1999] is studying in detail the slug initiation process, another mechanism that is not properly predicted by the existing one-dimensional two-fluid models.

The slug flow study has clearly shown that the numerical results are not reliable for cases on and probably above the Inviscid Kelvin Helmholtz (IKH) transition from stratified to slug flow, because they become very sensitive to the mesh size, which is characteristic of ill-posed initial-value problems. It worth nothing that the incompressible two-fluid model is no longer hyperbolic for this type of problems, and although the model was not investigated for cases below the IKH transition criteria, it is the understanding of the author that if the slug flow regime is observed, the numerical results will be more stable and reliable below a critical mesh size [Bonizzi et al., 2002]. In this case, the incompressible model will be very attractive compared to the compressible model (SPM-4), because the numerical time step is not limited by the acoustic wave speed, providing a solution generally hundred times faster than the compressible model.

It should be mentioned that all the simulations presented in this chapter were done using fixed boundary conditions, however, some recent work by Bonizzi et al. (2002) suggested that taking into account the time varying aspect of the inlet and outlet boundaries, may stabilize the flow for cases above the IKH criteria, and make the numerical solution insensitive for small mesh sizes. This last point requires further investigation, as it appears a bit controversial, because it seems to contradict the expected behaviour of ill-posed initial-value problems.

6.8 References - 6

- **Abdul-Majeed G. H., (2000)** "Liquid slug holdup in horizontal and slightly inclined two-phase slug flow". *Journal of Petroleum Science and Engineering*, **27**, 27-32.

- **AEA Technology (1996).** "PLAC User Guide and Technical Manual". PC version 5.3, (January 1996).

- **Andreussi P., Paglianti A., Vatistas N., Minervini A., and Bendiksen K., (1988)** "Analysis of slug flow in near horizontal and horizontal pipes". *European Two-Phase Flow Group Meeting*, Brussels, Belgium, 30 May to 1 June 1988, **Paper B2**.

- **Andreussi P., & Bendiksen K., (1989)** "An investigation of void fraction in liquid slugs for horizontal and inclined gas-liquid pipe flow". *Int. J. Multiphase Flow*, **15 (6)**, 937-946.

- **Andreussi P., Bendiksen K. H., and Nydal O. J., (1993)** "Void Distribution in Slug Flow". *Int. J. Multiphase Flow,* **19 (5)**, 817-828.

- **Andritsos N., & Hanratty T. J., (1987)** "Influence of interfacial waves in stratified gas-liquid flows". *AIChE Journal*, **33 (3)**, 444-454.

- **Barnea D., & Brauner N., (1985)** "Holdup of the liquid slug in two-phase intermittent flow". *Int. J. Multiphase Flow*, **11 (1)**, 43-49.

- **Bendiksen K. H., (1984)** "An experimental investigation of the motion of long bubbles in inclined tubes". *Int. J. Multiphase Flow*, **10**, 467-483.

- **Bendiksen K., Brandt I., Fuchs P., Linga H., Malnes D., and Moe R., (1986)** "Two-Phase Flow Research at SINTEF and IFE: Some Experimental Results and a Demonstration of the Dynamic Two-Phase Flow Simulator", presented at the 1986 Offshore Northern Seas Conference, Stavanger, (1986).

- **Bendiksen K., Malnes D., Moe R., & Nuland S., (1991)** "The Dynamic Two-Fluid Model OLGA: Theory and Application". *SPE Production Engineering*, **6**, 171-180.

- **Bendiksen K. H., Malnes D., & Nydal O.J., (1996)** "On the Modelling of Slug Flow". *Chem. Eng. Comm.,* **Vol. 141-142**, 71-102.

- **Benjamin, (1968)** "Gravity currents and related phenomena". *J. Fluid Mech.*, **31 (2)**, 209-248.

- **Bertola V., (2002)** "Slug velocity profiles in horizontal gas-liquid flow". *Experiments in Fluids*, **32**, 722-727.

- **Black P. S., Daniels L. C., Hoyle N. C., and Jepson W. P., (1990)** "Studying Transient Multiphase Flow using The Pipeline Analysis Code (PLAC)". *Journal of Energy Resources Technology*, **112**, 25-29, (March 1990).

- **Bonizzi M., Issa R. I., and Kempf M. H. W., (2001)** "Modelling of gas entrainment in horizontal slug flow". *Proceedings of the ICMF 2001 Conference*, **Paper 402**, May 27 – June 1, New Orleans, USA.

- **Brill J. P., Schmidt Z., Coberly W. A., Herring J. D., and Moore D. W., (1981)** "Analysis of Two-Phase Tests in Large-Diameter Flow Lines in Prudhoe Bay Field". *SPE Journal**, June 1981,*** 363-378.

- **Davis R. M., & Taylor G. I., (1950)** "The mechanics of large bubbles rising through extended liquids and through liquids in tubes". *Proc Roy. Soc.*, **200A**, 375-390.

- **Dukler A. E., & Hubbard M. G., (1975)** "A model for gas-liquid slug flow in horizontal and near horizontal tubes". *Ind. Eng. Chem. Fundam.*, **14 (4)**, 337-347.

- **Dukler A. E., Moalem Maron D., and Brauner N., (1985)** "A physical model for predicting the minimum stable slug length". *Chem. Eng. Sci.*, **40**, 1379-1385.

- **Dukler A. E., & Fabre J., (1994)** "Gas-Liquid Slug Flow Knots and Loose Ends". *Multiphase Science & technology*, ed. Hewitt et al., Begell House, **Chap. 7**, 355-469.

- **Fabre J., & Liné A., (1992)** "Modelling of two-phase slug flow". *Annual Rev. Fluid Mech.*, **24**, 21-46.

- **Ferré D., (1979)** "Ecoulements diphasiques a poches en conduite horizontale". *Rev. Inst. Fr. Pet.*, **34**, 113-142.

- **Ferschneider G, (1983)** "Ecoulement diphasiques gas-liquide a poches et a bouchons en conduits". *Revue Inst. Fr. Petrole,* **38**, 153.

- **Gomez L. E., Shoham O. & Taitel Y., (2000)** "Prediction of slug liquid holdup: horizontal to upward vertical flow". *Int. J. Multiphase Flow*, **26**, 517-521.

- **Gordon I. C., & Fairhurst C. P., (1987)** "Multi-phase pipeline and equipment design for marginal and deep water field development". *Paper A1, 3rd International Multiphase Flow Conference*, The Hague, May 18-20, 1-12.

- **Gregory G. A., & Scott D. S., (1969)** "Correlation of liquid slug velocity and frequency in horizontal co-current gas-liquid slug flow". *AIChE Journal*, **15 (6)**, 933-935.

- **Gregory G. A., Nicholson M. K., and Aziz K., (1978)** "Correlation of the liquid volume fraction in the slug for horizontal gas-liquid slug flow". *Int. J. Multiphase Flow*, **4**, 33-39.

- **Greskovish E. J., & Shrier A. L., (1971)** "Pressure drop and holdup in horizontal slug flow". *AIChE Journal*, **17 (5)**, 1214-1219.

- **Griffith P., & Wallis G. B., (1961)** "Two-Phase Slug Flow". *Journal of Heat Transfer*, Trans. ASME, Series C, **83**, 307-320.

- **Hale C. P., (1994)** "Modelling the slug flow regime". *Technical Report*, MPS/62, WASP/16, Department of Chemical Engineering, Imperial College of Science, Technology & Medicine, London, UK.

- **Hale C. P., (2000)** "Slug formation, growth and decay in gas-liquid flows". *PhD thesis*, Department of Chemical Engineering, Imperial College of Science, Technology & Medicine, London, UK.

- **Hand N. P., (1991)** "Gas-Liquid Co-Current Flow in a Horizontal Pipe". *PhD thesis*, Faculty of Engineering, The Queen's University of Belfast.

- **Hewitt G. F., (2002)** "Joint Project on Transient Multiphase Flows (TMF3)". *http://www.cranfield.ac.uk/sme/amac/tmf/tmf3_prospectus_final_version_may_2nd_2002.pdf (visited on the 02/12/2003)*

- **Heywood N. I., & Richardson J. F., (1979)** "Slug flow of air-water mixtures in a horizontal pipe: determination of liquid holdup by γ-ray absorption". *Chem. Eng. Sci.*, **34**, 17-30.

- **Hill T. J., & Wood D. G., (1990)** "A new approach to the prediction of slug frequency". *65th Annual Technical Conference and Exhibition of the Society of Petroleum Engineers*, September 23-26, New Orleans, USA, **SPE 20629**, 141-149.

- **Hughmark G. A., (1965)** "Holdup and heat transfer in horizontal slug gas-liquid flow". *Chemical Engineering Science*, **20**, 1007-1010.

- **Issa R. I. & Woodburn P. J., (1998),** "Numerical prediction of instabilities and slug formation in horizontal two-phase flows". *Proc. 3rd Int. Conf. Multiphase Flow*, Lyon, France, June 8-12.

- **King M. J. S., (1998)** "Experimental and modelling studies of transient slug flow". *PhD Thesis,* Department of Chemical Engineering and Chemical Technology*,* Imperial College of Science, Technology & Medicine, London, England.

- **Kowalski J. E., (1987)** "Wall and Interfacial Shear Stress in Stratified Flow in a Horizontal Pipe", *AIChE Journal*, **33** (2), 274-281.

- **Louaked M., Hanich L., and Thompson C., (2003)** "The Well-Posedness of Incompressible One-Dimensional Two- and Three-Phase Flow Models". *IMA Journal of Applied Mathematics*, **68/6**, 595-620.

- **Malnes D., (1982)** "Slug flow in vertical, horizontal and inclined pipes". Report IFE/KR/E-83/002*, V. Inst. for Energy technology,* Kjeller, Norway.

- **Mandhane J. M., Gregory G. A. & Aziz K., (1974),** "A flow pattern map for gas-liquid flow in horizontal pipes". *Int. J. Multiphase Flow*, **1**, 537-553.

- **Manfield P. D., (2000),** "Experimental, computational and analytical studies of slug flow", PhD thesis, Department of Chemical Engineering and Chemical Technology, Imperial College of Science, Technology & Medicine, UK.

- **Manolis I. G., (1995)** "High Pressure Gas-Liquid Slug Flow". *PhD thesis*, Department of Chemical Engineering and Chemical Technology, Imperial College of Science, Technology & Medicine, UK.

- **Marcano R., Chen T. X., Sarica C., and Brill J. P., (1998)** "A Study of Slug Characteristics for Two-Phase Horizontal Flow". **SPE 39856,** 213-219.

- **Mishima K., & Ishii M., (1980)** "Theoretical prediction of onset of horizontal slug flow". *Journal of Fluids Engineering***, 102,** 441-444.

- **Nadler N., & Mewes D. (1995)** "Effects of liquid viscosity on the phase distributions in horizontal gas-liquid slug flow". *Int. J. Multiphase Flow***, 21 (2),** 253-266.

- **Nicholson M. K., Aziz K., and Gregory G. A., (1978)** "Intermittent two-phase flow in horizontal pipes: Predictive models". *Can. J. Chem. Eng.*, **56**, 653-663.

- **Nicklin D. J., Wilkes J. O., and Davidson J. F., (1962)** "Two-phase flow in vertical tubes". *Trans. Inst. Chem. Eng.*, **40**, 61-68.

- **Nydal O. J., Pintus S., and Andreussi P., (1992)** "Statistical characterization of slug flow in horizontal pipes". *Int. J. Multiphase Flow*, **18 (3)**, 439-453.

- **Paglianti A., Trotta G., Andreussi P., and Nydal O. J., (1996)** "The effect of fluid properties and geometry on void distribution in slug flow". *6th International Conference on Multiphase Production*, June 16-18, Cannes, France, 193-203.

- **Paglianti A., Giona M., and Soldati A., (1996)** "Characterization of subregimes in two-phase slug flow". *Int. J. Multiphase Flow*, **22 (4)**, 783-796.

- **Petalas N., & Aziz K., (1998),** "A mechanistic model for multiphase flow in pipes". *49th Annual Technical Meeting of Petroleum Society of the Canadian Institute of Mining, Metallurgy & Petroleum*. **Paper 98-39**, Calgary, Alberta June 8-10, Canada.

- **Scott S. L., Shoham O., & Brill J. P., (1986)** "Prediction of slug length in horizontal large diameter pipes". Paper presented at the *SPE 56th Annual California Regional Meeting*, Oakland, California, April 1986.

- **Scott S. L., Shoham O., and Brill J. P., (1987)** "Modelling slug growth in large diameter pipes". *3rd International Conference on Multiphase Flow*, The Hague 18-20 May, **Paper B2**, 55-63.

- **Shaha J., (1999)** "Phase Interactions in Transient Stratified Flow". *PhD thesis*, Department of Chemical Engineering, Imperial College of Science, Technology & Medicine, London, UK.

- **Spedding P. L., & Hand N. P., (1997)** "Prediction in Stratified Gas-Liquid Co-Current Flow in Horizontal Pipelines". *Int. J. Heat Mass Transfe*r, **40 (8)**, 1923-1935.

- **Srichai S., (1994)** "High Pressure Separated Two-Phase Flow". *PhD thesis*, Department of Chemical Engineering, Imperial College, London, UK.

- **Stapelberg H. H., & Mewes D., (1994)** "Te Pressure Loss and Slug Frequency of Liquid-Liquid-Gas Slug Flow in Horizontal Pipes". *Int. J. Multiphase Flow,* **20 (2)**, 285.

- **Taitel Y., & Barnea D., (1990a)** "A Consistent Approach for Calculating Pressure Drop in Inclined Slug Flow". *Chem. Engineering Science*, **45**, 2089-2097.

- **Taitel Y., & Barnea D., (1990b)** "Two-Phase Slug Flow". *Advances in Heat Transfer*, **20**, 83-132.

- **Taitel Y., & Barnea D., (1998)** "Effect of gas compressibility on a slug tracking model". *Chemical Engineering Science*, **53 (11)**, 2089-2097.

- **Taitel Y., & Duckler A. E., (1976)** "A Model For Predicting Flow Regime Transitions in Horizontal and Near-Horizontal Gas-Liquid Flow". *AIChE Journal*, **22 (1)**, 47-55.

- **Taitel Y., & Dukler A. E., (1977)** "A model for slug frequency during gas-liquid flow in horizontal and near horizontal pipes". *Int. J. Multiphase Flow,* **3 (6)**, 585-596.

- **Théron B., (1989)** "Ecoulements diphasiques instationnaires en conduite horizontale". *PhD thesis*, Institut National Polytechnique de Toulouse, France.

- **Tronconi E., (1990)** "Prediction of slug frequency in horizontal two-phase flow". *AIChE Journal*, **36 (5)**, 701-709.

- **Vermeulen L. R., & Ryan J. T., (1971)** "Two-phase slug flow in horizontal and inclined tubes". *Can. J. Chem. Eng.*, **49**, 195-201.

- **Wallis G. B., (1969)** "One dimensional two-phase flow". *New York, McGraw-Hill*.

- **Watson M., (1990)** "Non Linear Waves in Pipeline Two-Phase Flows", Proceedings of the 3rd International Conference on Hyperbolic Problems, Uppsala, Sweden, (June 1990), Studentliterratur, Lund.

- **Weber M. E., (1981)** "Drift in Intermittent Two-Phase Flow in Horizontal Pipes". *Can. J. Chem. Eng.,* **59**, 398-399.

- **Woods D. B., & Hanratty T. J., (1996)** "Relation of Slug stability to shedding rate". *Int. J. Multiphase Flow,* **22 (5)**, 809-828.

- **Zabaras G. J., (1999)** "Prediction of Slug Frequency for Gas-Liquid Flows". *SPE Annual Technical Conference & Exhibition, October 3-6, Houston, Texas, USA***, SPE 56462**, 181-188.

- **Zigrang D. J. & Sylvester N. D., (1985)** "A Review of Explicit Friction Factor Equations". *Journal of Energy Resources Technology*, **107**, 280-283.

- **Zukoski E. E., (1966)** "Influence of viscosity, surface tension, and inclination angle on motion of long bubbles in closed tubes". *J. Fluid Mech.*, **25 (4)**, 821-837.

7 Chapter 7 – Conclusions and Future Work

The oil and natural gas production industry has an ongoing need to improve the understanding of transient multiphase flows. Such flows occur widely in hydrocarbon recovery and the industry needs to operate flow systems with more than one material to achieve optimum economy whilst ensuring safety and protecting the environment. Therefore, a good knowledge of the time varying flow characteristics, such as the fluid phase content or velocity, is very important to properly design flow lines, fluid treating and other separation facilities. In the first chapter, the specific goals of the present work were stated, and the progress made against these objectives as well as suggestions for future research are summarised in this chapter

7.1 Conclusions

After reviewing the modelling approaches existing in the literature in the second chapter, we presented and studied in detail the mathematical properties of three specific transient gas-liquid models, which were later implemented in a unique framework. These three models are the HEM-3 (Homogeneous Equilibrium Model) based on the homogeneous or "fully mixed" approach, and two other models based on the "two-fluid" approach. The first one assumes that both phase are incompressible, and is known as the PFM-2 (Pressure-Free Model), while the other one assumes the gas phase as a compressible fluid and is referred here as the SPM-4 (Single Pressure Model).

For numerical purposes and a better understanding of the main characteristics of these three models, we have performed their stability analysis, more specifically, we have analysed their hyperbolicity condition. Hence, we have shown that the homogeneous equilibrium model is always hyperbolic, and that the two-fluid incompressible model is hyperbolic for flow conditions below the inviscid Kelvin Helmholtz (IKH) condition (2.57). We have also shown that the four approximate eigenvalues of SPM-4 model are always real. However, it should be noted that these approximate eigenvalues are only valid for the small parameter $\theta \leq 5\%$, or more specifically, the relative flow velocity V_r should be less than 15 m/s if gas speed of sound is 300 m/s.

It is worth noting that the HEM-3 model was developed solely for testing and validating numerical schemes because while being simplistic, it contains most of the important features encountered in two-phase flow modelling. On the other hand, the incompressible two-fluid model PFM-2 is primarily used to assess the practical stratified and slug flow applications presented in this work. This model is only limited to flowing fluids with constant properties, therefore, a third model SPM-4 was proposed as an improvement of the later model because it takes into consideration the gas phase compressibility, allowing a true representation of the flow movement for cases such as slug flows when the change in volume of the gas becomes important due to compressibility effect.

Because of the complexity of multifluid models, i.e. the lack of hyperbolicity over the whole range of flowrates and the presence of non-conservative terms, the resolution techniques for these models remain an active field of research. Therefore, the third chapter of this thesis presents the explicit finite volume approach that we have adopted for solving our two-phase flow models, and described in detail the numerical schemes that we have implemented and investigated, during the course of this work. Various simulations and validation cases on uniform grids are presented, and these show that the high-resolution schemes developed here are robust, efficient and are able to capture strong discontinuities in the flow with a high accuracy. As suggestions for future work, we advocate using the modified flux corrected transport (FCT) scheme developed here for conservative models such as the HEM-3 or PFM-2, and a combination of two explicit schemes (TVD Lax Friedrichs and 2^{nd} order MinMod) for the single pressure model SPM-4.

Pipelines are extremely long in general and may require a large number of uniform grid cells in order to capture the finest possible feature of interest in the model. Therefore, in order to improve the efficiency and also the accuracy of the numerical models mentioned earlier, we describe in the fourth chapter the most consuming task of this research: an adaptive mesh refinement (AMR) technique, which provides the best means of achieving true multiscale capability in contemporary physical simulations.

The AMR strategy developed here is a combination of many elements from numerous researchers in the literature, but the underlying principle follows Berger & Oliger (1984) block-structured approach. The algorithm is validated with several numerical examples that showed that the AMR technique is robust and can achieve a similar level of accuracy for a fraction of cost of a calculation on a conventional uniform grid. More precisely, we have shown that this algorithmic technique can save as much as an order of magnitude in computational time for two-phase flow problems.

In the fifth chapter of this thesis, we present the first practical application for transient gas-liquid flow in pipelines. We studied the stratified flow pattern through a sudden increase of the gas flowrate and proposed a new combination of existing correlations for wall and interfacial friction factors valid for the full range of stratified flows (smooth and wavy). These models are defined by the Moody (1947) based equation (5.72) for the gas wall friction, the combined Moody (1947) and Kowalski (1987) based equation (5.73) for the liquid wall friction, and the modified Andritsos & Hanratty (1987) equation (5.74) for the

interface friction factor. The application of these simple correlations for the case presented shows prediction with less than 5% error compared to the experimental measurements.

Slug flow is an extreme case of time varying phenomena occurring in gas-liquid pipelines with continuous liquid and gas zones passing alternatively along the system. Therefore, the objective of our second application was to better understand this flow pattern by simulating a hydrodynamic slug flow case with the incompressible model developed here. The results presented in the penultimate chapter of this thesis, showed that the incompressible two-fluid model (PFM-2) is not able to accurately predict most of the features of this complex flow regime. Mechanisms such as the interfacial wave formation, the pipe bridging event, the slug growth and propagation can be predicted qualitatively observed, but critical flow characteristics such the slug length, frequency and velocity are not accurately determined.

Phenomena such as the entrainment of dispersed gas bubbles in the liquid slug are not however observed, which is expected as no mechanism was introduced in the basic equations to account for these turbulent effects. In addition, a team of researchers [Bonizzi et al., 2002] in the Imperial College London is currently investigating this important three-dimensional effect in slug flow, while another team in the same university [Hale & Hewitt, 1999] is studying in detail the slug initiation process, another mechanism that is not properly predicted by the existing one-dimensional two-fluid models.

The slug flow study has clearly shown that the numerical results are not reliable for cases on and probably above the Inviscid Kelvin Helmholtz (IKH) transition from stratified to slug flow, because they become very sensitive to the mesh size, which is characteristic of ill-posed initial-value problems. It worth nothing that the incompressible two-fluid model is no longer hyperbolic for this type of problems, and although the model was not investigated for cases below the IKH transition criteria, it is the understanding of the author that if the slug flow regime is observed, the numerical results will be more stable and reliable below a critical mesh size [Bonizzi et al., 2002]. In this case, the incompressible model will be very attractive compared to the compressible model (SPM-4), because the numerical time step is not limited by the acoustic wave speed, providing a solution generally hundred times faster than the compressible model.

All the modelling development and programming works mentioned above have led to the design of **EMAPS** (Eulerian Multiphase Adaptive Pipeline Solver), a unified and modular framework for one-dimensional multifluid models, which contains advanced numerical methods, and provides an easy way to add or modify appropriate physical correlations for the implemented mathematical models. The implementation of this framework is based on a robust adaptive mesh refinement (AMR) technique. The performance of this technique depends on the problem solved, but its automatic gradient-based error control mechanism highly improves the accuracy of the results and its local space and time adaptation strategy can increase the computational speed by an order of magnitude compared to uniform grids.

7.2 Suggestions for Future Work

Improving mathematical models and numerical methods for two-phase flows will remain an active research area for many years to come. And although we proposed two two-fluid models for gas-liquid flows, most of our reported simulations were performed using the incompressible model PFM-2, hence, further validation work is required for the single pressure model SPM-4. Furthermore, the reader should be warned against a confusion sometimes found in the literature, which suggests that this compressible two-fluid model is always hyperbolic. Though the approximate eigenvalues are always real, as shown in Chapter 2, the analytical values of the true eigenvalues can be complex, and a numerical evaluation of these analytical values reveals that the condition of hyperbolicity or limit of validity of the SPM-4 model is similar to the two-fluid incompressible model PFM-2 i.e. critical flow above the same IKH condition (2.57).

It will be therefore useful for future researchers to derive more complete models, which are applicable for the whole range of flowrates and for which change in flow patterns do not mean a complete change in the mathematical structure of the set of equations, and if that approach is not feasible for all the flow patterns, we will need to derive transition mechanisms, which allow us to switch from one model to another without losing accuracy.

During the course of this project, we have generated good information about gas-liquid stratified flow. There is also a very good understanding of the interfacial behaviour in the literature, including formation and types of travelling waves. A significant shortcoming of the present study was is emphasis on air-water data at low pressure. Additional tests at different pressures and with other fluids will help to further validate the empirical correlations for wall and interface friction factors proposed here for our transient two-fluid model.

Though not mentioned here, considerable basic work has been undertaken in the literature in measuring stratified flow wave, frequency, amplitude, transitions, and propagation velocity. It has not found its way into computer system codes because it is probably difficult, if not impossible, to incorporate it in present two-fluid models. We therefore advise future researchers to include these crucial effects in subsequent models, and hopefully, we will be able to predict accurately the onset of slugging in physical models and advance our understanding of slug flow.

8 Appendix-A (EMAPS)

8.1 Introduction

The **E**ulerian **M**ultiphase **A**daptive **P**ipeline **S**olver (EMAPS) is the computational framework in which all the results presented in this thesis were simulated. It is a general-purpose one-dimensional fluid flow code that is capable of simulating single-phase, two-phase or three-phase flow problems encountered in the oil and gas industry. The general vector-matrix form of the set of partial differential equations (PDEs) solved by the numerical schemes implemented in EMAPS is given in Appendix C, with three specific two-phase flow models.

The purpose of this appendix is not to describe all the modules implemented in the code but to give the reader a brief overview of the code main components; therefore we present in the next sections the general architecture of the code, and some of its main elements.

8.2 EMAPS Architecture

EMAPS is designed as a flexible collection of modules, and its complete structure involves three main parts:

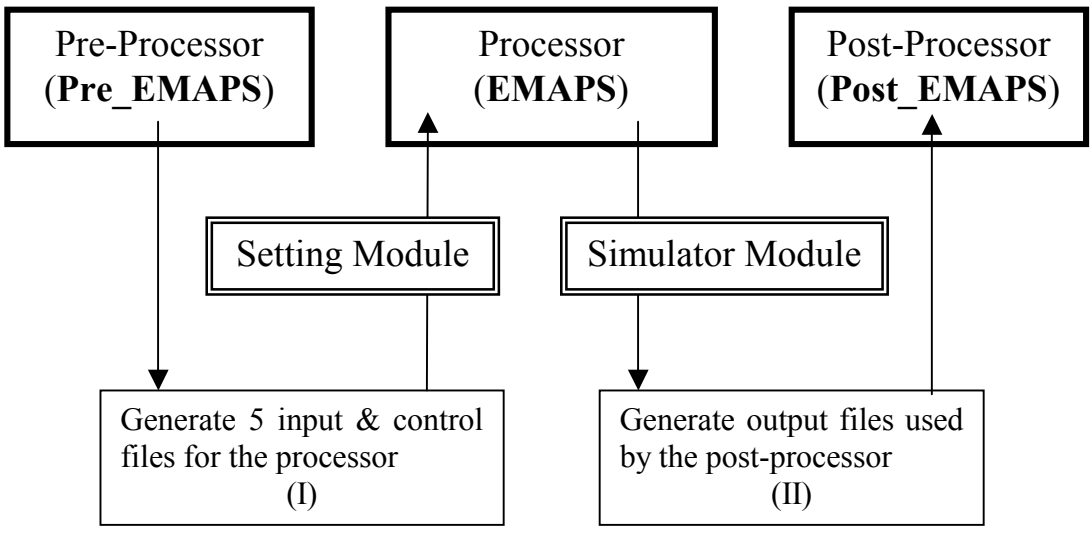

Figure 8-1: Architecture of EMAPS

1. The pre-processor for input text files (Pre-EMAPS)
2. The actual solver or processor (EMAPS)
3. The post-processor for analysing results of the simulation (Post-EMAPS)

The Figure A-1 shows a schematic diagram of the interaction between the three-parts.

8.3 The Pre-Processor

In its current version [Omgba-Essama & Hanich, 2002], the code requires five input and control data files to start a simulation. These input files are labelled:

1. Pipe.txt (for the pipe topography: length, diameter, inclination & mesh size,)
2. Fluids.txt (for the physical properties of the fluids)
3. Control.txt (time step information, numerical schemes…)
4. Problem.txt (test case name, initial & boundary condition data)
5. Model.txt (mathematical model, phase friction, interfacial pressure,)

The five input files are generated either using a text-based pre-processor written in Fortran 90, or a graphical user interface (Vassilas, 2002) written in Java. A detailed description, of all the appropriate data in each of the above files, is given in the code user manual [Omgba-Essama & Hanich, 2002], and it is not repeated here.

8.4 The Processor

The processor read the input files generated by the pre-processor, via the module **setting** (file setting.f90). This module contains, therefore, many functions that check and read the control data, and initialises all the internal variables, which are necessary for successful start of a simulation.

The module **simulator** (simulator.f90) actually contains steady and transient solvers, which make use of the adaptive mesh refinement techniques decribed in Chapter 4. The processor runs the solver selected by the user, using th appropriate numerical schemes and write the solution vector in various output files described in the code user manual.

As already mentioned, the code is composed of many modules, which make it programmer-friendly and also facilate its maintenance. The mjor modules that are present in the code are given in Figure A-2.

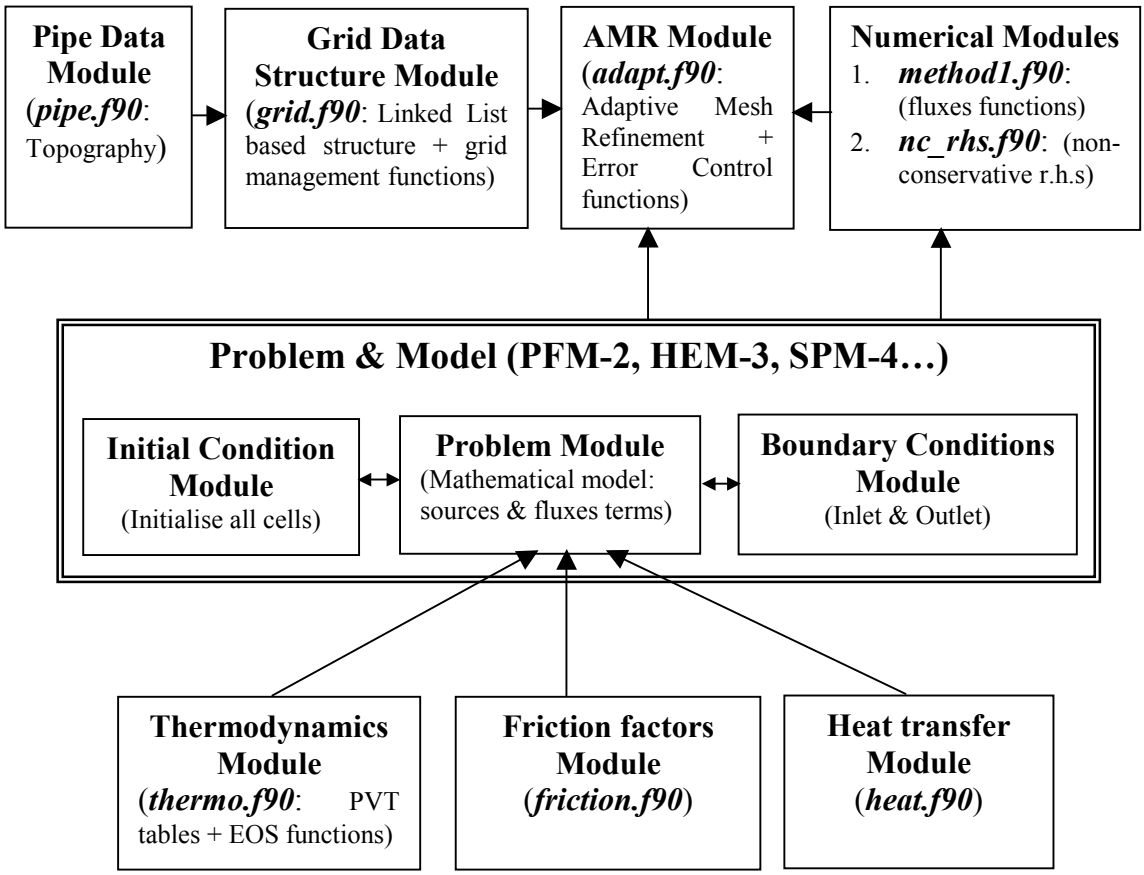

Figure 8-2: Main EMAPS Modules

In addition to these major modules, many accessory modules were implemented such the error handling module (error.f90) or the file operations module (io_files.f90). All these files will be fully described in the code technical manual, which we are currently writing.

The EMAPS files are identical for all the mathematical models simulated, except for the file or module implementing the vector-matrix formulation of the model (Appendix C). Hence, to run the code a specific executable must be created fore each of the mathematical models that the user is investigating.

8.5 The Post-Processor

In the current vesrion of the code, there is no real post-processor, which can automatically plot variables selected by the user, therefore to process the output files generated by the simulator and plot the required variables, we manually use a freeware called GNUPLOT.

8.6 References - A

- **Omgba-Essama C., & Hanich L., (2002)** "E.M.A.P.S.: Eulerian Multiphase Pipeline Solver". *User Guide*, **Version 2.75**, Applied Mathematics & Computing, Cranfield University.

- **Vassilas A., (2002)** "Graphical User Interface for the EMAPS Code". MSc Thesis, Applied Mathematics & Computing, Cranfield University.

9 Appendix-B (PFM-2)

9.1 Non-Conservative Formulation

Consider incompressible, gravitationally separated, two-phase flow of gas and liquid in a circular pipe of diameter **D**, inclined at an angle **β** to the horizontal, as shown in Figure B-1. If the flow properties are averaged over the pipe cross-section then the one-dimensional mass and momentum balance equations [Watson, 1990] for each fluid are:

- Conservation of gas mass:

$$\frac{\partial \rho_G A_G}{\partial t} + \frac{\partial \rho_G A_G V_G}{\partial x} = 0 \qquad \text{(B.1)}$$

- Conservation of gas momentum:

$$\frac{\partial \rho_G A_G V_G}{\partial t} + \frac{\partial \rho_G A_G V_G^{\,2}}{\partial x} = -A_G \frac{\partial P_I}{\partial x} - \rho_G A_G g \cos\beta \frac{\partial h_L}{\partial x} - \rho_G A_G g \sin\beta - \tau_I S_I - \tau_G S_G \qquad \text{(B.2)}$$

- Conservation of liquid mass:

$$\frac{\partial \rho_L A_L}{\partial t} + \frac{\partial \rho_L A_L V_L}{\partial x} = 0 \qquad \text{(B.3)}$$

- Conservation of liquid momentum:

$$\frac{\partial \rho_L A_L V_L}{\partial t} + \frac{\partial \rho_L A_L V_L^{\,2}}{\partial x} = -A_L \frac{\partial P_I}{\partial x} - \rho_L A_L g \cos\beta \frac{\partial h_L}{\partial x} - \rho_L A_L g \sin\beta + \tau_I S_I - \tau_L S_L \qquad \text{(B.4)}$$

The pairs (ρ_G, ρ_L), (V_G, V_L) and (A_G, A_L) are respectively the gas and liquid densities, velocities and cross-sectional areas. $\mathbf{P_I}$ is the interface pressure, and $\mathbf{h_L}$ is the liquid height, which is related to the pipe diameter and the fluids cross-section (see Section B.4).

$\mathbf{S_G}$ and $\mathbf{S_L}$ are the gas and liquid wetted perimeters, while $\mathbf{S_I}$ is the interfacial chord and their expressions are given in Section B.4. The interfacial drag force $\boldsymbol{\tau_I}$, and the gas and liquid wall shear stresses, $\boldsymbol{\tau_G}$ and $\boldsymbol{\tau_L}$ are defined as:

$$\tau_G = \frac{1}{2} f_G \rho_G V_G^2 \qquad \tau_L = \frac{1}{2} f_L \rho_L V_L^2 \tag{B.5}$$

$$\tau_I = \frac{1}{2} f_I \rho_G (V_G - V_L) \left| V_G - V_L \right| \tag{B.6}$$

Various correlations for the wall friction factors $\mathbf{f_G}$ and $\mathbf{f_L}$, and the interface friction $\mathbf{f_I}$ in Equations (B.5) and (B.6) are reviewed in Chapter 4.

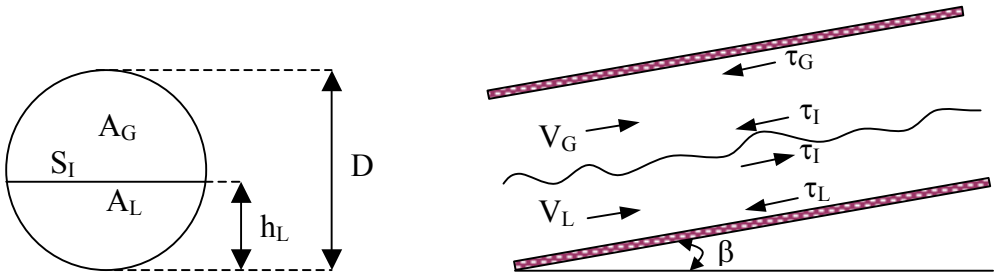

Figure 9-1: Cross-section and side views of a stratified flow in a circular pipe

9.2 Conservative Formulation

The set of partial differential equations [PDEs] (B.1) - (B.4) above is not in conservative form, and therefore not suitable for most finite difference numerical schemes for conservative hyperbolic systems. So instead of using this set for numerical purposes, we use the following set of equations, which were derived by Watson (1990) as follows:

- A total mass conservation is obtained by adding together (B.1) and (B.3) giving:

$$\frac{\partial}{\partial t}\left(\rho_L A_L + \rho_G A_G\right) + \frac{\partial}{\partial x}\left(\rho_L A_L V_L + \rho_G A_G V_G\right) = 0 \tag{B.7}$$

- A global momentum equation is obtained by combining (B.2) and (B.4) so as to eliminate the interfacial pressure p_I :

$$\frac{\partial}{\partial t}\left(\rho_L V_L - \rho_G V_G\right) + \frac{\partial}{\partial x}\left(\frac{1}{2}\rho_L V_L^{\,2} - \frac{1}{2}\rho_G V_G^{\,2} + \left(\rho_L - \rho_G\right) g h_L \cos\beta\right) = H \qquad \text{(B.8a)}$$

where

$$H = -\left(\rho_L - \rho_G\right) g \sin\beta + \tau_I S_I \left(\frac{1}{A_G} + \frac{1}{A_L}\right) + \frac{\tau_G S_G}{A_G} - \frac{\tau_L S_L}{A_L} \qquad \text{(B.8b)}$$

To solve the primitive variables (A_G, A_L, V_G, V_L), the two evolution equations (B.7) and (B.8) must be supplemented by two more relationships or closure relations. The first one is obtained from the two original mass conservation equations (B.1) and (B.3). Since the two fluids are assumed incompressible, by eliminating the fluid density in the mass conservation equations (B.1) and (B.3), they can be added to give the following relation:

$$\frac{\partial}{\partial x}\left(A_L V_L + A_G V_G\right) = 0\,. \qquad \text{(B.9)}$$

Hence we obtain the algebraic constraint C(t), which is a known function of time dependent on the inlet boundary flow parameters.

$$A_L V_L + A_G V_G = C(t) = \left(A_L V_L + A_G V_G\right)_{inlet} \qquad \text{(B.10)}$$

The other condition is obtained from the geometric constraint that the areas occupied by the liquid and gas phases must fill the pipe, so that

$$A_L + A_G = A \qquad \text{(B.11)}$$

Therefore we have reduced the original four partial differential equations (B.1) - (B.4) to just two PDEs (B.7) and (B.8), and two algebraic equations (B.10) and (B.11). It is this latter system of equations that was labelled **PFM-2** (for **P**ressure-**F**ree **M**odel) in Chapter 2 of this thesis.

9.3 Primitive Formulation

Selecting the vector $P = \left(A_L, V_G\right)^T$ as the primitive variables for the two PDEs (B.7) and (B.8), we can rewrite the total mass conservation equation (B.7) in the following form:

$$\left(\rho_L - \rho_G\right)\frac{\partial A_L}{\partial t} + \rho_L \frac{\partial\left(C(t) - A_G V_G\right)}{\partial x} + \rho_G A_G \frac{\partial V_G}{\partial x} - \rho_G V_G \frac{\partial A_L}{\partial x} = 0 \qquad \text{(B.12)}$$

$$(\rho_L - \rho_G)\frac{\partial A_L}{\partial t} + (\rho_L - \rho_G)V_G \frac{\partial A_L}{\partial x} - (\rho_L - \rho_G)A_G \frac{\partial V_G}{\partial x} = 0 \qquad \text{(B.13)}$$

Using the same primitive vector, we can transform the global momentum equation (B.8) in the following way:

$$\rho_L \frac{\partial V_L}{\partial t} - \rho_G \frac{\partial V_G}{\partial t} + \rho_L V_L \frac{\partial V_L}{\partial x} - \rho_G V_G \frac{\partial V_G}{\partial x} + (\rho_L - \rho_G) g \cos\beta \frac{dh_L}{dA_L}\frac{\partial A_L}{\partial x} = 0 \qquad \text{(B.15)}$$

The liquid velocity is given by $V_L = (C(t) - A_G V_G)/A_L$, which means that its derivatives to time and space are given by the following expressions:

$$\begin{cases} \dfrac{\partial V_L}{\partial t} = (C(t) - A_G V_G)\dfrac{\partial}{\partial t}\left(\dfrac{1}{A_L}\right) - \dfrac{A_G}{A_L}\dfrac{\partial V_G}{\partial t} + \dfrac{V_G}{A_L}\dfrac{\partial A_L}{\partial t} + \dfrac{1}{A_L}\dfrac{\partial C(t)}{\partial t} \\ \dfrac{\partial V_L}{\partial x} = (C(t) - A_G V_G)\dfrac{\partial}{\partial x}\left(\dfrac{1}{A_L}\right) - \dfrac{A_G}{A_L}\dfrac{\partial V_G}{\partial x} + \dfrac{V_G}{A_L}\dfrac{\partial A_L}{\partial x} \end{cases} \qquad \text{(B.16)}$$

For steady state problem, C(t) is not varying with time, which means that:

$$\frac{\partial V_L}{\partial z} = \frac{(V_G - V_L)}{A_L}\frac{\partial A_L}{\partial z} - \frac{A_G}{A_L}\frac{\partial V_G}{\partial z} \qquad \text{(B.17)}$$

where z is either the time variable t or the space variable x.

By using the relation (B.17) in Equation (B.15), we obtain the following momentum conservation equation:

$$\begin{aligned} &\rho_L \frac{(V_G - V_L)}{A_L}\frac{\partial A_L}{\partial t} + \left(\rho_L V_L \frac{(V_G - V_L)}{A_L} + \frac{(\rho_L - \rho_G) g \cos\beta}{A'_L}\right)\frac{\partial A_L}{\partial x} \\ &- \left(\rho_G + \rho_L \frac{A_G}{A_L}\right)\frac{\partial V_G}{\partial t} - \left(\rho_G V_G + \rho_L V_L \frac{A_G}{A_L}\right)\frac{\partial V_G}{\partial x} = 0 \end{aligned} \qquad \text{(B.18)}$$

where $A'_L = \dfrac{dA_L}{dh_L}$. Hence, if we define the relative velocity $V_r = V_G - V_L$ and the density difference $\Delta\rho = \rho_L - \rho_G$, we can recast the system of two equations (B.13) and (B.18) in the following primitive formulation:

$$M_A \frac{\partial P}{\partial t} + M_B \frac{\partial P}{\partial x} = S \ , \tag{B.19}$$

where the matrices M_A and M_B are given by:

$$M_A = \begin{bmatrix} \Delta\rho & 0 \\ \rho_L \dfrac{V_r}{A_L} & -\left(\rho_G + \rho_L \dfrac{A_G}{A_L}\right) \end{bmatrix} \tag{B.20}$$

$$M_B = \begin{bmatrix} \Delta\rho V_G & -\Delta\rho A_G \\ \rho_L V_L \dfrac{V_r}{A_L} + \dfrac{\Delta\rho g \cos\beta}{A'_L} & -\left(\rho_G V_G + \rho_L V_L \dfrac{A_G}{A_L}\right) \end{bmatrix} \tag{B.21}$$

9.4 Geometrical Relations

$A = \dfrac{\pi D^2}{4}$	Pipe cross-section
$A_L = AR_L$	Liquid cross-section
$A_G = AR_G$	Gas cross-section
$R_G + R_L = 1$	R_G and R_L are the gas and liquid volume fraction, (R_L is also known as the holdup, while R_G is also known as the void fraction).

The geometric relation between the liquid holdup R_L and the liquid height h_L for a circular cross-sectional pipe is:

$$R_L = \left(\frac{1}{\pi}\right)\left\{\pi - \cos^{-1}\left[2\frac{h_L}{D} - 1\right] + \left[2\frac{h_L}{D} - 1\right]\sqrt{\left(1 - \left[2\frac{h_L}{D} - 1\right]^2\right)}\right\}$$

$$R_L = \left(\frac{1}{\pi}\right)\left\{\pi - \cos^{-1}(X) + X\sqrt{(1 - X^2)}\right\}, \text{ where } X = 2\frac{h_L}{D} - 1$$

Knowing the liquid height h_L and the pipe diameter D, and assuming a flat gas-liquid interface, the wetted perimeters are given by the following relations [Taitel & Barnea, 1990b]:

$$S_L = D\left[\pi - \cos^{-1}\left(2\frac{h_L}{D} - 1\right)\right]$$

$$S_G = \pi D - S_L$$

$$S_I = D\sqrt{1 - \left(2\frac{h_L}{D} - 1\right)^2}$$

9.5 References - B

- **Taitel Y., & Barnea D., (1990b)** "Two-Phase Slug Flow". *Advances in Heat Transfer*, **20**, 83-132.

- **Watson M., (1990)** "Non Linear Waves in Pipeline Two-Phase Flows". Proceedings of the 3rd International Conference on Hyperbolic Problems, Uppsala, Sweden, (June 1990), Studentliterratur, Lund.

10 Appendix-C

10.1 Vector-Matrix Formulation

For a successful implementation of a mathematical model in the EMAPS code, the model has to be written in the following vector-matrix formulation:

$$\frac{\partial Q}{\partial t}+\frac{\partial F}{\partial x}=H\frac{\partial Q}{\partial x}+S \qquad (C.1)$$

where Q is a vector of unknowns, generally the conservative variables, F is a physical flux vector, H is a matrix containing non-conservative terms existing in the model, and S is a vector of algebraic source terms.

Hence, the three specific two-phase flow models described in Chapter 2, are explicitly re-written in the following sections.

10.2 HEM-3 (Homogeneous Equilibrium Model)

This hyperbolic model is fully conservative, hence the matrix H is null, and from equations (2.32), (2.33), and (2.34), the vectors Q, F, and S are given as:

$$Q=\begin{pmatrix}\rho_G R_G\\ \rho_L R_L\\ \rho_M V_M\end{pmatrix},\qquad F=\begin{pmatrix}\rho_G R_G V_M\\ \rho_L R_L V_M\\ \rho_M V_M^2+P\end{pmatrix},\qquad S=\begin{pmatrix}0\\ 0\\ T_w-\rho_M g\sin\beta\end{pmatrix} \qquad (C.2)$$

$$H=0 \qquad (C.3)$$

10.3 PFM-2 (Pressure-Free Model)

This incompressible two-fluid model is also fully conservative, therefore the matrix H is set to zero (C.3), and from relations (2.37) and (2.38), the vectors Q, F and S are given as:

$$Q = \begin{pmatrix} \rho_L R_L + \rho_G R_G \\ \rho_L V_L - \rho_G V_G \end{pmatrix}, \qquad F = \begin{pmatrix} \rho_L R_L V_L + \rho_G R_G V_G \\ \dfrac{\rho_L V_L^2 - \rho_G V_G^2}{2} + (\rho_L - \rho_G) g h_L \cos\beta \end{pmatrix} \tag{C.4a}$$

$$S = \begin{pmatrix} 0 \\ -(\rho_L - \rho_G) g \sin\beta + \tau_I S_I \left(\dfrac{1}{A_G} + \dfrac{1}{A_L} \right) + \dfrac{\tau_G S_G}{A_G} - \dfrac{\tau_L S_L}{A_L} \end{pmatrix} \tag{C.4b}$$

10.4 SPM-4 (Single Pressure Model)

This two-fluid model contains non-conservative terms; hence to obtain the vector-matrix formulation, we transform the momentum expression (2.42) as:

$$\begin{cases} \dfrac{\partial \rho_G R_G V_G}{\partial t} + \dfrac{\partial \left(\rho_G R_G V_G^2 + R_G P \right)}{\partial x} = P \dfrac{\partial R_G}{\partial x} + B_{fG} + T_I + T_{Gw} \\ \dfrac{\partial \rho_L R_L V_L}{\partial x} + \dfrac{\partial \left(\rho_L R_L V_L^2 + R_L P \right)}{\partial x} = (P - P_c) \dfrac{\partial R_L}{\partial x} + B_{fG} + T_I + T_{Gw} \end{cases} \tag{C.5}$$

And considering that the liquid phase is incompressible, the equation (C.5) can be further transformed as:

$$\begin{cases} \dfrac{\partial \rho_G R_G V_G}{\partial t} + \dfrac{\partial \left(\rho_G R_G V_G^2 + R_G P \right)}{\partial x} = -\dfrac{P}{\rho_L} \dfrac{\partial \rho_L R_L}{\partial x} + B_{fG} + T_I + T_{Gw} \\ \dfrac{\partial \rho_L R_L V_L}{\partial x} + \dfrac{\partial \left(\rho_L R_L V_L^2 + R_L P \right)}{\partial x} = \dfrac{(P - P_c)}{\rho_L} \dfrac{\partial \rho_L R_L}{\partial x} + B_{fG} + T_I + T_{Gw} \end{cases} \tag{C.6}$$

Hence, from relations (2.41) and (C.6), the vectors Q, F and S, and the matrix H are respectively given as:

$$Q = \begin{pmatrix} \rho_G R_G \\ \rho_L R_L \\ \rho_G R_G V_G \\ \rho_L R_L V_L \end{pmatrix}, \qquad F = \begin{pmatrix} \rho_G R_G V_G \\ \rho_L R_L V_L \\ \rho_G R_G V_G^2 + R_G P \\ \rho_L R_L V_L^2 + R_L P \end{pmatrix} \tag{C.7a}$$

$$S = \begin{bmatrix} 0 \\ 0 \\ B_{fG} + T_I + T_{Gw} \\ B_{fL} - T_I + T_{Lw} \end{bmatrix}, \qquad H = \begin{bmatrix} 0 & 0 & 0 & 0 \\ 0 & 0 & 0 & 0 \\ 0 & P/\rho_L & 0 & 0 \\ 0 & (P - P_c)/\rho_L & 0 & 0 \end{bmatrix} \qquad \text{(C.7b)}$$

From relation (C.7b), it appears that the non-conservative terms matrix H can be reduce into a vector, but EMAPS contains other mathematical models, such as three-phase flow ones, which require a matrix formulation for the non-conservative terms, and that is why a matrix form of these terms was selected as a default one.

11 Appendix-D (Extra Tables)

11.1 Dimensionless Numbers

Name	Symbol	Definition	Significance
Atwood	At	$(\rho' - \rho)/(\rho' + \rho)$	Density difference/Density sum
Bond	Bo	$(\rho' - \rho)gL^2/\sigma$	Gravitational force/Surface tension
Drag Coefficient	C_D	$(\rho' - \rho)gL/\rho' V^2$	Drag force/Inertial force
Eotvös	Eo	$(\rho' - \rho)gL^2/\sigma$	Gravitational force/Surface tension
Fourier	Fo	$k.t/\rho C_p L^2$	Current time/Steady state time
Froude	Fr	V^2/gL	Kinetic energy/Gravitational energy
Mach	M, Ma	V/C_s	Magnitude of compressibility effects
Reynolds	Re	$\rho LV/\mu$	Inertial forces/Viscous forces
Weber	We	$\rho LV^2/\sigma$	Inertial forces/Surface tension forces

Legend		***Unit***
C_p	Specific heat capacity at constant pressure	[J/(kg.K)]
C_s	Speed of sound	[m/s]
g	Gravitational constant	[m/s^2]
k	Thermal conductivity	[W/(m.K)]
L	Scale length, radius	[m]
t	Time	[s]
V	Characteristic flow velocity	[m/s]
μ	Viscosity coefficient	[kg/(m.s)]
ρ, ρ'	Mass density	[kg/m^3]
σ	Surface tension coefficient	[N/m]

Table 11-1: Dimensionless Numbers

11.2 Shaha Case: Comparative Tables

This section contains extra tables associated with the Shaha case figures in Chapter 5.

Liquid Wall Friction Effect

- **F_i = F_{wg} (Taitel & Dukler, 1976), F_{wg} = Moody (1947)**

Liquid Wall Friction Correlations	Numerical Holdup Value (Fully Developed Flow)		Experimental Holdup Value (R_L^{exp})		Error = $\frac{\left\|R_L^{exp} - R_L^{num}\right\|}{R_L^{exp}} \cdot 100$	
	Upstream	Downstream	Upstream	Downstream	Upstream	Downstream
Moody (1947)	0.178	0.149	0.182	0.137	2.2	8.8
Kowalski (1987)	0.198	0.172	0.182	0.137	8.8	25.5
Hand (1990)	0.195	0.166	0.182	0.137	7.1	21.2
Srichai (1994)	0.241	0.211	0.182	0.137	32.4	54.0

Table 11-2: Numerical and Experimental results for → Figure 5.6

- **F_i = Andritsos (1987), F_{wg} = Moody (1947)**

Liquid Wall Friction Correlations	Numerical Holdup Value (Fully Developed Flow)		Experimental Holdup Value (R_L^{exp})		Error = $\frac{\left\|R_L^{exp} - R_L^{num}\right\|}{R_L^{exp}} \cdot 100$	
	Upstream	Downstream	Upstream	Downstream	Upstream	Downstream
Moody (1947)	0.178	0.107	0.182	0.137	2.2	21.9
Kowalski (1987)	0.198	0.131	0.182	0.137	8.8	4.4
Hand (1990)	0.195	0.122	0.182	0.137	7.1	10.9
Srichai (1994)	0.241	0.162	0.182	0.137	32.4	18.2

Table 11-3: Numerical and Experimental results for → Figure 5.7

Gas-Liquid Interface Friction Effect (F_{wg} = Moody, F_{wl}= Moody)

Interface Friction Correlations	Numerical Holdup Value (Fully Developed Flow)		Experimental Holdup Value (R_L^{exp})		Error = $\frac{\left\|R_L^{exp} - R_L^{num}\right\|}{R_L^{exp}} \cdot 100$	
	Upstream	Downstream	Upstream	Downstream	Upstream	Downstream
Cohen & H. (1968)	0.139	0.112	0.182	0.137	23.6	18.2
Taitel & D. (1976)	0.178	0.149	0.182	0.137	2.2	8.8
Kowaski (1987)	0.119	0.084	0.182	0.137	34.6	38.7
Andritsos (1987)	0.178	0.107	0.182	0.137	2.2	21.9
Hart et al. (1989)	0.098	0.083	0.182	0.137	46.2	39.4
Tronconi (1990)	0.146	0.120	0.182	0.137	19.8	12.4
Hand (1990)	0127	0.099	0.182	0.137	30.2	27.7

Table 11-4: Numerical and Experimental results for → Figure 5.8

Best Combinations Of Interface Friction & Liquid Wall Friction (F_{wg} = Moody/Blasius)

(F_{wl}, F_i) Friction Correlations	Numerical Holdup Value (Fully Developed Flow)		Experimental Holdup Value (R_L^{exp})		Error = $\frac{\left\|R_L^{exp} - R_L^{num}\right\|}{R_L^{exp}} \cdot 100$	
	Upstream	Downstream	Upstream	Downstream	Upstream	Downstream
Kowalski / Tronconi	0.169	0.145	0.182	0.137	7.1	5.8
Hand / Tronconi	0.163	0.137	0.182	0.137	10.4	0.0
Moody / Andritsos2	0.178	0.132	0.182	0.137	2.2	3.6
(*) Blasius / Andreussi	0.175	0.146	0.182	0.137	3.8	6.6
Kowalski / Andritsos	0.198	0.131	0.182	0.137	8.8	4.4

Table 11-5: Numerical and Experimental results for → Figure 5.9

12 Nomenclature

Symbol	Definition	Unit
Roman		
A	Cross-sectional area of the pipe ($A = A_G + A_L = \pi D^2/4$)	[m^2]
A_G	Cross-sectional area of the gas phase	[m^2]
A_L	Cross-sectional area of the liquid phase	[m^2]
B_{fk}	Body or gravity force of the k-phase ($B_{fk} = -\rho_k R_k g \sin\beta$)	[Pa/m]
B_{fL}	Liquid body or gravity force	[Pa/m]
Bo	Bond number ($Bo = gD^2\Delta\rho/\sigma$)	-
Bo_L	Liquid Bond number ($Bo_L = gD^2\rho_L/\sigma$)	-
C_D	Drag coefficient	-
C_G	Gas speed of sound	[m/s]
C_M	Homogenous or mixture speed of sound	[m/s]
C_0	Translational velocity coefficient	-
C_1	Drift velocity coefficient	-
C_1, C_2, C_3	Dimensionless coefficients for the Friedel correlation	-
c	concentration term	-
c_{vm}, c_{vm}^0	Virtual mass coefficients	-
D	Pipe diameter	[m]
D_B	Bubble diameter	[m]
D_{hk}	Hydraulic diameter of the k-phase	[m]
D_G, D_{hG}	Gas hydraulic diameter	[m]
D_L, D_{hL}	Liquid hydraulic diameter	[m]
dP/dx	Pressure gradient	[Pa/m]
Eo	Eotvos number	-
F	Vector of the physical flux terms	
$\hat{F}$	Vector of the numerical flux terms	
Fr_k	Froude number of the k-phase $\left(Fr_k = J_k \big/ \sqrt{gD}\right)$	-
Fr_G	Gas Froude number	-
Fr_L	Liquid Froude number	-
Fr_M	Mixture Froude number $\left(Fr_M = V_M \big/ \sqrt{gD}\right)$	-
$\overline{Fr}_M$	Square of the mixture Froude number $\left(\overline{Fr}_M = V_M^2 \big/ gD\right)$	-
$\hat{Fr}_M$	Modified mixture Froude number	-
f	Wall friction factor for single-phase flow	-
f_I	Interfacial friction factor	-
f_k	Wall friction factor of the k-phase	-
f_w, f_M	Wall friction factor of the gas-liquid mixture	-
G_k	Mass velocity of k-phase ($G_k = \rho_k \, . \, J_k$)	[$kg/(m^2 s)$]

G_G	Mass velocity of gas-phase	[kg/(m^{2}s)]
G_L	Mass velocity of liquid-phase	[kg/(m^{2}s)]
G_T	Total mass velocity ($G_T = G_G + G_L$)	[kg/(m^{2}s)]
H	Matrix of non-conservative terms	
h_L	Liquid height	[m]
g	Gravitational acceleration constant	[m/s^2]
Grad	Average gradient for half of a patch (left or right)	
J	Jacobian of the flux vector F $\left(J = \partial F/\partial Q\right)$	
J_G	Gas superficial velocity ($J_G = V_G.R_G$)	[m/s]
J_L	Liquid superficial velocity ($J_L = V_L.R_L$)	[m/s]
L_B	Length of the Taylor bubble	[m]
L_S	Length of the slug body	[m]
M	Total number of cells or nodes	-
M_A, M_B	Matrices for system of equations	
M_1, M_2	Matrices used for computation of eigenvalues	
$\overline{M}_{ki}$	Average particle drag of the k-phase	[Pa/m]
M_{ki}	Interfacial stress force of the k-phase	[Pa/m]
M_{kw}	Wall stress force of the k-phase	[Pa/m]
N_f	Viscosity number	-
$P(x,\theta)$	Polynomial function of $x(\theta)$ and small parameter θ	
$P_k(x)$	Polynomial function of the k-index (k = 0, 1 or 2)	
P_k	Pressure of the k-phase	[Pa]
P_I, P	Interfacial common pressure	[Pa]
P_c	Pressure correction term of the liquid phase ($P_c = P_L – P_{Li}$)	[Pa]
P_{ki}	Interfacial pressure of the k-phase	[Pa]
P_G	Pressure of the gas phase	[Pa]
P_{Gi}	Interfacial pressure of the gas phase	[Pa]
P_L	Pressure of the liquid phase	[Pa]
P_{Li}	Interfacial pressure of the liquid phase	[Pa]
Q	Vector of conservative variables	
$\overline{Q}$	Intermediate vector solution	
r_B	Radius of small bubbles	[m]
R_d	Volume fraction of the discontinuous phase	-
R_k	Volume fraction or holdup of the k-phase	-
R_G	Volume fraction or holdup of the gas phase	-
R_L	Volume fraction or holdup of the liquid phase	-
R_{LE}	Equilibrium liquid holdup	-
R_{LS}	Liquid slug holdup	-
Re_k	Reynolds number of the k-phase	-
Re_G	Reynolds number of the gas-phase	-
Re_L	Reynolds number of the liquid-phase	-
Re_M	Reynolds number of the gas-liquid mixture	-
Re_S	Reynolds number of the liquid slug region	-
S	Vector of source terms	

S_i	Interfacial wetted perimeter	[m]
S_k	Wall wetted perimeter of the k-phase	[m]
t	Time variable	[s]
T	Flow temperature	[Kelvin]
T_{bk}	Time at which the wave "k" bridges the pipe	[s]
T_w	Wall shear force of the gas-liquid mixture	[Pa/m]
T_{Gw}	Wall shear force of the gas phase	[Pa/m]
T_{Lw}	Wall shear force of the liquid phase	[Pa/m]
T_I	Interfacial shear force	[Pa/m]
V_k	Velocity of the k-phase	[m/s]
V_{ki}	Interfacial velocity of the k-phase	[m/s]
V_D	Drift velocity	[m/s]
V_G	Gas phase velocity	[m/s]
V_L	Liquid phase velocity	[m/s]
V_M	Mixture velocity ($V_M = J_G + J_L$)	[m/s]
V_r	Relative velocity ($V_r = V_G - V_L$)	[m/s]
$\overline{V}_r$	Average local relative velocity $\left(\overline{V}_r \neq V_r\right)$	[m/s]
V_T	Translational velocity	[m/s]
We_M	Mixture Weber number	-
X^2	Martinelli parameter $\left(X^2 = (dP/dx)_L / (dP/dx)_G\right)$	-
X_{bk}	Location of the wave "k" when it bridges the pipe	[m]
x	Space variable	[m]
x_G	Gas quality	-
$x(\theta)$, $y(\theta)$	First order root approximations of the polynomial $P(z, \theta)$	
y	Unknown or variable of a quadratic equation	
y^+, y^-	Single roots of a quadratic equation	
Z^2	Chisholm parameter $\left(Z^2 = (dP/dx)_{GO} / (dP/dx)_{LO}\right)$	-
z	Unknown or variable of a quadratic equation	
z_1, z_2	Single roots of a dimensionless quadratic equation	-
$z_{1,4}$, $z_{2,3}$	Double roots of a dimensionless quadratic equation	-

Greek

α	Thermal diffusivity	-
β	Pipe inclination	[rad]
χ	Density ratio coefficient	-
δ	Density coefficient used for pressure correction terms	[kg/m^3]
δQ^{LR}	Spatial difference of two vectors ($\delta Q^{LR} = Q^R - Q^L$)	
$\delta\overline{Q}_j$	Difference of vectors with a limiter function	
ΔP_{ki}	Pressure correction term of the k-phase ($\Delta P_{ki} = P_k - P_{ki}$)	[Pa]

ΔP_{Gi}	Pressure correction term of the gas phase	[Pa]
$\Delta\rho$	Density difference ($\Delta\rho = \rho_L - \rho_G$)	[kg/m^3]
Δ^S	Discriminant for a stratified flow correction	
Δ^D	Discriminant for a dispersed flow correction	
Δt	Time step	[s]
Δx	Mesh size	[m]
ε	Pipe roughness	[m]
ϕ^2	Two-phase multiplier	-
γ	Angle subtended by the liquid wetted perimeter (Ch. 1)	[rad]
	Norm exponent parameter (Chapter 2)	-
Γ_k	Mass transfer of the k-phase	[kg/(m^{3}s)]
κ	Coefficient used for virtual mass force term	-
$\tilde{\lambda}$	Dimensionless characteristic value or eigenvalue	-
λ	Characteristic value or eigenvalue	[m/s]
λ_k	kth characteristic value or eigenvalue (k = 1, 2, 3, …)	[m/s]
λ_{max}	Maximum of the absolute value of eigenvalues	[m/s]
λ_L	Non-slip liquid holdup $\left(\lambda_L = J_L/(J_L + J_G)\right)$	-
θ	Small parameter for perturbation analysis ($\theta = V_r/C_G$)	-
ρ_k	Density of the k-phase	[kg/m^3]
ρ_G	Density of the gas phase	[kg/m^3]
ρ_L	Density of the liquid phase	[kg/m^3]
ρ_H	Homogeneous mixture density ($\rho_H = (1-\lambda_L)\rho_G + \lambda_L\rho_L$)	[kg/m^3]
ρ_M	Density of the gas-liquid mixture ($\rho_M = R_G\rho_G + R_L\rho_L$)	[kg/m^3]
μ_G	Viscosity of the gas phase	[kg/(m.s)]
μ_L	Viscosity of the liquid phase	[kg/(m.s)]
μ_M	Viscosity of the gas-liquid mixture	[kg/(m.s)]
μ	Anti-diffusion coefficient	-
ν	Diffusion coefficient	-
σ	Surface tension	[N/m]
τ	ratio timestep/mesh size ($\tau = \Delta t/\Delta x$)	[m/s]
τ_{Gi}, τ_I	Gas interfacial shear stress	[N/m^2]
τ_{ki}	Interfacial shear stress of the k-phase	[N/m^2]
τ_k	Wall shear stress or viscous stress of the k-phase	[N/m^2]
τ_k^{Re}	Reynolds or turbulent viscous stress of the k-phase	[N/m^2]
ξ, ξ_0	Coefficients used for pressure correction terms	-
Ψ	Vector of unknowns or flow variables	
Ψ^T	Transpose of the unknowns or flow variables vector	
ω_s	Slug frequency	-

Superscripts

B	Basset
C	Collision
CB	**C**hisholm & **B**aroczy pressure drop correlation
D	Drag, Dispersed
FCT	**F**lux **C**orrected **T**ransport numerical scheme
Force	**F**irst **Or**der **Ce**ntred numerical scheme
L	Lift (Chapter 1)
	Left State (Chapter 2)
LF	**L**ax-**F**riedrichs numerical scheme
LM	**L**ockhart & **M**artinelli pressure drop correlation
LR	Symmetric average of **L**eft and **R**ight states
R	Right state
RI	**Ri**chtmyer scheme
RUS	**Rus**anov scheme
TVDLF	**T**otal **V**ariation **D**iminishing (TVD) **L**ax-**F**riedrichs scheme
TD	**T**aitel & **D**ukler
V	Virtual mass
S	Stratified
′	First derivative
n	Current time step
n+1	Next time step
c	coarse patch / level
f	fine patch / level
d	diffuse
ad	**a**nti-**d**iffuse
cad	**c**orrect **a**nti-**d**iffuse
sep	**sep**arated flow

Subscripts

G	Gas phase
H	Homogenous gas-liquid
L	Liquid phase
M	Mixture gas-liquid
R	Reference
GO	**G**as **O**verall
LO	**L**iquid **O**verall
c	coarse patch / level
f	fine patch / level
w	wall
j	Cell centre index

j+1/2, j-1/2	Cell border indexes
norm	**norm**al atmospheric conditions
left	**left** half part of a patch (collection of cells)
right	**right** half part of a patch
fric	**fric**tion term
grav	**grav**ity term
acc	**acc**eleration term
x	axial coordinate
< >	Area-average

Acronyms

AMR	**A**daptive **M**esh **R**efinement
BBT	**B**lasius (gas) **B**lasius (liquid) **T**aitel & Dukler (interface) friction factors
CFD	**C**omputational **F**luid **D**ynamics
CFL	**C**ourant-**F**riedrichs-**L**evy number
DFM	**D**rift-**F**lux **M**odel
EMAPS	**E**ulerian **M**ultiphase **A**daptive **P**ipeline **S**olver
FCT	**F**lux **C**orrected **T**ransport (numerical scheme)
Force	**F**irst **Or**der **Ce**ntred (numerical scheme)
HEM	**H**omogeneous **E**quilibrium **M**odel
IKH	**I**nviscid **K**elvin-**H**elmholtz
IMF	**I**mplicit **M**ulti-**F**ield algorithm
IPSA	**I**nter-**P**hase **S**lip **A**lgorithm
LOCA	**L**oss **O**f **C**oolant **A**ccident
MUSCL	**M**onotonic **U**pstream **S**cheme for **C**onservation **L**aws
NCT	**N**on-**C**onservative **T**erms
NFT	**N**umerical **F**lux **T**erms
PDE	**P**artial **D**ifferential **E**quation
PeTra	**Pe**troleum **Tra**nsportation
PFM	**P**ressure-**F**ree **M**odel
PLAC	**P**ipe**L**ine **A**nalysis **C**ode
ProFes	**Pro**duced **F**luid **E**ngineering **S**oftware
PSD	**P**ower **S**pectral **D**ensity
PWR	**P**ressurized **W**ater **R**eactor
SETS	**S**tability **E**nhancing **T**wo-**S**tep (numerical scheme)
SPM	**S**ingle **P**ressure **M**odel
TFM	**T**wo-**F**luid **M**odel
TMF	**T**ransient **M**ultiphase **F**low
TPM	**T**wo-**P**ressure **M**odel
TRAC	**T**ransient **R**eactor **A**nalysis **C**ode
TVD	**T**otal **V**ariation **D**iminishing
VKH	**V**iscous **K**elvin-**H**elmholtz
VLW	**V**ery **L**ong **W**aves